Skin Friction at Very High Reynolds Numbers in the National Transonic Facility

Ralph D. Watson, John B. Anders, and Robert M. Hall
Langley Research Center, Hampton, Virginia

Since its founding, NASA has been dedicated to the advancement of aeronautics and space science. The NASA Scientific and Technical Information (STI) Program Office plays a key part in helping NASA maintain this important role.

The NASA STI Program Office is operated by Langley Research Center, the lead center for NASA's scientific and technical information. The NASA STI Program Office provides access to the NASA STI Database, the largest collection of aeronautical and space science STI in the world. The Program Office is also NASA's institutional mechanism for disseminating the results of its research and development activities. These results are published by NASA in the NASA STI Report Series, which includes the following report types:

- TECHNICAL PUBLICATION. Reports of completed research or a major significant phase of research that present the results of NASA programs and include extensive data or theoretical analysis. Includes compilations of significant scientific and technical data and information deemed to be of continuing reference value. NASA counterpart of peer-reviewed formal professional papers, but having less stringent limitations on manuscript length and extent of graphic presentations.

- TECHNICAL MEMORANDUM. Scientific and technical findings that are preliminary or of specialized interest, e.g., quick release reports, working papers, and bibliographies that contain minimal annotation. Does not contain extensive analysis.

- CONTRACTOR REPORT. Scientific and technical findings by NASA-sponsored contractors and grantees.

- CONFERENCE PUBLICATION. Collected papers from scientific and technical conferences, symposia, seminars, or other meetings sponsored or co-sponsored by NASA.

- SPECIAL PUBLICATION. Scientific, technical, or historical information from NASA programs, projects, and missions, often concerned with subjects having substantial public interest.

- TECHNICAL TRANSLATION. English-language translations of foreign scientific and technical material pertinent to NASA's mission.

Specialized services that complement the STI Program Office's diverse offerings include creating custom thesauri, building customized databases, organizing and publishing research results ... even providing videos.

For more information about the NASA STI Program Office, see the following:

- Access the NASA STI Program Home Page at *http://www.sti.nasa.gov*

- E-mail your question via the Internet to help@sti.nasa.gov

- Fax your question to the NASA STI Help Desk at (301) 621-0134

- Phone the NASA STI Help Desk at (301) 621-0390

- Write to:
  NASA STI Help Desk
  NASA Center for AeroSpace Information
  7121 Standard Drive
  Hanover, MD 21076-1320

Skin Friction at Very High Reynolds Numbers in the National Transonic Facility

Ralph D. Watson, John B. Anders, and Robert M. Hall
Langley Research Center, Hampton, Virginia

Available from:

Contents

List of Tables

List of Figures

Abstract

Skin friction coefficients were derived from measurements using standard measurement technologies on an axisymmetric cylinder in the Langley National Transonic Facility (NTF) at Mach numbers from 0.2 to 0.85. The pressure gradient was nominally zero, the wall temperature was nominally adiabatic, and the ratio of boundary layer thickness to model diameter within the measurement region was 0.10 to 0.14, varying with distance along the model. Reynolds numbers based on momentum thicknesses ranged from 37×10^3 to 605×10^3. Reynolds numbers based on axial distance ranged from 37×10^6 to 916×10^6. These measurements approximately doubled the range of available data for flat plate skin friction coefficients. Three different techniques were used to measure surface shear. The maximum error of Preston tube measurements was estimated to be 2.5 percent, while that of Clauser-derived measurements was estimated to be approximately 5 percent. Direct measurements by skin friction balance proved to be subject to large errors and were not considered reliable. The data lay above the Karman-Schoenherr prediction by about 5 percent at $R_\theta = 362 \times 10^3$.

Symbols

A	constant in equation (4)
B	constant in equation (4)
c_f	coefficient of friction
c_F	coefficient of average friction, drag/(q x area)
c_p	coefficient of pressure, $(p-p_\infty)/q$
C1	parameter in equation (15)
C2	parameter in equation (15)
d	outside diameter of Preston tube
d^+	$d \, u_\tau/\nu$
D	model diameter (12.75 inches)
E	constant in Spalding equations, equations (3) and (5)
F	constant in East equation, equation (14)

h	balance element height error (see Appendix C)
H	shape factor, δ^*/θ
l	mixing length
L	length of nose in equation (11)
M	Mach number
p	pressure
p^+	$(\mu/(\rho^2 u_\tau^2))(dp/dx)$
pw1, pw2, pw3	averaged pressures on model, see table 1(c)
Pr	Prandtl number
q	dynamic pressure
r	radial coordinate, see figure 10(a)
r_1	parameter in equation (11)
r_2	parameter in equation (11)
R	unit Reynolds number, $\rho u/\mu$, also D/2
s	distance along surface of model
T	temperature
Tw1, Tw2, Tw3	averaged temperatures on model, see table 1(d)
u	velocity
u_τ	shear velocity, $\sqrt{\tau_w/\rho_w}$
u^+	u/u_τ
w	Coles' wake function, see equation (13)
x	axial distance along model, inches, see figure 10(a)
x*	Patel's Preston tube parameter, see appendix D
y	coordinate normal to surface

y^+	$y\,u_\tau/\nu$
y^*	Patel's Preston tube parameter, see appendix D
z	lateral distance along model
Z	compressibility factor
α	model angle of attack
β'	pressure gradient parameter, $(\delta^{*\prime}/\tau_w)(dp/dx)$
γ	ratio of specific heats
δ	boundary layer thickness
δ_u	boundary layer thickness at $u/u_e = 0.995$
δ^*	displacement thickness
δ^+	value of y^+ at edge of boundary layer
$\Delta u/u_\tau$	strength of the wake component
θ	momentum thickness
κ	van Karman constant
μ	dynamic viscosity
ν	kinematic viscosity
Π	Coles' constant in equation (13)
ρ	density
τ	shear stress
ϕ	roll angle on model, see figure 10(a)

Subscripts

aw	adiabatic wall condition
e	at edge of boundary layer
max	maximum value
t	stagnation condition

3

w	at wall
x	based on x coordinate
y	based on y coordinate
θ	based on the integral quantity θ
∞	freestream condition
1, 2	denotes conditions at Stations 1 or 2

Superscript

( )'   reduced to incompressible form by Van Driest method for velocities and integral quantities; also by Sommer and Short T' method for temperature-dependent quantities

U.S. customary units are used throughout this paper unless otherwise noted.

Introduction

The optimum design of transport aircraft requires that accurate predictions of turbulent skin friction be made at flight Reynolds numbers and Mach numbers of approximately 0.8. Predictions are sometimes made by first calculating the flat plate incompressible skin friction and then correcting for various effects such as pressure gradients, three-dimensionality, surface roughness, and compressibility. In an attempt to provide a more accurate basis for this prediction at high Reynolds numbers, an experiment was designed to measure adiabatic flat plate skin friction values at Reynolds numbers as large as or larger than reported flight conditions and Mach numbers approaching flight conditions for modern transport aircraft (M=0.85 to 0.88). The measurements would also be useful to verify the prediction of calculation methods at very high Reynolds numbers. The most widely-used incompressible flat plate skin friction prediction method is the empirical Karman-Schoenherr method (ref. 1), based on data at a maximum length Reynolds number of 450×10^6. Using a standard incompressible flat plate relation between R_x and R_θ, the maximum equivalent R_θ of the data is 380×10^3. Flight Reynolds numbers are approximately 45×10^6 for wing sections, based on chord length, and 380×10^6 for the fuselage of a Boeing 747 at cruise conditions, based on a length of 225 feet. While the data of ref. 1 cover this range, additional data was desired in order to validate the results of ref. 1 at very high Reynolds numbers.

To measure skin friction at Reynolds numbers close to flight conditions, the Langley Research Center cryogenic transonic tunnels, the National Transonic Facility (NTF), and the 0.3-Meter Transonic Cryogenic Tunnel (TCT), were used. Unit Reynolds numbers as high as 100×10^6 per foot can be obtained in these tunnels, and length Reynolds numbers of 900×10^6 in NTF. Thus, Reynolds numbers obtainable in NTF could nearly double the range of data of ref. 1. Unfortunately, it is very difficult to obtain accurate skin friction measurements in cryogenic tunnels because the extremely low temperature often leads to problems with instrumentation, and the high Reynolds number of the flow can produce wall roughness effects if not carefully accounted for.

The idea of obtaining high Reynolds number c_f data utilizing the Langley cryogenic tunnels is not new

and, in fact, a program to do so was outlined in ref. 2. Many of the ideas presented in ref. 2 were used in planning the test described in this report, although the model to be used was different. It was determined in the early planning stage that a two-dimensional flat plate, as proposed in ref. 2, posed too many problems in mounting and maintaining the accuracy of the surface in the high dynamic pressure environment of NTF. For this reason, an axisymmetric model was designed for which transverse curvature effects were small, based on the thickness of the predicted boundary layer. In addition, it was necessary to determine if compressibility effects could be accurately accounted for at Mach numbers as high as 0.8. This was successfully done by applying the Van Driest transformation (ref. 3) to the data to determine equivalent incompressible flow conditions.

Early in the planning stage of the experiment it was decided that only off-the-shelf skin friction measuring techniques would be used. The program began in 1994, and this requirement eliminated the use of the nascent technologies of the time such as MEMS devices. Instrumentation development was considered too difficult, costly, and time-consuming to pursue in an already difficult and costly experiment. It was also required to measure the skin friction as accurately as possible, a notoriously difficult measurement to make at near-ambient temperature without the added challenge of making measurements at cryogenic temperatures. Three different standard techniques were used with the rationale that they would either provide consistency among themselves, or point out inadequacies in the experiment.

A skin friction balance was used, since it provides a direct measurement of skin friction. The two other methods used were Preston tubes and boundary layer surveys, from which skin friction was inferred by a Clauser method (ref. 4). The surveys also provided the boundary layer integral quantities such as the momentum and displacement thicknesses as well as the boundary layer thickness. It was known that problems existed with each technique; therefore, a series of risk-reduction experiments was conducted in the NASA Langley 0.3-Meter Transonic Cryogenic Tunnel. The range of Reynolds numbers of the Preston tube calibration was extended by testing Preston tubes in the Princeton Superpipe (ref. 5), a pipe-flow apparatus operating at high pressure and Reynolds number. These experiments are described in an appendix to this report. A discussion of the general methods available for measuring skin friction can be found in ref. 6.

The law-of-the-wall is used extensively in this report to present data and to infer skin friction coefficients from velocity profile measurements. There has been a renewed interest in the validity of the law-of-the-wall, as evidenced in the report of George and Castillo (ref. 7). The present data are examined in the parameters of ref. 7, but discussion of the relative merits of law-of-the-wall or of the power-law validity is not attempted.

This experiment extends the existing flat plate turbulent skin friction-Reynolds number database. Increased accuracy in the prediction of high Reynolds number skin friction coefficients can translate into savings in terms of fuel or increased payload. The monetary savings are directly proportional to fuel costs, which have risen sharply recently.

Experiment Design Considerations

In order to analyze flat plate adiabatic wall skin friction data, it is necessary to compare the measurements with the most reliable existing data and theory available. There are many theories for predicting skin friction; however, if a theory has been derived based on a limited amount of data it may be in error if extrapolated to other conditions.

5

Extraneous factors can often affect experiments. Tunnel flow may not be uniform and, if an axisymmetric model is used, the model must be large in relation its boundary layer in order to produce a flow approaching the required two-dimensionality. Also, in many wind tunnels the total temperature of the flow may change, producing a departure from adiabatic wall conditions.

In this section several factors pertaining to the analysis and measurement of flat plate skin friction and errors and uncertainties are discussed.

Flat Plate Skin Friction Methods

The most commonly used method for calculating turbulent incompressible flat plate skin friction is that of Karman-Schoenherr, ref. 1, covering a range of R_x from 2.8×10^5 to 450×10^6 for the turbulent data. The equivalent R_θ is from 800 to 3.8×10^5. The data were obtained by towing flat plates behind ships and correlating the drag with length Reynolds number using an equation of von Karman. The data, from a variety of sources, contains large scatter; however, the correlation has proved to be surprisingly accurate.

The Karman-Schoenherr equations are:

$$0.242 / \sqrt{c_F} = \log_{10}\left(c_F R_x\right) = \log_{10}\left(2R_\theta\right) \tag{1a}$$

$$c_f = 0.558\, c_F \left/ \left(0.558 + 2\sqrt{c_F}\right)\right. \tag{1b}$$

where c_F is the average skin friction coefficient, i.e. , total drag /(area x dynamic pressure). The local skin friction coefficient, c_f, was obtained in ref. 1 by differentiating equation (1a). Another more convenient formulation can be found in ref. 8, which can be solved directly for c_f in terms of R_θ:

$$1/c_f = 17.08\left(\log_{10} R_\theta\right)^2 + 25.11\,\log_{10} R_\theta + 6.012 \tag{2}$$

Several other methods for calculating c_f are discussed in Schlichting, ref. 9, and White, ref. 10. The Spalding equation for skin friction from ref. 11, used extensively in this report, is based on a velocity profile which includes the sublayer, buffer layer, and logarithmic regions, but not the outer (wake) region of the boundary layer. The Spalding equation for the velocity profile, derived in ref. 12 is :

$$y^+ = u^+ + \frac{1}{E}\left\{e^{\kappa u^+} - 1 - \kappa u^+ - \frac{\left(\kappa u^+\right)^2}{2!} - \frac{\left(\kappa u^+\right)^3}{3!} - \frac{\left(\kappa u^+\right)^4}{4!}\right\} \tag{3}$$

where κ and E are determined by a fit to the law of the wall :

$$u^+ = A \ln\left(y^+\right) + B$$
$$\text{where } A = \frac{1}{\kappa} \tag{4}$$

6

The equations for skin friction, derived from equation (3) in ref. 11, are:

$$R_x = \frac{\left(u_e^+\right)^4}{12} + \left(\frac{1}{\kappa^3 E}\right) \left\{ \left[6 - 4\kappa u_e^+ + \left(\kappa u_e^+\right)^2\right] e^{\kappa u_e^+} - 6 - 2\kappa u_e^+ - \frac{\left(\kappa u_e^+\right)^4}{12} - \frac{\left(\kappa u_e^+\right)^5}{20} - \frac{\left(\kappa u_e^+\right)^6}{60} - \frac{\left(\kappa u_e^+\right)^7}{252}\right\} \quad (5a)$$

$$R_\theta = \frac{\left(u_e^+\right)^2}{6} + \left(\frac{1}{\kappa E}\right) \left[\left(1 - \frac{2}{\kappa u_e^+}\right) e^{\kappa u_e^+} + \frac{2}{\kappa u_e^+} + 1 - \frac{\left(\kappa u_e^+\right)^2}{6} - \frac{\left(\kappa u_e^+\right)^3}{12} - \frac{\left(\kappa u_e^+\right)^4}{40} - \frac{\left(\kappa u_e^+\right)^5}{180}\right] \quad (5b)$$

$$\text{where} \quad c_f = \frac{2}{\left(u_e^+\right)^2} \quad \text{and} \quad E = e^{\kappa B}$$

In these equations, κ is the von Karman wall constant. In ref. 12 Spalding assumed values of 0.40 for κ and B=5.5 in the law-of-the-wall. The coefficient 1/E outside the brackets in equation (3) was set equal to 0.1108 in ref. 12, and thus was not adjustable for other values of B. In ref. 11 the coefficient was generalized to 1/E, and a value of E equal to 9.025 was used for the velocity profile, giving a profile equivalent to that in ref. 12. If E = 9.025 is used in equations (5a) and (5b) however, the skin friction prediction is too high. It was noted in ref. 11 that if E was taken to be 12.0 in equations (5a) and (5b), a better value for the skin friction coefficient is calculated. Thus, it is possible to use equation (3) for whatever values are required for κ and E for agreement with inner velocity profiles; however, the coefficient, E, also used in the skin friction equations (5a) and (5b) should be different in these equations, due to the neglect of the wake component in equation (3).

The reason for the discrepancy can be explained by referring to figure 1. Velocity profile data from this report taken at Mach numbers of 0.85, 0.6, and 0.4 are reduced to incompressible form by the Van Driest transformation, described in appendix A. The data are plotted along with Spalding's velocity profile (equation (3)) with $\kappa = 0.41$ and E = 9.535, and the law-of-the-wall (equation (4)) with $\kappa = 0.41$ and B = 5.5. The difference in u'/u_τ between the logarithmic law-of-the-wall and u_e'/u_τ at the edge of the boundary layer is due to the wake component of the boundary layer, denoted the "strength of the wake" parameter, $\Delta u'/u_\tau$. If the strength of the wake component is constant over the complete Reynolds number range, then equation (5b) with suitable values of κ and E should accurately predict u_e'/u_τ, and thus, c_f. This is not true for $R_\theta \geq 25{,}000$ (see section "Boundary Layer Profile Data Reduction"). Although equations (5a) and (5b) were based on the velocity profile of equation (3), the value of E in the velocity profile and skin friction equations should be considered separately. It is evident in figure 1 that law-of-the-wall coordinates can be used to plot skin friction laws (u_e^+ as a function of δ^+), as well as the velocity profile. A skin friction law would appear as a locus of points defined by the edge of the boundary layer in the figure. The use of 12.0 for E and 0.4 for κ in equation (3) gives an equivalent value for B = 6.212 in equation (4), which is the usual additive constant in the law-of-the-wall plus the strength-of-the-wake component.

Figure 2 compares the values of c_f obtained from equations (1a) and (1b) (Karman-Schoenherr) with that from equation (5b) (Spalding), and with the results from a finite-difference calculation by the method

of ref. 13. The large Reynolds number extent of the fit to data of the Karman-Schoenherr method and the range of Reynolds numbers covered in this experiment, which are nearly twice that of ref. 1, are noted in the figure. The Spalding equation was calculated with $\kappa=0.4$ and $E=12.0$, mentioned in ref. 11 as a good fit to data. It can be seen that the Spalding and Karman-Schoenherr methods agree at R_θ of about 6000. For larger R_θ, the Spalding method is higher than the Karman-Schoenherr and agrees with the finite-difference calculation.   At $R_\theta=300,000$, the difference between Karman-Schoenherr and Spalding is approximately 5 %.

Although not a consideration for high Reynolds numbers, theory should accurately predict low Reynolds number effects in the range of R_θ from 400 to 1000. The non-equilibrium turbulent boundary layer effect is not adequately predicted by either the Karman-Schoenherr or Spalding equations. This is illustrated by the data of Coles, ref. 14, and Purtell, ref. 15, shown in figure 3. The theory of ref. 7, also shown in figure 3, does predict increased c_f at low Reynolds numbers and agrees with the predictions of Spalding and finite-difference calculations at high Reynolds numbers. Parameters of interest for the method of ref. 7, calculated as a function of δ^+, are somewhat unwieldy. Refer to ref. 7 for the complete equations and constants required to calculate parameters of interest.

Initial Finite-Difference Calculations

Finite-difference calculations were made by the method of ref. 13 in order to estimate the surface shear levels required for designing a skin friction balance, to size a rake to capture the full extent of the boundary layer, to estimate the physical thickness corresponding to $y^+ = 5$ at the surface for estimating wall roughness effects, and to estimate the effects of transverse curvature. Sharp leading edge, two-dimensional, fully turbulent calculations at Mach 0.03 are compared to the Karman-Schoenherr and Spalding methods and the results of ref. 7 in figure 2. At high Reynolds numbers, the finite-difference calculations agree more closely with Spalding's theory, equation (5b), than with Karman-Schoenherr, equation (1).

Existing High Reynolds Number Skin Friction Data

In ref. 16, Fernholz and Finley assessed incompressible zero-pressure-gradient boundary layers as of 1996.   Two cases which they mentioned are of sufficiently high Reynolds number to be of interest here: those of Fernholz, et al, in ref. 17 and of Gaudet in refs. 18 and 19.   The data presented in ref. 18 is a reexamination of the data of ref. 19, where c_f was measured on the wall of a tunnel by floating element balance. The data, taken at a Mach number of 0.8, were reduced for this report using the Van Driest transformation for comparison with incompressible theories (see appendix A). The maximum compressible value of R_θ was 311×10^6 and the maximum transformed R_θ was 273×10^6. For the Preston tube data of ref. 17, no attempt was made to transform for compressibility effects since not enough information was given to do so. The data of Nagib and Hites in ref. 20 were also examined. There was no mention of how u_τ was obtained for these data; however, compressibility effects should not be present because of the low Mach number. Finally, the data of Smith and Walker from ref. 21 were considered. George and Castillo used the data of ref. 21, published in 1959, in deriving the constants for their skin friction theory in ref. 7.

These data are shown in figure 3, along with the theories discussed in the previous two sections of this report, an incompressible flow finite-difference calculation, the low pressure data of ref. 15, the low Reynolds number correlation of ref. 14, and the data of this report reduced from velocity surveys by the Clauser method (see Appendix B). In general, the agreement between data and incompressible theory is

very good. The Spalding theory matches the data well at high Reynolds numbers and the George and Castillo theory matches well over the whole Reynolds number range.

Factors Affecting Skin Friction Measurements

Six factors which affect the measurement of skin friction, apart from the errors associated with instrumentation, are: compressibility, pressure gradient effects, heat transfer effects, transverse curvature, surface roughness, and spanwise nonuniformity (three-dimensionality) of the flow. Each effect was examined before the test was begun to insure that it could be minimized to the extent that a "flat plate" skin friction could be measured.

Compressibility Effects

A range of Mach numbers from 0.2 to 0.85 was covered in the present data. Above approximately Mach 0.3, compressibility effects must be considered in the flow. One approach, and the one used by Allen in Preston tube reductions (ref. 22), is the use of the T' method in which temperature-dependent quantities such as ρ and μ are replaced by their values at a temperature intermediate between the wall and freestream values, i.e., the "T-prime" condition. Allen used the Sommer and Short method, ref. 23, which was a fit to supersonic data in air, and which works well for lower Mach numbers. The Sommer and Short T-prime method was used in this report for all Preston tube reductions, as was done in ref. 22. The equation defining T' is

$$\frac{T'}{T_e} = 1. + 0.035\, M_e^2 + 0.45\left(\frac{T_w}{T_e} - 1.0\right) \tag{8}$$

In order to present both velocity profile and skin friction data in incompressible form, velocity profiles and related quantities such as δ^*, θ, and R_θ, were transformed using the Van Driest method of ref. 3, which has been shown to work well for adiabatic wall boundary layers at Mach numbers as high as 10 in helium in ref. 24. This method, the basis of the Van Driest compressible skin friction law, is discussed in appendix A of this report. Spatial coordinates and τ_w are not transformed by this method. The transformation is larger at Mach 0.85 than at 0.4, as demonstrated in the appendix.

By transforming compressible results to equivalent incompressible results, errors in the correlation of skin friction by R_θ are negligible. The inference of c_f from profile data by the Clauser method is a measurement error, and will be discussed in a later section.

Pressure Gradient Effects

Preliminary tests were run in the Langley 0.3 Meter Transonic Cryogenic Tunnel (see appendix C for a description of the tests), and the effects of both favorable and adverse pressure gradients on measured skin friction were made. This was accomplished by moving the upper wall of the test section to produce pressure gradients of different magnitude on the flat side wall of the test section. Figure 4 shows the effects on Preston tube measured c_f in terms of β', the pressure gradient parameter used by Clauser to generate self-similar equilibrium profiles in ref. 4. Data are shown at Mach numbers of 0.6 and 0.8 at two different unit Reynolds numbers. β' is the transformed value calculated using the Van Driest transformed value of δ^*. Compressibility and Reynolds number effects are not completely removed using β'; however, the correlation is adequate for estimating pressure gradient effects. For these test conditions

9

$$\frac{c_f}{\left(c_f\right)_{\beta'=0}} = 1.0 - 0.7\,\beta' \qquad (9)$$

If $\beta' = \pm 0.015$, the resulting error in skin friction coefficient would be approximately $\pm 1\%$.

Heat Transfer Effects

The effects of nonadiabatic wall temperature (heat transfer) on incompressible skin friction, measured by Preston tubes in the 0.3 Meter Tunnel and reduced by the T-prime method, are shown in figure 5. The total temperature of this tunnel can be rapidly varied from above ambient temperature to 100 K, making it possible to measure c_f over a range of T_w/T_{aw}. The results are shown in figure 5 for Mach 0.6 and Mach 0.8. Two different runs are plotted to show the repeatability. The effects are larger at Mach 0.8 than 0.6, and the error in $c_f'/c_f'_{,Taw}$ is $\pm 0.5\ \%$ for T_w/T_{aw} between 0.98 and 1.02. It will be shown in the Results and Discussion section of this report that the actual variation was less than this amount. The effect of non-adiabatic wall temperature on c_f' is:

$$\frac{c_f'}{c_{f\,T,aw}'} = 1.139 - 0.139\left(T_w/T_{aw}\right) \quad \text{for Mach 0.6} \qquad (10a)$$

and

$$\frac{c_f'}{c_{f\,T,aw}'} = 1.246 - 0.246\left(T_w/T_{aw}\right) \quad \text{for Mach 0.8} \qquad (10b)$$

For most runs in the 0.3 Meter Tunnel, the wall was slightly off-adiabatic because of heat transfer through the tunnel wall to a plenum chamber behind the wall, and then to outside the tunnel.

Transverse Curvature Effects

In order to assess the suitability of an axisymmetric model for measuring "flat plate" skin friction, calculations were made to estimate the magnitude of the curvature effects to be expected in NTF. The effects of lateral divergence and longitudinal curvature on the nose of the model, as well as the purely geometric effect of transverse curvature on the cylindrical portion, are complicated by differences in transition and the initial growth of the boundary layer at different tunnel conditions. In order to estimate what these combined effects would be, boundary layer calculations were made using the finite-difference method of ref. 13 – see section on "Initial Finite-Difference Calculations." Calculations were made for Mach numbers of 0.2 and 0.9, covering the range of high and low Mach numbers of the test. At both Mach numbers, calculations were made for a zero-pressure-gradient ($c_p = 0$) fully turbulent flat plate and for axisymmetric bodies having diameters of 6 and 12 inches with 24-inch long ellipsoidal noses. Simple Newtonian impact theory, $c_p = c_{p,max}\,\sin^2(\theta)$, usually applied in hypersonic flow, was used to estimate pressures on the elliptical noses of the cylinders as an input to the calculations. Model geometry and pressures were generated by a simple Fortran program which produced the inputs in the required format for input to the method of ref. 13.

Plotting skin friction coefficients as a function of s, the surface distance, points out the problem of

10

correlating c_f with R_x or R_s. In Figure 6 the growth of θ on a flat plate at Mach 0.9 is compared with that on two axisymmetric bodies at Mach 0.9. Because of the initial development of the boundary layer in a three-dimensional flow subject to pressure gradients, the boundary layer at a specified location on the model will not be the same as that on a zero-pressure-gradient flat plate at the same location, even in the absence of transverse curvature effects. The transition location was input as 0.1 inch for the 2-D calculation and at 0.372 and 0.180 inches for the 12-inch and 6-inch diameter models, respectively. The unit Reynolds number was the same for all three cases. The initial growth of the boundary layer over the nose of the model is influenced strongly by the non-uniform external conditions from the stagnation point to the shoulder junction. Past the shoulder junction, θ diverges downstream between the 6-inch and 12-inch diameter models due to geometry effects.

Correlation is properly done using R_θ, which accounts for upstream history effects. This is illustrated in figures 7(a) and 7(b) where flat plate calculations at Mach 0.2 and 0.9 are compared with axisymmetric calculations for model diameters of 6 and 12 inches. The calculated values of R_θ at the measurement locations for the NTF model, designated Stations 1 and 2 (see section "Facility, Model, Instrumentation, and Data Reduction"), are noted on the figure.

For a 12-inch diameter model a maximum error of 1.17% occurs at Station 2 at Mach 0.2, less than the probable error of the skin friction measuring devices used. The error decreases with Mach number, corresponding to an increase in unit Reynolds number and the concomitant decrease in boundary layer thickness, and increases with R_θ, corresponding to downstream growth of the boundary layer. It was concluded from these simple calculations that an axisymmetric model would be suitable for measuring essentially flat-plate turbulent boundary layer characteristics, and that the maximum error in skin friction coefficient between the actual model and a flat plate, when compared on an R_θ basis, would be about 1 % at the lowest Reynolds numbers. At high Mach numbers, the calculated error was on the order of 0.5 %.

The final model, as constructed, was 12.75 inches in diameter and the axial nose length was 25.951 inches. See table 1(a) and the section entitled "Facility, Model, Instrumentation, and Data Reduction" for a discussion of the model design. The experimental value of δ/R was 0.15 at the second measurement station at $M = 0.2$, where the boundary layer was thickest and the Reynolds number was lowest, as discussed in the Results and Discussion of this report.

Surface Roughness Effects

In order to insure that the model was hydraulically smooth, finite-difference calculations were used to determined the $y^+ = 5$ height normal to the surface. Figure 8 shows y in inches plotted against y^+ for the most severe case, that at highest unit Reynolds number. To meet the criterion of roughness being less than 5 wall units, it was decided that the rms wall roughness should be smaller than 30 μin. When constructed, the model and skin friction balance element had a measured roughness of 4 μin.; thus, it was felt that surface roughness did not significantly affect the skin friction measurements of this test.

Spanwise Nonuniformity Effects

Turbulent boundary layers exhibit spanwise variations in skin friction coefficients and integral boundary layer properties, even in flat plate experiments where great care has been taken to insure the two-dimensionality of the outer flow. Spanwise plots of θ for nominally two-dimensional flows are always somewhat ragged, as are c_f measurements. The reason may be because of the raggedness in the transition process, and/or the presence of near wall structures in the boundary layer, inducing a standing pattern in the flow. Added to this, when there is finite three-dimensionality in the flow, these effects are

11

added to the usual two-dimensional variations.   In order to minimize the three-dimensionality of the flow on the model, the expected droop because of the model weight was calculated and found to be approximately 0.25 degree. Since the model could be adjusted within 0.01 degree, the effect should be minimized by careful alignment of the model in the vertical plane. Initial runs were devoted to model alignment. Rake, balance, and Preston tube measurements to determine skin friction were always made in the same azimuthal plane.

When measurements are made on the sidewall of tunnels, the effects are larger than found on models mounted in the freestream because of the initial establishment of the flow. In the Results and Discussion of this report, the spanwise variations measured on this model were about 2.5%.

Errors Due To Above Factors

Extraneous effects from several non-measurement sources were quantified as follows:

- Correlation errors due to compressibility: negligible

- Pressure gradient effects: see eq. (9) and Results and Discussion

- Non-adiabatic wall effects on Preston tube data: see eq. (10) and Results and Discussion

- Transverse curvature effects, R_θ dependent: 0.5 to 1.2 %

- Surface roughness effects: negligible

- Spanwise nonuniformity effects ± 2.5% max, see Instrumentation

Facility, Model, Instrumentation, Data Reduction, and Instrumentation and Measurement Errors

Facility

The National Transonic Facility at Langley Research Center is described in ref. 25. This tunnel is capable of Reynolds numbers as high as 147×10^6 per ft and Mach numbers as high as 1.22, using nitrogen gas at cryogenic temperatures as the test medium. In order to maintain a very low temperature, liquid nitrogen is injected into the tunnel through a set of nozzles. The nitrogen vaporizes, creating a gaseous test medium at temperatures just above the liquefaction point. Intermediate temperatures are achieved by allowing the flow to heat naturally during the run process, or by the use of a heat exchanger. The tunnel can also use air as the test medium if ambient temperature is required. For the present tests, both ambient and cryogenic temperatures were run to obtain the desired Reynolds number range.

The test section is approximately 8.2 ft square by 25 ft long, making it possible to mount very long models in the tunnel to produce large length Reynolds numbers. The model described in this report was 17.28 feet long.

Model

The design of the model was a compromise among several factors. It was desirable to have a long

model in order to produce high length Reynolds numbers. The diameter was required to be large enough so that the model would not sag significantly under its own weight and to allow room for the skin friction balance and other instrumentation to be mounted internally. Also, it was required to be large enough that transverse curvature effects would not be a significant factor affecting skin friction or boundary layer properties. It could not be too large, however, since model loads and blockage effects could not be excessive. A photograph of the axisymmetric 347 stainless steel model mounted in NTF is shown in figure 9, and a sketch of the model is shown in figure 10(a). The model consisted of a cylinder 12.75 inches in diameter and 17.3 feet long, having a modified-elliptical nose with 7 cylindrical sections downstream of the nose. Section coordinates are listed in table 1(a).

Instrumentation ports were mounted in the model at the stations listed in table 1(b). The model was instrumented with 147 pressure orifices, most of which were located in a row along the primary measurement ray of the model, although some were placed circumferentially around the model – see table 1(c). Thirty three thermocouples were located at various locations on the model with the thermocouples embedded in plugs, pressed into the surface, and final-machined. Three thermocouples were attached to the inner surface of the model, and two thermocouples were reserved for measurement of temperatures on and within the skin friction balance, see table 1(d). Skin friction was measured by a balance and Preston tubes at Station 2, and by inference from velocity profiles at Stations 1 and 2 (see figs. 10(a) and 10(b) for model dimensions in the vicinity of Stations 1 and 2). Skin friction instrumentation was mounted at two large ports four inches in diameter at Stations 1 and 2, and at six ports 1.85 inches in diameter at the same stations. Preston tubes were mounted circumferentially around the model at plugs mounted in the small ports at Station 2 for initial alignment of the model and to determine the symmetry of the boundary layer, from skin friction data. Mounting arrangement of the Preston tubes on the model plugs is shown in figures 10(c) and 10(d).

The nose was designed as a standard ellipse, blended with a super ellipse (ref. 26). The coordinates, plotted in figure 10(e), were described by the following equations:

$$r = r_1 \left(1.0 - \frac{x}{L}\right) + r_2 \frac{x}{L} \qquad \text{merged} \qquad (11a)$$

$$\text{where} \quad r_1 = \left[1.0 - \left(1.0 - \frac{x}{L}\right)^2\right]^{\frac{1}{2}} R \quad \text{ellipse} \qquad (11b)$$

$$\text{and} \quad r_2 = \left[1.0 - \left(1.0 - \frac{x}{L}\right)^3\right]^{\frac{1}{3}} R \quad \text{super ellipse} \qquad (11c)$$

Tabulation of the nose coordinates used in the manufacture of the model can be found in table 1(e).

Locations of the rake tubes used for measuring velocity profiles are shown in figure 10(f). The tubing tip was 0.0095 inch i.d.–0.018 inch o.d. hypodermic tubing mounted in 0.0195 inch i.d.–0.032 inch o.d. tubing. The larger tubing extended 0.8 inch from the tip of the rake body, while the smaller tubing extending 0.2 inch from the end of the large tubing.

13

The model was sting-mounted to avoid interference caused by strut mounts. The NTF sting mounting mechanism had roll and angle of attack capability, which could be used to set the model at nominally zero degree angle of attack in the vertical plane.

A preliminary estimation of blockage effects to be expected for a cylindrical model in NTF was made, based on area considerations. The NTF test section cross section is 8.2 ft sq (2.5 m sq), giving a free area of 67.240 ft^2. Calculations were made for different model radii to determine the solid blockage effect assuming a solid wall test section, even though the test section top and bottom walls are slotted with an openness area ratio 6%. The percent solid blockage is defined as (model cross-section area)/(diminished test section area x 100). Figure 11 shows the results with a blockage of 1.34% for the final model radius selected, 6.375 inches. The influence of the model will obviously be a function of the freestream Mach number.

Calculations of the flow over the final configuration were made by TLNS3D, refs. 26 and 27. It was determined from these calculations and the finite-difference calculations of ref. 13 that the pressure gradient would be close to zero at the first measurement station, and thus would not be a factor in measuring "flat plate" skin friction. Measurements confirmed this, as shown in the Results and Discussion section of this report

The whole model, including the nose, was polished to a surface finish of 4 μin, measured by the manufacturer and checked at Langley Research Center, and independently confirmed by optical measurements done on contract. No transition trips were used on the nose.

Instrumentation

Measured tunnel parameters included total pressure, static pressure, and total temperature. Total and static pressures were measured by fused-quartz pressure transducers having an accuracy of ± 0.012% of reading plus 0.006% of full scale. Four transducers having ranges of 30, 50, 100, and 150 psi were used. Total temperature was measured by two systems, (1) PRT indicators having an accuracy of ± 0.05 ^{o}K, and (2) copper constantan (type T) thermocouples having an accuracy of ± 1 ^{o}K. The tunnel Mach number was accurate to ± 0.002 from Mach 0.2 to 1.2. Model pressures were measured by an ESP system which was calibrated when the accuracy exceeded ± 0.19% of full scale of the module. Module sizes of 5, 15, and 45 psi were used. Model temperatures were measured by copper-constantan thermocouples having an accuracy of ± 1 ^{o}K. See ref. 28 for a discussion of the tunnel transducers, data acquisition system, and data reduction procedures.

As previously stated, a requirement of this test was that no instrumentation development would take place because of time and cost constraints. Three methods of determining skin friction were selected for the measurements: a skin friction balance, Preston tube measurements, and velocity profile measurements from which skin friction was inferred by a modified Clauser method.

Even though skin friction balances have been used extensively for many years, the problems anticipated by operating in a cryogenic environment required that a risk reduction experiment be conducted in a smaller, less expensive tunnel to operate. The results of these tests are discussed in appendix C of this report. The problems encountered were larger than anticipated, and greatly influenced the design of the final balance.

The balance was constructed of series 300 stainless steel, as was the model. It was mounted in the four-inch diameter ports at Stations 1 and 2. Its sensing element was 3 inches in diameter, with a surface

14

area of 7.075 square inches, subtending an angle of ± 13.24 deg of the model. The gap between the element and the case was 0.005 inches, and the lip thickness was 0.015 inches. It calibrated very accurately under laboratory conditions with excellent repeatability and linearity; however, during tunnel runs it often gave unreasonable readings. It was periodically disassembled, reassembled, and recalibrated – each a very tedious and time-consuming process. In addition to a standard calibration, the balance was subjected to vibration in the laboratory since it was anticipated that vibration would occur on the model when sting-mounted in NTF. No vibration problems were found. It was suspected that the balance material was a cause of erratic readings of the balance during tunnel runs due to the thermal cycling; however, no problems could be directly attributed to material properties.

The Preston tubes required no special design considerations except for minimal flow interference and sizing of the diameter for the boundary layer in which measurements were to be made. The tubes o.d. were 0.058 inches. Only one set of data covering the range anticipated for the present measurements was known to the authors (ref. 29). For this reason, a high Reynolds number Preston tube calibration was made at Princeton University in the Superpipe Facility, described in refs. 5 and 30. Details of the Princeton test are given in appendix D. Dimensions of the Preston tubes mounted on small and large model plugs are shown in figures 10(c) and 10(d).

Inference of skin friction from velocity surveys also required no special design considerations except for placement of the tubes at the desired locations within the turbulent boundary layer. The initial boundary layer calculations by the method of ref. 13 provided the guidelines for tube placement. There were 31 rake tubes with o.d. = 0.018, i.d. = 0.0095 inches. The lower 17 tubes were staggered, while the upper 14 tubes were in-line. They were mounted in a post tapered at 22 deg to a sharp leading edge front and back. The tip of the tubes was one inch upstream of the leading edge of the post. Measured tube locations for the rake are listed in table 2 and plotted in figure 10(f).

Photographs of the instruments are shown in figure 12; the balance in figure 12(a), a Preston tube mounted on an NTF model plug in figure 12(b), and the rake in figure 12(c).

Data Reduction

Calculation of Real-Gas Flow Properties

Properties of the flow in NTF were calculated using the Beattie-Bridgeman equation of state, discussed in ref. 31. Since the Mach number was not constant over the surface of the model, a nominal reference Mach number was calculated using the measured tunnel total pressure and an average of three static pressures on the model at orifices 60, 61, and 62 on Section 3 (see table 1(c) and figure 10(b). This Mach number was taken to be representative of the flow over the surface of the model for the purposes of calculating the local velocity, unit Reynolds number, and dynamic pressure. Test section blockage because of the model made this Mach number slightly different from the usual tunnel calculation of the freestream Mach number.

For the most accurate measure of local values of flow parameters at survey Stations 1 and 2, the wall pressure and local conditions were calculated from an average of data from 11 orifices surrounding the survey locations. For Station 1, orifices 65, 66, 76-82, 84, and 85 were used; for Station 2, orifices 116, 117, 127-133, 135, and 136 were used. Similarly for temperature, the nominal model temperature was found by averaging three temperatures at x = 69.95 for Station 1 and at x = 119.9 for Station 2. (See tables 1(c) and 1(d), and figure 10(b) for these pressure and temperature locations.)

15

Preston Tube Data Reduction

Four different methods of reducing Preston tube data were examined to determine the accuracy of each method. The methods examined were: Patel (ref. 32), Allen (ref. 33), Bertelrud (ref. 34), and Bradshaw (ref. 35). Since all methods had been derived using data at lower Mach numbers than would be encountered in this experiment, the basic formulation of each method was retained and new constants were fit to calibration data obtained at very high Reynolds numbers in the Princeton Superpipe (ref. 5). A discussion of the Princeton Preston tube calibrations at high Reynolds numbers can be found in appendix D. Using several input data cases, solutions were obtained for each of the modified methods and found to give the same results. That is, one method did not appear to be superior to another in calculating c_f from the input data. The Patel equation (equation D3 from appendix D) was used for the final data reduction since this equation was found to accurately predict the Princeton measurements with no modification and is the most commonly used method. Ref. 34 suggests parameters other than Patel's as being more suitable for data reduction, however Patel's parameters (x* and y*, see appendix D) were used for the data reduction of this report.

Three of the methods are for incompressible flow, the Bradshaw method being the exception, and the T' method (see discussion of compressibility effects) was used to account for compressibility effects as in ref. 22.

Boundary Layer Profile Data Reduction

The reduction of boundary layer pitot profiles to velocity profiles and the calculation of properties such as the displacement and momentum thicknesses are simple and straightforward, however, it is necessary to use care in the reduction scheme or the results can contain potentially large errors. For example, the survey points closest to the wall sometimes contain spurious effects caused by the interaction of the probe with the flow. In addition, it is necessary to provide a reasonable estimate of the profile between the wall and the first good data point in order to accurately calculate the integral thicknesses. The compressible routines used for the data reduction of this report, developed over a period of several years for the reduction of high Mach number profiles in helium, contain features which provide the means to evaluate experimental profiles for spurious effects and an accurate calculation of the boundary layer properties. The ideal gas assumptions of the program, originally used with fixed-gamma equations from ref. 36, were replaced with the real gas routines described in ref. 28 in order to account for the flow properties of nitrogen gas at very low temperatures.

Basic survey data consists of pitot pressures as a function of y along with the surface static pressure in the vicinity of the survey. It is assumed that there is no pressure gradient normal to the surface. Mach number profiles are calculated using the real gas method described in ref. 28. A Crocco relation [i.e., $(T_t-T_w)/(T_{t,e}-T_w) = fn(u/u_e)$] between the velocity profile and the total temperature was assumed in order to calculate the velocity, total temperature, static temperature, density, and velocity. The equation of Rotta, valid for all Mach numbers, from ref. 37 was used. This equation allows for non-adiabatic wall conditions and a smooth transition to the edge total temperature.

$$\frac{T}{T_e} = \frac{T_w}{T_e} + \left[\frac{T_{aw} - T_w}{T_e}\right]\frac{u}{u_e} - \sqrt[3]{Pr}\left(\frac{\gamma - 1}{2}\right)M_e^2\left(\frac{u}{u_e}\right)^2 \tag{12}$$

where $(Pr)^{1/3}$ has been substituted for the turbulent recovery factor

16

If the flow is turbulent, the profiles should be compared with the law-of-the-wall (equation (4)). The value of κ in equation 5 is usually 0.41 in the literature, however B varies considerably. The von Karman constant, κ, and the additive constant, B, in the law-of-the-wall are inputs to the data reduction program so that a "best fit" to the profiles can be determined.

The profiles should also be compared with the law-of-the-wake (ref. 38) to insure that there are no points with probe interference near the wall or that secondary flow effects are not present.

$$\frac{u}{u_t} = A \ln\left(y^+\right) + B + \frac{\Pi}{\kappa} w\left(\frac{y}{\delta}\right)$$

where A and B are the same as in equation (4)

and w is Coles's wake function

$$w = 1 - \cos\left(\pi \frac{y}{\delta}\right) \text{ for the present data reduction}$$

(13)

The law-of-the-wake and the law-of-the-wall components are sensitive indicators of secondary flow effects in boundary layers. Coles's Π for the law-of-the-wake is an input to equation (13) when data are plotted in these parameters. Coles determined that $\Pi = 0.55$ described equilibrium law-of-the-wall turbulent boundary layers for R_θ above 5500. Bull (ref. 39) finds values of Π lower than 0.55 for his data for R_θ from about 10,000 to 30,000. A good physical description of the strength-of-the-wake component can also be found in ref. 39. Reference 40 discusses the dependence of the strength-of-the-wake component on Reynolds number. Above R_θ of about 15,000, $\Delta u/u_\tau$ begins to decrease. The value of 2.2 found for the present data are characteristic of other high Reynolds number data. Π is then calculated to be 0.451 for the present data instead of Coles's 0.55. From equation (13), the sensitivity of c_f to Π is about 1.9 % at $\delta^+ = 1000$ and 1.35 % at $\delta^+ = 100,000$ for a change in Π of 0.10. An example of transformed profile data at Station 2 in law-of-the-wake coordinates is shown in figure 13(a) with Coles' Π of 0.55 and also with a value of 0.451. The agreement between theory and data is excellent, especially for the value of Π of 0.451.

The flow between the wall and the first data point is calculated using the profile of East (ref. 41). The East profile is

$$u^+ = \frac{1}{2\kappa} \ln\left[\frac{4}{F}\left(y^+\right)^2 + 1.0\right] + F\left[1.0 - \exp\left(\frac{-y^+}{F}\right)\right]$$

(14a)

where κ was 0.4 and F was 9.0 in ref. 41

at large y^+

$$u^+ = \frac{1}{\kappa} \ln y^+ + \frac{1}{2\kappa} \ln\left(\frac{\kappa}{F}\right) + F$$

(14b)

and in the parameter, B, of the law of the wall, Eq. (4)

$$B = \frac{1}{2\kappa} \ln\left(\frac{\kappa}{F}\right) + F$$

This equation gives a sublayer-buffer-log profile which merges with the law-of-the-wall having $\kappa =$

17

0.40 and B = 5.108. It gives essentially the same results as the Spalding equation, equation (3), however is easier to implement in a data reduction program since the solution for u^+ is a direct function of y^+, instead of vice-versa. As for equation (3), the wake region of the boundary layer is not calculated in equation (14a).

Experimental profiles were filled between the wall and the first data point using equation (14a) for accuracy in calculating integral quantities. Figure 13(b) shows the East profile calculated for κ=0.39, 0.41, and 0.43 and B=5.5, for κ=0.40 and B=5.108 as used by East, and compared with the law-of-the-wall with κ=0.41 and B=5.5. The profiles for κ=0.40, B=5.108 and κ=0.41, B=5.5 are almost indistinguishable in the range of y^+ from 100 to 10,000. By specifying only the two constants κ and B, a smooth profile from the sublayer through the buffer region to the logarithmic portion of the boundary layer can be used to accurately fill the profile between the wall and the first experimental point.

The Van Driest transformation was applied to the profile and the integral quantities θ and δ^* were calculated for both compressible and incompressible profiles. Finally, the surface shear was determined by fitting the transformed incompressible profile to the law-of-the-wall by a modified Clauser method. A detailed discussion of this method can be found in appendix B.

Iteration was involved in that a preliminary reduction of the profile was first performed and the boundary layer thicknesses, δ and δ_u, were determined. Delta is defined as the edge of the boundary layer which, for low speed flows, can be measured from the velocity profiles. In compressible flow this may not be the case, especially for gases such as helium where the thermal layer can be much thicker than the velocity layer at high Mach numbers. In this case the pitot profile is the proper indicator of the boundary layer thickness, being a function of both the velocity and density variations. At a value of the Mach number equal to approximately one the velocity and pitot thicknesses are equally sensitive indicators of the boundary layer thickness. The edge of the velocity layer is used in the definition of the wake profile. It does not depend on the thickness of the temperature layer, but only on the velocity. Thus it is necessary to define it separately from δ if the wake profile is to be considered. In addition, at high Mach numbers, the difference between δ and δ_u can be significant.

Edge values were calculated from the pitot data based on the input value of δ. Integration was carried only to δ, not the full measured profile, since the boundary layer code was developed for use in cases where there could be considerable variation in flow outside the boundary layer in the y-direction (e.g., hypersonic flow). The profile was examined in law-of-the-wall coordinates, bad points near the wall (because of plugged or partially-plugged orifices) were noted and removed, and a final reduction was made. At each reduction the value of u_τ was determined by iteration using interactive plotting.

Since the profiles were obtained on the external surface of an axisymmetric body, the axisymmetric definitions of integral quantities were used (ref. 42).

Instrumentation and Measurement Errors

A summary of errors due to instrumentation and data reduction is as follows:

- Pressure Measurement:

    o   Model Pressure: ± 0.01, 0.03, 0.09 psi, dependent on ESP module

    o   Tunnel Pressure: ± 0.03 psi, max

- Temperature Measurement: $\pm 1\ ^o$K

- Mach number calculation ± 0.002

- Inference of c_f by Clauser method – human bias: 0.5 %

- Calculation of c_f from Patel equation (see Appendix D) 0.15 %

Results and Discussion

Local Flow Conditions

Data were taken at the conditions shown in figure 14 at 7 nominal Mach numbers and 5 nominal Reynolds numbers per foot. The figure maps the conditions at which three different skin friction measuring techniques were used. Rake data were taken at model Stations 1 and 2, while balance and Preston tube data were taken at Station 2 only. Actual tunnel conditions for all runs, reduced by the method discussed in the section entitled "Calculation of Real-Gas Flow Properties," are listed in table 3.

Model Alignment

Before skin friction measurements were made, the model was aligned. The NTF sting-mount mechanism is designed so that the angle of attack can be varied during a tunnel run, and the model rolled 360 degrees as desired. The model cannot be adjusted nose left or right except when the model is initially mounted. The model roll was set to 0° and Preston tubes at Station 2 located on the model in the upper and lower vertical planes ($\phi = 0$ and 180 deg) were used to measure c_f as the angle of attack was set at small angles around 0°. The method of finding the vertical alignment is shown in figure 15 for Mach 0.4 and Mach 0.85. The figure shows c_f from the Preston tubes plotted to determine at what angle c_f would be the same on both the top and bottom tubes. The model was aligned when the angle of attack mechanism read -0.07 deg, and this value was used for all data acquisition. The angle setting could be read to ± 0.01 deg.

In order to determine if unexpected effects would be found with the model set at different roll angles, measurements of the boundary layer were made using the boundary layer rake mounted at Station 2. With the model at nominal 0° in the vertical plane, it was rolled in 15° increments to determine the state of the boundary layer away from $\phi = 0^o$. A pattern in the radial variation in c_f and R_θ, similar to the patterns found on the wall of low speed wind tunnels (ref. 43) is shown in figure 16. When c_f increases, R_θ decreases. Based on an angle of ± 13.24 deg. subtended by the balance element, the maximum variation in c_f' over the element would be 2%, integrated over the element surface. By plotting c_f against R_θ these effects are minimized, as shown in figure 17, validating the correlation of c_f with the boundary layer momentum thickness. The reason for the variation in c_f and R_θ with roll angle is not known; however, it appears that the variations found are not a reason for concern. Based on figure 17, the boundary layer is not perfectly symmetrical, but this was to be expected.

Model Pressures and Temperatures

Representative plots of model pressures and temperatures are shown in figure 18 and listed in table 4. Figure 18(a) shows measured pressure coefficients on the model at four different Mach numbers. The suction peak at x=13 inches was Mach number dependent; however, pressure coefficients on the

19

cylindrical portion of the model were not a strong function of Mach number. β' was determined to be zero at Station 1, and -0.0088 at Station 2, giving a maximum error in c_f of about $+ 0.6$ %, based on equation 9 in the "Factors Affecting Skin Friction Measurements" section of this report.

Figures 18(b) to 18(f) show model temperatures for an ambient run and for several cryogenic runs. As expected, model wall temperatures were more uniform at ambient temperatures than at cold wall conditions since the wall was near T_t at the beginning of the run. Based on the results shown in figure 5, c_f' will be within ± 0.5 % of $c_{f,Taw}'$ if T_w/T_{aw} is between 0.98 and 1.02. The values of T_w/T_t for this variation are shown in figure 18 (b) using $Pr^{(1/3)}$ for the turbulent recovery factor and an ideal gas calculation. For ambient conditions, at $T_t \cong 120$ deg. F, the wall would have to be held between ± 11 deg of T_{aw}, while for cold conditions, at $T_t \cong -250$ deg. F, the wall would have to be held between ± 4 deg. of T_{aw} to meet the desired criterion of 1 % or less error in adiabatic wall c_f'. Temperatures at Stations 1 and 2, the average of three T_w measurements were, in most cases, within ± 1 % of calculated ideal gas adiabatic wall conditions, see table 3. Seven wall temperatures were recorded and plotted in the vicinity of Stations 1 and 2, giving the variation of T_w around the full circumference of the model; however, only temperatures on the centerline and ± 30 degrees off-centerline were averaged for T_{w1} and T_{w2}.

It is evident from table 3 that temperature effects are negligible on Preston tube data at ambient temperatures. For cold runs, temperature effects may contribute errors of ± 0.5 % in the c_f data from Preston tube measurements. The effects of non-adiabatic wall conditions on c_f inferred from rake data were not quantified; however, a source of errors might be because of the Van Driest transformation.

Boundary Layer Rake Data

Following the alignment of the model and the measurement of model pressures and temperatures, the boundary rakes were installed at Stations 1 and 2 and the boundary layer pressure profiles were measured at different Mach numbers and Reynolds numbers. Nominal Reynolds numbers were set by manually adjusting the tunnel total temperature and pressure while holding the test Mach numbers constant, a procedure that has since been automated in this tunnel. Table 5 summarizes the integral and derived boundary layer properties, both in compressible and transformed form, while table 6 summarizes the velocity profile data at Stations 1 and 2. Figure 19(a) shows the difference in transformed skin friction coefficients inferred from Clauser plots using two different values of B, the additive constant in equation (4). The data were originally reduced using B = 5.0 and the result lies above both the Karman-Schoenherr and Spalding curves. A later reduction using B = 5.5 shifts the transformed data downward to within 3% of the Spalding curve at all Reynolds numbers. Figure 19(b) shows transformed profiles at Station 1, while figure 19(c) shows the profiles at Station 2 in law-of-the-wall coordinates. Also shown are the strength-of-the-wake component, $\Delta u/u_\tau = 2.2$, and the East profile used to fill between the wall and the first data point in data reduction.

Transformed shape factors are shown in figure 19(d) compared with the data of refs 14, 15, 17, 18, and 21, finite-difference calculations for a sharp leading edge flat plate at Mach 0.03, and calculations by the method of ref. 7. Although not shown, an analysis of the data shows that δ^*/δ, θ/δ, and H are not well-predicted by the method of ref. 7, even for the incompressible data of ref. 21. However, c_f as a function of R_θ is well predicted and R_θ as a function of δ^+ is accurately predicted. Transformed shape factors for the present data are independent of the value of B used to infer skin friction.

Profiles at Station 1 are shown in figure 19(e), and Station 2 in figure 19(f) in velocity defect parameters. Also shown are predictions from equation (13) for $\Pi=0.55$ and $\Pi=0.451$, which was determined to be appropriate for the present data (see section on Boundary Layer Profile Data Reduction).
20

Figure 19(g) shows the Station 1 data in the parameters of ref. 44, and figure 19(h) the profiles of Station 2. The parameters of ref. 45 give an excellent correlation of all profiles. (It has been shown in ref. 45 that there are only three profiles for all boundary layers when plotted in these parameters – zero-pressure-gradient, favorable pressure gradient, and adverse pressure gradient, independent of the magnitude of the pressure gradient.)

In order to plot Preston tube and skin friction balance data reduced to incompressible form by the T-prime method as a function of the transformed momentum thickness Reynolds number, transformed momentum thicknesses obtained from rake data were plotted as a function of Mach number and unit Reynolds number. Transformed R_θ's should also be a function of location on the model (Station 1 or Station 2); however, Preston tube and balance data were taken only at Station 2. Thus, only rake data at this position need to be considered. The following equation was found to predict R_θ' with an average error of 1% in R_θ' for Mach numbers from 0.4 to 0.85:

$$R_\theta' = C1 \left[R/ft \right]^{C2}$$

$$\text{where} \quad C1 = 0.1508 - 0.2883\,M + 0.1732\,M^2 \tag{15}$$

$$\text{and} \quad C2 = 0.7939 + 0.2822\,M - 0.1718 M^2$$

Figure 20 shows R_θ' from the rake at Station 2 along with the predicted values from equation (15).

Some balance data were taken at nominal Mach 0.2 and a simple linear relation was used to fit this data:

$$R_\theta' = 0.0078 \left[R/ft \right] + 8785.0 \tag{16}$$

Preston Tube Data

Measurements of skin friction by Preston tube were made at Station 2 for 7 different Reynolds numbers and 4 different Mach numbers. No data at Mach 0.2 were taken. The data are listed in table 7 sorted by "hot" (i.e., ambient) or "cold" tunnel conditions, and then by Mach number. Listed are the compressible and transformed skin friction coefficients calculated by the T-prime method (equation (8)), and transformed values of unit Reynolds number by the Van Driest transformation. For plotting the data as a function of the transformed momentum thickness Reynolds number, values of R_θ' were found by applying equation (15) to the measured values of compressible unit Reynolds number and Mach number for each Preston tube point.

Preston tube data are shown in compressible form in figure 21(a) at the four different Mach numbers of the test, and in figure 21(b) in transformed variables compared with the Karman-Schoenherr, Spalding, and George and Castillo incompressible theories. The data are 3 % higher than Karman-Schoenherr at R_θ' = 30,000 and 5 % higher at R_θ' = 362,000, the valid extent of the Karman-Schoenherr theory. There does not appear to be a significant, consistent difference in the data between ambient and cold wall conditions.

Balance Data

Balance data show large variations in measured c_f compared to rake and Preston tube data, both for ambient and cold tunnel conditions. This is illustrated in figure 22. Most of the data lie above the

21

theories, with no discernible difference in ambient and cold tunnel runs. Some few data points lie on or below the Spalding curve. Because of the large discrepancy between these data and the other two sets, the balance data were discounted when analyzing the c_f measurements.

An extensive development program would be necessary to produce a direct-measuring skin friction balance suitable for measuring c_f under cryogenic conditions. Initially, the present design looked promising and the instrument calibrated accurately in the laboratory under cryogenic conditions. In practice however, the instrument proved to be unreliable, possibly because of a combination of tunnel vibration coupled with the extreme temperature variations to which it was subjected. No indication of vibration/cryogenic problems were found during laboratory calibrations. The balance tended to give larger errors the longer it was run at cryogenic conditions.

Comparison of Preston Tube and Rake Data

A summary of rake and Preston tube data are shown in figure 23 compared with the Karman-Schoenherr, Spalding theories, and George and Castillo theories. Figure 23(a) shows the rake data as originally reduced with B = 5.0. It is obvious that the value of B = 5.0 for the rake data produces good agreement with the Preston tube data, although it is slightly higher than the Preston tube data at all Reynolds numbers and both measurements lie above theory. At $R_\theta' = 30,000$, where agreement between data and theory should be good, the rake data are high. For this reason, the rake data were again reduced with B = 5.5. The results are shown in figure 23(b). Here the data lie slightly below the Preston tube data, but agree well with the Spalding curve near $R_\theta' = 30,000$. It is not possible to determine the correct value of B without a direct, accurate measure of the skin friction. A rake reduction with B = 5.5 was considered here to be the more nearly correct reduction for the reasons stated above.

Skin friction coefficients derived from rake data with B = 5.5 and the Preston tube data were fit in a 2nd order polynomial in $\ln(R_\theta')$ between R_θ' of 30,000 and 300,000, and are compared with the above theories in figure 23(c). The Spalding and George and Castillo theories agree closely. These theories lie 1.9 % above the Karman-Schoenherr theory at $R_\theta' = 362,000$ and about 1.5 % above at $R_\theta' = 30,000$. The Preston tube data are 2.9 % higher than the Spalding/George and Castillo theories at $R_\theta' = 362,000$ and 1.4 % higher at $R_\theta' = 30,000$.

Summary of Errors

The sources of errors in this experimental program include: 1) errors associated with the calibration and sensitivity of instruments, 2) errors associated with data reduction, and 3) errors associated with model geometry and construction and flow non-uniformity. These errors have been discussed in previous sections, and are summarized as follows:

Errors due to extraneous effects:

Pressure gradient effects on c_f', based on eq. (9) and Results and Discussion, $+ 0.6 \%$

Non-adiabatic wall effects on c_f', based on eq. (10) and Results and Discussion, $\pm 0.5 \%$

Span wise non-uniformity for balance: $< 2.5 \%$

Transverse curvature effects: 0.5% to 1.2%

22

Errors in measurement:

      Pressures: $\pm$ 0.03 to 0.09 psia

      Temperatures: $\pm$ 1 $^{\circ}$K

      Balance: unknown large errors

Errors in calculating skin friction related to Preston tube calibration and law-of-the-wall:

      Preston tube from eq. (D3): 0.15 %

      Rake, B and κ dependent:

            Variation in B from 5 to 5.5, 3 %

            Variation in κ, probably negligible

            Human bias in estimation of c_f' by Clauser method, $\pm$ 0.5 %

Maximum cumulative error in Preston tube measurements: 2.5 %

Maximum cumulative error in rake-inferred measurements: 5 %

Conclusions

An experimental program in NASA Langley National Transonic Tunnel has extended the data base for skin friction at very high Reynolds numbers. The maximum equivalent incompressible R_θ obtained for the data were 605,000. Data were obtained by two basic methods – the Preston tube, and a modified Clauser method. The Preston tube data are considered the least subject to errors in data reduction since they are based on a high Reynolds number calibration with no "adjustable" constants. The two sets of data agree well with each other when reasonable values of law-of-the-wall constants are used in the Clauser reduction for the velocity profiles. It is generally agreed that κ is not Reynolds number dependent, and is equal to 0.41. There is no generally-accepted value for the additive constant in the law-of-the-wall for canonical flat plate boundary layers. For the present study, the absolute level of skin friction using the Clauser method is bounded to within about 3% for values of B between 5.0 and 5.5. The data lie above Karman-Schoenherr theory at the highest Reynolds numbers, and closer to theories of Spalding and George and Castillo. Measurements by skin friction balance were attempted, however unreasonable balance reading were often measured during tunnel runs. The problems were assumed to be associated with thermal cycling of the balance from ambient to cryogenic temperatures; however, no reason was found for the erratic behavior of the balance, and these data were not considered valid.

Tests were performed for Mach numbers as high as 0.85, and the skin friction coefficients, when reduced to the incompressible case by Sommer and Short T-prime method and R_θ' by the Van Driest transformation, compared well with existing incompressible data at lower Reynolds numbers. Velocity profiles transformed by the Van Driest transformation gave values of shape factor and strength-of-the-wake component which agreed well with other reliable incompressible turbulent boundary layer data.

Appendix A

Transformation of Compressible Boundary Layer Profiles to Incompressible Profiles

The law-of-the-wall can be derived for both incompressible and compressible flow and the compressible boundary layer velocity profile can be transformed to an incompressible velocity profile if the following assumptions are made:

1. For turbulent flow the mixing length hypothesis can be used to calculate the velocity profile from the definition of the turbulent shear stress.
2. The shear stress distribution through the boundary layer for both laminar and turbulent flow is the same for incompressible and compressible boundary layers up to Mach 5 (ref. 46).
3. The density distribution through the boundary layer or the temperature distribution, its equivalent in law-of-the-wall flows, is known. This is the same as assuming that the relation between the temperature and velocity profile is known.

Van Driest assumed that the velocity profile is modified by the density change through the boundary layer and used this in the formulation of his compressible skin friction theory in ref. 3. Maise and McDonald (ref. 46) called a resulting equivalent incompressible profile a "generalized" profile. Bradshaw also relied on the insensitivity of flow structure to changes because of compressibility in ref. 47.

For turbulent boundary layers the mixing-length definition of turbulent shear stress provides the necessary relation between velocity profiles in compressible and incompressible flows. In the case of laminar boundary layers, the compressible flow can be calculated accurately and transformation functions can be derived from relations between the calculated boundary layers and calculated incompressible boundary layers. Ideal gas properties are assumed; thus, the density change between the wall and freestream can be calculated for different gases using the appropriate γ. Transformation functions, if determined by a series of calculations of compressible and incompressible profiles, can be used in a manner similar to the reference temperature methods used by Eckert (ref. 48) and Sommer and Short (ref. 23).

The turbulent shear stress, defined in terms of the mixing length, is $\tau = \rho \, l^2 \, (du/dy)'$. Where the mixing length is usually defined as $l = \kappa y$ for the log region and $l/\delta = 0.085$ for the wake region. Equations for the velocity profile in terms of y^+ are:

$$\text{incompressible flow} \qquad\qquad\qquad \text{compressible flow}$$

$$du^+ = \sqrt{\frac{\tau}{\tau_w}} \, \frac{1}{\kappa} \, d\left(\ln\left(y^+\right)\right) \qquad \sqrt{\frac{\rho}{\rho_w}} \, du^+ = \sqrt{\frac{\tau}{\tau_w}} \, \frac{1}{\kappa} \, d\left(\ln\left(y^+\right)\right) \qquad (A1)$$

If it is assumed that $\sqrt{\tau / \tau_w}$ is the same for incompressible and compressible flow, the only difference between the two equations is on the left hand side. An equivalent incompressible velocity can be defined in terms of the compressible velocity and density as

24

$$\left(u^+\right)' = \int_0^{u^+} \sqrt{\frac{\rho}{\rho_w}} \, du^+ \quad \text{or} \quad u' = \int_0^{u} \sqrt{\frac{\rho}{\rho_w}} \, du \qquad \text{(A2)}$$

Compressible flow with different temperatures and densities at the wall and in the freestream is thus transformed into a flow with constant density and temperature equal to that at the wall.

For laminar flow the shear stress is defined as $\tau = \mu \, (du/dy)$ and the following equations result for incompressible and compressible flow:

<u>incompressible flow</u>   <u>compressible flow</u>

$$du^+ = \frac{\tau}{\tau_w} \, dy^+ \quad \text{or} \quad du = \frac{\tau}{\tau_w} \, dy \qquad \left(\frac{\rho_w}{\rho}\right)^{\omega} du^+ = \frac{\tau}{\tau_w} \, dy^+ \quad \text{or} \quad \left(\frac{\rho_w}{\rho}\right)^{\omega} du = \frac{\tau}{\tau_w} \, dy \qquad \text{(A3)}$$

and, as for turbulent flow,

$$\left(u^+\right)' = \int_0^{u^+} \left(\frac{\rho}{\rho_w}\right)^{\omega} du^+ \quad \text{or} \quad u' = \int_0^{u} \left(\frac{\rho}{\rho_w}\right)^{\omega} du \qquad \text{(A4)}$$

where $\omega = 0.76$ for air (ref. 36)

As assumed for turbulent flow, the laminar incompressible and compressible shear stresses are assumed to be the same in both cases in order to transform the compressible flow. For laminar boundary layers, or in the sublayer of a turbulent boundary layer, a slightly different transformation from the turbulent transformation applies. But since the region for which $(\rho/\rho_w)^{\omega}$ changes is very small, the turbulent transformation is used throughout the boundary layer in this report.

Figure A1 (a) shows the shear stress distribution through a laminar boundary layer from Howarth's calculations (ref. 9), and figure A1 (b) shows the measured turbulent distribution from Klebanoff (ref. 49). Simple approximations to the distributions are also shown in the figures. While it is not necessary to know the distribution of shear stress through the boundary layer for the compressible-incompressible transformation, the distributions are different in laminar and turbulent flows. Using analytical expressions for the shear distributions, simplified calculations of both incompressible and compressible boundary layers can be made by integrating equations (A1) and (A2) with the proper definition of mixing length for the logarithmic and wake regions of turbulent boundary layers.

The edge velocity is different for the transformed compressible and incompressible cases, as is the edge density and viscosity. The y-coordinate remains unchanged. The compressible unit Reynolds number, $\rho_e u_e/\mu_e$ becomes $\rho_w u_e'/\mu_w$ for the transformed flow. Not only is the unit Reynolds number different between the two flows, but the integral quantities θ', $\delta^{*\prime}$, and H' must be calculated using the transformed velocity profile, not the compressible profile without the density term. The skin friction coefficient is different because of the difference in dynamic pressure between the two flows.

The following table compares some quantities between compressible and transformed flows:

Quantities Transformed by Van Driest Method

Compressible Quantity	Transformed Quantity
c_f	$c_f^{'}$
H	$H^{'}$
M	0.
q	$q^{'}$
R/inch	R'/inch
T	T_w
u	u'
u/u_e	$u^{'}/u_e^{'}$
δ^*	$\delta^{*'}$
θ	$\theta^{'}$
ρ	ρ_w
ρ/ρ_e	1.0

Not transformed are x, y, p, δ, τ, and u_τ.

It is possible to assume a Crocco relation between the velocity profile and the temperature through the boundary layer for compressible flow, such as that used by Rotta (ref. 37), or to use a linear or quadratic Crocco relation in performing the transformation. Of course the method can be applied to more general cases. No attempt is made here to calculate the transformation functions between R_θ and R_θ' and c_f and c_f' for a range of Mach numbers. Rather, for the boundary layer reduction used for the data of this report, the incompressible transformation is calculated at the same time that pitot profiles are reduced to Mach number and velocity profiles. The transformed incompressible parameters are calculated for each profile.

The application of the method is shown in figure A2 where compressible profiles are compared with their transformed profiles and with the incompressible law-of-the-wall. For adiabatic wall and cold wall compressible flows the density increases from the wall to the freestream; thus, the transformed turbulent velocity profile is fuller than the compressible profile. This is evident in figure A2. The shear velocity, u_τ, is obtained iteratively, as explained in appendix B, and incompressible and compressible skin friction coefficients calculated from the result.

Two profiles are shown: point 927 at M = 0.4 and point 856 at M = 0.85. In the absence of measured T_t profiles for the present data, a quadratic Crocco relation was assumed in the data reduction. At adiabatic wall conditions and the Mach numbers of this test, the variation in T_t through the boundary layer is small, and it was found that constant T_t could be assumed with insignificant effect on the final result. Also shown is the profile of East modified for the data reduction procedure used here (see section

"Boundary Layer Profile Data Reduction," equation (14)). Figure A3 compares the compressible wake profile with its transformed profile and the law-of-the-wall wake profile of Coles (ref. 38) with $\Pi = 0.451$. See main text "Boundary Layer Profile Data Reduction" for discussion of the strength-of-the-wake parameter and its relation to Coles' Π. The comparison is very good.

An early check on the validity of the present method was made using the thirteen profiles of Gaudet from ref. 18. The measured values of skin friction were an input to the reduction, and transformed values of c_f were an output of the program. Integral quantities were derived from the transformed velocity profiles. The method appeared to give excellent results, and the data are discussed and presented in the "Results and Discussion" section of this report.

Appendix B

Inference of Skin Friction From Velocity Profiles – The Clauser Method

The inference of skin friction from boundary layer profile data, presented in a paper by Clauser (ref. 50), consists of plotting the experimental velocity profile, u/u_e, against R_y and finding the best fit of the data to a series of theoretical profiles calculated for different values of c_f. The profile in this form is different from a law-of-the-wall profile, and the different regions of the boundary layer (sublayer, buffer layer, log layer, and wake) may be hard to determine. If the unit Reynolds number is high enough it may be difficult or impossible to obtain measurements in the sublayer, as was the case for the experiments in NTF, so that only the outer part of the boundary layer is present. It was desirable to look at profiles having different degrees of compressibility in a standardized way so as to be able to identify their different regions. To accomplish this, velocity profiles were transformed into equivalent incompressible profiles using the Van Driest transformation and then plotted in law-of-the-wall coordinates.

Values of u_τ required to fit the data to the theoretical law-of-the-wall were obtained by trial-and-error. A first guess for incompressible c_f was made using the transformed value of R_θ for the profile and a table lookup from Coles (ref. 14) for the incompressible c_f. The compressible value of c_f was then calculated from the Van Driest transformation. In appendix A it is noted that τ_w and u_τ are the same for both compressible and transformed flows; however, c_f is different, because of the difference in dynamic pressure between the two flows. By iterating on u_τ, a value was found which collapsed the data onto the incompressible law-of-the-wall. Values of c_f obtained by this method were consistently within 0.5 % when the fitting was done by different people, giving confidence in the accuracy of the procedure.

The application of the original Clauser method to the present data would be applied by plotting the transformed u/u_e profile against the transformed y-Reynolds number. An "incompressible" value of c_f would be obtained by this method. Note that here is a difference between the compressible and transformed u/u_e profiles, as discussed in appendix A.

Profile 856 is used to illustrate the application of the Clauser method, as usually applied and as applied herein. Figure B1 shows the Mach 0.852 profile plotted in law-of-the-wall coordinates, both as compressible and as transformed data. Also shown are the East profile (see equation (14a) used to fill in the profile between the wall and the first data point, and the strength-of-the-wake component (ref. 40) with $\Delta u/u_\tau = 2.2$. Figure B2 shows the application of the usual Clauser method applied to the transformed data of this profile. The incompressible value of c_f was 0.0015087, and the compressible c_f was 0.00139. Figure B3 shows the same profile plotted in law-of-the-wall coordinates as done for obtaining u_τ by the present method. Different values of u_τ are chosen using an interactive plotting-data reduction program to fit the data to the law-of-the-wall. The result is the same as for the original Clauser method, however, plotting the data in law-of-the-wall coordinates gives a clearer picture of the different regions of the boundary layer.

The Clauser method of extracting skin friction from velocity profiles (finding u_τ iteratively) is not a primary method for measuring skin friction since two constants must be chosen to define the law-of-the-wall. The von Karman constant, κ, is generally accepted to be 0.41, the value which Clauser used. The additive constant, B, is known to vary with flow conditions such as inflow/outflow conditions and other nonuniformities in the flow, and varies considerably in the literature. Clauser used a value of 4.9, whereas a value of 5.5 was used for the present data.

A problem in inferring c_f from boundary layer rake data is that the rake body causes a pressure disturbance in the immediate vicinity of the rake. This could cause a local thickening of the boundary layer. The rake design was optimized for minimum pressure disturbance effects during risk reduction experiments in the 0.3 Meter Cryogenic Tunnel, discussed in appendix C. Disturbances can be minimized, but not totally eliminated, by performing a survey with a single tube traversed through the boundary layer; however, such a survey was impractical for the NTF test.

In many tests, boundary layer surveys are necessary to establish important parameters of the flow such as δ^* and θ, which are used to calculate the momentum thickness Reynolds number. The Clauser method, or a modified Clauser method used in this report, offers extra and useful information obtained from the profiles. The c_f obtained is subject to human bias, the assumptions that the profiles are accurately transformed to incompressible profiles, and the assumption that the theoretical values of κ and B are correct in the law-of-the-wall.

A few caveats and a detailed description of the Clauser method can be found in ref. 51; however, the only experimental example discussed concerned low Reynolds number effects, which are not a present concern.

Appendix C

Risk Reduction Experiments in 0.3 Meter Transonic Cryogenic Tunnel

A series of risk-reduction experiments was performed in the 0.3 Meter Transonic Cryogenic Tunnel (TCT) as a necessary step in preparation for runs in NTF. Many issues regarding instrumentation, test techniques, and data reduction were identified and several problems were addressed before runs in NTF were made. Not all problems with the skin friction balance were solved, attested to by the unreliability of the balance data in NTF. For short periods of time the balance appeared to be stable and very repeatable; however, over a longer period of time, it is evident that the operation of the balance was adversely affected by the cryogenic environment of the flow. Only one entry was originally planned for the TCT; however, because of the many problems found during this test, two other entries were required before runs in NTF were made. A final entry was made after the NTF test was completed.

Tunnel

The Langley 0.3 Meter Transonic Cryogenic Tunnel, described in ref. 52, operates at Mach numbers from 0.2 to 0.95 and unit Reynolds numbers as high as 100×10^6 per foot. The stagnation temperature is usually 100 K. Based on a preliminary reduction of data presented in ref. 53, boundary layer profiles measured in this tunnel appeared to be near-equilibrium, showing law-of-the-wall constants in good agreement with the majority of reliable flat plate boundary layer data. Because of this, the tunnel was considered suitable for testing instrumentation and checking techniques to be used in measuring skin friction in NTF.

The 0.3 Meter Tunnel utilizes adaptive upper and lower walls in the test section to control the flow for airfoil testing. Thus, it was possible to set desired pressure gradients to determine their effects on skin friction measured by various techniques.

The test section cross-section is 13 by 13 inches. The right sidewall section 60.2 inches long was replaced with a new aluminum test surface designed for mounting Preston tubes, a self-nulling aluminum skin friction balance of the type described in ref. 54, and a boundary layer rake.

Because of the variation in tunnel Mach number, a transformation technique was used to reduce measured parameters to an equivalent incompressible condition – see appendix A. The flow properties for cryogenic nitrogen were calculated by the method described in refs. 28 and 31. Local flow parameters were calculated using measured total pressure and local pressures on the test surface.

Test Surface and Instrumentation

The overall dimensions of the new sidewall are shown in figure C1(a). The test surface and plug inserts were constructed of type 6061-T6 aluminum. The skin friction balance was mounted in a 4-inch diameter plug, which could be mounted in one of three survey locations. The balance was calibrated in a cryostat at ambient and cryogenic nitrogen temperature. The boundary layer rake and Preston tubes were mounted on 1- by 3-inch plugs, which could be mounted off centerline as well as on centerline by mounting the small plug in a larger 4-inch plug.

The plate was instrumented with 58 pressure orifices as shown in figure C1(b). An additional 12

orifices were installed in a 4-inch diameter plug in which the rake was mounted, and one orifice on the 1-by 3-inch plug in which the Preston tubes were mounted. Top thermocouple locations, numbering 22, are shown in figure C1(c). Another 10 thermocouples measured temperatures on the underside of the test surface and at other locations on the balance, rake, and a terminal strip used to connect the thermocouples. Locations of plugs, pressure orifices, and thermocouples in the vicinity of survey locations are shown in figure C2. Also, locations of the survey stations, plugs, and pressure and thermocouple locations are listed in table C1. Tube locations of a 30-tube boundary layer rake are listed in table C2.

Tunnel Entries – Purpose and Results

First Entry: Tests 357, 358, 359, and 360.

Test 357 was run to measure flow properties using the new test surface and to check data acquisition and reduction techniques using routines developed for use in a cryogenic nitrogen environment. Surface pressures and the spanwise non-uniformity in surface shear across the test surface were measured with a Preston tube bar containing eleven Preston tubes.

Test 358 checked the operation of Preston tubes in a cryogenic environment, along with the sensitivity of the measurements to non-adiabatic wall temperature and pressure gradient effects. Preston tube diameters of 0.059 and 0.083 inches were tested. Preston tube data were reduced using Patel's method and the calibration constants from the Princeton calibration before it was determined that roughness effects were present in the data (see appendix D). Thus, the absolute levels of the Preston tube data are inaccurate, as determined from later Princeton measurements; however, for comparative purposes the data are valid. For the compressible flow Mach numbers of this test, it was found that for β' as large as $\pm$ 0.06, c_f measurements will be correct to within $\pm$ 5 %. β' for the NTF test was much less than this. The Preston tubes were found to be sensitive to non-adiabatic wall temperature effects. For temperature effects, if T_w = T_{aw} within 5 % at Mach 0.8, then c_f measurements will be correct to within 3 %. In most cases data acquisition was taken with T_w = T_{aw} within 1 % in NTF.

Test 359 checked the operation of a skin friction balance designed for use in a cryogenic environment, considered the primary, direct measurement of skin friction. Sensitivity to gap effects (the space between the edge of the sensing element and the case) and the effects of element tilt, vertical misalignment, and pressure and temperature gradient effects on the output were determined at Mach 0.6. Balance gaps of 0.035, 0.015, and 0.005 inches, and height mismatches of 0.006, 0.003, 0.0, -0.005, and –0.0025 inches were tested. The Preston tube bar, used to measure the spanwise skin friction in the TCT, indicated that the reading of the skin friction balance should be very slightly higher than that of a Preston tube reading at the center of the balance sensing element because of the spanwise variation of c_f across the tunnel. The balance integrated the shear levels over a three-inch diameter sensing area.

For a gap of 0.035 - Runs in which the balance was removed from the tunnel and reinstalled repeated within about 1 %. When the balance element element was raised above the case, c_f increased: when it was lowered, c_f decreased. For most runs, the element was not perfectly aligned with the surface, i.e., setting the gap perfectly uniform was a difficult trial-and-error procedure. When it was aligned, it agreed well with the misaligned runs, showing that misalignment was not important for this gap size. This is in agreement with the results of Allen, ref. 55, which show that sensitivity to misalignment to be less with large gap size.

For gaps of 0.015 and 0.005 – As gap size decreased, the measured value of c_f decreased at nominal h = 0. Allen's data at a lower Reynolds number did not show a gap size effect (ref. 55).

31

Test 360 checked the performance of a boundary layer rake for measuring velocity profiles, necessary for determining boundary layer integral quantities and to infer skin friction by the Clauser method. Pressure disturbances on the wall in the immediate vicinity of the rake were measured, which could produce possible errors in the profile data. Obviously, the pressure disturbances could distort the boundary layer and it was not known how to estimate the errors which this might produce. Also, the tubes were not located as accurately as would be required for the NTF test. The rake was redesigned with less frontal area for lower pressure disturbance, and refabricated with improved accuracy in the tube locations.

Also, the suitability of reducing compressible data to an equivalent incompressible condition was checked using the Van Driest transformation, discussed in appendix A.

Second Entry: Test 365.

The purpose of the second entry was fourfold: 1) to check the operation of a new steel balance, 2) to resolve the effects of gap size on c_f measurements, 3) to check the operation of a new rake design, and 4) to check the sensitivity of Preston tubes to mounting arrangement. A mounting arrangement different from the one used in the first entry was used for this test.

Gap size studies were made for the steel balance at ambient conditions for the following conditions: Mach 0.6, and 0.7, at R/ft = 20 x 10^6 and Mach 0.8 at R/ft = 22 x 10^6. Gap settings of 0.005, 0.0075, 0.010, 0.0125, 0.015, and 0.020 inches were tested.

The Preston tube data were reduced using Allen's (ref. 33) and Patel's (ref. 32) methods modified by the Princeton initial calibration (see appendix D). The tube outside diameter was 0.058 inches. Both modified (ref. 56) and standard Preston tubes were used. Three tubes were run in the modified mode to check mounting sensitivity. Two tubes were run as standard tubes to check the sensitivity to mounting, pressure gradient, and T_w/T_t effects.

Major problems appeared when the balance was run cold. The balance worked until its temperature reached about −180 F. Skin friction data were higher than for Test 359, the first entry.

A new boundary layer rake worked well. The frontal area was less than for the previous rake design, and this design was adopted for use in NTF.

It was found that standard Preston tubes showed less sensitivity to tube mounting than did modified Preston tubes. For this reason it was decided to use standard Preston tubes for the NTF test. The sensitivity to T_w/T_{aw} and pressure gradient effects was the same as for the first TCT entry.

Third Entry: Test 372.

The purpose of the third entry was to resolve effects of gap size and element misalignment on c_f measurements. The balance was laboratory-calibrated cold many times before the TCT test with no problems. Height and longitudinal element misalignment studies were made at the following tunnel conditions:

(a) M = 0.4, R/ft = 6, 10 and 15 x 10^6
(b) M = 0.6, R/ft = 6, 10, 15, and 20 x 10^6
(c) M = 0.8, R/ft = 6, 10, 15, and 22 x 10^6

32

(d) Gaps were 0.005, 0.0075, 0.010, and 0.0125 inches
(e) Longitudinal offset was 0.0029 inches
(f) Height offsets were 0., +0.001, and –0.001 inches

Problems appeared immediately when the balance was run cold in the tunnel. The problems may be associated with the rate of cooling or the temperature difference which exists between the flow side of the plate and the back side. The effect of longitudinal offset on the element was probably negligible. The effect of height offset was very large. The worst case was for negative height offset.

Fourth Entry: Test 502.

The final risk reduction experiment was made in the 0.3 Meter Tunnel after runs in NTF had been completed. The purpose was to further quantify element offset, lip thickness, and height effects for a balance gap of 0.005 inches, as run in NTF.

Offset Effects – The element was offset 0.0025 in a 0.005 gap, both upstream and downstream. The effect was to decrease the reading by 2.5 % in both cases at all Mach numbers, and decreased with increasing Reynolds number.

Height Effects – Five cases were run; h = +0.001, -0.001, +0.002, and -0.002 inches, and a curved element simulating the element used in NTF; i.e., h = -0.001 inch on the center and +0.001 inch on the edges parallel to the flow.

For positive heights, 0.001 produced very little effect at all Mach numbers, however 0.002 produced an increase in c_f of 5 %. For negative heights, -0.001 produced about the same effect as –0.002, with a change in the slope of c_f with Reynolds number. Max error was at low Reynolds numbers, being about 2.5 %. Repeat runs for h = - 0.001 showed excellent repeatability. For the curved element, the effects of low center (-0.001) and high edges (+0.001) are an increase of 2.5 % at low Reynolds numbers and 5 % at high Reynolds numbers. The change in slope with Reynolds number is the opposite of that for a flat element.

Lip Thickness Effects – Lip thicknesses of 0.005 and 0.015 inches were tested at a gap size of 0.005 inch. When the lip was decreased from 0.015 to 0.005 inch, the skin friction coefficients decreased by 2.5 % over the Mach–Reynolds number range. While this is significant, it is much less than the large skin friction coefficients measured in NTF

33

Appendix D

Preston Tube Calibrations At High Reynolds Numbers

Only one Preston tube calibration known to the authors (ref. 29) covered the range of Reynolds numbers as high as estimated for the NTF test, in terms of x^* from about 7.5 to 10.0 The calibration was augmented by testing Preston tubes in the high pressure pipe flow apparatus at Princeton University, the Superpipe described in ref. 5. Tube diameters of 0.058, 0.083, and 0.203 inches were tested. Skin friction coefficients were obtained by the usual measurement of the longitudinal pipe pressure gradient. Figure D1 shows a Preston tube mounted on a wall plug for the Superpipe.

The data were published by Zagarola in appendix A of ref. 5 and in ref. 30. The original data were taken before it became apparent that the roughness of the pipe might be an issue. The data were compared with the Patel calibration (ref. 32) and, based on the initial results, it appeared that Patel's equation should be modified at very high Reynolds numbers. This modification was made along with modifications to three other methods, which were considered for reducing the data of the NTF test: those of Allen (ref. 33), Bertelrud (ref. 34), and Bradshaw (ref. 35). The coefficients for all methods were determined by fitting the Princeton data at high Reynolds numbers in the parameters of the several methods. Essentially identical answers were obtained when reducing several data test cases by the four methods. Since no one method appeared to be superior to the other, the method of Patel was selected for data reduction as being the most commonly used method.

Patel's presented three different equations for different ranges of x^* as follows:

$$y^* = 0.5 \, x^* + 0.037$$
$$\text{for } y^* < 1.5; \, x^* < 2.93$$

(D1)

$$y^* = 0.8287 - 0.1381 \, x^* + 0.1437 \left(x^*\right)^2 - 0.006 \left(x^*\right)^3$$
$$\text{for } \quad 1.5 < y^* < 3.5; \, 2.93 < x^* < 5.6$$

(D2)

$$x^* = y^* + 2.0 \, \log\left[1.95 \, y^* + 4.10\right]$$
$$\text{for } 3.5 < y^* < 5.3; \quad 5.6 < x^* < 7.6$$

(D3)

$$\text{where } \quad x^* = \log\left[\frac{\Delta\rho \, d^2}{4\rho v^2}\right] = \log\left[\frac{\Delta\rho}{\tau_w}\left(\frac{d^+}{2}\right)^2\right]$$

$$y^* = \log\left[\frac{\tau_w d^2}{4\rho v^2}\right] = \log\left[\left(\frac{d^+}{2}\right)^2\right]$$

$$d^+ = u_\tau d / \nu$$

$$\Delta p = p_{Pr\,eston} - p_{static} = \frac{1}{2} \rho\, u^2$$

in incompressible flow

In ref. 32, Patel gives the limits on p^+ for which τ will be within 3% of the correct value in pressure gradients:

for adverse gradients, $p^+ < 0.010,\ \ d^+ <= 200$

favorable gradients, $p^+ > -0.005,\ \ d^+ <= 200$

$$\text{where}\quad p^+ = \frac{\mu}{\rho^2 u_\tau^2}\, \frac{dp}{dx}$$

The results from a risk-reduction experiment, wherein errors in c_f were correlated with β' are used in this report, rather than Patel's p^+ criteria. The maximum error on this basis amounts to about 0.6% at Station 2 – see the section "Pressure Gradient Effects" and figure 4 in this report.

After initial Preston tube data were taken, analysis of velocity profiles taken in the pipe indicated that the pipe might not have been hydraulically smooth. The pipe was rehoned and more Preston tube data taken, including data at higher values of x^* and y^* than originally taken. This data set agreed closely with the original calibration of Patel. Accordingly, equation (D3) was used for the final reduction of the Preston tube data from NTF. As noted in ref. 5, this equation fit the Preston tube results from Princeton within 0.15 %. A slight modification to equation (D3), which fits the data to within 0.10 %, can be found in ref. 5. Figure (D2) shows the Princeton data compared with Patel's unmodified high Reynolds number equation and the data of Ozarapoglu, ref. 29. Also shown is the range of x^* covered in the NTF experiment. Both sets of data agree well with equation (D3).

The data reduction at Princeton used the virial form of the equation of state (ref. 5) to calculate the compressibility function, Z, and a real-gas calculation of the viscosity because of high-density effects (ref. 25). For the pressures encountered in the Superpipe, Z ranged from 0.98 to 1.05, and the viscosity was as much as 30% higher than the Sutherland air value at the highest pressures. It is evident that Patel's method, unmodified, is applicable to very high Reynolds numbers. The data extends the upper limit in y^* of the Patel calibration from 5.3 to 8.7 and x^* from 7.6 to 11.3.

Controversy concerning the scaling of the pipe velocity profiles and the hydraulic smoothness of the pipe can be found in refs. 57, 58, and 59; however, the Princeton group believes the pipe to be hydraulically smooth.

Acknowledgements

References

1. Schoenherr, K. E.: *Resistance of Flat Surfaces Moving Through a Fluid*, Transactions SNAME, 40, 1932, pp 279-313.

2. Saric, W. S.; and Peterson, J. B., Jr.: Design of High-Reynolds-Number Flat-Plate Experiments in the NTF, *AIAA-84-0588,* presented at AIAA 13th Aerodynamics Testing Conference, San Diego, CA, March 5-7, 1984.

3. Van Driest, E. R.: Turbulent Boundary Layer in Compressible Fluids, *Journal of the Aeronautical Sciences*, 18, no. 3, March, 1951, pp 145-160, 216.

4. Clauser, F. H.: *The Turbulent Boundary Layer*, Advances in Applied Mechanics IV, 1956, pp 1-51.

5. Zagarola, M. V.: Mean-Flow Scaling of Turbulent Pipe Flow, Ph.D. Thesis, Mechanical and Aerospace Engineering, Princeton University, June, 1996.

6. Winter, K. G.: An outline of the techniques available for the measurement of skin friction in turbulent boundary layers, *Progress in Aerospace Sciences*, vol. 18, 1977, Pergamon Press, pp 1-57.

7. George, W. K.; and Castillo, L.: Zero-pressure-gradient turbulent boundary layer, *Applied Mechanics Reviews*, vol. 50, no. 12, part 1, December, 1997, pp 689-729.

8. Hopkins, E. J.; and Inouye, M.: An Evaluation of Theories for Predicting Turbulent Skin Friction and Heat Transfer on Flat Plates at Supersonic and Hypersonic Mach Numbers, *AIAA Journal*, vol. 9, no. 6, June, 1971, pp 993-1003.

9. Schlichting, Hermann: *Boundary-Layer Theory*, McGraw-Hill Book Company, 1968.

10. .White, F. M.: *Viscous Fluid Flow*, Second Edition, McGraw-Hill Book Company, 1991.

11. Spalding, D. B.: A New Analytical Expression for the Drag of a Flat Plate Valid for Both the Turbulent and Laminar Regimes*, International Journal of Heat and Mass Transfer*, 5, 1962, pp 1133-1138.

12. Spalding, D. B.: A Single Formula for the "Law-of-the-wall", *Journal of Applied Mechanics*, vol. 28, series E, number 3, September, 1961, pp. 455-458

13. Harris, J. E.; and Blanchard, D. K.: *Computer Program for Solving Laminar, Transitional, or Turbulent Compressible Boundary-Layer equations for Two-Dimensional and Axisymmetric Flow*, NASA Technical Memorandum 83207, NASA Langley, February, 1982.

14. Coles, D.: *The Turbulent Boundary Layer in a Compressible Fluid*, R-403-PR, Rand Corp., September, 1962.

15. Purtell, L. P.: The Turbulent Boundary Layer at Low Reynolds Number, Ph.D. Thesis, Graduate School, Mechanical Engineering, University of Maryland, 1978.

16. Fernholz, H. H.; and Finley, P. J.: The Incompressible Zero-Pressure-Gradient Turbulent Boundary Layer: An Assessment of the Data. *Progress in Aerospace Sciences*, Vol. 32, No. 4, Haines, A.B. and Orlik-Ruckemann, K. J., eds, Pergamon Press, August, 1996, pp 245-311.

17. Fernholz, H. H.; Krause, E.; Nockemann, M.; and Schober, M.: Comparative measurements in the canonical boundary layer at $Re_{d2} \leq 6x10^4$ on the wall of the German-Dutch windtunnel. *The Physics of Fluids*, Vol. 7, Number 6, June, 1995, pp 1275-1281.

18. Gaudet, L.: *Experimental Investigation of the Turbulent Boundary Layer at High Reynolds Numbers and a Mach Number of 0.8*, Technical Report 84094, Royal Aircraft Establishment, September, 1984.

19. Winter, K. G.; and Gaudet, L.: *Turbulent boundary-layer studies at high Reynolds numbers at Mach numbers between 0.2 and 2.8.* R & M 3712, Royal Aircraft Establishment, December, 1970.

20. Nagib, H.; and Hites, M.: High Reynolds Number Boundary-Layer Measurements in the NDF. *AIAA 95-0786*, 33rd Aerospace Sciences Meeting and Exhibit. Reno, NV, Jan 9-12, 1995.

21. Smith, Donald W.; and Walker, John H.: *Skin-Friction Measurements in Incompressible Flow.* NASA Technical Report R-26, 1959.

22. Allen, J. M.: *Evaluation of Compressible-Flow Preston Tube Calibrations*, NASA TN D-7190, May, 1973.

23. Sommer, S. C.; and Short, B. J.: *Free-Flight Measurements of Turbulent-Boundary-Layer Skin Friction in the Presence of Severe Aerodynamic Heating at Mach Numbers from 2.8 to 7.0*, NACA-TN-3391, NASA, Ames, March, 1955.

24. Watson, R. D.: Generalized Velocities in the Outer Region of Hypersonic Turbulent Boundary Layers, *AIAA Journal*, 17, Number 8, August, 1979, pp 919-921.

25. Bruce, W. E., Jr.: *The U.S. National Transonic Facility, Parts I and II.* Papers No. 14 and 15, AGARD-R-722, AGARD, April, 1985.

26. Private communication with Dr. Richard Campbell, NASA, Langley Research Center.

27. Vatsa, Veer N.; and Singer, Bart A.: Evaluation of a Second-Order Accurate Navier-Stokes Code for Detached Eddy Simulation Past a Circular Cylinder, *AIAA 2003-4085*, , presented at 21st AIAA Applied Aerodynamics Conference, Orlando, FL, June 23-26, 2003.

28. Foster, J. M.; and Adcock, J. B.: *User's Guide for the National Transonic Facility Research Data System*, NASA Technical Memorandum 110242, April 1996.

37

29. Ozarapoglu, V.: Measurements in Incompressible Turbulent Flows, Ph.D. Thesis, Laval University, February, 1973.

30. Zagarola, M. V.; Williams, D. R.; and Smits, A. J.:   Calibration of the Preston probe for high Reynolds number flows. *Measurement Science and Technology*, vol. 12, 2001, pp 495-501.

31. Adcock, J. B.: *Real-Gas Effects Associated With One-Dimensional Transonic Flow of Cryogenic Nitrogen,* NASA TN D-8274, NASA, December, 1976.

32. Patel, V. C.: Calibration of the Preston tube and limitations on its use in pressure gradients, *Journal of Fluid Mechanics*, vol. 23, pt. 1, September, 1965, pp 185-208.

33. Allen, J. M.: *Reevaluation of Compressible-Flow Preston Tube Calibrations*, NASA TM X-3488, February, 1977.

34. Bertelrud, A.: *Pipe Flow Calibration of Preston Tubes of Different Diameters and Relative Lengths Including Recommendations on Data Presentation for Best Accuracy*, FFA Report 125, Aeronautical Research Institute of Sweden, 1974.

35. Bradshaw, P.; and Unsworth, K.: *A Note on Preston Tube Calibrations in Compressible Flow*, IC Aero Report 73-07, Imperial College of Science and Technology, September, 1973.

36. Ames Research Staff: *Equations, Tables, and Charts for Compressible Flow*, NACA Report 1135, NASA, 1953.

37. Rotta, J. C.: *Critical Review of Experimental Heat Transfer Coefficients and Temperature Distributions in Turbulent Boundary Layers at Supersonic and Hypersonic Flow*, NASA TTF 10,905, 1967.

38. Coles, D. E.: The law-of-the-wake in the turbulent boundary layer, *JFM*, Vol. 1, Pt. 2, 1956, pp 191-226.

39. Bull, M. K.: Velocity Profiles of Turbulent Boundary Layers. *The Aeronautical Journal of the Royal Aeronautical Society*, Feb, 1969, Vol. 73,   pp 143-147.

40. Gad-el-Hak, M.; and Bandyopadhyay, P.: Reynolds number effects in wall-bounded turbulent flows. *Applied Mechanics Reviews*, Vol. 45, No. 8, August, 994, American Society of Mechanical Engineers, pp 307-365.

41. East, L.F.: *A prediction of the law-of-the-wall in compressible three-dimensional boundary layers*. RAE Technical Report 72178, 1972.

42. Cebeci, Tuncer; and Bradshaw, Peter: *Physical and Computational Aspects of Convective Heat Transfer*. Springer-Verlag, New York, 1988.

43. Motallebi, F.: Mean Flow Study of Two-Dimensional Subsonic Turbulent Boundary Layers, *AIAA Journal*, 32, November, 1994, pp 2153-2161.

44. Zagarola, Mark V.; and Smits, Alexander J.: A New Mean Velocity Scaling for Turbulent boundary Layers. *FEDSM98-4950, Proceedings of FEDSM'98*, 1998 ASME Fluids Engineering Division Summer Meeting, June 21-25, 1998, Washington, DC.

45. Castillo, L.; Walker, D. J.; and Wosnik, M.: The Effect of the Upstream Conditions on the Mean Velocity Deficit of Turbulent Boundary layers. *AIAA2000-2309.* Fluids 2000 Conference & Exhibit, June 19-22, 2000, Denver, CO.

46. Maise, George; and McDonald, Henry: Mixing Length and Kinematic Eddy Viscosity in a Compressible Boundary Layer, *AIAA Journal*, vol. 6, No. 1, January, 1968, pp 73-80.

47. Bradshaw, P.: *The Insensitivity of Turbulent Flow to Changes in Reynolds Number and Mach Number*. NPL Aero Note 1057, National Physical Laboratory, Aerodynamics Division, May, 1967.

48. Eckert, E. R. G.: Engineering Relations for Friction and Heat Transfer to Surfaces in High Velocity Flow. *Journal of the Aeronautical Sciences*, Vol. 22, No. 8, August, 1955, pp 585-587.

49. Klebanoff, P. S.: *Characteristics of Turbulence in a Boundary Layer with Zero Pressure Gradient*. NACA Report 1247, 1955.

50. Clauser, Francis H.: Turbulent Boundary Layers in Adverse Pressure Gradients. *Journal of the Aeronautical Sciences*. February, 1954, pp 91-108.

51. Wei, Tie; Schmidt, Rodney; and McMurty, Patrick: Comment on the Clauser chart method for determining the friction velocity. *Experiments in Fluids*, Vol. 38, 2005, pp 695-699.

52. Mineck, Raymond E.; and Hill, Acquilla S.: *Calibration of the 13- by 13-Inch Adaptive Wall Test Section for the Langley 0.3-Meter Transonic Cryogenic Tunnel*. NASA Technical Paper 3049, December 1990.

53. Plentovitch, E. B.; Chu, Julio; and Tracey, M. B.: *Effects of Yaw Angle and Reynolds Number on Rectangular-Box Cavities at Subsonic and Transonic Speeds*. NASA Technical Paper 3099, July, 1991.

54. Tcheng, Ping; and Supplee, Frank H., Jr.: Skin friction balance. Patent, Accession No. N88-29145. June 6, 1989.

55. Allen, Jerry M.: *Systemic Study of Error Sources in Supersonic Skin-Friction Balance Measurements*. NASA TN D-8291, October, 1976.

56. Bertelrud, A.: Total Head/Static Measurements of Skin Friction and Surface Pressure. *AIAA Journal,* Vol. 15, No. 3, March, 1977, pp 436-438.

57. Zagarola, M. V.; Perry, A.E.; and Smits, A. J.: Log laws or power laws: The scaling in the overlap region. *Physics of Fluids*, Vol. 9, no. 7, July, 1997, pp 2094-2100.

58. Barenblatt, G.I.; Chorin, A.J.; and Prostokishin, V. M.: Scaling laws for fully developed turbulent flow in pipes. *Applied Mechanics Review*, vol. 50, no. 7, July, 1997, pp 413-429.

59. Perry, A. E.; Hafez, S.; and Chong, M. S.: A possible reinterpretation of the Princeton superpipe data. *J. Fluid Mech.*, vol. 439, 2001, pp 395-401.

Table 1. Model and Instrumentation Locations
(a) Section Coordinates, Inches

r=6.375 at end of Section 1

see Figure 10(a)

Section	at end of section		
	x	s	
1	25.951	27.877	nose
2	55.951	57.877	
3	79.951	81.877	Station 1
4	103.951	105.877	
5	127.951	129.877	Station 2
6	151.951	153.877	
7	179.376	181.302	
8	207.376	209.302	

Table 1. Continued
(b) Plug, Preston Tube, Rake, and Balance Locations

see Figures 10 (a) and (b) for coordinate definitions

Device	x	s	ϕ

SECTION 3 - STATION 1, x = 73.95

LARGE PLUG

Device	x	s	ϕ
...	73.951	75.877	0.00

SMALL PLUGS

Device	x	s	ϕ
1-3	74.951	76.877	0.00
2-3	74.951	76.877	45.00
3-3	74.951	76.877	135.00
4-3	74.951	76.877	180.00
5-3	74.951	76.877	-45.00
6-3	74.951	76.877	-135.00

PRESTON TUBES, TO TIP

Device	x	s	ϕ
1	73.140	75.066	0.00
2	73.140	75.066	45.00
3	73.140	75.066	135.00
4	73.140	75.066	180.00
5	73.140	75.066	-45.00
6	73.140	75.066	-135.00

RAKE NO. 2, TO TIPS

Device	x	s	ϕ
...	73.140	75.066	

BALANCE

Device	x	s	ϕ
...	73.951	75.877	

SECTION 5 - STATION 2, x = 121.95

LARGE PLUG

Device	x	s	ϕ
...	121.951	123.877	0.00

SMALL PLUGS

Device	x	s	ϕ
1-5	122.951	124.877	0.00
2-5	122.951	124.877	45.00
3-5	122.951	124.877	135.00
4-5	122.951	124.877	180.00
5-5	122.951	124.877	-45.00
6-5	122.951	124.877	-135.00

PRESTON TUBES, TO TIP

Device	x	s	ϕ
1	121.140	123.066	0.00
2	121.140	123.066	45.00
3	121.140	123.066	135.00
4	121.140	123.066	180.00
5	121.140	123.066	-45.00
6	121.140	123.066	-135.00

RAKE NO. 2, TO TIPS

Device	x	s	ϕ
...	121.140	123.066	

BALANCE

Device	x	s	ϕ
...	121.951	123.877	

Table 1. Continued
(c) Pressure Orifice Locations, Inches

see Figure 10 for coordinate definitions

SECTION 1 - from NASA drawing LD1079601

Orifice	x	r	ϕ
1	0.000	0.000	0
2	0.957	1.779	0
3	2.652	2.971	0
4	4.533	3.848	0
5	6.495	4.527	0
6	6.495	4.527	30
7	6.495	4.527	330
8	8.502	5.058	0
9	10.537	5.472	0
10	12.590	5.788	0
11	14.654	6.021	0
12	14.654	6.021	30
13	14.654	6.021	330
14	16.724	6.183	0
15	18.798	6.288	0
16	20.874	6.345	0
17	22.951	6.375	0
18	22.951	6.375	30
19	22.951	6.375	330

SECTION 2 - from NASA drawing LD1079606

Orifice	x	s	ϕ
20	26.951	28.877	0
21	26.951	28.877	30
22	26.951	28.877	60
23	26.951	28.877	90
24	26.951	28.877	120
25	26.951	28.877	180
26	26.951	28.877	210
27	26.951	28.877	240
28	26.951	28.877	270
29	26.951	28.877	300
30	26.951	28.877	330
31	28.951	30.877	0
32	28.951	30.877	30
33	28.951	30.877	330
34	30.951	32.877	0
35	32.951	34.877	0
36	34.951	36.877	0
37	34.951	36.877	30
38	34.951	36.877	330
39	36.951	38.877	0

41

Table 1. Continued
(c) Continued

40	38.951	40.877	0
41	40.951	42.877	0
42	40.951	42.877	30
43	40.951	42.877	330
44	42.951	44.877	0
45	44.951	46.877	0
46	46.951	48.877	0
47	46.951	48.877	30
48	46.951	48.877	330
49	48.951	50.877	0
50	50.951	52.877	0
51	52.951	54.877	0
52	52.951	54.877	30
53	52.951	54.877	330

SECTION 3 - from NASA drawing LD1079606

54	56.951	58.877	0
55	58.951	60.877	0
56	58.951	60.877	30
57	58.951	60.877	330
58	60.951	62.877	0
59	62.951	64.877	0
60	64.951	66.877	0[1]
61	64.951	66.877	30[1]
62	64.951	66.877	330[1]
63	66.951	68.877	0
64	68.951	70.877	0
65	70.951	72.877	0[2]
66	70.951	72.877	30[2]
67	70.951	72.877	60
68	70.951	72.877	90
69	70.951	72.877	120
70	70.951	72.877	150
71	70.951	72.877	180
72	70.951	72.877	210
73	70.951	72.877	240
74	70.951	72.877	270
75	70.951	72.877	300
76	70.951	72.877	330[2]
77	72.451	74.377	30[2]
78	72.451	74.377	330[2]
79	73.951	75.877	30[2]
80	73.951	75.877	330[2]
81	75.451	77.377	30[2]
82	75.451	77.377	330[2]
83	76.951	78.877	0
84	76.951	78.877	30[2]

Table 1. Continued
(c) Continued

85	76.951	78.877	330[2]

SECTION 4 - from NASA drawing LD1079606

86	80.951	82.877	0
87	82.951	84.877	0
88	82.951	84.877	30
89	82.951	84.877	330
90	84.951	86.877	0
91	86.951	88.877	0
92	88.951	90.877	0
93	88.951	90.877	30
94	88.951	90.877	330
95	90.951	92.877	0
96	92.951	94.877	0
97	94.951	96.877	0
98	94.951	96.877	30
99	94.951	96.877	330
100	96.951	98.877	0
101	98.951	100.877	0
102	100.951	102.877	0
103	100.951	102.877	30
104	100.951	102.877	330

SECTION 5 - from NASA drawing LD1079606

105	104.951	106.877	0
106	106.951	108.877	0
107	106.951	108.877	30
108	106.951	108.877	330
109	108.951	110.877	0
110	110.951	112.877	0
111	112.951	114.877	0
112	112.951	114.877	30
113	112.951	114.877	330
114	114.951	116.877	0
115	116.951	118.877	0
116	118.951	120.877	0[3]
117	118.951	120.877	30[3]
118	118.951	120.877	60
119	118.951	120.877	90
120	118.951	120.877	120
121	118.951	120.877	150
122	118.951	120.877	180
123	118.951	120.877	210
124	118.951	120.877	240
125	118.951	120.877	270
126	118.951	120.877	300
127	118.951	120.877	330[3]

Table 1. Continued
(c) Continued

128	120.451	122.377	30^3
129	120.451	122.377	330^3
130	121.951	123.877	30^3
131	121.951	123.877	330^3
132	123.451	125.377	30^3
133	123.451	125.377	330^3
134	124.951	126.877	0
135	124.951	126.877	30^3
136	124.951	126.877	330^3

SECTION 6 - from NASA drawing LD1079606

137	128.951	130.877	0
138	130.951	132.877	0
139	130.951	132.877	30
140	130.951	132.877	330
141	132.951	134.877	0
142	134.951	136.877	0
143	136.951	138.877	0
144	136.951	138.877	30
145	136.951	138.877	330
146	138.951	140.877	0
147	140.951	142.877	0

Notes: 1 = averaged for p1
2 = averaged for pw1
3 = averaged for pw2

Table 1. Continued
(d) Thermocouple Locations, Inches

see Figure 10 for coordinate definitions

SECTION 1 - from NASA drawing LD1079601

Thermocouple	x	r	ϕ
1	15.688	6.110	0

SECTION 2 - from NASA drawing LD1079606

Thermocouple	x	s	ϕ
2	27.951	29.877	0
3	39.951	41.877	0
4	45.951	47.877	0
5	45.951	47.877	30
6	45.951	47.877	330
7	51.951	53.877	0

Table 1. Continued
(d) Continued

SECTION 3 - from NASA drawing LD1079606

8	57.951	59.877	0
9	63.951	65.877	0
10	69.951	71.877	0^1
11	69.951	71.877	30^1
12	69.951	71.877	90
13	69.951	71.877	150
14	69.951	71.877	210
15	69.951	71.877	270
16	69.951	71.877	330^1

SECTION 4 - from NASA drawing LD1079606

17	81.951	83.877	0
18	87.951	89.877	0
19	93.951	95.877	0
20	93.951	95.877	30
21	93.951	95.877	330
22	99.951	101.877	0

SECTION 5 - from NASA drawing LD1079606

23	105.951	107.877	0
24	111.951	113.877	0
25	117.951	119.877	0^2
26	117.951	119.877	30^2
27	117.951	119.877	90
28	117.951	119.877	150
29	117.951	119.877	210
30	117.951	119.877	270
31	117.951	119.877	330^2

SECTION 6 - from NASA drawing LD1079606

32	129.951	131.877	0
33	135.951	137.877	0

THERMOCOUPLES ON INNER WALL OF MODEL
  at Sections 3, 4, and 5

34	69.951	71.877	0
35	73.951	75.877	0
36	117.951	119.877	0

THERMOCOUPLES ON BALANCE

37	on base of balance
38	internal, at linear differential transformer

Notes: 1=averaged for Tw1, see Figure 10(b).
        2=averaged for Tw2, see Figure 10(b).

Table 1. Concluded
(e) Nose Coordinates, Inches

from NASA drawing LD1079602

Point	x	r	s
1	0.0000	0.0000	0.0000
2	0.1924	0.7890	0.8121
3	0.6104	1.4158	1.5655
4	1.1978	1.9928	2.3889
5	1.9292	2.5351	3.2994
6	2.7877	3.0443	4.2976
7	3.7598	3.5217	5.3806
6	4.8337	3.9649	6.5423
9	5.9988	4.3722	7.7766
10	7.2448	4.7417	9.0762
11	8.5627	5.0723	10.4349
12	9.9426	5.3629	11.8451
13	11.3757	5.6126	13.2998
14	12.8527	5.8224	14.7916
15	14.3648	5.9929	16.3133
16	15.9032	6.1267	17.8575
17	17.4591	6.2264	19.4166
16	19.0240	6.2959	20.9830
19	20.5891	6.3398	22.5488
20	22.1464	6.3634	24.1062
21	23.6873	6.3731	25.6472
22	25.2041	6.3750	27.1640
23	25.951[*]	6.3750	27.9109

Notes: * at junction of section 2
s at end of nose (x=25.500) = 27.426
s at junction of sections 1 and 2 = 27.877

Table 2. Boundary Layer Rake Tube Locations

Rake No. 2, as tested in NTF

Tube	DESIGN		AS CONSTRUCTED		LATE MEASUREMENT		USED IN DATA REDUCTION
	z,ideal	y,ideal	z,measured	y, measured	z, measured	y, measured	y
1	-0.1500	0.0230	-0.1500	0.0229	-0.1500	0.0218	0.0240
2	-0.0630	0.0320	-0.0634	0.0312	-0.0625	0.0300	0.0330
3	0.0150	0.0400	0.0147	0.0390	0.0163	0.0417	0.0420
4	0.0850	0.0490	0.0843	0.0496	0.0854	0.4730	0.0500
5	0.1500	0.0570	0.1493	0.0578	0.1502	0.0583	0.0580
6	-0.1100	0.0690	-0.1092	0.0690	-0.1095	0.0698	0.0700
7	-0.0300	0.0820	-0.0298	0.0816	-0.0297	0.0826	0.0840
8	0.0400	0.0950	0.0393	0.0951	0.0393	0.0932	0.0960
9	0.1100	0.1080	0.1086	0.1092	0.1110	0.1075	0.1100
10	-0.0800	0.1250	-0.0814	0.1255	-0.0802	0.1256	0.1257
11	-0.0050	0.1450	-0.0051	0.1444	-0.0051	0.1445	0.1470
12	0.0600	0.1750	0.0592	0.1745	0.0607	0.1735	0.1760
13	-0.0650	0.2150	-0.0643	0.2148	-0.0640	0.2142	0.2150
14	0.0400	0.2650	0.0389	0.2655	0.0403	0.2644	0.2660
15	-0.0300	0.3250	-0.0306	0.3253	-0.0297	0.3241	0.3260
16	0.0300	0.3950	0.0302	0.3950	0.0293	0.3944	0.3960
17	-0.0250	0.4750	-0.0262	0.4761	-0.0249	0.4749	0.4750
18	0.0000	0.5550	-0.0012	0.5558	0.0005	0.5538	0.5660
19	0.0000	0.6350	-0.0006	0.6354	-0.0012	0.6347	0.6360
20	0.0000	0.7150	-0.0005	0.7157	-0.0008	0.7141	0.7165
21	0.0000	0.7950	0.0000	0.7950	0.0003	0.7938	0.7960
22	0.0000	0.8750	-0.0012	0.8756	-0.0005	0.8753	0.8780
23	0.0000	0.9760	-0.0017	0.9769	-0.0007	0.9749	0.9770
24	0.0000	1.0760	0.0000	1.0767	-0.0002	1.0753	1.0770
25	0.0000	1.1990	-0.0005	1.2000	-0.0001	1.1981	1.2010
26	0.0000	1.3230	0.0000	1.3228	-0.0006	1.3220	1.3240
27	0.0000	1.4750	0.0000	1.4750	-0.0002	1.4748	1.4755
28	0.0000	1.6270	0.0000	1.6270	-0.0005	1.6269	1.6280
29	0.0000	1.8140	-0.0013	1.8145	-0.0008	1.8130	1.8150
30	0.0000	2.0000	-0.0005	2.0003	0.0004	1.9994	2.0005
31	0.0000	2.2000	-0.0005	2.2003	0.0003	2.1988	2.2000

Table 3. Measured Tunnel and Model Test Conditions

	Parameters From Standard Tunnel Reduction							Calculated Flow Quantities				Station 1 and 2 Quantities				(ideal gas)
	Run	Point	p_t , psia	T_t , deg F	α , deg	roll, deg	time	M_e	p_e , psia	q_e , psf	R/ft	pw1, psia	pw2, psia	Tw1, deg F	Tw2, deg F	$T_{w,ave}/T_{aw}$
Preston Tube Data																
1	39	352	95.614	120.998	-0.005	0.018	14:43:55	0.401	85.538	1395.010	1.504E+07	85.531	85.554	120.409	120.381	1.0022
2	39	353	95.613	121.042	-0.005	0.016	14:44:07	0.401	85.546	1393.290	1.503E+07	85.542	85.562	120.455	120.441	1.0022
3	39	354	95.617	120.961	-0.005	0.021	14:44:19	0.401	85.550	1393.950	1.504E+07	85.542	85.570	120.461	120.447	1.0024
4	39	358	95.615	120.718	0.190	0.018	14:45:52	0.401	85.538	1394.290	1.505E+07	85.537	85.553	120.484	120.469	1.0028
5	39	359	95.612	120.888	0.190	0.015	14:46:04	0.401	85.541	1393.930	1.504E+07	85.537	85.550	120.506	120.492	1.0026
6	39	360	95.615	120.956	0.190	0.014	14:46:16	0.401	85.541	1394.100	1.504E+07	85.539	85.561	120.539	120.511	1.0025
7	39	370	95.616	119.771	0.063	0.188	14:50:32	0.401	85.548	1394.170	1.508E+07	85.539	85.557	120.430	120.346	1.0043
8	39	371	95.616	119.716	0.063	0.187	14:50:43	0.401	85.552	1393.360	1.508E+07	85.545	85.559	120.327	120.257	1.0042
9	39	372	95.612	119.647	0.063	0.182	14:50:55	0.401	85.549	1393.430	1.508E+07	85.541	85.558	120.266	120.196	1.0043
10	40	373	95.617	118.961	0.061	0.005	14:53:36	0.401	85.554	1393.180	1.510E+07	85.547	85.563	119.386	119.413	1.0040
11	40	374	95.614	118.740	0.060	0.006	14:54:15	0.401	85.546	1393.890	1.511E+07	85.539	85.556	119.230	119.230	1.0041
12	40	375	95.618	119.062	0.060	0.005	14:54:53	0.401	85.556	1393.200	1.510E+07	85.548	85.559	119.053	119.067	1.0032
13	40	379	95.613	118.942	0.191	-0.004	14:57:30	0.401	85.546	1393.780	1.510E+07	85.539	85.555	118.991	118.990	1.0033
14	40	380	95.617	118.892	0.191	-0.002	14:58:09	0.401	85.557	1392.720	1.510E+07	85.551	85.563	118.930	118.930	1.0033
15	40	381	95.614	118.945	0.191	-0.002	14:58:46	0.401	85.555	1392.660	1.510E+07	85.548	85.562	118.897	118.911	1.0032
16	42	395	95.634	119.864	-0.028	0.179	20:56:28	0.401	85.533	1397.070	1.509E+07	85.535	85.546	119.454	119.496	1.0026
17	42	396	95.629	120.021	-0.029	0.169	20:56:52	0.401	85.525	1397.410	1.509E+07	85.528	85.541	119.565	119.593	1.0025
18	42	397	95.632	120.019	-0.029	0.169	20:57:17	0.401	85.533	1397.170	1.509E+07	85.533	85.545	119.621	119.649	1.0026
19	42	401	95.593	120.064	0.129	0.167	20:59:18	0.401	85.492	1397.250	1.508E+07	85.493	85.506	119.746	119.773	1.0027
20	42	402	95.590	120.168	0.132	0.174	21:00:20	0.401	85.492	1396.880	1.508E+07	85.493	85.506	119.820	119.819	1.0026
21	42	403	95.594	120.170	0.132	0.174	21:00:44	0.401	85.495	1396.850	1.508E+07	85.497	85.512	119.875	119.875	1.0027
22	43	413	95.591	120.661	-0.019	0.177	21:06:21	0.402	85.489	1397.680	1.507E+07	85.488	85.504	120.357	120.314	1.0027
23	43	414	95.595	120.671	-0.019	0.182	21:06:44	0.401	85.496	1397.350	1.506E+07	85.493	85.508	120.394	120.351	1.0027
24	43	415	95.593	120.704	-0.019	0.173	21:07:09	0.401	85.500	1396.570	1.506E+07	85.497	85.508	120.416	120.402	1.0027
25	47	451	38.321	119.386	-0.025	0.178	21:53:17	0.401	34.280	557.550	6.068E+06	34.291	34.286	115.455	115.314	0.9963
26	47	452	38.316	119.802	-0.025	0.178	21:53:41	0.401	34.275	557.550	6.062E+06	34.285	34.279	115.789	115.648	0.9962
27	47	453	38.317	119.733	-0.025	0.179	21:54:06	0.401	34.275	557.500	6.063E+06	34.287	34.284	116.114	115.987	0.9969
28	47	457	38.319	120.009	0.129	0.18	21:55:53	0.401	34.278	557.540	6.060E+06	34.289	34.283	117.213	117.072	0.9983
29	47	458	38.321	120.034	0.129	0.178	21:56:18	0.401	34.279	557.770	6.061E+06	34.289	34.283	117.391	117.264	0.9986
30	47	459	38.318	120.330	0.129	0.178	21:56:48	0.401	34.276	557.690	6.056E+06	34.287	34.283	117.621	117.494	0.9984
31	48	469	38.318	120.693	-0.022	0.184	22:02:19	0.401	34.275	557.960	6.053E+06	34.284	34.281	119.029	118.888	1.0002
32	48	470	38.319	120.644	-0.022	0.185	22:02:43	0.401	34.281	557.790	6.053E+06	34.287	34.285	119.094	118.968	1.0005
33	48	471	38.320	120.691	-0.023	0.180	22:03:05	0.401	34.279	557.740	6.052E+06	34.288	34.286	119.132	119.019	1.0004
34	49	473	25.240	121.429	-0.080	-0.002	22:33:58	0.701	18.169	901.760	6.053E+06	18.170	18.148	116.964	116.809	1.0015
35	49	474	25.198	122.631	-0.080	-0.001	22:34:25	0.701	18.140	900.270	6.037E+06	18.140	18.120	117.410	117.227	1.0002
36	49	475	25.201	121.851	-0.081	-0.003	22:34:50	0.702	18.135	900.880	6.050E+06	18.137	18.114	117.715	117.560	1.0021
37	50	476	22.675	119.834	-0.032	0.183	22:39:46	0.848	14.158	1028.250	6.046E+06	14.156	14.120	119.368	119.242	1.0123
38	50	477	22.712	122.894	-0.032	0.181	22:40:09	0.849	14.172	1030.360	6.016E+06	14.174	14.136	119.289	119.162	1.0069
39	50	478	22.697	125.075	-0.032	0.183	22:40:38	0.850	14.140	1031.710	5.988E+06	14.143	14.107	119.729	119.602	1.0039
40	50	482	22.700	123.257	0.123	0.183	22:42:39	0.850	14.148	1031.450	6.012E+06	14.149	14.112	119.914	119.816	1.0074
41	50	483	22.710	121.275	0.123	0.179	22:43:02	0.850	14.158	1031.790	6.041E+06	14.156	14.122	119.821	119.736	1.0107
42	50	484	22.712	121.390	0.123	0.179	22:43:26	0.850	14.162	1031.560	6.039E+06	14.161	14.127	119.619	119.549	1.0101
43	51	495	22.706	122.042	-0.022	0.186	22:49:21	0.850	14.153	1031.780	6.030E+06	14.151	14.115	119.727	119.432	1.0090
44	51	496	22.708	121.706	-0.022	0.183	22:49:50	0.850	14.155	1031.950	6.035E+06	14.152	14.118	119.671	119.404	1.0095
45	51	497	22.707	121.498	-0.022	0.184	22:50:14	0.850	14.158	1031.610	6.037E+06	14.154	14.119	119.572	119.347	1.0097
46	52	498	22.706	121.660	-0.022	0.185	22:51:35	0.850	14.157	1031.300	6.034E+06	14.156	14.118	119.417	119.262	1.0092

Table 3. Continued

	Run	Point	p_t, psia	T_t, deg F	α, deg	roll, deg	time	M_e	p_e, psia	q_e, psf	R/ft	pw1, psia	pw2, psia	Tw1, deg F	Tw2, deg F	$T_{w,ave}/T_{aw}$
47	52	499	22.706	121.506	-0.022	0.186	22:51:57	0.850	14.158	1031.170	6.035E+06	14.159	14.121	119.379	119.238	1.0094
48	52	500	22.706	121.229	-0.022	0.184	22:52:21	0.850	14.152	1031.620	6.040E+06	14.153	14.115	119.294	119.196	1.0098
49	53	513	22.707	120.800	-0.022	0.187	22:58:52	0.850	14.160	1031.220	6.045E+06	14.159	14.122	118.079	117.812	1.0083
50	53	514	22.707	120.847	-0.022	0.185	22:59:15	0.850	14.157	1031.610	6.046E+06	14.155	14.118	118.089	117.863	1.0083
51	53	515	22.707	120.921	-0.023	0.186	22:59:40	0.850	14.158	1031.400	6.044E+06	14.157	14.118	118.130	117.933	1.0082
52	60	555	101.802	-250.224	-0.126	-0.057	13:30:48	0.604	79.723	2904.780	9.048E+07	79.726	79.729	-256.185	-254.684	0.9821
53	60	556	101.799	-250.357	-0.124	-0.057	13:31:13	0.601	79.907	2883.880	9.025E+07	79.900	79.836	-256.162	-254.614	0.9828
54	60	559	101.798	-250.343	0.031	-0.062	13:32:45	0.601	79.921	2883.620	9.024E+07	79.901	79.837	-256.264	-254.579	0.9826
55	60	560	101.800	-250.332	0.033	-0.059	13:33:08	0.601	79.900	2885.210	9.026E+07	79.890	79.821	-256.307	-254.603	0.9824
56	60	567	101.804	-250.102	-0.117	0.191	13:37:18	0.601	79.899	2886.850	9.013E+07	79.880	79.824	-256.328	-254.582	0.9813
57	60	568	101.802	-250.128	-0.116	0.190	13:37:42	0.601	79.918	2884.210	9.011E+07	79.900	79.827	-256.256	-254.492	0.9818
58	61	569	90.496	-250.047	-0.118	-0.067	13:41:22	0.601	71.018	2567.390	8.010E+07	70.998	70.951	-255.744	-253.893	0.9841
59	61	570	90.496	-250.188	-0.120	-0.080	13:41:47	0.601	71.016	2567.130	8.018E+07	71.000	70.945	-255.635	-253.822	0.9852
60	62	571	81.303	-250.497	-0.114	-0.068	13:46:00	0.700	58.730	2883.130	8.034E+07	58.703	58.638	-256.085	-254.340	0.9866
61	62	572	81.306	-250.438	-0.113	-0.062	13:46:19	0.700	58.745	2882.280	8.029E+07	58.714	58.633	-256.115	-254.381	0.9861
62	63	573	73.538	-250.811	-0.116	-0.072	13:48:05	0.601	57.678	2090.570	6.552E+07	57.658	57.622	-254.915	-253.104	0.9916
63	63	574	73.536	-250.800	-0.118	-0.075	13:48:28	0.601	57.678	2090.040	6.551E+07	57.661	57.621	-254.636	-252.879	0.9928
64	64	575	66.067	-250.237	-0.117	-0.096	13:50:13	0.701	47.703	2346.150	6.520E+07	47.675	47.609	-255.000	-253.153	0.9909
65	64	576	66.065	-250.307	-0.116	-0.098	13:50:36	0.700	47.729	2343.990	6.520E+07	47.693	47.633	-255.023	-253.318	0.9907
66	65	577	59.006	-250.210	-0.115	-0.031	13:53:25	0.848	36.968	2664.490	6.506E+07	36.928	36.851	-255.897	-254.135	0.9900
67	65	578	59.001	-250.139	-0.115	-0.051	13:53:48	0.849	36.927	2667.040	6.505E+07	36.896	36.815	-255.981	-254.343	0.9890
68	65	581	59.008	-250.278	0.028	-0.087	13:55:18	0.849	36.926	2666.970	6.512E+07	36.903	36.833	-256.338	-254.923	0.9873
69	65	582	59.003	-250.313	0.028	-0.086	13:55:41	0.850	36.889	2670.380	6.517E+07	36.861	36.779	-256.366	-254.990	0.9873
70	66	589	56.461	-250.312	-0.127	-0.037	14:02:09	0.601	44.296	1604.040	5.014E+07	44.279	44.253	-255.309	-254.236	0.9856
71	66	590	56.461	-250.413	-0.127	-0.043	14:02:33	0.601	44.275	1606.580	5.005E+07	44.258	44.236	-255.285	-254.202	0.9862
72	67	591	50.655	-250.618	-0.123	-0.056	14:04:00	0.701	36.559	1799.940	5.015E+07	36.545	36.507	-254.639	-253.414	0.9929
73	67	592	50.652	-250.729	-0.123	-0.061	14:04:22	0.701	36.551	1801.190	5.021E+07	36.530	36.489	-254.277	-252.944	0.9954
74	68	593	45.401	-249.800	-0.123	-0.103	14:06:47	0.850	28.369	2057.040	4.998E+07	28.344	28.290	-254.628	-253.447	0.9928
75	68	594	45.392	-250.228	-0.125	-0.110	14:07:09	0.849	28.385	2054.300	5.010E+07	28.363	28.312	-254.705	-253.554	0.9944
76	70	601	39.513	-250.881	-0.092	0.011	21:57:06	0.600	30.998	1122.460	3.525E+07	30.989	30.975	-250.176	-249.487	1.0121
77	70	602	39.511	-250.835	-0.091	0.011	21:57:29	0.600	31.000	1122.350	3.524E+07	30.989	30.977	-250.208	-249.416	1.0119
78	71	603	35.497	-250.961	-0.094	0.002	22:00:22	0.700	25.633	1260.020	3.523E+07	25.623	25.600	-252.012	-250.959	1.0068
79	71	604	35.499	-250.910	-0.093	0.005	22:00:47	0.700	25.628	1261.080	3.523E+07	25.616	25.592	-251.808	-250.754	1.0076
80	72	605	31.709	-250.749	-0.134	0.185	22:04:15	0.849	19.828	1434.780	3.512E+07	19.819	19.788	-253.195	-252.018	1.0042
81	72	606	31.711	-250.850	-0.135	0.177	22:04:37	0.850	19.806	1436.930	3.517E+07	19.798	19.763	-252.987	-251.808	1.0058
82	72	609	31.711	-250.547	0.002	0.186	22:06:33	0.850	19.806	1437.490	3.510E+07	19.791	19.758	-252.461	-251.394	1.0066
83	72	610	31.710	-250.719	0.003	0.179	22:06:58	0.849	19.831	1434.840	3.512E+07	19.820	19.795	-252.383	-251.259	1.0079
84	73	617	23.502	-251.071	-0.136	0.180	22:14:57	0.402	21.033	342.140	1.519E+07	21.028	21.035	-252.679	-251.727	0.9978
85	73	618	23.503	-250.777	-0.135	0.181	22:15:20	0.402	21.030	342.340	1.516E+07	21.027	21.033	-252.437	-251.520	0.9975
86	73	621	23.502	-250.842	0.013	0.184	22:16:49	0.402	21.036	341.660	1.516E+07	21.032	21.039	-251.988	-251.096	0.9999
87	73	622	23.503	-250.711	0.013	0.181	22:17:13	0.402	21.027	342.640	1.516E+07	21.025	21.031	-251.765	-250.871	1.0003
88	74	629	55.028	-250.484	-0.089	0.005	22:35:27	0.402	49.265	798.310	3.526E+07	49.256	49.256	-248.637	-247.470	1.0149
89	74	630	55.018	-251.461	-0.089	0.002	22:35:50	0.402	49.265	797.180	3.548E+07	49.255	49.256	-249.344	-248.154	1.0163
90	75	631	78.690	-251.389	-0.097	0.002	22:43:50	0.402	70.447	1141.120	5.067E+07	70.440	70.438	-250.520	-249.094	1.0109
91	75	632	78.682	-250.885	-0.097	0.000	22:44:14	0.401	70.476	1136.520	5.038E+07	70.467	70.464	-250.853	-249.503	1.0066
92	76	633	102.380	-251.195	-0.131	0.161	22:51:44	0.401	91.698	1479.000	6.566E+07	91.689	91.682	-251.666	-250.206	1.0045
93	76	634	102.381	-251.149	-0.133	0.163	22:52:06	0.402	91.683	1480.960	6.568E+07	91.675	91.667	-251.805	-250.317	1.0037
94	76	637	102.384	-251.029	0.021	0.161	22:53:42	0.402	91.691	1480.470	6.561E+07	91.682	91.673	-252.133	-250.618	1.0016
95	76	638	102.386	-251.005	0.023	0.161	22:54:07	0.401	91.700	1479.230	6.557E+07	91.693	91.686	-252.198	-250.609	1.0013

Table 3. Continued

	Run	Point	p_t, psia	T_t, deg F	α, deg	roll, deg	time	M_e	p_e, psia	q_e, psf	R/ft	pw1, psia	pw2, psia	Tw1, deg F	Tw2, deg F	$T_{w,ave}/T_{aw}$
Rake Data																
96	79	671	95.603	121.543	-0.105	0.005	21:28:40	0.401	85.499	1397.560	1.504E+07	85.500	85.513	121.614	121.333	1.0031
97	81	692	72.612	119.811	-0.095	0.009	21:53:35	0.201	70.599	287.540	6.043E+06	70.595	70.597	116.608	116.495	0.9952
98	83	713	38.317	121.061	-0.108	0.006	22:15:06	0.402	34.276	558.430	6.050E+06	34.280	34.275	119.349	119.166	1.0001
99	85	734	27.835	120.930	-0.093	0.001	22:46:38	0.602	21.783	797.040	6.058E+06	21.780	21.769	120.050	119.825	1.0053
100	87	752	22.675	123.745	-0.093	0.006	23:02:22	0.849	14.143	1029.380	5.996E+06	14.143	14.097	119.132	118.949	1.0051
101	93	793	105.422	-250.577	-0.138	-0.002	13:15:39	0.201	102.486	416.310	3.533E+07	102.501	102.498	-248.667	-247.445	1.0129
102	94	811	105.427	-250.230	-0.132	0.185	13:23:51	0.202	102.481	418.870	3.535E+07	102.488	102.480	-249.018	-252.454	0.9984
103	95	813	102.500	-250.949	-0.137	-0.021	13:27:18	0.401	91.806	1478.250	6.556E+07	91.815	91.790	-254.267	-241.397	1.0182
104	96	824	101.759	-249.818	-0.136	0.001	13:36:59	0.600	79.876	2881.270	8.984E+07	79.881	79.781	-254.336	-251.389	0.9924
105	96	825	101.757	-249.710	-0.136	-0.009	13:37:22	0.601	79.863	2882.760	8.980E+07	79.867	79.777	-254.245	-251.459	0.9920
106	96	837	101.757	-250.030	-0.141	0.185	13:45:32	0.601	79.845	2885.650	9.005E+07	79.842	79.755	-253.561	-252.893	0.9917
107	97	839	90.503	-249.963	-0.138	-0.071	13:49:46	0.601	71.003	2567.880	8.006E+07	71.001	70.925	-252.806	-252.471	0.9942
108	98	841	73.435	-250.579	-0.136	-0.064	13:54:19	0.601	57.604	2085.450	6.529E+07	57.596	57.536	-251.031	-251.069	1.0048
109	99	848	73.502	-250.957	-0.104	-0.006	21:30:08	0.601	57.675	2085.010	6.550E+07	57.669	57.614	-254.117	-248.582	1.0051
110	100	855	59.006	-249.723	-0.146	0.153	21:39:16	0.849	36.925	2666.740	6.490E+07	36.904	36.781	-253.764	-252.836	0.9960
111	100	856	59.004	-249.594	-0.145	0.154	21:39:40	0.849	36.908	2667.250	6.480E+07	36.897	36.787	-253.679	-252.812	0.9956
112	101	867	54.985	-249.973	-0.142	0.151	21:51:53	0.401	49.241	794.490	3.520E+07	49.242	49.232	-248.835	-249.467	1.0072
113	102	879	39.503	-250.444	-0.150	0.152	22:01:31	0.601	30.979	1123.100	3.520E+07	30.974	30.951	-250.082	-249.735	1.0096
114	105	915	31.695	-249.537	-0.142	0.153	22:25:16	0.849	19.822	1433.980	3.480E+07	19.812	19.762	-248.671	-248.805	1.0171
115	106	927	23.505	-249.511	-0.145	0.155	22:38:25	0.402	21.041	341.650	1.500E+07	21.035	21.032	-247.600	-248.453	1.0103
116	108	945	45.376	-250.097	-0.104	-0.027	22:58:30	0.849	28.373	2052.700	5.000E+07	28.362	28.277	-250.029	-249.790	1.0142
117	128	1209	95.571	121.296	-0.068	0.057	10:37:57	0.402	85.473	1397.730	1.500E+07	85.467	85.487	120.766	120.668	1.0022
118	148	1494	95.562	120.193	-0.067	0.172	13:08:36	0.402	85.467	1397.420	1.510E+07	85.460	85.479	119.903	119.903	1.0027
119	153	1569	72.644	120.015	-0.060	0.183	13:53:03	0.201	70.619	288.570	6.053E+06	70.620	70.624	118.564	118.452	0.9982
120	154	1575	22.683	120.398	-0.078	0.175	14:33:26	0.850	14.140	1031.290	6.047E+06	14.131	14.100	117.905	117.863	1.0089
121	158	1625	22.682	119.372	-0.072	0.177	15:00:12	0.850	14.143	1031.030	6.060E+06	14.133	14.106	116.438	116.353	1.0081
122	160	1661	22.683	119.444	-0.072	0.176	15:16:28	0.850	14.142	1030.840	6.059E+06	14.136	14.106	116.593	116.438	1.0081
123	161	1668	38.298	120.274	-0.071	0.176	16:03:11	0.401	34.267	557.700	6.055E+06	34.266	34.266	118.512	118.427	1.0001
Balance Data																
124	175	1790	95.621	120.442	-0.061	0.003	12:53:20	0.401	85.557	1393.300	1.510E+07	85.550	85.568	120.481	120.436	1.0033
125	175	1791	95.621	120.511	-0.061	0.004	12:53:44	0.401	85.561	1392.660	1.510E+07	85.555	85.571	120.476	120.462	1.0032
126	175	1792	95.620	120.576	-0.061	0.005	12:54:08	0.401	85.553	1393.530	1.510E+07	85.548	85.566	120.482	120.496	1.0031
127	177	1820	95.622	120.765	-0.062	-0.017	13:08:52	0.401	85.558	1393.440	1.500E+07	85.550	85.567	120.886	120.936	1.0035
128	177	1821	95.621	120.781	-0.062	-0.023	13:09:14	0.401	85.565	1392.480	1.500E+07	85.557	85.572	120.870	120.948	1.0035
129	177	1822	95.621	120.848	-0.062	-0.019	13:09:37	0.401	85.560	1393.090	1.500E+07	85.552	85.567	120.892	120.962	1.0034
130	179	1858	95.621	120.733	-0.060	-0.097	13:29:40	0.400	85.565	1391.630	1.500E+07	85.563	85.574	120.811	120.889	1.0034
131	179	1859	95.622	120.726	-0.060	-0.096	13:30:05	0.401	85.565	1392.000	1.500E+07	85.561	85.571	120.789	120.881	1.0034
132	179	1860	95.621	120.751	-0.060	-0.103	13:30:29	0.401	85.561	1392.250	1.500E+07	85.558	85.567	120.784	120.877	1.0034
133	185	1934	95.630	120.771	-0.059	-0.087	14:37:26	0.401	85.526	1397.530	1.510E+07	85.527	85.601	120.813	120.883	1.0034
134	185	1935	95.627	120.808	-0.060	-0.088	14:37:53	0.401	85.523	1397.670	1.510E+07	85.524	85.594	120.813	120.898	1.0033
135	185	1936	95.631	120.809	-0.059	-0.085	14:38:16	0.401	85.528	1397.460	1.510E+07	85.529	85.599	120.846	120.930	1.0034
136	205	2220	95.615	120.197	-0.062	-0.068	17:31:32	0.402	85.508	1398.190	1.509E+07	85.507	85.580	120.279	120.391	1.0035
137	205	2221	95.613	120.192	-0.062	-0.068	17:31:56	0.401	85.510	1397.510	1.508E+07	85.511	85.582	120.273	120.399	1.0035
138	205	2222	95.616	120.167	-0.063	-0.068	17:32:20	0.401	85.510	1397.840	1.508E+07	85.511	85.585	120.268	120.395	1.0035
139	206	2241	95.616	120.184	-0.057	-0.025	17:42:08	0.401	85.510	1397.800	1.508E+07	85.512	85.584	120.293	120.349	1.0035
140	206	2242	95.615	120.202	-0.057	-0.068	17:42:31	0.402	85.506	1398.340	1.509E+07	85.506	85.581	120.328	120.369	1.0035
141	206	2243	95.614	120.193	-0.057	-0.064	17:42:55	0.401	85.510	1397.380	1.508E+07	85.513	85.582	120.320	120.390	1.0035
142	207	2249	72.616	119.693	-0.064	-0.06	18:09:34	0.201	70.593	287.420	6.044E+06	70.600	70.616	117.328	117.370	0.9968
143	207	2250	72.616	119.859	-0.064	-0.059	18:09:57	0.200	70.595	287.330	6.041E+06	70.601	70.616	117.525	117.554	0.9968
144	207	2251	72.614	119.804	-0.064	-0.057	18:10:22	0.200	70.589	287.350	6.041E+06	70.598	70.613	117.748	117.733	0.9973

50

Table 3. Continued

	Run	Point	p_t, psia	T_t, deg F	α, deg	roll, deg	time	M_e	p_e, psia	q_e, psf	R/ft	pw1, psia	pw2, psia	Tw1, deg F	Tw2, deg F	$T_{w,ave}/T_{aw}$
145	208	2270	72.614	119.910	-0.063	0.040	18:20:13	0.201	70.590	287.840	6.050E+06	70.595	70.612	118.725	118.725	0.9988
146	208	2271	72.614	119.930	-0.061	-0.051	18:20:36	0.201	70.591	287.870	6.050E+06	70.595	70.614	118.761	118.775	0.9988
147	208	2272	72.615	119.891	-0.060	-0.044	18:20:59	0.201	70.591	287.720	6.040E+06	70.596	70.614	118.823	118.823	0.9990
148	211	2303	38.383	121.714	-0.070	-0.049	18:42:25	0.401	34.334	558.950	6.050E+06	34.342	34.370	117.870	117.870	0.9966
149	211	2304	38.377	121.822	-0.070	-0.051	18:42:48	0.401	34.328	559.030	6.050E+06	34.336	34.365	118.228	118.229	0.9970
150	211	2305	38.381	121.561	-0.070	-0.050	18:43:12	0.402	34.330	559.230	6.050E+06	34.338	34.367	118.506	118.506	0.9980
151	212	2324	38.384	120.896	-0.065	-0.039	18:53:13	0.402	34.336	559.360	6.060E+06	34.340	34.372	120.154	120.126	1.0019
152	212	2325	38.383	120.963	-0.065	-0.042	18:53:39	0.401	34.336	559.130	6.060E+06	34.341	34.374	120.171	120.170	1.0019
153	212	2326	38.382	120.935	-0.065	-0.043	18:54:04	0.401	34.335	559.150	6.060E+06	34.340	34.372	120.164	120.164	1.0019
154	215	2358	27.753	120.064	-0.071	0.023	19:41:59	0.602	21.723	793.640	6.050E+06	21.725	21.756	117.901	117.915	1.0033
155	215	2359	27.746	121.309	-0.071	0.024	19:42:53	0.602	21.713	793.670	6.030E+06	21.718	21.750	118.358	118.344	1.0019
156	215	2360	27.751	120.391	-0.071	0.026	19:43:16	0.601	21.721	793.190	6.040E+06	21.726	21.761	118.425	118.468	1.0037
157	216	2379	27.750	120.664	-0.065	-0.058	19:53:20	0.602	21.717	794.090	6.040E+06	21.717	21.758	119.180	119.138	1.0044
158	216	2380	27.750	120.693	-0.065	-0.056	19:53:43	0.602	21.721	793.960	6.040E+06	21.719	21.761	119.161	119.119	1.0044
159	216	2381	27.750	120.598	-0.065	-0.054	19:54:08	0.602	21.721	793.840	6.040E+06	21.720	21.762	119.145	119.145	1.0045
160	219	2412	22.663	121.298	-0.075	-0.069	20:16:35	0.850	14.126	1029.850	6.030E+06	14.125	14.190	119.052	119.066	1.0094
161	219	2413	22.662	122.046	-0.075	-0.069	20:17:00	0.850	14.131	1029.180	6.020E+06	14.131	14.196	119.019	119.033	1.0080
162	219	2414	22.660	122.330	-0.075	-0.067	20:17:24	0.850	14.130	1028.970	6.010E+06	14.131	14.193	119.049	119.091	1.0076
163	220	2433	22.663	121.357	-0.067	-0.056	20:27:13	0.850	14.127	1029.940	6.030E+06	14.123	14.193	118.981	118.784	1.0090
164	220	2434	22.662	121.417	-0.067	-0.058	20:27:36	0.850	14.134	1029.410	6.030E+06	14.129	14.197	118.918	118.763	1.0088
165	220	2435	22.661	121.456	-0.067	-0.059	20:28:00	0.850	14.132	1029.020	6.020E+06	14.131	14.195	118.896	118.756	1.0087
166	223	2463	22.662	120.638	-0.071	-0.060	20:46:38	0.850	14.128	1029.250	6.040E+06	14.130	14.192	117.914	117.914	1.0085
167	223	2464	22.661	120.633	-0.071	-0.062	20:47:03	0.850	14.121	1029.380	6.040E+06	14.127	14.187	117.915	117.929	1.0085
168	223	2465	22.661	120.604	-0.071	-0.057	20:47:27	0.850	14.122	1029.320	6.040E+06	14.128	14.188	117.886	117.900	1.0085
169	225	2499	22.663	120.226	-0.069	-0.067	21:04:28	0.849	14.129	1028.940	6.040E+06	14.134	14.190	117.842	117.772	1.0090
170	225	2500	22.663	120.220	-0.069	-0.072	21:04:52	0.850	14.126	1029.160	6.040E+06	14.131	14.188	117.764	117.694	1.0089
171	225	2501	22.661	120.242	-0.069	-0.071	21:05:18	0.850	14.127	1029.030	6.040E+06	14.131	14.190	117.720	117.692	1.0088
172	228	2551	22.663	120.221	-0.067	-0.051	21:31:26	0.850	14.128	1029.380	6.040E+06	14.129	14.189	117.106	116.824	1.0076
173	228	2552	22.662	120.218	-0.067	-0.053	21:31:49	0.850	14.129	1029.440	6.040E+06	14.128	14.189	117.140	116.900	1.0077
174	228	2553	22.661	120.259	-0.068	-0.056	21:32:14	0.850	14.126	1029.330	6.040E+06	14.128	14.187	117.186	116.946	1.0077
175	233	2615	105.298	-251.168	-0.131	-0.035	15:25:17	0.202	102.380	416.590	3.560E+07	102.375	102.383	-247.410	-241.545	1.0329
176	233	2616	105.294	-251.721	-0.131	-0.041	15:25:43	0.201	102.379	416.330	3.560E+07	102.373	102.388	-248.057	-242.114	1.0328
177	233	2617	105.290	-252.340	-0.131	-0.042	15:26:07	0.201	102.376	416.220	3.580E+07	102.370	102.384	-248.587	-242.795	1.0329
178	234	2633	105.295	-249.264	-0.133	-0.027	15:34:15	0.202	102.381	417.430	3.500E+07	102.367	102.376	-249.280	-245.403	1.0100
179	234	2634	105.296	-249.290	-0.133	-0.031	15:34:45	0.202	102.381	417.280	3.500E+07	102.369	102.372	-249.153	-245.263	1.0107
180	234	2635	105.299	-249.172	-0.133	-0.028	15:35:09	0.201	102.392	416.750	3.500E+07	102.375	102.384	-249.099	-245.263	1.0103
181	235	2636	102.464	-249.010	-0.133	-0.009	15:42:45	0.401	91.791	1477.890	6.460E+07	91.782	91.821	-250.692	-245.262	1.0082
182	235	2637	102.467	-248.988	-0.132	-0.009	15:43:16	0.401	91.782	1479.720	6.470E+07	91.771	91.813	-250.351	-245.126	1.0092
183	235	2638	102.469	-249.025	-0.132	-0.008	15:43:40	0.401	91.800	1477.820	6.460E+07	91.787	91.829	-250.245	-245.155	1.0095
184	236	2654	102.465	-250.354	-0.136	0.001	15:54:32	0.401	91.775	1481.500	6.530E+07	91.755	91.795	-250.736	-248.349	1.0071
185	236	2655	102.468	-250.402	-0.136	-0.007	15:54:55	0.401	91.786	1480.630	6.540E+07	91.765	91.800	-250.611	-248.321	1.0077
186	236	2656	102.466	-250.286	-0.138	-0.002	15:55:19	0.401	91.787	1480.050	6.530E+07	91.767	91.808	-250.518	-248.267	1.0075
187	240	2709	101.759	-250.647	-0.131	0.010	22:26:47	0.601	79.881	2882.290	9.040E+07	79.872	79.939	-254.128	-249.003	1.0026
188	241	2714	54.936	-250.518	-0.135	0.008	23:21:56	0.401	49.185	795.370	3.520E+07	49.186	49.214	-249.915	-247.833	1.0111
189	241	2715	54.932	-250.375	-0.134	0.007	23:22:19	0.401	49.188	794.580	3.510E+07	49.189	49.218	-250.039	-247.888	1.0100
190	241	2716	54.936	-250.525	-0.134	0.006	23:22:43	0.401	49.186	795.460	3.520E+07	49.186	49.216	-250.198	-247.874	1.0104
191	242	2732	54.935	-250.571	-0.150	0.020	23:30:51	0.401	49.187	795.670	3.520E+07	49.183	49.210	-250.797	-248.551	1.0076
192	242	2733	54.935	-250.444	-0.151	0.010	23:31:15	0.401	49.189	795.820	3.520E+07	49.182	49.210	-250.644	-248.456	1.0075
193	242	2734	54.935	-250.451	-0.151	0.012	23:31:38	0.401	49.188	795.850	3.520E+07	49.182	49.207	-250.527	-248.402	1.0080
194	243	2735	39.561	-249.286	-0.152	0.027	23:37:22	0.601	31.021	1125.910	3.490E+07	31.010	31.050	-249.921	-248.225	1.0081
195	243	2736	39.563	-249.416	-0.153	0.017	23:37:47	0.601	31.023	1125.980	3.500E+07	31.011	31.051	-249.719	-248.048	1.0096

Table 3. Concluded

	Run	Point	p_t, psia	T_t, deg F	α, deg	roll, deg	time	M_e	p_e, psia	q_e, psf	R/ft	pw1, psia	pw2, psia	Tw1, deg F	Tw2, deg F	$T_{w,ave}/T_{aw}$
196	243	2737	39.563	-249.264	-0.153	0.024	23:38:09	0.601	31.020	1126.340	3.490E+07	31.008	31.047	-249.587	-247.959	1.0094
197	246	2789	39.559	-249.099	-0.148	0.045	0:01:56	0.601	31.009	1126.970	3.490E+07	30.999	31.040	-248.454	-247.981	1.0113
198	246	2790	39.561	-249.266	-0.149	0.042	0:02:18	0.601	31.017	1126.660	3.490E+07	31.004	31.046	-248.349	-247.887	1.0125
199	246	2791	39.562	-249.136	-0.151	0.044	0:02:41	0.602	31.009	1127.550	3.490E+07	30.997	31.038	-248.266	-247.816	1.0123
200	247	2792	31.654	-249.737	-0.150	0.050	0:08:33	0.849	19.782	1433.800	3.480E+07	19.768	19.832	-249.035	-248.527	1.0179
201	247	2793	31.652	-249.740	-0.152	0.049	0:08:58	0.849	19.800	1432.340	3.480E+07	19.782	19.848	-248.848	-248.457	1.0185
202	247	2794	31.653	-249.781	-0.153	0.046	0:09:20	0.849	19.787	1433.490	3.480E+07	19.771	19.834	-248.821	-248.362	1.0190
203	248	2810	31.654	-249.891	-0.159	0.055	0:17:24	0.850	19.771	1434.990	3.490E+07	19.755	19.825	-248.546	-248.275	1.0204
204	248	2811	31.652	-249.623	-0.158	0.051	0:17:48	0.850	19.758	1435.610	3.480E+07	19.746	19.817	-248.423	-248.214	1.0196
205	248	2812	31.653	-249.886	-0.159	0.055	0:18:10	0.850	19.763	1435.330	3.490E+07	19.751	19.819	-248.384	-248.147	1.0211
206	249	2813	23.490	-249.637	-0.159	0.053	0:24:31	0.402	21.016	342.520	1.500E+07	21.014	21.033	-248.710	-248.776	1.0075
207	249	2814	23.492	-249.544	-0.158	0.057	0:24:53	0.402	21.023	342.060	1.500E+07	21.019	21.040	-248.560	-248.593	1.0079
208	249	2815	23.492	-249.628	-0.157	0.057	0:25:16	0.402	21.019	342.060	1.500E+07	21.019	21.037	-248.445	-248.529	1.0087
209	250	2831	23.492	-249.811	-0.154	0.062	0:33:25	0.402	21.019	342.440	1.510E+07	21.016	21.039	-248.088	-248.248	1.0111
210	250	2832	23.492	-249.748	-0.154	0.060	0:33:50	0.402	21.022	341.910	1.500E+07	21.020	21.043	-248.041	-248.145	1.0112
211	250	2833	23.491	-249.581	-0.153	0.061	0:34:16	0.402	21.018	342.350	1.500E+07	21.016	21.038	-247.946	-248.090	1.0107
212	256	2881	73.500	-250.615	-0.166	0.421	13:30:43	0.601	57.663	2087.582	6.540E+07	57.645	57.701	-251.884	-250.295	1.0048
213	256	2882	73.500	-250.689	-0.166	0.420	13:31:08	0.601	57.662	2087.712	6.540E+07	57.644	57.705	-251.701	-250.066	1.0061
214	256	2883	73.500	-250.582	-0.166	0.419	13:31:31	0.601	57.680	2085.336	6.530E+07	57.664	57.726	-251.629	-249.991	1.0059
215	257	2900	73.501	-250.456	-0.915	0.252	13:39:37	0.601	57.666	2087.366	6.540E+07	57.648	57.713	-251.018	-250.161	1.0064
216	257	2901	73.503	-250.603	-0.915	0.251	13:40:00	0.601	57.651	2089.123	6.540E+07	57.635	57.703	-250.922	-250.076	1.0075
217	257	2902	73.500	-250.654	-0.920	0.253	13:42:08	0.601	57.660	2088.490	6.540E+07	57.637	57.709	-250.742	-249.826	1.0088
218	257	2903	101.774	-250.464	-0.922	0.330	13:46:46	0.601	79.874	2885.472	9.030E+07	79.861	79.950	-252.279	-251.373	1.0005
219	258	2904	101.776	-250.332	-0.921	0.269	13:47:09	0.601	79.887	2885.530	9.030E+07	79.863	79.954	-252.446	-251.510	0.9991
220	258	2905	101.788	-250.147	-0.920	0.258	13:47:33	0.601	79.889	2886.869	9.020E+07	79.864	79.952	-252.505	-251.573	0.9979
221	259	2912	39.539	-250.599	-0.147	0.137	14:13:34	0.601	31.012	1123.747	3.520E+07	31.006	31.047	-250.101	-249.686	1.0104
222	259	2913	39.943	-250.843	-0.146	0.125	14:13:59	0.600	31.028	1122.912	3.530E+07	31.017	31.062	-249.756	-249.324	1.0133
223	259	2914	39.947	-250.742	-0.145	0.128	14:14:26	0.600	31.004	1126.195	3.530E+07	30.993	31.037	-249.517	-249.063	1.0140
224	259	2924	39.542	-250.395	-0.145	0.065	14:19:08	0.601	31.002	1124.620	3.518E+07	31.002	31.046	-248.611	-248.027	1.0170
225	259	2925	39.545	-250.602	-0.144	0.059	14:19:30	0.601	31.007	1124.470	3.523E+07	31.006	31.051	-248.590	-248.038	1.0181
226	259	2926	39.544	-250.578	-0.143	0.061	14:19:54	0.601	31.008	1124.710	3.523E+07	31.003	31.049	-248.524	-247.972	1.0183
227	260	2936	39.542	-250.273	-0.147	0.048	14:24:38	0.601	31.002	1125.300	3.516E+07	30.995	31.045	-248.372	-247.894	1.0173
228	260	2937	39.545	-250.537	-0.146	0.043	14:25:01	0.601	31.005	1125.240	3.522E+07	30.999	31.046	-248.416	-247.966	1.0183
229	260	2938	39.545	-250.504	-0.146	0.039	14:25:24	0.601	31.004	1125.780	3.522E+07	30.994	31.042	-248.358	-247.935	1.0184
230	261	2939	23.535	-249.940	-0.148	0.042	14:30:19	0.402	21.058	342.620	1.509E+07	21.057	21.074	-248.566	-248.230	1.0106
231	261	2940	23.536	-250.318	-0.148	0.041	14:30:43	0.402	21.059	342.780	1.514E+07	21.057	21.074	-248.402	-248.078	1.0132
232	261	2941	23.536	-250.480	-0.148	0.041	14:31:06	0.402	21.059	342.860	1.515E+07	21.057	21.075	-248.292	-248.042	1.0144
233	263	2975	23.535	-250.173	-0.133	0.068	14:46:06	0.402	21.055	342.374	1.510E+07	21.060	21.080	-247.789	-247.893	1.0144
234	263	2976	23.534	-250.251	-0.133	0.068	14:46:28	0.402	21.053	342.590	1.510E+07	21.058	21.075	-247.703	-247.796	1.0152
235	263	2977	23.535	-250.165	-0.132	0.069	14:46:51	0.402	21.054	342.590	1.510E+07	21.058	21.078	-247.611	-247.715	1.0152
236	266	3023	23.535	-250.164	-0.144	0.056	15:07:35	0.403	21.055	343.270	1.513E+07	21.053	21.076	-247.472	-247.531	1.0160
237	266	3024	23.535	-250.155	-0.143	0.053	15:07:58	0.403	21.052	343.750	1.514E+07	21.049	21.072	-247.452	-247.495	1.0161
238	266	3025	23.535	-250.234	-0.143	0.052	15:08:20	0.403	21.053	343.880	1.515E+07	21.048	21.070	-247.430	-247.517	1.0165

Table 4. Representative Model Surface Pressures and Mach Numbers

φ = 0 deg		Point 451		Point 574		Point 473		Point 606	
Orifice	x	c_p	M	c_p	M	c_p	M	c_p	M
1	0	1.0352	0.0000	1.0911	0.0000	1.1256	0.0000	1.1970	0.0000
2	0.957	0.4246	0.3041	0.4337	0.4521	0.4851	0.5046	0.5303	0.5889
3	2.652	0.1110	0.3776	0.1352	0.5571	0.1503	0.6427	0.1886	0.7585
4	4.533	-0.0161	0.4045	-0.0013	0.6018	-0.0071	0.7040	0.0191	0.8405
5	6.495	-0.1054	0.4226	-0.0981	0.6327	-0.1148	0.7452	-0.1140	0.9055
8	8.502	-0.1461	0.4307	-0.1635	0.6533	-0.1645	0.7642	-0.1925	0.9443
9	10.537	-0.1626	0.4339	-0.1822	0.6591	-0.1932	0.7752	-0.2284	0.9623
10	12.59	-0.1825	0.4378	-0.2141	0.6691	-0.1956	0.7760	-0.2689	0.9827
11	14.654	-0.1750	0.4363	-0.1948	0.6631	-0.1935	0.7752	-0.2546	0.9755
14	16.724	-0.1439	0.4302	-0.1670	0.6544	-0.1686	0.7658	-0.2211	0.9586
15	18.798	-0.1142	0.4243	-0.1213	0.6400	-0.1337	0.7524	-0.1624	0.9294
16	20.874	-0.1059	0.4227	-0.1076	0.6357	-0.1206	0.7474	-0.1380	0.9173
17	22.951	-0.0831	0.4181	-0.0879	0.6294	-0.0902	0.7358	-0.1042	0.9006
20	26.951	-0.0362	0.4086	-0.0350	0.6126	-0.0346	0.7145	-0.0359	0.8672
31	28.951	-0.0334	0.4080	-0.0351	0.6126	-0.0309	0.7131	-0.0351	0.8668
34	30.951	-0.0234	0.4060	-0.0192	0.6075	-0.0198	0.7089	-0.0192	0.8591
35	32.951	-0.0179	0.4048	-0.0103	0.6047	-0.0141	0.7067	-0.0115	0.8554
36	34.951	-0.0166	0.4046	-0.0135	0.6057	-0.0126	0.7061	-0.0131	0.8561
39	36.951	-0.0141	0.4041	-0.0041	0.6027	-0.0099	0.7050	-0.0105	0.8549
40	38.951	-0.0112	0.4035	-0.0138	0.6058	-0.0071	0.7040	-0.0101	0.8547
41	40.951	-0.0107	0.4033	-0.0066	0.6035	-0.0068	0.7038	-0.0052	0.8523
44	42.951	-0.0049	0.4022	0.0002	0.6013	-0.0020	0.7020	0.0008	0.8494
45	44.951	-0.0072	0.4026	-0.0016	0.6019	-0.0027	0.7023	-0.0017	0.8506
46	46.951	-0.0118	0.4036	-0.0172	0.6069	-0.0086	0.7045	-0.0133	0.8562
49	48.951	-0.0049	0.4022	-0.0020	0.6020	-0.0017	0.7019	-0.0019	0.8507
50	50.951	-0.0039	0.4019	0.0026	0.6005	0.0003	0.7011	0.0025	0.8485
51	52.951	-0.0041	0.4020	0.0039	0.6001	0.0004	0.7011	0.0022	0.8487
54	56.951	-0.0077	0.4027	-0.0051	0.6030	-0.0053	0.7033	-0.0019	0.8507
55	58.951	-0.0030	0.4018	-0.0019	0.6020	-0.0007	0.7015	-0.0023	0.8509
58	60.951	-0.0031	0.4018	0.0010	0.6010	0.0003	0.7011	0.0008	0.8494
59	62.951	-0.0034	0.4018	0.0002	0.6013	0.0003	0.7011	0.0005	0.8495
60	64.951	-0.0028	0.4017	0.0043	0.6000	-0.0011	0.7016	0.0021	0.8487
63	66.951	-0.0021	0.4016	-0.0010	0.6017	-0.0002	0.7013	-0.0002	0.8499
64	68.951	-0.0043	0.4020	-0.0012	0.6017	-0.0004	0.7014	-0.0016	0.8506
65	70.951	-0.0015	0.4015	0.0019	0.6007	0.0006	0.7010	0.0023	0.8486
83	76.951	-0.0004	0.4012	-0.0007	0.6016	-0.0014	0.7018	-0.0003	0.8499
86	80.951	-0.0040	0.4020	-0.0044	0.6028	-0.0036	0.7026	-0.0034	0.8514
87	82.951	-0.0015	0.4014	0.0002	0.6013	-0.0011	0.7016	0.0012	0.8492
90	84.951	-0.0057	0.4023	-0.0165	0.6067	-0.0043	0.7029	-0.0106	0.8549
91	86.951	-0.0008	0.4013	0.0012	0.6010	0.0002	0.7012	0.0016	0.8490
92	88.951	0.0007	0.4010	0.0006	0.6012	0.0005	0.7010	0.0016	0.8490
95	90.951	-0.0035	0.4019	-0.0116	0.6051	-0.0022	0.7020	-0.0064	0.8529
96	92.951	-0.0010	0.4013	0.0002	0.6013	-0.0002	0.7013	0.0006	0.8495
97	94.951	-0.0006	0.4013	-0.0004	0.6015	-0.0016	0.7018	0.0000	0.8497
100	96.951	-0.0021	0.4016	0.0022	0.6006	-0.0007	0.7015	0.0017	0.8489
101	98.951	-0.0028	0.4017	-0.0037	0.6026	-0.0026	0.7022	-0.0022	0.8508
102	100.951	-0.0065	0.4025	-0.0190	0.6075	-0.0075	0.7041	-0.0142	0.8566
105	104.951	-0.0041	0.4020	-0.0084	0.6041	-0.0040	0.7028	-0.0071	0.8532
106	106.951	-0.0094	0.4031	-0.0211	0.6081	-0.0081	0.7043	-0.0165	0.8578
110	110.951	-0.0005	0.4012	-0.0020	0.6020	-0.0029	0.7023	-0.0014	0.8504
111	112.951	-0.0037	0.4019	-0.0177	0.6070	-0.0064	0.7037	-0.0132	0.8562
114	114.951	-0.0080	0.4028	-0.0210	0.6081	-0.0091	0.7047	-0.0162	0.8576
115	116.951	-0.0039	0.4020	-0.0066	0.6035	-0.0050	0.7031	-0.0055	0.8524
137	128.951	-0.0024	0.4016	-0.0057	0.6032	-0.0046	0.7030	-0.0066	0.8530
138	130.951	-0.0021	0.4016	-0.0092	0.6043	-0.0056	0.7034	-0.0105	0.8549
141	132.951	-0.0002	0.4012	-0.0043	0.6027	-0.0042	0.7028	-0.0071	0.8532
142	134.951	-0.0010	0.4013	-0.0038	0.6026	-0.0052	0.7032	-0.0092	0.8542
143	136.951	-0.0044	0.4021	-0.0122	0.6053	-0.0072	0.7040	-0.0134	0.8563
146	138.951	-0.0018	0.4015	-0.0042	0.6027	-0.0047	0.7030	-0.0084	0.8538
147	140.951	0.0004	0.4011	-0.0040	0.6026	-0.0048	0.7031	-0.0091	0.8542

Table 4. Continued

φ = 30 deg		Point 451		Point 574		Point 473		Point 606	
Orifice	x	c_p	M	c_p	M	c_p	M	c_p	M
6	6.495	-0.0880	0.4191	-0.0997	0.6332	-0.1070	0.7423	-0.1108	0.9039
12	14.654	-0.1994	0.4411	-0.2458	0.6789	-0.1919	0.7746	-0.2940	0.9955
18	22.951	-0.0769	0.4168	-0.0693	0.6235	-0.0851	0.7339	-0.0925	0.8949
21	26.951	-0.0372	0.4088	-0.0340	0.6123	-0.0337	0.7142	-0.0365	0.8675
32	28.951	-0.0311	0.4075	-0.0277	0.6103	-0.0277	0.7119	-0.0285	0.8636
37	34.951	-0.0172	0.4047	-0.0113	0.6050	-0.0116	0.7057	-0.0121	0.8556
42	40.951	-0.0082	0.4028	0.0051	0.5997	-0.0039	0.7027	0.0010	0.8493
47	46.951	-0.0047	0.4021	0.0023	0.6006	-0.0011	0.7016	0.0000	0.8498
52	52.951	-0.0072	0.4026	-0.0097	0.6045	-0.0034	0.7025	-0.0059	0.8526
56	58.951	-0.0045	0.4021	-0.0023	0.6021	-0.0018	0.7019	-0.0036	0.8515
77	72.451	-0.0012	0.4014	-0.0043	0.6028	-0.0012	0.7017	-0.0031	0.8513
79	73.951	0.0025	0.4006	0.0045	0.5999	0.0027	0.7002	0.0064	0.8466
81	75.451	0.0008	0.4010	0.0011	0.6010	0.0005	0.7010	0.0027	0.8485
84	76.951	-0.0008	0.4013	0.0020	0.6007	-0.0007	0.7015	0.0007	0.8494
88	82.951	-0.0024	0.4016	0.0003	0.6013	-0.0001	0.7013	0.0015	0.8491
93	88.951	-0.0018	0.4015	-0.0004	0.6015	-0.0013	0.7017	-0.0006	0.8501
98	94.951	-0.0008	0.4013	0.0006	0.6012	-0.0007	0.7015	0.0006	0.8495
103	100.951	-0.0014	0.4014	-0.0005	0.6015	-0.0010	0.7016	-0.0003	0.8499
107	106.951	-0.0098	0.4032	-0.0276	0.6102	-0.0093	0.7048	-0.0203	0.8596
112	112.951	-0.0018	0.4015	-0.0036	0.6025	-0.0040	0.7027	-0.0027	0.8511
117	118.951	-0.0023	0.4016	-0.0032	0.6024	-0.0041	0.7028	-0.0042	0.8518
128	120.451	-0.0015	0.4014	-0.0030	0.6023	-0.0035	0.7026	-0.0041	0.8517
130	121.951	-0.0001	0.4012	-0.0010	0.6017	-0.0018	0.7019	-0.0012	0.8504
132	123.451	-0.0019	0.4015	-0.0036	0.6025	-0.0033	0.7025	-0.0043	0.8519
135	124.951	-0.0016	0.4015	-0.0058	0.6032	-0.0056	0.7034	-0.0071	0.8532
139	130.951	-0.0052	0.4022	-0.0191	0.6075	-0.0078	0.7042	-0.0154	0.8573
144	136.951	-0.0019	0.4015	-0.0132	0.6056	-0.0066	0.7038	-0.0133	0.8562
φ = 330 deg									
7	6.495	-0.1025	0.4220	-0.0940	0.6314	-0.1095	0.7432	-0.1075	0.9023
13	14.654	-0.1685	0.4351	-0.2048	0.6662	-0.1934	0.7752	-0.2572	0.9768
19	22.951	-0.0805	0.4176	-0.0889	0.6298	-0.0918	0.7364	-0.1049	0.9010
30	26.951	-0.0383	0.4090	-0.0365	0.6131	-0.0370	0.7154	-0.0381	0.8683
33	28.951	-0.0296	0.4072	-0.0255	0.6096	-0.0266	0.7115	-0.0254	0.8621
38	34.951	-0.0163	0.4045	-0.0126	0.6054	-0.0121	0.7059	-0.0126	0.8559
43	40.951	-0.0095	0.4031	-0.0048	0.6029	-0.0049	0.7031	-0.0039	0.8517
48	46.951	-0.0078	0.4028	-0.0113	0.6050	-0.0041	0.7028	-0.0081	0.8537
53	52.951	-0.0053	0.4022	0.0000	0.6014	-0.0007	0.7015	0.0011	0.8492
57	58.951	-0.0038	0.4019	-0.0030	0.6023	-0.0003	0.7014	-0.0004	0.8500
62	64.951	-0.0006	0.4013	0.0042	0.6000	0.0018	0.7005	0.0033	0.8481
76	70.951	-0.0001	0.4012	0.0053	0.5996	-0.0003	0.7013	0.0005	0.8495
78	72.451	0.0000	0.4012	-0.0006	0.6015	-0.0007	0.7015	0.0002	0.8496
80	73.951	0.0011	0.4009	-0.0003	0.6015	0.0000	0.7012	-0.0011	0.8503
82	75.451	0.0002	0.4011	-0.0073	0.6037	0.0002	0.7011	-0.0065	0.8529
85	76.951	-0.0010	0.4013	-0.0023	0.6021	-0.0011	0.7016	-0.0021	0.8508
89	82.951	-0.0024	0.4017	-0.0010	0.6017	-0.0007	0.7015	-0.0006	0.8500
94	88.951	-0.0023	0.4016	-0.0037	0.6025	-0.0008	0.7015	-0.0015	0.8505
99	94.951	-0.0029	0.4017	-0.0103	0.6047	-0.0021	0.7020	-0.0062	0.8528
104	100.951	-0.0018	0.4015	-0.0030	0.6023	-0.0026	0.7022	-0.0020	0.8507
108	106.951	0.0001	0.4011	0.0024	0.6006	-0.0017	0.7019	0.0009	0.8493
127	118.951	-0.0011	0.4014	-0.0029	0.6023	-0.0028	0.7023	-0.0021	0.8508
129	120.451	-0.0012	0.4014	-0.0005	0.6015	-0.0028	0.7023	-0.0016	0.8505
131	121.951	-0.0005	0.4013	-0.0016	0.6019	-0.0027	0.7023	-0.0012	0.8504
133	123.451	-0.0006	0.4013	-0.0010	0.6017	-0.0028	0.7023	-0.0023	0.8509
136	124.951	-0.0018	0.4015	-0.0050	0.6030	-0.0057	0.7034	-0.0069	0.8531
140	130.951	0.0014	0.4009	0.0032	0.6003	-0.0023	0.7021	-0.0038	0.8516
145	136.951	0.0008	0.4010	-0.0032	0.6024	-0.0034	0.7025	-0.0076	0.8534
Span 1, x = 26.951									
20	26.951	-0.0362	0.4086	-0.0350	0.6126	-0.0346	0.7145	-0.0359	0.8672
21	26.951	-0.0372	0.4088	-0.0340	0.6123	-0.0337	0.7142	-0.0365	0.8675
22	26.951	-0.0387	0.4091	-0.0348	0.6125	-0.0369	0.7154	-0.0372	0.8679
23	26.951	-0.0416	0.4097	-0.0473	0.6165	-0.0393	0.7163	-0.0450	0.8717

Table 4. Concluded

Span 1, x = 26.951, cont		Point 451		Point 574		Point 473		Point 606	
Orifice	x	c_p	M	c_p	M	c_p	M	c_p	M
24	26.951	-0.0378	0.4089	-0.0364	0.6130	-0.0370	0.7154	-0.0385	0.8685
25	26.951	-0.0367	0.4087	-0.0349	0.6126	-0.0353	0.7148	-0.0374	0.8679
26	26.951	-0.0396	0.4093	-0.0368	0.6132	-0.0379	0.7158	-0.0391	0.8688
27	26.951	-0.0398	0.4093	-0.0380	0.6136	-0.0371	0.7155	-0.0389	0.8687
28	26.951	-0.0388	0.4091	-0.0378	0.6135	-0.0380	0.7158	-0.0388	0.8687
29	26.951	-0.0381	0.4090	-0.0332	0.6120	-0.0345	0.7145	-0.0357	0.8672
30	26.951	-0.0383	0.4090	-0.0365	0.6131	-0.0370	0.7154	-0.0381	0.8683
Span 2, x = 70.951									
65	70.951	-0.0015	0.4015	0.0019	0.6007	0.0006	0.7010	0.0023	0.8486
67	70.951	-0.0003	0.4012	-0.0013	0.6018	-0.0016	0.7018	-0.0007	0.8501
68	70.951	-0.0025	0.4017	-0.0028	0.6023	-0.0027	0.7022	-0.0036	0.8515
69	70.951	0.0002	0.4011	0.0013	0.6009	0.0002	0.7011	0.0013	0.8492
70	70.951	-0.0016	0.4015	-0.0014	0.6018	-0.0020	0.7020	-0.0025	0.8510
71	70.951	-0.0077	0.4027	-0.0229	0.6087	-0.0060	0.7035	-0.0153	0.8572
72	70.951	0.0010	0.4009	0.0100	0.5981	-0.0001	0.7013	0.0054	0.8471
73	70.951	-0.0033	0.4018	-0.0150	0.6062	-0.0040	0.7028	-0.0096	0.8544
74	70.951	0.0001	0.4011	0.0030	0.6004	0.0003	0.7011	0.0028	0.8484
75	70.951	-0.0020	0.4016	-0.0009	0.6017	-0.0014	0.7018	0.0000	0.8497
76	70.951	-0.0001	0.4012	0.0053	0.5996	-0.0003	0.7013	0.0005	0.8495
Span 3, x = 118.951									
116	118.951	0.0559	0.3894	0.0579	0.5826	0.0800	0.6702	0.0880	0.8071
117	118.951	-0.0023	0.4016	-0.0032	0.6024	-0.0041	0.7028	-0.0042	0.8518
118	118.951	0.0016	0.4008	0.0047	0.5998	-0.0014	0.7018	0.0008	0.8494
119	118.951	-0.0086	0.4029	-0.0250	0.6094	-0.0099	0.7050	-0.0195	0.8592
120	118.951	0.0008	0.4010	-0.0018	0.6019	-0.0017	0.7019	-0.0007	0.8501
121	118.951	0.0011	0.4009	-0.0004	0.6015	-0.0005	0.7014	0.0004	0.8496
123	118.951	-0.0032	0.4018	-0.0081	0.6040	-0.0043	0.7029	-0.0078	0.8536
126	118.951	-0.0013	0.4014	-0.0021	0.6020	-0.0014	0.7018	-0.0018	0.8506
127	118.951	-0.0011	0.4014	-0.0029	0.6023	-0.0028	0.7023	-0.0021	0.8508

Table 5. Summary of Profile Parameters
(a) Standard Quantities and Inferred Skin Friction

STATION 1 — Standard Quantities / Inferred Quantities

Point	M_e	u_e, fps	R/ft	R_θ	δ	δ_u	δ^*	θ	H	u_τ	c_f
1569	0.203	239.170	6.096E+06	3.776E+04	1.280	0.751	0.1374	0.0743	1.849	7.810	2.120E-03
1668	0.403	468.380	6.034E+06	3.765E+04	1.300	0.761	0.1430	0.0749	1.909	15.327	2.080E-03
1209	0.400	466.420	1.495E+07	8.189E+04	1.450	0.702	0.1363	0.0657	2.074	14.371	1.840E-03
1494	0.400	465.950	1.498E+07	8.115E+04	1.450	0.694	0.1357	0.0650	2.088	14.320	1.830E-03
1575	0.852	940.050	5.998E+06	3.568E+04	1.300	0.753	0.1548	0.0714	2.169	31.752	2.000E-03
1625	0.850	937.200	5.994E+06	3.571E+04	1.300	0.756	0.1550	0.0715	2.168	31.554	1.990E-03
1661	0.850	937.590	5.997E+06	3.556E+04	1.300	0.753	0.1546	0.0712	2.173	31.571	1.990E-03

STATION 2

Point	Mach	u_e, fps	R/ft	R_θ	δ	δ_u	δ^*	θ	H	u_τ	c_f
692	0.203	238.800	6.089E+06	5.342E+04	1.800	1.080	0.1954	0.1053	1.856	7.504	1.970E-03
793	0.200	133.930	3.680E+07	3.073E+05	1.700	1.099	0.1864	0.1002	1.861	3.737	1.510E-03
811	0.201	134.540	3.682E+07	2.628E+05	1.500	0.937	0.1563	0.0856	1.825	3.811	1.610E-03
713	0.402	467.360	6.006E+06	5.726E+04	1.650	1.156	0.2071	0.1144	1.810	14.767	1.940E-03
671	0.402	469.010	1.504E+07	1.326E+05	1.700	1.132	0.1966	0.1059	1.857	13.896	1.700E-03
927	0.403	272.870	1.503E+07	1.230E+05	1.700	1.037	0.1876	0.0982	1.910	8.380	1.740E-03
867	0.401	278.610	3.560E+07	2.645E+05	1.700	0.975	0.1749	0.0892	1.961	7.772	1.560E-03
813	0.402	265.410	6.853E+07	5.361E+05	1.700	1.053	0.1887	0.0939	2.011	7.353	1.390E-03
734	0.603	688.050	6.013E+06	5.367E+04	1.700	1.124	0.2085	0.1071	1.947	22.006	1.910E-03
879	0.601	403.990	3.540E+07	2.570E+05	1.700	0.975	0.1803	0.0871	2.070	11.670	1.540E-03
841	0.603	397.950	6.715E+07	4.852E+05	1.700	1.002	0.1798	0.0867	2.074	11.007	1.410E-03
848	0.602	396.700	6.726E+07	4.951E+05	1.700	1.002	0.1840	0.0883	2.083	11.059	1.410E-03
839	0.603	394.950	8.307E+07	5.676E+05	1.600	0.937	0.1688	0.0820	2.058	10.766	1.380E-03
824	0.604	393.040	9.402E+07	6.364E+05	1.700	0.951	0.1728	0.0812	2.127	10.681	1.360E-03
825	0.604	393.300	9.397E+07	6.376E+05	1.700	0.959	0.1729	0.0814	2.123	10.682	1.360E-03
837	0.604	399.410	9.032E+07	6.304E+05	1.600	0.940	0.1147	0.0838	1.370	10.811	1.360E-03
752	0.854	944.480	5.956E+06	5.728E+04	1.800	1.199	0.2393	0.1154	2.074	30.629	1.850E-03
915	0.852	557.380	3.501E+07	2.597E+05	1.700	1.029	0.1968	0.0890	2.210	16.329	1.480E-03
945	0.852	553.110	5.063E+07	3.579E+05	1.700	0.994	0.1907	0.0848	2.248	15.893	1.420E-03
855	0.852	549.720	6.603E+07	4.491E+05	1.700	0.964	0.1845	0.0816	2.260	15.523	1.390E-03
856	0.852	559.370	6.489E+07	4.592E+05	1.700	0.967	0.1289	0.0849	1.518	15.772	1.390E-03

Table 5. Concluded
(b) Transformed Quantities and Inferred Skin Friction

STATION 1

			Transformed Quantities						Inferred
Point	M_e	R/ft	u_e', fps	R_θ'	$\delta^{*'}$	θ'	H'	$u_e'(\delta^{*'}/\delta_u)$	c_f'
1569	0.203	6.096E+06	239.377	3.974E+04	0.0984	0.0890	1.245	31.364	2.129E-03
1668	0.403	6.034E+06	470.694	3.864E+04	0.1008	0.0806	1.251	62.347	2.121E-03
1209	0.400	1.495E+07	469.019	8.403E+04	0.0879	0.0709	1.239	58.728	1.878E-03
1494	0.400	1.498E+07	468.601	8.329E+04	0.0872	0.0702	1.243	58.879	1.868E-03
1575	0.852	5.998E+06	961.422	3.273E+04	0.1015	0.0809	1.255	129.594	2.181E-03
1625	0.850	5.994E+06	958.222	3.282E+04	0.1018	0.0810	1.257	129.030	2.169E-03
1661	0.850	5.997E+06	958.675	3.268E+04	0.1014	0.0806	1.258	129.096	2.169E-03

STATION 2

Point	M_e	R/ft	u_e', fps	R_θ'	$\delta^{*'}$	θ'	H'	$u_e'(\delta^{*'}/\delta_u)$	c_f'
692	0.203	6.089E+06	238.813	5.626E+04	0.1383	0.1115	1.241	30.581	1.975E-03
793	0.200	3.680E+07	135.142	3.130E+05	0.1297	0.1068	1.214	15.949	1.529E-03
811	0.201	3.682E+07	134.323	2.787E+05	0.1095	0.0905	1.209	15.697	1.610E-03
713	0.402	6.006E+06	469.624	5.849E+04	0.1524	0.1224	1.245	61.912	1.977E-03
671	0.402	1.504E+07	471.720	1.350E+05	0.1390	0.1134	1.225	57.923	1.736E-03
927	0.403	1.503E+07	275.241	1.234E+05	0.1290	0.1055	1.222	34.239	1.781E-03
867	0.401	3.560E+07	280.820	2.663E+05	0.1158	0.0959	1.208	33.353	1.595E-03
813	0.402	6.853E+07	272.902	5.053E+05	0.1238	0.1027	1.206	32.085	1.452E-03
734	0.603	6.013E+06	696.277	5.251E+04	0.1455	0.1170	1.244	90.132	1.998E-03
879	0.601	3.540E+07	410.675	2.454E+05	0.1158	0.0955	1.212	48.776	1.615E-03
841	0.603	6.715E+07	405.284	4.654E+05	0.1143	0.0950	1.203	46.231	1.475E-03
848	0.602	6.726E+07	405.816	4.657E+05	0.1171	0.0973	1.204	47.426	1.485E-03
839	0.603	8.307E+07	401.612	5.519E+05	0.1077	0.0897	1.201	46.162	1.437E-03
824	0.604	9.402E+07	400.856	6.143E+05	0.1069	0.0891	1.200	45.059	1.420E-03
825	0.604	9.397E+07	400.995	6.161E+05	0.1070	0.0893	1.199	44.741	1.419E-03
837	0.604	9.032E+07	406.405	5.999E+05	0.1065	0.0888	1.199	46.045	1.415E-03
752	0.854	5.956E+06	965.089	5.242E+04	0.1609	0.1297	1.240	129.510	2.014E-03
915	0.852	3.501E+07	573.562	2.266E+05	0.1223	0.1008	1.213	68.170	1.621E-03
945	0.852	5.063E+07	570.105	3.126E+05	0.1160	0.0961	1.207	66.531	1.554E-03
855	0.852	6.603E+07	565.102	4.012E+05	0.1108	0.0921	1.203	64.952	1.509E-03
856	0.852	6.489E+07	574.957	4.020E+05	0.1118	0.0929	1.203	66.474	1.509E-03

57

Table 6. Boundary Layer Profiles
(a) Profiles at Station 1

y, in.	pitot pressure, psia	y/δ	M/M$_e$	u/u$_e$	ρ/ρ$_e$	T$_t$/T$_{t,e}$	(T$_t$-T$_w$)/(T$_{t,e}$-T$_w$)	y$^+$	u$^+$	u'/u$_\tau$	(u'-u$_e$')/u$_\tau$	y/δ$_u$	u'/u$_e$'

Point 1569, M=0.20

y, in.	pitot pressure, psia	y/δ	M/M$_e$	u/u$_e$	ρ/ρ$_e$	T$_t$/T$_{t,e}$	(T$_t$-T$_w$)/(T$_{t,e}$-T$_w$)	y$^+$	u$^+$	u'/u$_\tau$	(u'-u$_e$')/u$_\tau$	y/δ$_u$	u'/u$_e$'
0.0240	71.485	0.0187	0.6486	0.6498	0.9637	0.9989	0.5571	393.76	19.900	19.906	-10.433	0.0320	0.6494
0.0330	71.593	0.0258	0.6877	0.6889	0.9640	0.9990	0.6015	541.42	21.096	21.103	-9.235	0.0439	0.6885
0.0420	71.649	0.0328	0.7071	0.7082	0.9642	0.9991	0.6240	689.09	21.690	21.698	-8.641	0.0559	0.7079
0.0500	71.702	0.0391	0.7250	0.7261	0.9644	0.9991	0.6450	820.34	22.237	22.245	-8.094	0.0666	0.7257
0.0580	71.669	0.0453	0.7139	0.7150	0.9643	0.9991	0.6320	951.60	21.898	21.906	-8.433	0.0772	0.7147
0.0700	71.715	0.0547	0.7293	0.7304	0.9644	0.9991	0.6501	1148.48	22.369	22.377	-7.961	0.0932	0.7301
0.0840	71.827	0.0656	0.7655	0.7665	0.9647	0.9992	0.6935	1378.17	23.474	23.484	-6.855	0.1119	0.7662
0.0960	71.835	0.0750	0.7680	0.7690	0.9647	0.9992	0.6966	1575.05	23.551	23.561	-6.778	0.1278	0.7687
0.1100	71.826	0.0859	0.7651	0.7662	0.9647	0.9992	0.6932	1804.75	23.464	23.475	-6.864	0.1465	0.7659
0.1257	71.876	0.0982	0.7807	0.7817	0.9649	0.9993	0.7122	2062.34	23.941	23.952	-6.387	0.1674	0.7814
0.1470	71.933	0.1148	0.7981	0.7991	0.9650	0.9993	0.7337	2411.80	24.472	24.484	-5.855	0.1957	0.7988
0.1760	72.013	0.1375	0.8219	0.8228	0.9653	0.9994	0.7634	2887.60	25.198	25.212	-5.127	0.2344	0.8225
0.2150	72.042	0.1680	0.8304	0.8312	0.9654	0.9994	0.7740	3527.47	25.456	25.470	-4.869	0.2863	0.8310
0.2660	72.114	0.2078	0.8510	0.8518	0.9656	0.9995	0.8003	4364.21	26.085	26.100	-4.239	0.3542	0.8515
0.3260	72.201	0.2547	0.8752	0.8759	0.9658	0.9996	0.8316	5348.62	26.824	26.841	-3.498	0.4341	0.8757
0.3960	72.337	0.3094	0.9118	0.9123	0.9662	0.9997	0.8797	6497.10	27.939	27.958	-2.381	0.5273	0.9121
0.4750	72.390	0.3711	0.9256	0.9261	0.9664	0.9997	0.8981	7793.24	28.361	28.381	-1.958	0.6325	0.9259
0.5660	72.487	0.4422	0.9504	0.9507	0.9667	0.9998	0.9316	9286.26	29.116	29.138	-1.201	0.7537	0.9506
0.6360	72.536	0.4969	0.9627	0.9629	0.9668	0.9999	0.9484	10434.73	29.490	29.513	-0.826	0.8469	0.9628
0.7165	72.639	0.5598	0.9880	0.9880	0.9672	1.0000	0.9832	11755.48	30.259	30.284	-0.054	0.9541	0.9880
0.7960	72.656	0.6219	0.9921	0.9921	0.9672	1.0000	0.9889	13059.82	30.384	30.410	0.071	1.0599	0.9921
0.8780	72.688	0.6859	0.9998	0.9998	0.9673	1.0000	0.9997	14405.18	30.618	30.644	0.306	1.1691	0.9998
0.9770	72.678	0.7633	0.9974	0.9974	0.9673	1.0000	0.9963	16029.46	30.545	30.571	0.232	1.3009	0.9974
1.0770	72.697	0.8414	1.0019	1.0019	0.9673	1.0000	1.0027	17670.14	30.683	30.710	0.371	1.4341	1.0019
1.2010	72.689	0.9383	1.0000	1.0000	0.9673	1.0000	1.0000	19704.58	30.625	30.652	0.313	1.5992	1.0000
1.3240	72.689	1.0000	1.0000	1.0000	0.9673	1.0000	1.0000	21722.62	30.625	30.652	0.313	1.763	1.0000
1.4755	72.655	1.1527	0.9918	0.9919	0.9672	1.0000	0.9886	24208.25	30.377	30.402	0.064	1.9647	0.9919
1.6280	72.694	1.2719	1.0012	1.0012	0.9673	1.0000	1.0017	26710.29	30.662	30.688	0.349	2.1678	1.0012
1.8150	72.688	1.4180	0.9998	0.9998	0.9673	1.0000	0.9997	29778.37	30.618	30.644	0.306	2.4168	0.9998
2.0005	72.669	1.5629	0.9952	0.9952	0.9673	1.0000	0.9933	32821.83	30.479	30.505	0.167	2.6638	0.9952
2.2000	72.674	1.7188	0.9964	0.9964	0.9673	1.0000	0.9950	36094.99	30.516	30.542	0.203	2.9294	0.9964

Point 1668, M=0.40

y, in.	pitot pressure, psia	y/δ	M/M$_e$	u/u$_e$	ρ/ρ$_e$	T$_t$/T$_{t,e}$	(T$_t$-T$_w$)/(T$_{t,e}$-T$_w$)	y$^+$	u$^+$	u'/u$_\tau$	(u'-u$_e$')/u$_\tau$	y/δ$_u$	u'/u$_e$'
0.0240	35.874	0.0185	0.6368	0.6423	0.9508	0.9982	0.3975	374.89	19.628	19.669	-10.727	0.0315	0.6405
0.0330	36.092	0.0254	0.6779	0.6832	0.9523	0.9983	0.4526	515.47	20.877	20.926	-9.470	0.0434	0.6814
0.0420	36.189	0.0323	0.6953	0.7005	0.9530	0.9984	0.4770	656.05	21.407	21.460	-8.936	0.0552	0.6988
0.0500	36.258	0.0385	0.7074	0.7125	0.9535	0.9985	0.4943	781.01	21.775	21.830	-8.566	0.0657	0.7108
0.0580	36.289	0.0446	0.7128	0.7179	0.9537	0.9985	0.5021	905.98	21.938	21.994	-8.402	0.0762	0.7162
0.0700	36.367	0.0538	0.7261	0.7311	0.9542	0.9985	0.5216	1093.42	22.342	22.402	-7.994	0.0920	0.7294
0.0840	36.501	0.0646	0.7484	0.7532	0.9551	0.9986	0.5551	1312.10	23.017	23.082	-7.314	0.1104	0.7516

58

Table 6. Continued

(a) Continued

y, in.	pitot pressure, psia	y/δ	M/M$_e$	u/u$_e$	ρ/ρ$_e$	T$_t$/T$_{t,e}$	(T$_t$-T$_w$)/(T$_{t,e}$-T$_w$)	y$^+$	u$^+$	u'/u$_\tau$	(u'-u$_e$')/u$_\tau$	y/δ$_u$	u'/u$_e$'
0.0960	36.567	0.0738	0.7591	0.7638	0.9556	0.9987	0.5716	1499.55	23.341	23.409	-6.987	0.1261	0.7623
0.1100	36.594	0.0846	0.7635	0.7681	0.9557	0.9987	0.5783	1718.23	23.473	23.542	-6.854	0.1445	0.7666
0.1257	36.673	0.0967	0.7760	0.7805	0.9563	0.9988	0.5980	1963.47	23.852	23.924	-6.472	0.1652	0.7790
0.1470	36.749	0.1131	0.7879	0.7922	0.9568	0.9988	0.6168	2296.18	24.210	24.285	-6.111	0.1932	0.7908
0.1760	36.877	0.1354	0.8074	0.8115	0.9577	0.9989	0.6485	2749.17	24.799	24.880	-5.516	0.2313	0.8102
0.2150	36.978	0.1654	0.8225	0.8263	0.9583	0.9990	0.6735	3358.36	25.253	25.339	-5.057	0.2825	0.8251
0.2660	37.152	0.2046	0.8478	0.8512	0.9595	0.9991	0.7163	4155.00	26.012	26.106	-4.290	0.3495	0.8501
0.3260	37.316	0.2508	0.8708	0.8739	0.9606	0.9993	0.7564	5092.22	26.705	26.806	-3.590	0.4284	0.8729
0.3960	37.536	0.3046	0.9007	0.9032	0.9621	0.9994	0.8100	6185.64	27.601	27.712	-2.684	0.5204	0.9024
0.4750	37.749	0.3654	0.9286	0.9305	0.9635	0.9996	0.8616	7419.64	28.435	28.557	-1.839	0.6242	0.9299
0.5660	37.949	0.4354	0.9540	0.9552	0.9648	0.9997	0.9097	8841.09	29.192	29.324	-1.072	0.7438	0.9548
0.6360	38.106	0.4892	0.9734	0.9741	0.9659	0.9998	0.9473	9934.51	29.769	29.909	-0.487	0.8357	0.9739
0.7165	38.201	0.5512	0.9849	0.9854	0.9665	0.9999	0.9700	11191.94	30.112	30.256	-0.140	0.9415	0.9852
0.7960	38.270	0.6123	0.9932	0.9934	0.9669	1.0000	0.9864	12433.75	30.358	30.506	0.110	1.0460	0.9933
0.8780	38.269	0.6754	0.9931	0.9933	0.9669	1.0000	0.9862	13714.62	30.354	30.502	0.106	1.1537	0.9932
0.9770	38.334	0.7515	1.0008	1.0008	0.9674	1.0000	1.0016	15261.03	30.584	30.735	0.339	1.2838	1.0008
1.0770	38.287	0.8285	0.9952	0.9954	0.9670	1.0000	0.9904	16823.06	30.418	30.567	0.171	1.4152	0.9953
1.2010	38.324	0.9238	0.9996	0.9996	0.9673	1.0000	0.9992	18759.97	30.548	30.699	0.303	1.5782	0.9996
1.3240	38.328	1.0000	1.0001	1.0001	0.9673	1.0000	1.0002	20681.27	30.562	30.713	0.317	1.7398	1.0000
1.4755	38.317	1.1350	0.9988	0.9988	0.9672	1.0000	0.9976	23047.74	30.524	30.674	0.278	1.9389	0.9988
1.6280	38.282	1.2523	0.9946	0.9948	0.9670	1.0000	0.9893	25429.84	30.400	30.549	0.153	2.1393	0.9947
1.8150	38.283	1.3962	0.9948	0.9949	0.9670	1.0000	0.9895	28350.83	30.404	30.552	0.157	2.3850	0.9949
2.0005	38.295	1.5388	0.9962	0.9963	0.9671	1.0000	0.9923	31248.40	30.446	30.595	0.200	2.6288	0.9963
2.2000	38.302	1.6923	0.9970	0.9971	0.9671	1.0000	0.9940	34364.64	30.471	30.620	0.225	2.8909	0.9971

Point 1209, M=0.40

y, in.	pitot pressure, psia	y/δ	M/M$_e$	u/u$_e$	ρ/ρ$_e$	T$_t$/T$_{t,e}$	(T$_t$-T$_w$)/(T$_{t,e}$-T$_w$)	y$^+$	u$^+$	u'/u$_\tau$	(u'-u$_e$')/u$_\tau$	y/δ$_u$	u'/u$_e$'
0.0240	89.935	0.0166	0.6748	0.6804	0.9515	0.9991	-0.0298	871.18	22.084	22.146	-10.162	0.0342	0.6785
0.0330	90.361	0.0228	0.7057	0.7110	0.9527	0.9991	0.0400	1197.87	23.078	23.148	-9.160	0.0470	0.7092
0.0420	90.571	0.0290	0.7203	0.7256	0.9533	0.9992	0.0753	1524.56	23.550	23.624	-8.684	0.0598	0.7238
0.0500	90.693	0.0345	0.7287	0.7339	0.9537	0.9992	0.0961	1814.95	23.820	23.896	-8.412	0.0712	0.7322
0.0580	90.825	0.0400	0.7377	0.7428	0.9541	0.9992	0.1187	2105.34	24.108	24.187	-8.122	0.0826	0.7411
0.0700	90.976	0.0483	0.7478	0.7528	0.9545	0.9992	0.1449	2540.93	24.432	24.514	-7.794	0.0997	0.7511
0.0840	91.225	0.0579	0.7641	0.7689	0.9552	0.9993	0.1886	3049.11	24.956	25.043	-7.265	0.1197	0.7673
0.0960	91.371	0.0662	0.7735	0.7782	0.9557	0.9993	0.2145	3484.70	25.258	25.348	-6.960	0.1368	0.7766
0.1100	91.461	0.0759	0.7792	0.7839	0.9559	0.9993	0.2305	3992.89	25.442	25.533	-6.775	0.1567	0.7823
0.1257	91.694	0.0867	0.7939	0.7983	0.9566	0.9993	0.2724	4562.78	25.911	26.007	-6.301	0.1791	0.7968
0.1470	91.896	0.1014	0.8063	0.8106	0.9572	0.9994	0.3091	5335.95	26.309	26.409	-5.899	0.2094	0.8092
0.1760	92.154	0.1214	0.8219	0.8260	0.9579	0.9994	0.3565	6388.62	26.808	26.914	-5.394	0.2507	0.8246
0.2150	92.441	0.1483	0.8389	0.8427	0.9587	0.9995	0.4096	7804.28	27.350	27.462	-4.846	0.3063	0.8414
0.2660	92.825	0.1834	0.8611	0.8644	0.9598	0.9995	0.4816	9655.53	28.056	28.176	-4.132	0.3789	0.8633
0.3260	93.298	0.2248	0.8875	0.8903	0.9612	0.9996	0.5714	11833.47	28.897	29.027	-3.281	0.4644	0.8894
0.3960	93.785	0.2731	0.9138	0.9161	0.9625	0.9997	0.6650	14374.40	29.733	29.874	-2.434	0.5641	0.9153

Table 6. Continued

(a) Continued

y, in.	pitot pressure, psia	y/δ	M/M_e	u/u_e	ρ/ρ_e	$T_t/T_{t,e}$	$(T_r-T_w)/(T_{t,e}-T_w)$	y^+	u^+	u'/u_τ	$(u'-u_e')/u_\tau$	y/δ_u	u'/u_e'
0.4750	94.178	0.3276	0.9344	0.9362	0.9636	0.9998	0.7412	17242.02	30.386	30.537	-1.771	0.6766	0.9356
0.5660	94.657	0.3903	0.9589	0.9601	0.9650	0.9998	0.8348	20545.23	31.160	31.322	-0.987	0.8063	0.9597
0.6360	95.028	0.4386	0.9774	0.9780	0.9660	0.9999	0.9079	23086.16	31.744	31.913	-0.395	0.9060	0.9778
0.7165	95.336	0.4941	0.9924	0.9926	0.9669	1.0000	0.9688	26008.22	32.218	32.395	0.087	1.0207	0.9926
0.7960	95.447	0.5490	0.9978	0.9978	0.9672	1.0000	0.9908	28893.99	32.386	32.566	0.258	1.1339	0.9978
0.8780	95.586	0.6055	1.0044	1.0043	0.9676	1.0000	1.0184	31870.51	32.596	32.779	0.471	1.2507	1.0043
0.9770	95.538	0.6738	1.0021	1.0021	0.9674	1.0000	1.0088	35464.11	32.524	32.706	0.398	1.3917	1.0021
1.0770	95.512	0.7428	1.0009	1.0009	0.9674	1.0000	1.0037	39094.01	32.485	32.666	0.358	1.5342	1.0009
1.2010	95.555	0.8283	1.0029	1.0029	0.9675	1.0000	1.0122	43595.08	32.549	32.732	0.424	1.7108	1.0029
1.3240	95.565	0.9131	1.0034	1.0033	0.9675	1.0000	1.0142	48059.86	32.564	32.747	0.439	1.8860	1.0034
1.4755	95.479	1.0000	0.9993	0.9993	0.9673	1.0000	0.9971	53559.15	32.435	32.615	0.307	2.1019	1.0000
1.6280	95.414	1.1228	0.9962	0.9963	0.9671	1.0000	0.9842	59094.75	32.336	32.515	0.207	2.3191	0.9963
1.8150	95.528	1.2517	1.0017	1.0016	0.9674	1.0000	1.0069	65882.66	32.509	32.690	0.382	2.5855	1.0016
2.0005	95.574	1.3797	1.0039	1.0037	0.9675	1.0000	1.0160	72616.12	32.578	32.761	0.453	2.8497	1.0038
2.2000	95.693	1.5172	1.0095	1.0092	0.9679	1.0000	1.0397	79857.77	32.756	32.942	0.634	3.1339	1.0093

Point 1494, M=0.40

y, in.	pitot pressure, psia	y/δ	M/M_e	u/u_e	ρ/ρ_e	$T_t/T_{t,e}$	$(T_r-T_w)/(T_{t,e}-T_w)$	y^+	u^+	u'/u_τ	$(u'-u_e')/u_\tau$	y/δ_u	u'/u_e'
0.0240	89.885	0.0166	0.6717	0.6773	0.9512	0.9992	-0.6060	870.34	22.039	22.102	-10.283	0.0346	0.6754
0.0330	90.294	0.0228	0.7014	0.7069	0.9524	0.9992	-0.5097	1196.71	23.001	23.072	-9.313	0.0476	0.7051
0.0420	90.498	0.0290	0.7158	0.7211	0.9530	0.9993	-0.4597	1523.09	23.465	23.540	-8.846	0.0605	0.7194
0.0500	90.646	0.0345	0.7260	0.7313	0.9535	0.9993	-0.4226	1813.20	23.795	23.872	-8.513	0.0720	0.7295
0.0580	90.797	0.0400	0.7363	0.7415	0.9539	0.9993	-0.3842	2103.31	24.126	24.206	-8.179	0.0836	0.7397
0.0700	90.938	0.0483	0.7458	0.7508	0.9543	0.9993	-0.3478	2538.48	24.430	24.514	-7.872	0.1009	0.7491
0.0840	91.227	0.0579	0.7647	0.7696	0.9552	0.9994	-0.2716	3046.17	25.041	25.130	-7.255	0.1210	0.7680
0.0960	91.358	0.0662	0.7732	0.7779	0.9556	0.9994	-0.2365	3481.34	25.312	25.404	-6.981	0.1383	0.7763
0.1100	91.408	0.0759	0.7764	0.7811	0.9557	0.9994	-0.2230	3989.04	25.415	25.508	-6.877	0.1585	0.7795
0.1257	91.683	0.0867	0.7937	0.7982	0.9565	0.9994	-0.1478	4558.38	25.971	26.069	-6.316	0.1811	0.7967
0.1470	91.846	0.1014	0.8038	0.8081	0.9570	0.9994	-0.1025	5330.81	26.294	26.396	-5.989	0.2118	0.8066
0.1760	92.105	0.1214	0.8195	0.8236	0.9577	0.9995	-0.0296	6382.46	26.798	26.905	-5.480	0.2536	0.8222
0.2150	92.476	0.1483	0.8414	0.8452	0.9588	0.9995	0.0768	7796.76	27.500	27.616	-4.769	0.3098	0.8439
0.2660	92.817	0.1834	0.8611	0.8644	0.9598	0.9996	0.1764	9646.22	28.128	28.251	-4.135	0.3833	0.8633
0.3260	93.271	0.2248	0.8865	0.8893	0.9611	0.9997	0.3114	11822.06	28.937	29.070	-3.315	0.4697	0.8884
0.3960	93.777	0.2731	0.9138	0.9161	0.9625	0.9997	0.4648	14360.54	29.808	29.953	-2.432	0.5706	0.9153
0.4750	94.193	0.3276	0.9356	0.9374	0.9637	0.9998	0.5929	17225.39	30.502	30.656	-1.729	0.6844	0.9368
0.5660	94.693	0.3903	0.9611	0.9622	0.9651	0.9999	0.7489	20525.42	31.310	31.476	-0.910	0.8156	0.9619
0.6360	95.054	0.4386	0.9791	0.9797	0.9661	0.9999	0.8628	23063.90	31.877	32.052	-0.334	0.9164	0.9795
0.7165	95.350	0.4941	0.9935	0.9937	0.9669	1.0000	0.9569	25983.15	32.333	32.515	0.129	1.0324	0.9936
0.7960	95.461	0.5490	0.9988	0.9989	0.9672	1.0000	0.9923	28866.13	32.502	32.686	0.301	1.1470	0.9989
0.8780	95.588	0.6055	1.0049	1.0048	0.9676	1.0000	1.0330	31839.78	32.694	32.881	0.496	1.2651	1.0048
0.9770	95.554	0.6738	1.0033	1.0032	0.9675	1.0000	1.0221	35429.92	32.643	32.829	0.444	1.4078	1.0032
1.0770	95.506	0.7428	1.0010	1.0010	0.9674	1.0000	1.0067	39056.31	32.570	32.755	0.370	1.5519	1.0010
1.2010	95.542	0.8283	1.0027	1.0026	0.9675	1.0000	1.0182	43553.05	32.624	32.811	0.425	1.7305	1.0027

Table 6. Continued

(a) Continued

y, in.	pitot pressure, psia	y/δ	M/M_e	u/u_e	ρ/ρ_e	$T_t/T_{t,e}$	$(T_t-T_w)/(T_{t,e}-T_w)$	y^+	u^+	u'/u_τ	$(u'-u_e')/u_\tau$	y/δ_u	u'/u_e'
1.3240	95.579	0.9131	1.0045	1.0044	0.9676	1.0000	1.0301	48013.52	32.680	32.867	0.482	1.9078	1.0044
1.4755	95.466	1.0000	0.9991	0.9991	0.9673	1.0000	0.9939	53507.51	32.510	32.694	0.309	2.1261	1.0000
1.6280	95.418	1.1228	0.9968	0.9969	0.9671	1.0000	0.9786	59037.77	32.437	32.620	0.235	2.3458	0.9968
1.8150	95.512	1.2517	1.0013	1.0013	0.9674	1.0000	1.0086	65819.14	32.579	32.765	0.379	2.6153	1.0013
2.0005	95.567	1.3797	1.0039	1.0038	0.9675	1.0000	1.0262	72546.11	32.662	32.849	0.464	2.8826	1.0038
2.2000	95.664	1.5172	1.0085	1.0083	0.9678	1.0000	1.0573	79780.77	32.808	32.997	0.612	3.1700	1.0084

Point 1575, M=0.85

y, in.	pitot pressure, psia	y/δ	M/M_e	u/u_e	ρ/ρ_e	$T_t/T_{t,e}$	$(T_t-T_w)/(T_{t,e}-T_w)$	y^+	u^+	u'/u_τ	$(u'-u_e')/u_\tau$	y/δ_u	u'/u_e'
0.0240	17.159	0.0185	0.6267	0.6510	0.8964	0.9957	0.0046	320.79	19.274	19.465	-10.496	0.0319	0.6429
0.0330	17.527	0.0254	0.6610	0.6847	0.9016	0.9960	0.0705	441.08	20.272	20.493	-9.468	0.0438	0.6768
0.0420	17.776	0.0323	0.6830	0.7061	0.9051	0.9962	0.1157	561.37	20.906	21.148	-8.813	0.0558	0.6984
0.0500	17.895	0.0385	0.6932	0.7160	0.9067	0.9963	0.1375	668.30	21.199	21.451	-8.510	0.0664	0.7084
0.0580	18.005	0.0446	0.7025	0.7250	0.9082	0.9964	0.1577	775.23	21.464	21.725	-8.236	0.0770	0.7175
0.0700	18.156	0.0538	0.7149	0.7370	0.9103	0.9965	0.1854	935.62	21.819	22.093	-7.868	0.0930	0.7296
0.0840	18.406	0.0646	0.7349	0.7561	0.9137	0.9967	0.2315	1122.75	22.387	22.682	-7.279	0.1116	0.7491
0.0960	18.492	0.0738	0.7416	0.7626	0.9149	0.9968	0.2474	1283.14	22.576	22.879	-7.082	0.1275	0.7556
0.1100	18.628	0.0846	0.7520	0.7725	0.9167	0.9969	0.2725	1470.27	22.871	23.186	-6.776	0.1461	0.7657
0.1257	18.768	0.0967	0.7626	0.7825	0.9186	0.9970	0.2984	1680.11	23.168	23.494	-6.467	0.1669	0.7759
0.1470	18.988	0.1131	0.7787	0.7979	0.9215	0.9972	0.3390	1964.81	23.622	23.967	-5.994	0.1952	0.7915
0.1760	19.224	0.1354	0.7955	0.8137	0.9246	0.9973	0.3825	2352.42	24.092	24.457	-5.504	0.2337	0.8077
0.2150	19.478	0.1654	0.8131	0.8302	0.9279	0.9975	0.4291	2873.70	24.579	24.967	-4.994	0.2855	0.8246
0.2660	19.862	0.2046	0.8387	0.8540	0.9328	0.9978	0.4994	3555.37	25.285	25.706	-4.255	0.3533	0.8490
0.3260	20.277	0.2508	0.8651	0.8785	0.9380	0.9982	0.5747	4357.33	26.008	26.466	-3.496	0.4329	0.8741
0.3960	20.782	0.3046	0.8956	0.9065	0.9443	0.9986	0.6653	5292.96	26.838	27.340	-2.621	0.5259	0.9029
0.4750	21.213	0.3654	0.9205	0.9291	0.9496	0.9989	0.7417	6348.87	27.507	28.048	-1.914	0.6308	0.9263
0.5660	21.683	0.4354	0.9466	0.9525	0.9552	0.9992	0.8239	7565.18	28.201	28.783	-1.178	0.7517	0.9506
0.6360	22.103	0.4892	0.9689	0.9725	0.9602	0.9996	0.8963	8500.81	28.791	29.411	-0.551	0.8446	0.9713
0.7165	22.391	0.5512	0.9837	0.9857	0.9636	0.9998	0.9454	9576.77	29.181	29.826	-0.135	0.9515	0.9850
0.7960	22.600	0.6123	0.9943	0.9950	0.9660	0.9999	0.9807	10639.37	29.457	30.121	0.159	1.0571	0.9948
0.8780	22.668	0.6754	0.9977	0.9980	0.9668	1.0000	0.9922	11735.39	29.546	30.215	0.254	1.1660	0.9979
0.9770	22.644	0.7515	0.9965	0.9969	0.9665	0.9999	0.9882	13058.63	29.515	30.182	0.221	1.2975	0.9968
1.0770	22.700	0.8285	0.9993	0.9994	0.9671	1.0000	0.9976	14395.23	29.587	30.259	0.298	1.4303	0.9993
1.2010	22.700	0.9238	0.9993	0.9994	0.9671	1.0000	0.9976	16052.62	29.587	30.259	0.298	1.5950	0.9993
1.3240	22.718	1.0000	1.0002	1.0002	0.9674	1.0000	1.0006	17696.65	29.611	30.284	0.323	1.7583	1.0000
1.4755	22.700	1.1350	0.9993	0.9994	0.9671	1.0000	0.9976	19721.60	29.588	30.259	0.298	1.9595	0.9993
1.6280	22.672	1.2523	0.9979	0.9981	0.9668	1.0000	0.9929	21759.93	29.551	30.221	0.259	2.1620	0.9981
1.8150	22.688	1.3962	0.9987	0.9988	0.9670	1.0000	0.9956	24259.38	29.572	30.243	0.282	2.4104	0.9988
2.0005	22.692	1.5388	0.9989	0.9990	0.9671	1.0000	0.9962	26738.78	29.577	30.248	0.287	2.6567	0.9990
2.2000	22.680	1.6923	0.9983	0.9985	0.9669	1.0000	0.9942	29405.31	29.562	30.232	0.271	2.9216	0.9984

Point 1625, M=0.85

y, in.	pitot pressure, psia	y/δ	M/M_e	u/u_e	ρ/ρ_e	$T_t/T_{t,e}$	$(T_t-T_w)/(T_{t,e}-T_w)$	y^+	u^+	u'/u_τ	$(u'-u_e')/u_\tau$	y/δ_u	u'/u_e'
0.0240	17.122	0.0185	0.6243	0.6484	0.8966	0.9954	0.0970	320.28	19.260	19.447	-10.609	0.0317	0.6404

Table 6. Continued

(a) Continued

y, in.	pitot pressure, psia	y/δ	M/M$_e$	u/u$_e$	ρ/ρ$_e$	T$_t$/T$_{t,e}$	(T$_t$-T$_w$)/(T$_{t,e}$-T$_w$)	y$^+$	u$^+$	u'/u$_\tau$	(u'-u$_e$')/u$_\tau$	y/δ$_u$	u'/u$_e$'
0.0330	17.501	0.0254	0.6600	0.6835	0.9020	0.9957	0.1602	440.38	20.301	20.519	-9.538	0.0437	0.6757
0.0420	17.765	0.0323	0.6835	0.7064	0.9056	0.9960	0.2046	560.49	20.980	21.219	-8.837	0.0556	0.6987
0.0500	17.871	0.0385	0.6926	0.7152	0.9071	0.9961	0.2225	667.25	21.243	21.491	-8.565	0.0661	0.7077
0.0580	17.967	0.0446	0.7007	0.7231	0.9084	0.9961	0.2387	774.01	21.477	21.733	-8.323	0.0767	0.7157
0.0700	18.152	0.0538	0.7161	0.7379	0.9109	0.9963	0.2700	934.14	21.916	22.188	-7.868	0.0926	0.7306
0.0840	18.325	0.0646	0.7300	0.7513	0.9133	0.9964	0.2993	1120.97	22.315	22.601	-7.455	0.1111	0.7442
0.0960	18.477	0.0738	0.7420	0.7628	0.9153	0.9966	0.3250	1281.11	22.655	22.954	-7.102	0.1270	0.7559
0.1100	18.573	0.0846	0.7494	0.7698	0.9166	0.9967	0.3412	1467.94	22.865	23.173	-6.883	0.1455	0.7631
0.1257	18.707	0.0967	0.7596	0.7796	0.9184	0.9968	0.3638	1677.46	23.154	23.473	-6.583	0.1663	0.7730
0.1470	18.939	0.1131	0.7768	0.7959	0.9215	0.9970	0.4029	1961.70	23.639	23.978	-6.078	0.1944	0.7896
0.1760	19.157	0.1354	0.7925	0.8107	0.9243	0.9972	0.4395	2348.71	24.080	24.437	-5.619	0.2328	0.8047
0.2150	19.442	0.1654	0.8124	0.8294	0.9280	0.9974	0.4871	2869.16	24.635	25.017	-5.039	0.2844	0.8238
0.2660	19.825	0.2046	0.8381	0.8534	0.9329	0.9977	0.5507	3549.75	25.346	25.762	-4.294	0.3519	0.8483
0.3260	20.269	0.2508	0.8665	0.8796	0.9385	0.9981	0.6235	4350.45	26.126	26.581	-3.475	0.4312	0.8753
0.3960	20.705	0.3046	0.8930	0.9040	0.9439	0.9985	0.6941	5284.59	26.851	27.344	-2.712	0.5238	0.9004
0.4750	21.172	0.3654	0.9203	0.9288	0.9496	0.9988	0.7687	6338.84	27.586	28.120	-1.936	0.6283	0.9260
0.5660	21.645	0.4354	0.9466	0.9525	0.9553	0.9992	0.8431	7553.23	28.291	28.867	-1.189	0.7487	0.9506
0.6360	22.069	0.4892	0.9693	0.9728	0.9603	0.9995	0.9088	8487.37	28.893	29.507	-0.550	0.8413	0.9716
0.7165	22.363	0.5512	0.9845	0.9863	0.9638	0.9998	0.9537	9561.64	29.295	29.934	-0.122	0.9478	0.9857
0.7960	22.535	0.6123	0.9933	0.9941	0.9658	0.9999	0.9798	10622.56	29.525	30.179	0.123	1.0529	0.9938
0.8780	22.645	0.6754	0.9988	0.9989	0.9670	1.0000	0.9963	11716.85	29.669	30.334	0.278	1.1614	0.9989
0.9770	22.620	0.7515	0.9975	0.9978	0.9667	1.0000	0.9926	13037.99	29.637	30.299	0.243	1.2923	0.9977
1.0770	22.664	0.8285	0.9997	0.9998	0.9673	1.0000	0.9992	14372.49	29.694	30.360	0.304	1.4246	0.9998
1.2010	22.650	0.9238	0.9990	0.9992	0.9671	1.0000	0.9971	16027.26	29.676	30.341	0.285	1.5886	0.9991
1.3240	22.674	1.0000	1.0002	1.0002	0.9674	1.0000	1.0007	17668.68	29.707	30.374	0.318	1.7513	1.0000
1.4755	22.641	1.1350	0.9986	0.9988	0.9670	1.0000	0.9957	19690.44	29.664	30.328	0.272	1.9517	0.9987
1.6280	22.611	1.2523	0.9971	0.9974	0.9666	1.0000	0.9912	21725.54	29.625	30.286	0.230	2.1534	0.9973
1.8150	22.652	1.3962	0.9991	0.9992	0.9671	1.0000	0.9974	24221.04	29.679	30.343	0.287	2.4008	0.9992
2.0005	22.641	1.5388	0.9986	0.9988	0.9670	1.0000	0.9957	26696.53	29.664	30.328	0.272	2.6462	0.9987
2.2000	22.647	1.6923	0.9989	0.9990	0.9671	1.0000	0.9966	29358.84	29.672	30.336	0.280	2.9101	0.9990

Point 1661, M=0.85

y, in.	pitot pressure, psia	y/δ	M/M$_e$	u/u$_e$	ρ/ρ$_e$	T$_t$/T$_{t,e}$	(T$_t$-T$_w$)/(T$_{t,e}$-T$_w$)	y$^+$	u$^+$	u'/u$_\tau$	(u'-u$_e$')/u$_\tau$	y/δ$_u$	u'/u$_e$'
0.0240	17.144	0.0185	0.6258	0.6500	0.8967	0.9955	0.0839	320.37	19.304	19.493	-10.566	0.0319	0.6419
0.0330	17.497	0.0254	0.6590	0.6826	0.9017	0.9958	0.1435	440.50	20.272	20.489	-9.570	0.0438	0.6747
0.0420	17.770	0.0323	0.6833	0.7062	0.9055	0.9960	0.1900	560.64	20.974	21.214	-8.845	0.0558	0.6986
0.0500	17.880	0.0385	0.6928	0.7154	0.9070	0.9961	0.2088	667.43	21.246	21.495	-8.563	0.0664	0.7079
0.0580	17.967	0.0446	0.7001	0.7226	0.9082	0.9962	0.2237	774.22	21.458	21.714	-8.344	0.0770	0.7151
0.0700	18.155	0.0538	0.7157	0.7376	0.9108	0.9963	0.2559	934.40	21.905	22.177	-7.882	0.0930	0.7303
0.0840	18.323	0.0646	0.7293	0.7506	0.9131	0.9965	0.2848	1121.28	22.291	22.577	-7.481	0.1116	0.7435
0.0960	18.459	0.0738	0.7400	0.7609	0.9149	0.9966	0.3081	1281.47	22.596	22.894	-7.165	0.1275	0.7539
0.1100	18.578	0.0846	0.7492	0.7697	0.9165	0.9967	0.3285	1468.35	22.857	23.165	-6.894	0.1461	0.7629
0.1257	18.732	0.0967	0.7609	0.7808	0.9186	0.9968	0.3549	1677.92	23.188	23.509	-6.550	0.1669	0.7742

62

Table 6. Continued

(a) Continued

y, in.	pitot pressure, psia	y/δ	M/M_e	u/u_e	ρ/ρ_e	$T_t/T_{t,e}$	$(T_t-T_w)/(T_{t,e}-T_w)$	y^+	u^+	u'/u_τ	$(u'-u_e')/u_\tau$	y/δ_u	u'/u_e'
0.1470	18.934	0.1131	0.7758	0.7950	0.9212	0.9970	0.3895	1962.25	23.610	23.948	-6.111	0.1952	0.7887
0.1760	19.181	0.1354	0.7936	0.8118	0.9245	0.9972	0.4316	2349.36	24.108	24.468	-5.591	0.2337	0.8058
0.2150	19.450	0.1654	0.8123	0.8294	0.9280	0.9974	0.4772	2869.95	24.631	25.014	-5.045	0.2855	0.8238
0.2660	19.827	0.2046	0.8376	0.8529	0.9328	0.9977	0.5408	3550.73	25.330	25.746	-4.312	0.3533	0.8479
0.3260	20.289	0.2508	0.8671	0.8802	0.9386	0.9981	0.6179	4351.65	26.141	26.598	-3.461	0.4329	0.8759
0.3960	20.732	0.3046	0.8940	0.9049	0.9441	0.9985	0.6909	5286.05	26.875	27.370	-2.688	0.5259	0.9014
0.4750	21.179	0.3654	0.9200	0.9286	0.9496	0.9988	0.7635	6340.59	27.577	28.112	-1.947	0.6308	0.9258
0.5660	21.646	0.4354	0.9460	0.9520	0.9552	0.9992	0.8383	7555.31	28.272	28.849	-1.210	0.7517	0.9501
0.6360	22.076	0.4892	0.9690	0.9726	0.9603	0.9995	0.9061	8489.72	28.883	29.497	-0.562	0.8446	0.9714
0.7165	22.370	0.5512	0.9842	0.9861	0.9637	0.9998	0.9519	9564.28	29.284	29.925	-0.134	0.9515	0.9855
0.7960	22.576	0.6123	0.9947	0.9953	0.9661	0.9999	0.9837	10625.50	29.558	30.217	0.158	1.0571	0.9951
0.8780	22.671	0.6754	0.9994	0.9995	0.9672	1.0000	0.9983	11720.08	29.683	30.350	0.291	1.1660	0.9995
0.9770	22.647	0.7515	0.9982	0.9985	0.9669	1.0000	0.9946	13041.59	29.652	30.316	0.258	1.2975	0.9984
1.0770	22.676	0.8285	0.9997	0.9997	0.9672	1.0000	0.9991	14376.46	29.690	30.357	0.298	1.4303	0.9997
1.2010	22.687	0.9238	1.0002	1.0002	0.9674	1.0000	1.0007	16031.68	29.704	30.372	0.313	1.5950	1.0002
1.3240	22.681	1.0000	0.9999	0.9999	0.9673	1.0000	0.9998	17673.56	29.696	30.364	0.305	1.7583	1.0000
1.4755	22.650	1.1350	0.9984	0.9986	0.9669	1.0000	0.9951	19695.88	29.656	30.321	0.262	1.9595	0.9985
1.6280	22.620	1.2523	0.9969	0.9973	0.9666	1.0000	0.9905	21731.54	29.616	30.279	0.220	2.1620	0.9971
1.8150	22.640	1.3962	0.9979	0.9981	0.9668	1.0000	0.9935	24227.73	29.642	30.307	0.248	2.4104	0.9981
2.0005	22.635	1.5388	0.9976	0.9979	0.9668	1.0000	0.9928	26703.90	29.636	30.300	0.241	2.6567	0.9978
2.2000	22.678	1.6923	0.9998	0.9998	0.9673	1.0000	0.9994	29366.95	29.692	30.360	0.301	2.9216	0.9998

63

Table 6. Continued
(b) Profiles at Station 2

y, in.	pitot pressure, psia	y/δ	M/M_e	u/u_e	ρ/ρ_e	$T_t/T_{t,e}$	$(T_t-T_w)/(T_{t,e}-T_w)$	y^+	u^+	u'/u_τ	$(u'-u_e')/u_\tau$	y/δ_u	u'/u_e'
Point 692, M=0.20													
0.0240	71.363	0.0133	0.6114	0.6122	0.9648	0.9975	0.5562	380.65	19.483	19.478	-12.047	0.0222	0.6121
0.0330	71.451	0.0183	0.6455	0.6463	0.9649	0.9977	0.5922	523.40	20.565	20.560	-10.965	0.0306	0.6461
0.0420	71.541	0.0233	0.6784	0.6792	0.9651	0.9979	0.6278	666.15	21.615	21.610	-9.915	0.0389	0.6791
0.0500	71.616	0.0278	0.7047	0.7055	0.9652	0.9980	0.6564	793.03	22.451	22.446	-9.079	0.0463	0.7053
0.0580	71.640	0.0322	0.7129	0.7137	0.9652	0.9981	0.6654	919.92	22.712	22.707	-8.818	0.0537	0.7135
0.0700	71.663	0.0389	0.7207	0.7215	0.9653	0.9981	0.6740	1110.24	22.959	22.954	-8.571	0.0648	0.7213
0.0840	71.698	0.0467	0.7324	0.7331	0.9653	0.9982	0.6869	1332.29	23.330	23.325	-8.200	0.0778	0.7330
0.0960	71.715	0.0533	0.7380	0.7387	0.9654	0.9982	0.6931	1522.62	23.508	23.503	-8.022	0.0889	0.7386
0.1100	71.746	0.0611	0.7481	0.7488	0.9654	0.9983	0.7044	1744.67	23.829	23.824	-7.701	0.1019	0.7486
0.1257	71.748	0.0698	0.7487	0.7495	0.9654	0.9983	0.7051	1993.68	23.850	23.845	-7.680	0.1164	0.7493
0.1470	71.807	0.0817	0.7676	0.7683	0.9655	0.9984	0.7262	2331.51	24.448	24.444	-7.081	0.1361	0.7681
0.1760	71.858	0.0978	0.7835	0.7842	0.9656	0.9985	0.7442	2791.47	24.954	24.949	-6.576	0.1630	0.7840
0.2150	71.900	0.1194	0.7963	0.7970	0.9657	0.9986	0.7588	3410.03	25.362	25.358	-6.167	0.1991	0.7968
0.2660	71.987	0.1478	0.8223	0.8229	0.9659	0.9988	0.7885	4218.92	26.187	26.183	-5.342	0.2463	0.8228
0.3260	72.050	0.1811	0.8406	0.8412	0.9660	0.9989	0.8096	5170.56	26.768	26.764	-4.761	0.3019	0.8410
0.3960	72.173	0.2200	0.8752	0.8757	0.9663	0.9991	0.8499	6280.80	27.865	27.862	-3.663	0.3667	0.8755
0.4750	72.226	0.2639	0.8897	0.8901	0.9664	0.9992	0.8670	7533.79	28.324	28.322	-3.203	0.4398	0.8900
0.5660	72.305	0.3144	0.9108	0.9112	0.9665	0.9994	0.8920	8977.10	28.995	28.993	-2.532	0.5241	0.9111
0.6360	72.353	0.3533	0.9234	0.9237	0.9666	0.9995	0.9071	10087.35	29.394	29.393	-2.132	0.5889	0.9236
0.7165	72.403	0.3981	0.9363	0.9366	0.9668	0.9996	0.9226	11364.13	29.804	29.803	-1.722	0.6634	0.9365
0.7960	72.461	0.4422	0.9511	0.9513	0.9669	0.9997	0.9404	12625.04	30.273	30.272	-1.253	0.7370	0.9513
0.8780	72.495	0.4878	0.9597	0.9598	0.9670	0.9997	0.9507	13925.61	30.544	30.543	-0.981	0.8130	0.9598
0.9770	72.574	0.5428	0.9792	0.9793	0.9671	0.9999	0.9745	15495.81	31.164	31.164	-0.360	0.9046	0.9793
1.0770	72.620	0.5983	0.9904	0.9905	0.9672	0.9999	0.9883	17081.87	31.519	31.520	-0.005	0.9972	0.9905
1.2010	72.646	0.6672	0.9967	0.9967	0.9673	1.0000	0.9960	19048.59	31.718	31.719	0.194	1.1120	0.9967
1.3240	72.673	0.7356	1.0032	1.0032	0.9673	1.0000	1.0039	20999.45	31.923	31.925	0.400	1.2259	1.0032
1.4755	72.648	0.8197	0.9972	0.9972	0.9673	1.0000	0.9966	23402.33	31.734	31.734	0.210	1.3662	0.9972
1.6280	72.667	0.9044	1.0018	1.0018	0.9673	1.0000	1.0022	25821.07	31.878	31.879	0.354	1.5074	1.0018
1.8150	72.659	1.0000	0.9998	0.9998	0.9673	1.0000	0.9998	28787.00	31.817	31.818	0.293	1.6806	1.0000
2.0005	72.642	1.1114	0.9958	0.9958	0.9673	1.0000	0.9948	31729.15	31.688	31.689	0.164	1.8523	0.9958
2.2000	72.664	1.2222	1.0010	1.0010	0.9673	1.0000	1.0013	34893.34	31.855	31.856	0.331	2.0370	1.0010
Point 793, M=0.20													
0.0240	103.755	0.0141	0.6615	0.6660	0.9547	1.0052	0.6540	1945.27	23.870	24.037	-11.772	0.0218	0.6647
0.0330	103.838	0.0194	0.6829	0.6873	0.9554	1.0049	0.6756	2674.74	24.633	24.808	-11.001	0.0300	0.6860
0.0420	103.945	0.0247	0.7095	0.7138	0.9563	1.0045	0.7027	3404.22	25.581	25.766	-10.043	0.0382	0.7125
0.0500	103.974	0.0294	0.7166	0.7207	0.9566	1.0043	0.7098	4052.64	25.831	26.020	-9.789	0.0455	0.7195
0.0580	104.052	0.0341	0.7352	0.7392	0.9572	1.0041	0.7287	4701.07	26.492	26.689	-9.121	0.0528	0.7380
0.0700	104.042	0.0412	0.7328	0.7369	0.9571	1.0041	0.7263	5673.70	26.409	26.604	-9.205	0.0637	0.7357
0.0840	104.104	0.0494	0.7473	0.7512	0.9577	1.0039	0.7411	6808.44	26.924	27.125	-8.684	0.0764	0.7501
0.0960	104.174	0.0565	0.7633	0.7671	0.9582	1.0036	0.7574	7781.07	27.493	27.701	-8.108	0.0874	0.7660
0.1100	104.170	0.0647	0.7624	0.7662	0.9582	1.0036	0.7565	8915.81	27.461	27.668	-8.141	0.1001	0.7651

64

Table 6. Continued

(b) Continued

y, in.	pitot pressure, psia	y/δ	M/M_e	u/u_e	ρ/ρ_e	$T_t/T_{t,e}$	$(T_t-T_w)/(T_{t,e}-T_w)$	y^+	u^+	u'/u_τ	$(u'-u_e')/u_\tau$	y/δ_u	u'/u_e'
0.1257	104.215	0.0739	0.7726	0.7762	0.9585	1.0035	0.7668	10188.34	27.820	28.032	-7.777	0.1144	0.7752
0.1470	104.251	0.0865	0.7806	0.7842	0.9588	1.0034	0.7750	11914.77	28.104	28.320	-7.489	0.1338	0.7831
0.1760	104.338	0.1035	0.7996	0.8030	0.9595	1.0031	0.7944	14265.30	28.779	29.003	-6.807	0.1601	0.8020
0.2150	104.415	0.1265	0.8161	0.8193	0.9601	1.0028	0.8112	17426.36	29.362	29.593	-6.216	0.1956	0.8183
0.2660	104.449	0.1565	0.8232	0.8263	0.9604	1.0027	0.8185	21560.06	29.615	29.850	-5.960	0.2420	0.8254
0.3260	104.573	0.1918	0.8488	0.8516	0.9613	1.0023	0.8447	26423.23	30.520	30.767	-5.043	0.2966	0.8508
0.3960	104.688	0.2329	0.8719	0.8743	0.9622	1.0020	0.8683	32096.93	31.334	31.591	-4.218	0.3603	0.8736
0.4750	104.783	0.2794	0.8905	0.8926	0.9629	1.0017	0.8874	38500.11	31.989	32.256	-3.554	0.4322	0.8920
0.5660	104.877	0.3329	0.9085	0.9103	0.9636	1.0014	0.9058	45875.92	32.623	32.899	-2.911	0.5150	0.9098
0.6360	104.987	0.3741	0.9291	0.9305	0.9644	1.0011	0.9270	51549.62	33.349	33.634	-2.175	0.5787	0.9301
0.7165	105.065	0.4215	0.9434	0.9446	0.9650	1.0009	0.9417	58074.37	33.853	34.146	-1.664	0.6520	0.9442
0.7960	105.144	0.4682	0.9577	0.9586	0.9656	1.0007	0.9564	64518.07	34.355	34.655	-1.154	0.7243	0.9583
0.8780	105.195	0.5165	0.9668	0.9675	0.9660	1.0005	0.9658	71164.41	34.675	34.980	-0.829	0.7989	0.9673
0.9770	105.290	0.5747	0.9835	0.9839	0.9666	1.0003	0.9830	79188.64	35.262	35.576	-0.233	0.8890	0.9838
1.0770	105.319	0.6335	0.9886	0.9888	0.9668	1.0002	0.9882	87293.93	35.439	35.756	-0.054	0.9800	0.9888
1.2010	105.368	0.7065	0.9971	0.9971	0.9672	1.0000	0.9970	97344.48	35.736	36.057	0.248	1.0928	0.9971
1.3240	105.366	0.7788	0.9967	0.9968	0.9672	1.0001	0.9966	107313.98	35.724	36.045	0.236	1.2047	0.9968
1.4755	105.385	0.8679	1.0000	1.0000	0.9673	1.0000	1.0000	119593.49	35.838	36.161	0.352	1.3426	1.0000
1.6280	105.379	0.9576	0.9989	0.9990	0.9673	1.0000	0.9989	131954.05	35.802	36.125	0.315	1.4813	0.9990
1.8150	105.395	1.0000	1.0017	1.0016	0.9674	1.0000	1.0017	147110.93	35.899	36.222	0.413	1.6515	1.0000

Point 811, M=0.20

y, in.	pitot pressure, psia	y/δ	M/M_e	u/u_e	ρ/ρ_e	$T_t/T_{t,e}$	$(T_t-T_w)/(T_{t,e}-T_w)$	y^+	u^+	u'/u_τ	$(u'-u_e')/u_\tau$	y/δ_u	u'/u_e'
0.0240	103.826	0.0160	0.6824	0.6827	0.9665	0.9962	0.6450	2096.21	24.100	24.064	-10.829	0.0256	0.6827
0.0330	103.929	0.0220	0.7079	0.7082	0.9665	0.9965	0.6722	2882.29	25.000	24.962	-9.930	0.0352	0.7082
0.0420	104.034	0.0280	0.7329	0.7332	0.9665	0.9968	0.6992	3668.36	25.885	25.845	-9.047	0.0448	0.7333
0.0500	103.993	0.0333	0.7232	0.7236	0.9665	0.9967	0.6888	4367.10	25.543	25.504	-9.388	0.0534	0.7236
0.0580	104.085	0.0387	0.7448	0.7451	0.9665	0.9969	0.7121	5065.84	26.304	26.263	-8.629	0.0619	0.7452
0.0700	104.180	0.0467	0.7664	0.7667	0.9665	0.9972	0.7356	6113.94	27.066	27.024	-7.868	0.0747	0.7668
0.0840	104.221	0.0560	0.7755	0.7758	0.9666	0.9973	0.7456	7336.73	27.389	27.346	-7.547	0.0896	0.7759
0.0960	104.234	0.0640	0.7784	0.7787	0.9666	0.9973	0.7487	8384.83	27.490	27.447	-7.445	0.1025	0.7787
0.1100	104.225	0.0733	0.7764	0.7767	0.9666	0.9973	0.7466	9607.62	27.420	27.377	-7.515	0.1174	0.7768
0.1257	104.308	0.0838	0.7945	0.7948	0.9666	0.9975	0.7665	10978.89	28.060	28.016	-6.877	0.1342	0.7949
0.1470	104.321	0.0980	0.7973	0.7976	0.9666	0.9976	0.7696	12839.27	28.159	28.115	-6.778	0.1569	0.7977
0.1760	104.492	0.1173	0.8333	0.8336	0.9667	0.9980	0.8095	15372.19	29.427	29.381	-5.512	0.1878	0.8336
0.2150	104.497	0.1433	0.8343	0.8346	0.9667	0.9980	0.8106	18778.53	29.464	29.417	-5.475	0.2295	0.8346
0.2660	104.561	0.1773	0.8474	0.8476	0.9667	0.9981	0.8252	23232.97	29.924	29.876	-5.016	0.2839	0.8477
0.3260	104.684	0.2173	0.8719	0.8721	0.9668	0.9984	0.8527	28473.49	30.788	30.738	-4.154	0.3479	0.8721
0.3960	104.762	0.2640	0.8870	0.8873	0.9668	0.9986	0.8699	34587.43	31.323	31.272	-3.620	0.4226	0.8873
0.4750	104.850	0.3167	0.9038	0.9041	0.9669	0.9988	0.8890	41487.45	31.915	31.864	-3.029	0.5069	0.9041
0.5660	104.953	0.3773	0.9231	0.9233	0.9670	0.9991	0.9110	49435.57	32.594	32.542	-2.351	0.6041	0.9233
0.6360	105.048	0.4240	0.9405	0.9407	0.9670	0.9993	0.9310	55549.51	33.207	33.154	-1.739	0.6788	0.9407
0.7165	105.102	0.4777	0.9503	0.9504	0.9671	0.9994	0.9422	62580.54	33.551	33.497	-1.396	0.7647	0.9504
0.7960	105.166	0.5307	0.9617	0.9618	0.9671	0.9995	0.9554	69524.22	33.953	33.899	-0.994	0.8495	0.9618
0.8780	105.259	0.5853	0.9780	0.9781	0.9672	0.9997	0.9744	76686.27	34.529	34.473	-0.419	0.9370	0.9781

Table 6. Continued

(b) Continued

y, in.	pitot pressure, psia	y/δ	M/M_e	u/u_e	ρ/ρ_e	$T_t/T_{t,e}$	$(T_t-T_w)/(T_{t,e}-T_w)$	y^+	u^+	u'/u_τ	$(u'-u_e')/u_\tau$	y/δ_u	u'/u_e'
0.9770	105.375	0.6513	0.9980	0.9981	0.9673	1.0000	0.9977	85333.12	35.233	35.177	0.284	1.0427	0.9981
1.0770	105.384	0.7180	0.9996	0.9996	0.9673	1.0000	0.9995	94067.32	35.287	35.231	0.338	1.1494	0.9996
1.2010	105.424	0.8007	1.0064	1.0064	0.9673	1.0001	1.0075	104897.73	35.527	35.469	0.577	1.2818	1.0064
1.3240	105.449	0.8827	1.0106	1.0106	0.9674	1.0001	1.0124	115640.79	35.675	35.618	0.725	1.4130	1.0106
1.4755	105.376	0.9837	0.9982	0.9982	0.9673	1.0000	0.9979	128873.11	35.239	35.183	0.290	1.5747	0.9982
1.6280	105.441	1.0000	1.0092	1.0092	0.9674	1.0001	1.0108	142192.76	35.628	35.570	0.678	1.7375	1.0000
1.8150	105.385	1.2100	0.9998	0.9998	0.9673	1.0000	0.9997	158525.71	35.294	35.237	0.344	1.9370	0.9998

Point 713, M=0.40

y, in.	pitot pressure, psia	y/δ	M/M_e	u/u_e	ρ/ρ_e	$T_t/T_{t,e}$	$(T_t-T_w)/(T_{t,e}-T_w)$	y^+	u^+	u'/u_τ	$(u'-u_e')/u_\tau$	y/δ_u	u'/u_e'
0.0240	35.667	0.0145	0.5949	0.6005	0.9496	0.9979	0.3620	360.55	19.004	19.038	-12.462	0.0208	0.5986
0.0330	35.893	0.0200	0.6407	0.6461	0.9511	0.9981	0.4188	495.76	20.449	20.491	-11.010	0.0285	0.6443
0.0420	36.046	0.0255	0.6698	0.6751	0.9522	0.9982	0.4570	630.97	21.365	21.413	-10.087	0.0363	0.6733
0.0500	36.085	0.0303	0.6770	0.6822	0.9525	0.9983	0.4667	751.16	21.592	21.641	-9.859	0.0433	0.6805
0.0580	36.154	0.0352	0.6895	0.6947	0.9529	0.9983	0.4839	871.34	21.987	22.039	-9.462	0.0502	0.6930
0.0700	36.222	0.0424	0.7016	0.7067	0.9534	0.9984	0.5007	1051.62	22.368	22.423	-9.078	0.0606	0.7050
0.0840	36.348	0.0509	0.7235	0.7285	0.9542	0.9985	0.5318	1261.94	23.056	23.115	-8.385	0.0727	0.7268
0.0960	36.402	0.0582	0.7327	0.7375	0.9546	0.9985	0.5451	1442.22	23.343	23.405	-8.095	0.0830	0.7359
0.1100	36.421	0.0667	0.7359	0.7407	0.9547	0.9985	0.5498	1652.54	23.443	23.506	-7.994	0.0952	0.7391
0.1257	36.460	0.0762	0.7424	0.7472	0.9550	0.9986	0.5594	1888.41	23.648	23.712	-7.789	0.1087	0.7456
0.1470	36.601	0.0891	0.7654	0.7700	0.9560	0.9987	0.5939	2208.40	24.369	24.440	-7.061	0.1272	0.7685
0.1760	36.665	0.1067	0.7756	0.7801	0.9564	0.9987	0.6095	2644.07	24.689	24.762	-6.738	0.1522	0.7786
0.2150	36.744	0.1303	0.7881	0.7923	0.9569	0.9988	0.6288	3229.97	25.077	25.154	-6.347	0.1860	0.7909
0.2660	36.898	0.1612	0.8116	0.8156	0.9580	0.9989	0.6661	3996.15	25.813	25.897	-5.604	0.2301	0.8143
0.3260	37.012	0.1976	0.8286	0.8323	0.9587	0.9990	0.6936	4897.53	26.343	26.432	-5.069	0.2820	0.8311
0.3960	37.151	0.2400	0.8488	0.8522	0.9596	0.9991	0.7270	5949.15	26.972	27.068	-4.433	0.3426	0.8511
0.4750	37.268	0.2879	0.8654	0.8685	0.9604	0.9992	0.7550	7135.98	27.489	27.589	-3.911	0.4109	0.8675
0.5660	37.438	0.3430	0.8889	0.8916	0.9616	0.9993	0.7955	8503.08	28.218	28.327	-3.173	0.4896	0.8907
0.6360	37.566	0.3855	0.9062	0.9085	0.9624	0.9994	0.8258	9554.70	28.753	28.868	-2.632	0.5502	0.9077
0.7165	37.675	0.4342	0.9206	0.9226	0.9631	0.9995	0.8516	10764.06	29.199	29.320	-2.181	0.6198	0.9219
0.7960	37.850	0.4824	0.9432	0.9446	0.9643	0.9996	0.8927	11958.40	29.898	30.027	-1.473	0.6886	0.9442
0.8780	37.966	0.5321	0.9578	0.9589	0.9650	0.9997	0.9198	13190.29	30.350	30.485	-1.015	0.7595	0.9586
0.9770	38.100	0.5921	0.9744	0.9751	0.9659	0.9998	0.9510	14677.58	30.862	31.004	-0.496	0.8452	0.9749
1.0770	38.145	0.6527	0.9799	0.9805	0.9662	0.9999	0.9614	16179.89	31.032	31.176	-0.324	0.9317	0.9803
1.2010	38.280	0.7279	0.9962	0.9963	0.9671	1.0000	0.9927	18042.76	31.534	31.685	0.185	1.0389	0.9963
1.3240	38.332	0.8024	1.0024	1.0024	0.9674	1.0000	1.0047	19890.60	31.724	31.879	0.378	1.1453	1.0024
1.4755	38.286	0.8942	0.9969	0.9970	0.9671	1.0000	0.9941	22166.60	31.556	31.708	0.207	1.2764	0.9970
1.6280	38.312	0.9867	1.0000	1.0000	0.9673	1.0000	1.0001	24457.63	31.651	31.804	0.304	1.4083	1.0000
1.8150	38.309	1.0000	0.9997	0.9997	0.9673	1.0000	0.9994	27266.95	31.640	31.793	0.293	1.5701	1.0000
2.0005	38.284	1.2124	0.9967	0.9968	0.9671	1.0000	0.9936	30053.74	31.548	31.700	0.200	1.7305	0.9968
2.2000	38.343	1.3333	1.0037	1.0036	0.9675	1.0000	1.0072	33050.85	31.764	31.919	0.419	1.9031	1.0037

Point 671, M=0.40

y, in.	pitot pressure, psia	y/δ	M/M_e	u/u_e	ρ/ρ_e	$T_t/T_{t,e}$	$(T_t-T_w)/(T_{t,e}-T_w)$	y^+	u^+	u'/u_τ	$(u'-u_e')/u_\tau$	y/δ_u	u'/u_e'
0.0240	89.498	0.0141	0.6343	0.6402	0.9495	0.9992	-1.2426	841.40	21.608	21.665	-11.948	0.0212	0.6382
0.0330	89.924	0.0194	0.6668	0.6725	0.9508	0.9992	-1.1277	1156.93	22.698	22.764	-10.849	0.0292	0.6706

66

Table 6. Continued
(b) Continued

y, in.	pitot pressure, psia	y/δ	M/M_e	u/u_e	ρ/ρ_e	$T_t/T_{t,e}$	$(T_t-T_w)/(T_{t,e}-T_w)$	y^+	u^+	u'/u_τ	$(u'-u_e')/u_\tau$	y/δ_u	u'/u_e'
0.0420	90.212	0.0247	0.6878	0.6934	0.9517	0.9993	-1.0443	1472.46	23.404	23.475	-10.138	0.0371	0.6915
0.0500	90.406	0.0294	0.7016	0.7071	0.9522	0.9993	-0.9858	1752.93	23.865	23.940	-9.672	0.0442	0.7052
0.0580	90.541	0.0341	0.7110	0.7164	0.9526	0.9993	-0.9441	2033.39	24.181	24.259	-9.354	0.0512	0.7146
0.0700	90.652	0.0412	0.7186	0.7240	0.9530	0.9993	-0.9092	2454.10	24.437	24.517	-9.096	0.0618	0.7222
0.0840	90.879	0.0494	0.7340	0.7392	0.9536	0.9993	-0.8363	2944.91	24.951	25.035	-8.578	0.0742	0.7375
0.0960	91.045	0.0565	0.7450	0.7502	0.9541	0.9994	-0.7818	3365.62	25.319	25.407	-8.206	0.0848	0.7484
0.1100	91.202	0.0647	0.7553	0.7603	0.9546	0.9994	-0.7293	3856.44	25.661	25.753	-7.860	0.0972	0.7586
0.1257	91.319	0.0739	0.7628	0.7678	0.9549	0.9994	-0.6896	4406.85	25.913	26.007	-7.606	0.1110	0.7661
0.1470	91.511	0.0865	0.7751	0.7798	0.9555	0.9994	-0.6235	5153.60	26.321	26.418	-7.194	0.1299	0.7782
0.1760	91.705	0.1035	0.7872	0.7918	0.9560	0.9994	-0.5556	6170.30	26.725	26.827	-6.786	0.1555	0.7903
0.2150	91.974	0.1265	0.8037	0.8081	0.9568	0.9995	-0.4596	7537.58	27.273	27.381	-6.231	0.1899	0.8066
0.2660	92.265	0.1565	0.8211	0.8252	0.9577	0.9995	-0.3536	9325.56	27.853	27.967	-5.646	0.2350	0.8239
0.3260	92.595	0.1918	0.8404	0.8442	0.9586	0.9996	-0.2309	11429.07	28.493	28.614	-4.998	0.2880	0.8429
0.3960	93.019	0.2329	0.8645	0.8678	0.9598	0.9996	-0.0697	13883.17	29.290	29.421	-4.191	0.3498	0.8667
0.4750	93.379	0.2794	0.8843	0.8873	0.9609	0.9997	0.0699	16652.79	29.947	30.087	-3.526	0.4196	0.8863
0.5660	93.703	0.3329	0.9018	0.9044	0.9618	0.9997	0.1976	19843.12	30.524	30.671	-2.941	0.5000	0.9035
0.6360	93.995	0.3741	0.9172	0.9194	0.9626	0.9998	0.3141	22297.21	31.033	31.187	-2.426	0.5618	0.9187
0.7165	94.366	0.4215	0.9364	0.9382	0.9637	0.9998	0.4639	25119.42	31.664	31.827	-1.786	0.6330	0.9376
0.7960	94.648	0.4682	0.9507	0.9521	0.9645	0.9998	0.5791	27906.57	32.134	32.304	-1.309	0.7032	0.9516
0.8780	94.888	0.5165	0.9626	0.9637	0.9652	0.9999	0.6779	30781.37	32.527	32.702	-0.910	0.7756	0.9634
0.9770	95.160	0.5747	0.9760	0.9767	0.9659	0.9999	0.7907	34252.16	32.965	33.147	-0.465	0.8631	0.9765
1.0770	95.359	0.6335	0.9856	0.9861	0.9665	1.0000	0.8738	37758.01	33.281	33.468	-0.144	0.9514	0.9859
1.2010	95.563	0.7065	0.9954	0.9955	0.9670	1.0000	0.9593	42105.27	33.601	33.794	0.181	1.0610	0.9955
1.3240	95.594	0.7788	0.9969	0.9970	0.9671	1.0000	0.9724	46417.47	33.649	33.843	0.230	1.1696	0.9969
1.4755	95.665	0.8679	1.0003	1.0002	0.9673	1.0000	1.0023	51728.83	33.760	33.955	0.342	1.3034	1.0002
1.6280	95.640	0.9576	0.9991	0.9991	0.9673	1.0000	0.9917	57075.25	33.721	33.915	0.303	1.4382	0.9991
1.8150	95.691	1.0000	1.0015	1.0014	0.9674	1.0000	1.0132	63631.19	33.800	33.996	0.383	1.6034	1.0000
2.0005	95.625	1.1768	0.9984	0.9984	0.9672	1.0000	0.9854	70134.55	33.697	33.892	0.279	1.7672	0.9984
2.2000	95.618	1.2941	0.9980	0.9981	0.9672	1.0000	0.9825	77128.72	33.687	33.881	0.268	1.9435	0.9981

Point 927, M=0.40

y, in.	pitot pressure, psia	y/δ	M/M_e	u/u_e	ρ/ρ_e	$T_t/T_{t,e}$	$(T_t-T_w)/(T_{t,e}-T_w)$	y^+	u^+	u'/u_τ	$(u'-u_e')/u_\tau$	y/δ_u	u'/u_e'
0.0240	22.092	0.0141	0.6610	0.6678	0.9480	1.0011	0.7735	837.13	22.201	22.302	-10.873	0.0231	0.6655
0.0330	22.137	0.0194	0.6746	0.6813	0.9486	1.0011	0.7848	1151.05	22.651	22.757	-10.418	0.0318	0.6791
0.0420	22.195	0.0247	0.6918	0.6983	0.9495	1.0010	0.7987	1464.98	23.217	23.329	-9.846	0.0405	0.6962
0.0500	22.224	0.0294	0.7002	0.7067	0.9499	1.0010	0.8054	1744.02	23.494	23.609	-9.566	0.0482	0.7045
0.0580	22.256	0.0341	0.7094	0.7157	0.9503	1.0009	0.8127	2023.07	23.796	23.914	-9.261	0.0559	0.7136
0.0700	22.332	0.0412	0.7306	0.7368	0.9514	1.0009	0.8292	2441.63	24.495	24.621	-8.554	0.0675	0.7347
0.0840	22.393	0.0494	0.7472	0.7531	0.9523	1.0008	0.8417	2929.96	25.039	25.172	-8.003	0.0810	0.7512
0.0960	22.361	0.0565	0.7386	0.7446	0.9518	1.0008	0.8352	3348.52	24.755	24.884	-8.290	0.0926	0.7426
0.1100	22.439	0.0647	0.7594	0.7652	0.9529	1.0008	0.8508	3836.85	25.441	25.579	-7.596	0.1061	0.7633
0.1257	22.509	0.0739	0.7777	0.7832	0.9539	1.0007	0.8641	4384.47	26.038	26.183	-6.991	0.1212	0.7814
0.1470	22.557	0.0865	0.7899	0.7952	0.9545	1.0006	0.8728	5127.42	26.438	26.589	-6.586	0.1418	0.7935
0.1760	22.601	0.1035	0.8009	0.8061	0.9551	1.0006	0.8806	6138.96	26.799	26.955	-6.220	0.1697	0.8044
0.2150	22.632	0.1265	0.8086	0.8136	0.9556	1.0006	0.8859	7499.29	27.050	27.209	-5.966	0.2073	0.8120

Table 6. Continued
(b) Continued

y, in.	pitot pressure, psia	y/δ	M/M_e	u/u_e	ρ/ρ_e	$T_t/T_{t,e}$	$(T_t-T_w)/(T_{t,e}-T_w)$	y^+	u^+	u'/u_τ	$(u'-u_e')/u_\tau$	y/δ_u	u'/u_e'
0.2660	22.728	0.1565	0.8319	0.8365	0.9569	1.0005	0.9016	9278.20	27.809	27.979	-5.196	0.2565	0.8350
0.3260	22.802	0.1918	0.8493	0.8536	0.9579	1.0004	0.9131	11371.02	28.378	28.556	-4.619	0.3144	0.8522
0.3960	22.891	0.2329	0.8698	0.8736	0.9591	1.0004	0.9262	13812.65	29.044	29.232	-3.942	0.3819	0.8724
0.4750	22.960	0.2794	0.8853	0.8887	0.9600	1.0003	0.9359	16568.21	29.547	29.744	-3.431	0.4581	0.8876
0.5660	23.097	0.3329	0.9153	0.9179	0.9618	1.0002	0.9538	19742.33	30.517	30.730	-2.445	0.5458	0.9171
0.6360	23.170	0.3741	0.9308	0.9330	0.9628	1.0002	0.9628	22183.96	31.018	31.240	-1.935	0.6133	0.9323
0.7165	23.203	0.4215	0.9377	0.9397	0.9632	1.0002	0.9667	24991.83	31.241	31.467	-1.708	0.6909	0.9391
0.7960	23.285	0.4682	0.9546	0.9561	0.9643	1.0001	0.9761	27764.83	31.788	32.023	-1.152	0.7676	0.9557
0.8780	23.345	0.5165	0.9668	0.9679	0.9651	1.0001	0.9827	30625.02	32.180	32.422	-0.752	0.8467	0.9676
0.9770	23.430	0.5747	0.9838	0.9843	0.9662	1.0000	0.9917	34078.18	32.725	32.978	-0.197	0.9421	0.9842
1.0770	23.481	0.6335	0.9938	0.9940	0.9669	1.0000	0.9968	37566.23	33.047	33.306	0.131	1.0386	0.9939
1.2010	23.494	0.7065	0.9963	0.9965	0.9671	1.0000	0.9981	41891.40	33.128	33.389	0.214	1.1581	0.9964
1.3240	23.513	0.7788	1.0000	1.0000	0.9673	1.0000	1.0000	46181.69	33.246	33.510	0.335	1.2768	1.0000
1.4755	23.517	0.8679	1.0008	1.0008	0.9674	1.0000	1.0004	51466.08	33.271	33.535	0.360	1.4229	1.0008
1.6280	23.516	0.9576	1.0006	1.0006	0.9674	1.0000	1.0003	56785.35	33.265	33.529	0.354	1.5699	1.0006
1.8150	23.508	1.0000	0.9990	0.9991	0.9673	1.0000	0.9995	63307.99	33.215	33.478	0.303	1.7502	1.0000
2.2000	23.520	1.2941	1.0014	1.0013	0.9674	1.0000	1.0007	76736.95	33.290	33.554	0.379	2.1215	1.0013

Point 867, M=0.40

y, in.	pitot pressure, psia	y/δ	M/M_e	u/u_e	ρ/ρ_e	$T_t/T_{t,e}$	$(T_t-T_w)/(T_{t,e}-T_w)$	y^+	u^+	u'/u_τ	$(u'-u_e')/u_\tau$	y/δ_u	u'/u_e'
0.0240	51.770	0.0141	0.6721	0.6791	0.9479	1.0002	0.9181	1882.57	23.840	23.975	-11.069	0.0246	0.6770
0.0330	51.889	0.0194	0.6873	0.6942	0.9487	1.0002	0.9271	2588.54	24.373	24.513	-10.531	0.0338	0.6922
0.0420	52.083	0.0247	0.7115	0.7182	0.9499	1.0001	0.9402	3294.50	25.214	25.364	-9.680	0.0431	0.7162
0.0500	52.183	0.0294	0.7236	0.7302	0.9505	1.0001	0.9463	3922.03	25.635	25.790	-9.254	0.0513	0.7283
0.0580	52.242	0.0341	0.7307	0.7371	0.9509	1.0001	0.9497	4549.55	25.880	26.038	-9.006	0.0595	0.7352
0.0700	52.329	0.0412	0.7410	0.7473	0.9514	1.0001	0.9544	5490.84	26.236	26.398	-8.646	0.0718	0.7454
0.0840	52.479	0.0494	0.7583	0.7644	0.9523	1.0001	0.9619	6589.01	26.836	27.007	-8.037	0.0862	0.7626
0.0960	52.561	0.0565	0.7676	0.7736	0.9529	1.0001	0.9657	7530.30	27.158	27.333	-7.711	0.0985	0.7718
0.1100	52.634	0.0647	0.7758	0.7816	0.9533	1.0001	0.9689	8628.46	27.441	27.619	-7.425	0.1128	0.7799
0.1257	52.734	0.0739	0.7868	0.7925	0.9539	1.0001	0.9729	9859.98	27.823	28.006	-7.038	0.1289	0.7908
0.1470	52.869	0.0865	0.8015	0.8069	0.9547	1.0001	0.9778	11530.77	28.328	28.519	-6.525	0.1508	0.8053
0.1760	52.962	0.1035	0.8114	0.8166	0.9553	1.0000	0.9809	13805.54	28.671	28.866	-6.178	0.1805	0.8151
0.2150	53.122	0.1265	0.8282	0.8331	0.9563	1.0000	0.9856	16864.72	29.248	29.452	-5.592	0.2205	0.8317
0.2660	53.273	0.1565	0.8437	0.8482	0.9572	1.0000	0.9895	20865.19	29.781	29.993	-5.051	0.2728	0.8469
0.3260	53.473	0.1918	0.8637	0.8678	0.9584	1.0000	0.9937	25571.63	30.468	30.691	-4.353	0.3344	0.8667
0.3960	53.656	0.2329	0.8816	0.8853	0.9595	1.0000	0.9967	31062.47	31.082	31.314	-3.730	0.4062	0.8842
0.4750	53.882	0.2794	0.9032	0.9063	0.9609	1.0000	0.9995	37259.27	31.819	32.063	-2.980	0.4872	0.9054
0.5660	54.037	0.3329	0.9177	0.9204	0.9618	1.0000	1.0008	44397.37	32.312	32.565	-2.478	0.5805	0.9196
0.6360	54.274	0.3741	0.9393	0.9413	0.9632	1.0000	1.0019	49888.21	33.048	33.315	-1.729	0.6523	0.9407
0.7165	54.424	0.4215	0.9527	0.9543	0.9641	1.0000	1.0021	56202.67	33.504	33.779	-1.265	0.7349	0.9538
0.7960	54.601	0.4682	0.9682	0.9693	0.9651	1.0000	1.0019	62438.70	34.032	34.316	-0.728	0.8164	0.9690
0.8780	54.715	0.5165	0.9781	0.9789	0.9658	1.0000	1.0016	68870.83	34.366	34.657	-0.387	0.9005	0.9786
0.9770	54.849	0.5747	0.9895	0.9899	0.9666	1.0000	1.0009	76636.45	34.753	35.052	0.008	1.0021	0.9898
1.0770	54.936	0.6335	0.9969	0.9970	0.9671	1.0000	1.0003	84480.50	35.002	35.305	0.262	1.1046	0.9969
1.2010	54.927	0.7065	0.9961	0.9962	0.9670	1.0000	1.0003	94207.14	34.976	35.279	0.235	1.2318	0.9962

68

Table 6. Continued
(b) Continued

y, in.	pitot pressure, psia	y/δ	M/M_e	u/u_e	ρ/ρ_e	$T_r/T_{t,e}$	$(T_r-T_w)/(T_{t,e}-T_w)$	y^+	u^+	u'/u_τ	$(u'-u_e')/u_\tau$	y/δ_u	u'/u_e'
1.3240	54.940	0.7788	0.9972	0.9973	0.9671	1.0000	1.0003	103855.33	35.013	35.317	0.273	1.3579	0.9973
1.4755	54.984	0.8679	1.0009	1.0009	0.9674	1.0000	0.9999	115739.07	35.138	35.444	0.400	1.5133	1.0009
1.6280	54.968	0.9576	0.9995	0.9996	0.9673	1.0000	1.0000	127701.26	35.093	35.398	0.354	1.6697	0.9996
1.8150	54.982	1.0000	1.0007	1.0007	0.9674	1.0000	0.9999	142369.65	35.133	35.438	0.395	1.8615	1.0000
2.2000	54.956	1.2941	0.9985	0.9986	0.9672	1.0000	1.0001	172569.27	35.059	35.363	0.320	2.2564	0.9986

Point 813, M=0.40

y, in.	pitot pressure, psia	y/δ	M/M_e	u/u_e	ρ/ρ_e	$T_r/T_{t,e}$	$(T_r-T_w)/(T_{t,e}-T_w)$	y^+	u^+	u'/u_τ	$(u'-u_e')/u_\tau$	y/δ_u	u'/u_e'
0.0240	96.553	0.0141	0.6739	0.6889	0.9274	1.0146	0.6803	3183.33	24.865	25.406	-11.323	0.0228	0.6846
0.0330	96.844	0.0194	0.6939	0.7084	0.9295	1.0137	0.7001	4377.08	25.570	26.136	-10.594	0.0313	0.7042
0.0420	97.089	0.0247	0.7102	0.7244	0.9313	1.0130	0.7164	5570.82	26.146	26.732	-9.997	0.0399	0.7203
0.0500	97.218	0.0294	0.7186	0.7326	0.9322	1.0126	0.7247	6631.93	26.442	27.040	-9.690	0.0475	0.7286
0.0580	97.359	0.0341	0.7277	0.7415	0.9333	1.0122	0.7338	7693.04	26.762	27.371	-9.358	0.0551	0.7375
0.0700	97.538	0.0412	0.7391	0.7525	0.9345	1.0117	0.7450	9284.71	27.161	27.785	-8.944	0.0665	0.7487
0.0840	97.788	0.0494	0.7547	0.7676	0.9363	1.0110	0.7604	11141.65	27.707	28.351	-8.378	0.0798	0.7639
0.0960	97.885	0.0565	0.7606	0.7734	0.9370	1.0107	0.7663	12733.31	27.914	28.567	-8.162	0.0912	0.7697
0.1100	97.917	0.0647	0.7626	0.7753	0.9372	1.0106	0.7683	14590.26	27.983	28.638	-8.091	0.1045	0.7717
0.1257	98.182	0.0739	0.7786	0.7907	0.9390	1.0099	0.7840	16672.68	28.539	29.217	-7.513	0.1194	0.7872
0.1470	98.340	0.0865	0.7879	0.7997	0.9401	1.0095	0.7933	19497.89	28.865	29.555	-7.174	0.1396	0.7964
0.1760	98.506	0.1035	0.7976	0.8090	0.9413	1.0090	0.8028	23344.41	29.201	29.905	-6.824	0.1671	0.8058
0.2150	98.859	0.1265	0.8178	0.8284	0.9437	1.0081	0.8227	28517.32	29.901	30.634	-6.095	0.2042	0.8254
0.2660	99.086	0.1565	0.8305	0.8406	0.9452	1.0075	0.8352	35281.89	30.340	31.091	-5.638	0.2526	0.8377
0.3260	99.475	0.1918	0.8518	0.8609	0.9478	1.0066	0.8561	43240.21	31.073	31.856	-4.874	0.3096	0.8583
0.3960	99.795	0.2329	0.8689	0.8771	0.9500	1.0058	0.8728	52524.92	31.659	32.468	-4.262	0.3761	0.8748
0.4750	100.207	0.2794	0.8904	0.8975	0.9527	1.0049	0.8938	63003.38	32.393	33.234	-3.495	0.4511	0.8955
0.5660	100.559	0.3329	0.9082	0.9143	0.9550	1.0041	0.9112	75073.50	33.002	33.871	-2.858	0.5375	0.9127
0.6360	100.927	0.3741	0.9265	0.9315	0.9574	1.0033	0.9290	84358.20	33.623	34.521	-2.208	0.6040	0.9302
0.7165	101.262	0.4215	0.9428	0.9468	0.9595	1.0025	0.9448	95035.62	34.174	35.099	-1.631	0.6804	0.9457
0.7960	101.583	0.4682	0.9582	0.9611	0.9616	1.0018	0.9596	105580.39	34.691	35.641	-1.089	0.7559	0.9603
0.8780	101.836	0.5165	0.9701	0.9722	0.9632	1.0013	0.9711	116456.77	35.091	36.060	-0.669	0.8338	0.9716
0.9770	102.094	0.5747	0.9820	0.9833	0.9648	1.0008	0.9827	129588.00	35.492	36.481	-0.248	0.9278	0.9830
1.0770	102.297	0.6335	0.9913	0.9919	0.9661	1.0004	0.9916	142851.86	35.803	36.808	0.078	1.0228	0.9918
1.2010	102.433	0.7065	0.9975	0.9977	0.9670	1.0001	0.9976	159299.06	36.010	37.024	0.295	1.1406	0.9976
1.3240	102.495	0.7788	1.0003	1.0003	0.9674	1.0000	1.0003	175613.62	36.103	37.122	0.393	1.2574	1.0003
1.4755	102.487	0.8679	0.9999	0.9999	0.9673	1.0000	0.9999	195708.38	36.091	37.110	0.381	1.4012	0.9999
1.6280	102.479	0.9576	0.9995	0.9996	0.9673	1.0000	0.9996	215935.78	36.079	37.097	0.368	1.5461	0.9996
1.8150	102.505	1.0000	1.0007	1.0007	0.9674	1.0000	1.0007	240739.21	36.118	37.138	0.409	1.7236	1.0000
2.2000	102.527	1.2941	1.0017	1.0016	0.9676	0.9999	1.0016	291805.11	36.151	37.173	0.444	2.0893	1.0016

Point 734, M=0.60

y, in.	pitot pressure, psia	y/δ	M/M_e	u/u_e	ρ/ρ_e	$T_r/T_{t,e}$	$(T_r-T_w)/(T_{t,e}-T_w)$	y^+	u^+	u'/u_τ	$(u'-u_e')/u_\tau$	y/δ_u	u'/u_e'
0.0240	23.872	0.0141	0.6054	0.6183	0.9276	0.9977	-0.1878	340.55	19.331	19.425	-11.896	0.0214	0.6139
0.0330	24.155	0.0194	0.6435	0.6561	0.9306	0.9979	-0.1146	468.25	20.513	20.624	-10.696	0.0294	0.6518
0.0420	24.333	0.0247	0.6662	0.6785	0.9325	0.9980	-0.0665	595.96	21.215	21.337	-9.984	0.0374	0.6744
0.0500	24.468	0.0294	0.6828	0.6949	0.9339	0.9980	-0.0292	709.47	21.727	21.859	-9.462	0.0445	0.6909
0.0580	24.505	0.0341	0.6873	0.6993	0.9343	0.9981	-0.0188	822.99	21.865	21.999	-9.322	0.0516	0.6953

Table 6. Continued
(b) Continued

y, in.	pitot pressure, psia	y/δ	M/M_e	u/u_e	ρ/ρ_e	$T_t/T_{t,e}$	$(T_t-T_w)/(T_{t,e}-T_w)$	y^+	u^+	u'/u_τ	$(u'-u_e')/u_\tau$	y/δ_u	u'/u_e'
0.0700	24.593	0.0412	0.6978	0.7097	0.9352	0.9981	0.0060	993.26	22.189	22.328	-8.993	0.0623	0.7057
0.0840	24.774	0.0494	0.7189	0.7303	0.9371	0.9982	0.0577	1191.91	22.835	22.986	-8.334	0.0747	0.7265
0.0960	24.863	0.0565	0.7289	0.7402	0.9380	0.9983	0.0835	1362.19	23.144	23.301	-8.019	0.0854	0.7364
0.1100	24.942	0.0647	0.7378	0.7489	0.9388	0.9983	0.1065	1560.84	23.414	23.576	-7.744	0.0979	0.7451
0.1257	25.022	0.0739	0.7466	0.7575	0.9397	0.9983	0.1300	1783.61	23.683	23.851	-7.470	0.1118	0.7538
0.1470	25.139	0.0865	0.7592	0.7698	0.9409	0.9984	0.1646	2085.85	24.069	24.245	-7.076	0.1308	0.7663
0.1760	25.301	0.1035	0.7763	0.7865	0.9425	0.9985	0.2130	2497.34	24.591	24.777	-6.544	0.1566	0.7831
0.2150	25.473	0.1265	0.7940	0.8037	0.9443	0.9986	0.2648	3050.73	25.128	25.326	-5.995	0.1913	0.8004
0.2660	25.634	0.1565	0.8102	0.8193	0.9459	0.9987	0.3136	3774.39	25.616	25.826	-5.495	0.2367	0.8162
0.3260	25.866	0.1918	0.8327	0.8411	0.9482	0.9988	0.3846	4625.76	26.298	26.524	-4.797	0.2900	0.8383
0.3960	26.048	0.2329	0.8499	0.8576	0.9500	0.9989	0.4406	5619.02	26.815	27.054	-4.266	0.3523	0.8551
0.4750	26.311	0.2794	0.8740	0.8808	0.9526	0.9991	0.5221	6739.98	27.538	27.796	-3.524	0.4226	0.8785
0.5660	26.553	0.3329	0.8955	0.9013	0.9550	0.9992	0.5973	8031.22	28.179	28.455	-2.866	0.5036	0.8993
0.6360	26.732	0.3741	0.9110	0.9160	0.9567	0.9993	0.6531	9024.48	28.639	28.929	-2.392	0.5658	0.9143
0.7165	26.952	0.4215	0.9295	0.9336	0.9588	0.9995	0.7219	10166.73	29.190	29.496	-1.825	0.6375	0.9322
0.7960	27.119	0.4682	0.9433	0.9466	0.9605	0.9996	0.7741	11294.79	29.598	29.916	-1.404	0.7082	0.9455
0.8780	27.315	0.5165	0.9591	0.9616	0.9623	0.9997	0.8354	12458.33	30.065	30.399	-0.922	0.7811	0.9608
0.9770	27.505	0.5747	0.9741	0.9757	0.9641	0.9998	0.8949	13863.08	30.508	30.856	-0.465	0.8692	0.9752
1.0770	27.641	0.6335	0.9847	0.9857	0.9654	0.9999	0.9374	15282.03	30.818	31.176	-0.144	0.9582	0.9853
1.2010	27.805	0.7065	0.9973	0.9974	0.9670	1.0000	0.9887	17041.52	31.186	31.557	0.236	1.0685	0.9974
1.3240	27.882	0.7788	1.0031	1.0029	0.9677	1.0000	1.0127	18786.82	31.356	31.733	0.413	1.1779	1.0029
1.4755	27.853	0.8679	1.0009	1.0008	0.9674	1.0000	1.0037	20936.52	31.292	31.667	0.346	1.3127	1.0009
1.6280	27.827	0.9576	0.9989	0.9990	0.9672	1.0000	0.9956	23100.41	31.235	31.607	0.287	1.4484	0.9990
1.8150	27.864	1.0000	1.0017	1.0016	0.9675	1.0000	1.0071	25753.83	31.316	31.692	0.371	1.6148	1.0000
2.0005	27.884	1.1768	1.0032	1.0030	0.9677	1.0000	1.0134	28385.97	31.361	31.738	0.417	1.7798	1.0031
2.2000	27.877	1.2941	1.0027	1.0025	0.9676	1.0000	1.0112	31216.77	31.345	31.722	0.401	1.9573	1.0026

Point 879, M=0.60

y, in.	pitot pressure, psia	y/δ	M/M_e	u/u_e	ρ/ρ_e	$T_t/T_{t,e}$	$(T_t-T_w)/(T_{t,e}-T_w)$	y^+	u^+	u'/u_τ	$(u'-u_e')/u_\tau$	y/δ_u	u'/u_e'
0.0240	34.520	0.0141	0.6630	0.6774	0.9272	0.9998	1.0588	1752.24	23.451	23.683	-11.151	0.0246	0.6730
0.0330	34.754	0.0194	0.6835	0.6977	0.9292	0.9998	1.0658	2409.32	24.151	24.398	-10.435	0.0338	0.6933
0.0420	35.005	0.0247	0.7048	0.7185	0.9313	0.9998	1.0715	3066.41	24.874	25.138	-9.696	0.0431	0.7143
0.0500	35.108	0.0294	0.7133	0.7269	0.9322	0.9998	1.0734	3650.49	25.162	25.433	-9.400	0.0513	0.7227
0.0580	35.249	0.0341	0.7248	0.7381	0.9334	0.9997	1.0755	4234.57	25.550	25.831	-9.003	0.0595	0.7340
0.0700	35.361	0.0412	0.7338	0.7468	0.9343	0.9997	1.0768	5110.69	25.853	26.141	-8.693	0.0718	0.7428
0.0840	35.588	0.0494	0.7515	0.7641	0.9362	0.9997	1.0787	6132.83	26.452	26.755	-8.079	0.0862	0.7603
0.0960	35.686	0.0565	0.7591	0.7714	0.9371	0.9997	1.0792	7008.94	26.705	27.014	-7.819	0.0985	0.7677
0.1100	35.801	0.0647	0.7678	0.7799	0.9380	0.9997	1.0795	8031.08	26.997	27.315	-7.519	0.1128	0.7762
0.1257	35.948	0.0739	0.7787	0.7905	0.9392	0.9997	1.0796	9177.34	27.365	27.692	-7.141	0.1289	0.7869
0.1470	36.116	0.0865	0.7910	0.8024	0.9406	0.9997	1.0791	10732.45	27.776	28.115	-6.718	0.1508	0.7989
0.1760	36.332	0.1035	0.8065	0.8173	0.9424	0.9997	1.0779	12849.73	28.293	28.647	-6.187	0.1805	0.8140
0.2150	36.534	0.1265	0.8207	0.8309	0.9440	0.9997	1.0761	15697.12	28.765	29.132	-5.701	0.2205	0.8278
0.2660	36.824	0.1565	0.8405	0.8499	0.9464	0.9998	1.0726	19420.62	29.422	29.809	-5.024	0.2728	0.8471
0.3260	37.131	0.1918	0.8609	0.8694	0.9489	0.9998	1.0676	23801.21	30.096	30.504	-4.329	0.3344	0.8668
0.3960	37.405	0.2329	0.8786	0.8862	0.9511	0.9998	1.0622	28911.90	30.678	31.105	-3.728	0.4062	0.8839

Table 6. Continued
(b) Continued

y, in.	pitot pressure, psia	y/δ	M/M_e	u/u_e	ρ/ρ_e	$T_t/T_{t,e}$	$(T_t-T_w)/(T_{t,e}-T_w)$	y⁺	u⁺	u'/u_τ	(u'-u_e')/u_τ	y/δ_u	u'/u_e'
0.4750	37.746	0.2794	0.9000	0.9065	0.9538	0.9998	1.0544	34679.67	31.380	31.831	-3.003	0.4872	0.9045
0.5660	38.020	0.3329	0.9167	0.9223	0.9559	0.9998	1.0474	41323.57	31.927	32.397	-2.437	0.5805	0.9206
0.6360	38.367	0.3741	0.9374	0.9417	0.9587	0.9999	1.0375	46434.26	32.599	33.093	-1.740	0.6523	0.9404
0.7165	38.594	0.4215	0.9506	0.9540	0.9604	0.9999	1.0306	52311.55	33.027	33.537	-1.296	0.7349	0.9530
0.7960	38.861	0.4682	0.9658	0.9683	0.9625	0.9999	1.0219	58115.83	33.519	34.048	-0.785	0.8164	0.9675
0.8780	39.070	0.5165	0.9775	0.9792	0.9641	0.9999	1.0148	64102.64	33.896	34.440	-0.393	0.9005	0.9787
0.9770	39.288	0.5747	0.9895	0.9903	0.9658	1.0000	1.0071	71330.61	34.282	34.841	0.008	1.0021	0.9901
1.0770	39.415	0.6335	0.9964	0.9967	0.9668	1.0000	1.0024	78631.60	34.504	35.072	0.239	1.1046	0.9966
1.2010	39.460	0.7065	0.9989	0.9990	0.9672	1.0000	1.0008	87684.82	34.581	35.153	0.320	1.2318	0.9989
1.3240	39.504	0.7788	1.0013	1.0012	0.9675	1.0000	0.9991	96665.03	34.657	35.232	0.399	1.3579	1.0012
1.4755	39.486	0.8679	1.0003	1.0003	0.9674	1.0000	0.9998	107726.02	34.626	35.200	0.367	1.5133	1.0003
1.6280	39.480	0.9576	1.0000	1.0000	0.9673	1.0000	1.0000	118860.02	34.616	35.189	0.356	1.6697	1.0000
1.8150	39.482	1.0000	1.0001	1.0001	0.9673	1.0000	1.0000	132512.86	34.619	35.193	0.360	1.8615	1.0000
2.2000	39.489	1.2941	1.0004	1.0004	0.9674	1.0000	0.9997	160621.65	34.632	35.205	0.372	2.2564	1.0004

Point 841, M=0.60

y, in.	pitot pressure, psia	y/δ	M/M_e	u/u_e	ρ/ρ_e	$T_t/T_{t,e}$	$(T_t-T_w)/(T_{t,e}-T_w)$	y⁺	u⁺	u'/u_τ	(u'-u_e')/u_τ	y/δ_u	u'/u_e'
0.0240	64.538	0.0141	0.6790	0.6941	0.9268	0.9979	0.1009	3192.53	25.094	25.406	-11.033	0.0240	0.6900
0.0330	64.774	0.0194	0.6899	0.7048	0.9279	0.9979	0.1235	4389.73	25.481	25.802	-10.637	0.0329	0.7008
0.0420	65.258	0.0247	0.7116	0.7261	0.9302	0.9981	0.1704	5586.93	26.251	26.591	-9.848	0.0419	0.7222
0.0500	65.471	0.0294	0.7209	0.7352	0.9312	0.9981	0.1913	6651.11	26.581	26.929	-9.510	0.0499	0.7314
0.0580	65.762	0.0341	0.7335	0.7474	0.9326	0.9982	0.2199	7715.29	27.022	27.381	-9.058	0.0579	0.7437
0.0700	65.950	0.0412	0.7414	0.7552	0.9334	0.9982	0.2386	9311.55	27.302	27.669	-8.771	0.0699	0.7515
0.0840	66.315	0.0494	0.7566	0.7699	0.9351	0.9983	0.2749	11173.86	27.834	28.215	-8.224	0.0838	0.7663
0.0960	66.517	0.0565	0.7648	0.7779	0.9361	0.9983	0.2951	12770.13	28.122	28.512	-7.928	0.0958	0.7744
0.1100	66.726	0.0647	0.7732	0.7860	0.9370	0.9984	0.3160	14632.44	28.416	28.814	-7.625	0.1098	0.7826
0.1257	67.001	0.0739	0.7841	0.7965	0.9383	0.9985	0.3437	16720.89	28.797	29.205	-7.234	0.1254	0.7932
0.1470	67.301	0.0865	0.7958	0.8078	0.9397	0.9985	0.3739	19554.26	29.204	29.624	-6.815	0.1467	0.8046
0.1760	67.593	0.1035	0.8070	0.8185	0.9410	0.9986	0.4035	23411.91	29.592	30.024	-6.415	0.1756	0.8155
0.2150	68.031	0.1265	0.8234	0.8343	0.9430	0.9987	0.4479	28599.77	30.161	30.611	-5.828	0.2146	0.8314
0.2660	68.533	0.1565	0.8417	0.8518	0.9453	0.9988	0.4990	35383.90	30.795	31.264	-5.175	0.2655	0.8491
0.3260	69.028	0.1918	0.8594	0.8685	0.9476	0.9989	0.5495	43365.23	31.400	31.890	-4.550	0.3253	0.8661
0.3960	69.618	0.2329	0.8798	0.8879	0.9502	0.9991	0.6098	52676.79	32.100	32.613	-3.826	0.3952	0.8858
0.4750	70.253	0.2794	0.9011	0.9080	0.9531	0.9992	0.6746	63185.54	32.827	33.365	-3.074	0.4741	0.9062
0.5660	70.849	0.3329	0.9206	0.9263	0.9558	0.9994	0.7355	75290.56	33.488	34.050	-2.390	0.5649	0.9248
0.6360	71.365	0.3741	0.9370	0.9416	0.9581	0.9995	0.7881	84602.11	34.043	34.626	-1.814	0.6347	0.9404
0.7165	71.862	0.4215	0.9525	0.9561	0.9603	0.9996	0.8387	95310.40	34.564	35.167	-1.273	0.7151	0.9551
0.7960	72.325	0.4682	0.9666	0.9692	0.9623	0.9997	0.8857	105885.66	35.038	35.659	-0.780	0.7944	0.9685
0.8780	72.673	0.5165	0.9770	0.9788	0.9639	0.9998	0.9209	116793.48	35.388	36.023	-0.416	0.8762	0.9784
0.9770	73.015	0.5747	0.9872	0.9882	0.9654	0.9999	0.9555	129962.68	35.725	36.374	-0.065	0.9750	0.9879
1.0770	73.271	0.6335	0.9946	0.9951	0.9665	1.0000	0.9814	143264.90	35.975	36.634	0.195	1.0749	0.9950
1.2010	73.360	0.7065	0.9972	0.9975	0.9669	1.0000	0.9904	159759.65	36.061	36.723	0.284	1.1986	0.9974
1.3240	73.457	0.7788	1.0000	1.0000	0.9673	1.0000	1.0001	176121.38	36.154	36.821	0.382	1.3214	1.0000
1.4755	73.429	0.8679	0.9992	0.9993	0.9672	1.0000	0.9973	196274.24	36.127	36.793	0.354	1.4726	0.9993
1.6280	73.461	0.9576	1.0002	1.0001	0.9673	1.0000	1.0005	216560.12	36.158	36.825	0.386	1.6248	1.0001

Table 6. Continued

(b) Continued

y, in.	pitot pressure, psia	y/δ	M/M_e	u/u_e	ρ/ρ_e	$T_t/T_{t,e}$	$(T_t-T_w)/(T_{t,e}-T_w)$	y^+	u^+	u'/u_τ	$(u'-u_e')/u_\tau$	y/δ_u	u'/u_e'
1.8150	73.447	1.0000	0.9998	0.9998	0.9673	1.0000	0.9991	241435.27	36.145	36.811	0.372	1.8114	1.0000
2.2000	73.459	1.2941	1.0001	1.0001	0.9673	1.0000	1.0003	292648.82	36.156	36.823	0.384	2.1956	1.0001

Point 848, M=0.60

y, in.	pitot pressure, psia	y/δ	M/M_e	u/u_e	ρ/ρ_e	$T_t/T_{t,e}$	$(T_t-T_w)/(T_{t,e}-T_w)$	y^+	u^+	u'/u_τ	$(u'-u_e')/u_\tau$	y/δ_u	u'/u_e'
0.0240	64.499	0.0141	0.6745	0.6916	0.9215	1.0024	0.7872	3131.36	24.807	25.200	-11.127	0.0240	0.6867
0.0330	64.844	0.0194	0.6905	0.7073	0.9234	1.0023	0.8000	4305.62	25.371	25.780	-10.547	0.0329	0.7025
0.0420	65.270	0.0247	0.7097	0.7260	0.9256	1.0021	0.8152	5479.88	26.044	26.474	-9.853	0.0419	0.7214
0.0500	65.481	0.0294	0.7190	0.7351	0.9268	1.0020	0.8224	6523.67	26.369	26.809	-9.518	0.0499	0.7306
0.0580	65.726	0.0341	0.7297	0.7454	0.9281	1.0019	0.8304	7567.45	26.739	27.191	-9.136	0.0579	0.7410
0.0700	66.029	0.0412	0.7425	0.7579	0.9297	1.0018	0.8401	9133.13	27.187	27.654	-8.673	0.0699	0.7536
0.0840	66.357	0.0494	0.7562	0.7711	0.9314	1.0017	0.8502	10959.76	27.661	28.144	-8.184	0.0838	0.7669
0.0960	66.473	0.0565	0.7610	0.7757	0.9320	1.0017	0.8537	12525.44	27.826	28.314	-8.013	0.0958	0.7716
0.1100	66.689	0.0647	0.7697	0.7841	0.9331	1.0016	0.8600	14352.06	28.129	28.628	-7.700	0.1098	0.7801
0.1257	66.999	0.0739	0.7821	0.7960	0.9348	1.0015	0.8688	16400.49	28.556	29.070	-7.258	0.1254	0.7922
0.1470	67.293	0.0865	0.7937	0.8071	0.9363	1.0014	0.8769	19179.58	28.952	29.481	-6.847	0.1467	0.8034
0.1760	67.593	0.1035	0.8052	0.8182	0.9378	1.0013	0.8848	22963.30	29.349	29.892	-6.436	0.1756	0.8146
0.2150	67.938	0.1265	0.8183	0.8306	0.9396	1.0012	0.8937	28051.76	29.796	30.355	-5.973	0.2146	0.8272
0.2660	68.405	0.1565	0.8355	0.8470	0.9420	1.0011	0.9051	34705.90	30.384	30.966	-5.361	0.2655	0.8439
0.3260	69.003	0.1918	0.8570	0.8674	0.9451	1.0009	0.9189	42534.30	31.114	31.725	-4.603	0.3253	0.8645
0.3960	69.529	0.2329	0.8754	0.8847	0.9477	1.0008	0.9304	51667.43	31.734	32.370	-3.957	0.3952	0.8821
0.4750	70.147	0.2794	0.8963	0.9043	0.9508	1.0006	0.9431	61974.82	32.440	33.105	-3.222	0.4741	0.9021
0.5660	70.700	0.3329	0.9146	0.9214	0.9536	1.0005	0.9538	73847.89	33.051	33.743	-2.585	0.5649	0.9195
0.6360	71.204	0.3741	0.9308	0.9364	0.9561	1.0004	0.9631	82981.02	33.592	34.308	-2.019	0.6347	0.9349
0.7165	71.771	0.4215	0.9487	0.9530	0.9589	1.0003	0.9730	93484.12	34.184	34.928	-1.400	0.7151	0.9518
0.7960	72.218	0.4682	0.9625	0.9656	0.9611	1.0002	0.9805	103856.75	34.640	35.404	-0.924	0.7944	0.9648
0.8780	72.659	0.5165	0.9758	0.9779	0.9633	1.0001	0.9876	114555.56	35.079	35.864	-0.464	0.8762	0.9773
0.9770	73.047	0.5747	0.9873	0.9884	0.9652	1.0001	0.9936	127472.42	35.457	36.261	-0.066	0.9750	0.9881
1.0770	73.310	0.6335	0.9951	0.9955	0.9665	1.0000	0.9975	140519.75	35.710	36.527	0.199	1.0749	0.9954
1.2010	73.430	0.7065	0.9985	0.9987	0.9671	1.0000	0.9993	156698.43	35.825	36.647	0.319	1.1986	0.9986
1.3240	73.468	0.7788	0.9997	0.9997	0.9673	1.0000	0.9998	172746.65	35.861	36.684	0.357	1.3214	0.9997
1.4755	73.463	0.8679	0.9995	0.9996	0.9672	1.0000	0.9998	192513.36	35.856	36.679	0.352	1.4726	0.9995
1.6280	73.478	0.9576	0.9999	0.9999	0.9673	1.0000	1.0000	212410.53	35.870	36.694	0.367	1.6248	0.9999
1.8150	73.483	1.0000	1.0001	1.0001	0.9673	1.0000	1.0000	236809.04	35.875	36.699	0.372	1.8114	1.0000
2.2000	73.479	1.2941	1.0000	1.0000	0.9673	1.0000	1.0000	287041.26	35.871	36.695	0.368	2.1956	1.0000

Point 839, M=0.60

y, in.	pitot pressure, psia	y/δ	M/M_e	u/u_e	ρ/ρ_e	$T_t/T_{t,e}$	$(T_t-T_w)/(T_{t,e}-T_w)$	y^+	u^+	u'/u_τ	$(u'-u_e')/u_\tau$	y/δ_u	u'/u_e'
0.0240	79.664	0.0150	0.6834	0.6980	0.9288	0.9948	0.5650	3959.20	25.606	25.904	-11.012	0.0256	0.6944
0.0330	80.064	0.0206	0.6983	0.7126	0.9303	0.9950	0.5833	5443.90	26.141	26.451	-10.465	0.0352	0.7090
0.0420	80.674	0.0262	0.7202	0.7341	0.9325	0.9953	0.6109	6928.60	26.930	27.257	-9.659	0.0448	0.7307
0.0500	80.863	0.0312	0.7269	0.7405	0.9332	0.9954	0.6193	8248.34	27.168	27.501	-9.415	0.0534	0.7372
0.0580	81.167	0.0362	0.7374	0.7508	0.9342	0.9956	0.6328	9568.07	27.545	27.887	-9.029	0.0619	0.7475
0.0700	81.626	0.0438	0.7530	0.7660	0.9359	0.9958	0.6529	11547.67	28.101	28.456	-8.460	0.0747	0.7628
0.0840	81.972	0.0525	0.7645	0.7771	0.9371	0.9960	0.6679	13857.21	28.511	28.876	-8.040	0.0896	0.7740
0.0960	82.150	0.0600	0.7703	0.7828	0.9378	0.9961	0.6755	15836.81	28.718	29.089	-7.828	0.1025	0.7797

72

Table 6. Continued
(b) Continued

y, in.	pitot pressure, psia	y/δ	M/Mₑ	u/uₑ	ρ/ρₑ	Tₜ/Tₜ,ₑ	(Tₜ-Tᵥ)/(Tₜ,ₑ-Tᵥ)	y⁺	u⁺	u'/uτ	(u'-uₑ')/uτ	y/δᵤ	u'/uₑ'
0.1100	82.367	0.0687	0.7773	0.7896	0.9385	0.9962	0.6848	18146.34	28.968	29.345	-7.571	0.1174	0.7866
0.1257	82.751	0.0786	0.7896	0.8015	0.9399	0.9964	0.7011	20736.32	29.403	29.791	-7.125	0.1342	0.7986
0.1470	83.051	0.0919	0.7990	0.8106	0.9410	0.9966	0.7137	24250.11	29.737	30.134	-6.782	0.1569	0.8078
0.1760	83.535	0.1100	0.8140	0.8249	0.9427	0.9968	0.7338	29034.15	30.264	30.675	-6.241	0.1878	0.8223
0.2150	84.006	0.1344	0.8282	0.8386	0.9444	0.9970	0.7532	35467.85	30.764	31.189	-5.727	0.2295	0.8361
0.2660	84.649	0.1663	0.8471	0.8567	0.9467	0.9974	0.7792	43881.16	31.429	31.872	-5.044	0.2839	0.8544
0.3260	85.333	0.2037	0.8667	0.8753	0.9491	0.9977	0.8065	53779.16	32.113	32.577	-4.339	0.3479	0.8733
0.3960	85.974	0.2475	0.8846	0.8923	0.9514	0.9980	0.8316	65326.84	32.734	33.217	-3.699	0.4226	0.8904
0.4750	86.752	0.2969	0.9057	0.9122	0.9541	0.9983	0.8616	78359.21	33.465	33.971	-2.945	0.5069	0.9106
0.5660	87.533	0.3537	0.9263	0.9315	0.9569	0.9987	0.8912	93371.18	34.173	34.703	-2.213	0.6041	0.9302
0.6360	88.211	0.3975	0.9436	0.9478	0.9592	0.9990	0.9165	104918.86	34.770	35.320	-1.597	0.6788	0.9468
0.7165	88.724	0.4478	0.9565	0.9598	0.9610	0.9992	0.9354	118198.68	35.210	35.775	-1.141	0.7647	0.9590
0.7960	89.267	0.4975	0.9699	0.9722	0.9629	0.9995	0.9552	131313.54	35.667	36.248	-0.668	0.8495	0.9717
0.8780	89.830	0.5487	0.9836	0.9848	0.9649	0.9997	0.9754	144840.81	36.130	36.728	-0.188	0.9370	0.9845
0.9770	90.206	0.6106	0.9925	0.9931	0.9662	0.9999	0.9888	161172.52	36.434	37.043	0.127	1.0427	0.9930
1.0770	90.362	0.6731	0.9962	0.9965	0.9668	0.9999	0.9943	177669.20	36.559	37.173	0.257	1.1494	0.9965
1.2010	90.511	0.7506	0.9997	0.9998	0.9673	1.0000	0.9996	198125.07	36.678	37.296	0.380	1.2818	0.9998
1.3240	90.579	0.8275	1.0013	1.0012	0.9675	1.0000	1.0020	218415.99	36.731	37.352	0.436	1.4130	1.0013
1.4755	90.501	0.9222	0.9995	0.9995	0.9672	1.0000	0.9993	243408.45	36.670	37.288	0.372	1.5747	0.9995
1.6280	90.527	1.0000	1.0001	1.0001	0.9673	1.0000	1.0002	268565.88	36.690	37.309	0.393	1.7375	1.0000
1.8150	90.448	1.1344	0.9983	0.9984	0.9671	1.0000	0.9974	299414.66	36.628	37.244	0.328	1.9370	0.9984
2.2000	90.605	1.3750	1.0019	1.0018	0.9676	1.0000	1.0029	362926.86	36.752	37.373	0.457	2.3479	1.0018

Point 824, M=0.60

y, in.	pitot pressure, psia	y/δ	M/Mₑ	u/uₑ	ρ/ρₑ	Tₜ/Tₜ,ₑ	(Tₜ-Tᵥ)/(Tₜ,ₑ-Tᵥ)	y⁺	u⁺	u'/uτ	(u'-uₑ')/uτ	y/δᵤ	u'/uₑ'
0.0240	89.699	0.0141	0.6857	0.7015	0.9259	0.9963	0.5029	4408.44	25.815	26.184	-10.963	0.0252	0.6977
0.0330	90.247	0.0194	0.7036	0.7191	0.9278	0.9965	0.5275	6061.60	26.461	26.847	-10.300	0.0347	0.7153
0.0420	90.701	0.0247	0.7181	0.7332	0.9293	0.9966	0.5477	7714.76	26.981	27.381	-9.766	0.0442	0.7295
0.0500	91.219	0.0294	0.7341	0.7489	0.9311	0.9968	0.5705	9184.24	27.558	27.973	-9.174	0.0526	0.7453
0.0580	91.470	0.0341	0.7418	0.7563	0.9320	0.9969	0.5815	10653.72	27.832	28.254	-8.893	0.0610	0.7528
0.0700	91.657	0.0412	0.7474	0.7618	0.9327	0.9969	0.5897	12857.94	28.033	28.461	-8.686	0.0736	0.7583
0.0840	92.136	0.0494	0.7616	0.7755	0.9343	0.9971	0.6105	15429.52	28.540	28.982	-8.165	0.0883	0.7722
0.0960	92.433	0.0565	0.7703	0.7839	0.9353	0.9972	0.6233	17633.74	28.848	29.299	-7.848	0.1009	0.7806
0.1100	92.865	0.0647	0.7827	0.7959	0.9368	0.9973	0.6418	20205.33	29.288	29.752	-7.395	0.1157	0.7927
0.1257	93.067	0.0739	0.7884	0.8014	0.9375	0.9974	0.6504	23089.18	29.490	29.960	-7.187	0.1322	0.7983
0.1470	93.626	0.0865	0.8039	0.8163	0.9394	0.9976	0.6741	27001.67	30.040	30.526	-6.621	0.1546	0.8133
0.1760	93.915	0.1035	0.8118	0.8239	0.9404	0.9977	0.6863	32328.53	30.318	30.813	-6.334	0.1851	0.8210
0.2150	94.591	0.1265	0.8300	0.8412	0.9427	0.9979	0.7145	39492.23	30.955	31.471	-5.676	0.2261	0.8385
0.2660	95.228	0.1565	0.8466	0.8570	0.9449	0.9981	0.7408	48860.16	31.538	32.072	-5.075	0.2797	0.8545
0.3260	95.918	0.1918	0.8642	0.8737	0.9473	0.9983	0.7690	59881.25	32.151	32.706	-4.441	0.3428	0.8714
0.3960	96.779	0.2329	0.8855	0.8938	0.9502	0.9985	0.8038	72739.18	32.891	33.472	-3.675	0.4164	0.8918
0.4750	97.581	0.2794	0.9048	0.9119	0.9529	0.9988	0.8357	87250.28	33.558	34.163	-2.984	0.4995	0.9102
0.5660	98.441	0.3329	0.9249	0.9307	0.9558	0.9990	0.8696	103965.60	34.250	34.880	-2.267	0.5952	0.9294
0.6360	99.227	0.3741	0.9428	0.9474	0.9585	0.9993	0.9001	116823.54	34.863	35.517	-1.630	0.6688	0.9463
0.7165	100.040	0.4215	0.9609	0.9641	0.9612	0.9995	0.9313	131610.16	35.479	36.157	-0.990	0.7534	0.9634

Table 6. Continued
(b) Continued

y, in.	pitot pressure, psia	y/δ	M/M_e	u/u_e	ρ/ρ_e	$T_t/T_{t,e}$	$(T_t-T_w)/(T_{t,e}-T_w)$	y^+	u^+	u'/u_τ	$(u'-u_e')/u_\tau$	y/δ_u	u'/u_e'
0.7960	100.736	0.4682	0.9761	0.9780	0.9635	0.9997	0.9577	146213.11	35.992	36.690	-0.457	0.8370	0.9776
0.8780	101.119	0.5165	0.9842	0.9856	0.9648	0.9998	0.9721	161275.26	36.269	36.979	-0.168	0.9232	0.9853
0.9770	101.425	0.5747	0.9907	0.9915	0.9658	0.9999	0.9836	179460.06	36.488	37.207	0.060	1.0273	0.9913
1.0770	101.767	0.6335	0.9979	0.9981	0.9670	1.0000	0.9963	197828.54	36.730	37.459	0.312	1.1325	0.9981
1.2010	101.774	0.7065	0.9981	0.9982	0.9670	1.0000	0.9966	220605.45	36.735	37.464	0.317	1.2629	0.9982
1.3240	101.733	0.7788	0.9972	0.9974	0.9669	1.0000	0.9950	243198.69	36.706	37.434	0.287	1.3922	0.9974
1.4755	102.022	0.8679	1.0032	1.0030	0.9678	1.0000	1.0058	271026.93	36.909	37.645	0.498	1.5515	1.0030
1.6280	101.775	0.9576	0.9981	0.9983	0.9670	1.0000	0.9966	299038.87	36.736	37.465	0.318	1.7119	0.9982
1.8150	102.013	1.0000	1.0030	1.0028	0.9678	1.0000	1.0054	333387.93	36.902	37.638	0.491	1.9085	1.0000
2.2000	101.661	1.2941	0.9957	0.9961	0.9666	0.9999	0.9924	404106.58	36.655	37.381	0.234	2.3134	0.9960

Point 825, M=0.60

y, in.	pitot pressure, psia	y/δ	M/M_e	u/u_e	ρ/ρ_e	$T_t/T_{t,e}$	$(T_t-T_w)/(T_{t,e}-T_w)$	y^+	u^+	u'/u_τ	$(u'-u_e')/u_\tau$	y/δ_u	u'/u_e'
0.0240	89.726	0.0141	0.6865	0.7022	0.9263	0.9960	0.5217	4412.15	25.853	26.216	-10.931	0.0250	0.6984
0.0330	90.243	0.0194	0.7034	0.7187	0.9280	0.9962	0.5442	6066.71	26.463	26.841	-10.306	0.0344	0.7150
0.0420	90.807	0.0247	0.7213	0.7362	0.9300	0.9964	0.5686	7721.26	27.107	27.502	-9.646	0.0438	0.7326
0.0500	91.185	0.0294	0.7330	0.7476	0.9313	0.9965	0.5848	9191.98	27.527	27.933	-9.214	0.0521	0.7441
0.0580	91.473	0.0341	0.7418	0.7562	0.9323	0.9966	0.5970	10662.69	27.841	28.256	-8.892	0.0605	0.7527
0.0700	91.625	0.0412	0.7463	0.7606	0.9328	0.9967	0.6035	12868.77	28.005	28.424	-8.723	0.0730	0.7572
0.0840	92.155	0.0494	0.7621	0.7758	0.9346	0.9969	0.6257	15442.52	28.566	29.001	-8.147	0.0876	0.7726
0.0960	92.435	0.0565	0.7702	0.7837	0.9355	0.9970	0.6374	17648.60	28.856	29.300	-7.848	0.1001	0.7805
0.1100	92.803	0.0647	0.7808	0.7939	0.9368	0.9971	0.6527	20222.35	29.232	29.686	-7.462	0.1147	0.7908
0.1257	93.034	0.0739	0.7873	0.8002	0.9376	0.9972	0.6622	23108.63	29.464	29.924	-7.223	0.1311	0.7972
0.1470	93.635	0.0865	0.8040	0.8163	0.9396	0.9974	0.6869	27024.42	30.055	30.534	-6.614	0.1533	0.8134
0.1760	93.887	0.1035	0.8109	0.8229	0.9405	0.9975	0.6971	32355.76	30.298	30.784	-6.364	0.1835	0.8201
0.2150	94.609	0.1265	0.8303	0.8414	0.9429	0.9977	0.7262	39525.51	30.979	31.486	-5.662	0.2242	0.8388
0.2660	95.303	0.1565	0.8484	0.8586	0.9453	0.9979	0.7538	48901.32	31.613	32.140	-5.008	0.2774	0.8562
0.3260	95.990	0.1918	0.8658	0.8751	0.9476	0.9982	0.7808	59931.70	32.221	32.769	-4.379	0.3399	0.8729
0.3960	96.871	0.2329	0.8875	0.8956	0.9506	0.9985	0.8150	72800.47	32.977	33.551	-3.597	0.4129	0.8938
0.4750	97.623	0.2794	0.9056	0.9126	0.9531	0.9987	0.8437	87323.79	33.601	34.197	-2.951	0.4953	0.9110
0.5660	98.451	0.3329	0.9249	0.9307	0.9559	0.9990	0.8750	104053.19	34.267	34.887	-2.261	0.5902	0.9293
0.6360	99.196	0.3741	0.9419	0.9465	0.9584	0.9992	0.9028	116921.96	34.849	35.490	-1.657	0.6632	0.9454
0.7165	99.987	0.4215	0.9595	0.9628	0.9610	0.9994	0.9319	131721.05	35.449	36.114	-1.034	0.7471	0.9620
0.7960	100.636	0.4682	0.9737	0.9758	0.9632	0.9996	0.9555	146336.29	35.929	36.613	-0.535	0.8300	0.9753
0.8780	101.052	0.5165	0.9826	0.9840	0.9646	0.9998	0.9705	161411.14	36.232	36.927	-0.220	0.9155	0.9837
0.9770	101.413	0.5747	0.9902	0.9911	0.9658	0.9999	0.9834	179611.26	36.490	37.197	0.049	1.0188	0.9909
1.0770	101.767	0.6335	0.9977	0.9979	0.9669	1.0000	0.9960	197995.21	36.741	37.458	0.310	1.1230	0.9978
1.2010	101.790	0.7065	0.9982	0.9983	0.9670	1.0000	0.9969	220791.32	36.757	37.474	0.327	1.2523	0.9983
1.3240	101.751	0.7788	0.9973	0.9976	0.9669	1.0000	0.9955	243403.58	36.730	37.446	0.298	1.3806	0.9975
1.4755	102.064	0.8679	1.0039	1.0035	0.9679	1.0001	1.0066	271255.28	36.949	37.674	0.527	1.5386	1.0036
1.6280	101.793	0.9576	0.9982	0.9984	0.9670	1.0000	0.9970	299290.81	36.759	37.477	0.329	1.6976	0.9983
1.8150	102.015	1.0000	1.0028	1.0026	0.9678	1.0000	1.0048	333668.81	36.915	37.639	0.491	1.8926	1.0000
2.2000	101.692	1.2941	0.9961	0.9964	0.9667	0.9999	0.9934	404447.04	36.688	37.402	0.255	2.2941	0.9964

Table 6. Continued
(b) Continued

y, in.	pitot pressure, psia	y/δ	M/M_e	u/u_e	ρ/ρ_e	$T_t/T_{t,e}$	$(T_t-T_w)/(T_{t,e}-T_w)$	y^+	u^+	u'/u_τ	$(u'-u_e')/u_\tau$	y/δ_u	u'/u_e'
Point 837, M=0.60													
0.0240	89.573	0.0150	0.6828	0.6977	0.9593	0.9942	0.5785	4311.72	25.776	26.095	-11.127	0.0255	0.6942
0.0330	90.048	0.0206	0.6985	0.7131	0.9609	0.9945	0.5974	5928.62	26.345	26.677	-10.545	0.0351	0.7097
0.0420	90.690	0.0262	0.7190	0.7332	0.9631	0.9948	0.6226	7545.52	27.088	27.437	-9.785	0.0447	0.7299
0.0500	91.021	0.0312	0.7293	0.7433	0.9642	0.9950	0.6354	8982.76	27.461	27.818	-9.404	0.0532	0.7400
0.0580	91.440	0.0362	0.7422	0.7558	0.9656	0.9952	0.6515	10420.00	27.923	28.292	-8.930	0.0617	0.7526
0.0700	91.711	0.0438	0.7503	0.7637	0.9665	0.9954	0.6617	12575.86	28.216	28.592	-8.630	0.0745	0.7606
0.0840	92.134	0.0525	0.7629	0.7759	0.9679	0.9956	0.6776	15091.03	28.665	29.053	-8.169	0.0894	0.7729
0.0960	92.389	0.0600	0.7703	0.7831	0.9688	0.9957	0.6871	17246.89	28.932	29.326	-7.896	0.1021	0.7801
0.1100	92.718	0.0687	0.7798	0.7923	0.9699	0.9959	0.6992	19762.07	29.270	29.673	-7.549	0.1170	0.7894
0.1257	93.069	0.0786	0.7897	0.8019	0.9710	0.9961	0.7121	22582.65	29.625	30.037	-7.185	0.1337	0.7990
0.1470	93.445	0.0919	0.8002	0.8120	0.9723	0.9963	0.7257	26409.31	29.998	30.421	-6.801	0.1564	0.8092
0.1760	93.999	0.1100	0.8154	0.8266	0.9741	0.9965	0.7455	31619.31	30.537	30.974	-6.248	0.1872	0.8240
0.2150	94.494	0.1344	0.8286	0.8393	0.9758	0.9968	0.7630	38625.86	31.006	31.456	-5.766	0.2287	0.8368
0.2660	95.316	0.1663	0.8501	0.8598	0.9785	0.9972	0.7916	47788.27	31.763	32.235	-4.987	0.2830	0.8575
0.3260	96.107	0.2037	0.8701	0.8788	0.9812	0.9975	0.8186	58567.58	32.467	32.960	-4.262	0.3468	0.8768
0.3960	96.834	0.2475	0.8881	0.8958	0.9836	0.9979	0.8430	71143.44	33.093	33.606	-3.616	0.4213	0.8940
0.4750	97.646	0.2969	0.9076	0.9141	0.9863	0.9982	0.8697	85336.19	33.771	34.306	-2.916	0.5053	0.9126
0.5660	98.476	0.3537	0.9270	0.9323	0.9890	0.9986	0.8966	101684.81	34.443	35.000	-2.222	0.6021	0.9311
0.6360	99.246	0.3975	0.9445	0.9487	0.9916	0.9989	0.9211	114260.67	35.048	35.626	-1.596	0.6766	0.9477
0.7165	99.832	0.4478	0.9576	0.9608	0.9935	0.9992	0.9395	128722.91	35.496	36.090	-1.132	0.7622	0.9601
0.7960	100.456	0.4975	0.9712	0.9735	0.9956	0.9994	0.9589	143005.49	35.964	36.575	-0.647	0.8468	0.9730
0.8780	101.026	0.5487	0.9835	0.9848	0.9974	0.9997	0.9763	157737.21	36.383	37.009	-0.213	0.9340	0.9845
0.9770	101.481	0.6106	0.9931	0.9937	0.9989	0.9999	0.9901	175523.07	36.711	37.349	0.127	1.0394	0.9936
1.0770	101.661	0.6731	0.9969	0.9972	0.9995	0.9999	0.9956	193488.59	36.840	37.483	0.261	1.1457	0.9971
1.2010	101.738	0.7506	0.9985	0.9986	0.9998	1.0000	0.9979	215765.83	36.894	37.539	0.317	1.2777	0.9986
1.3240	101.817	0.8275	1.0002	1.0002	1.0000	1.0000	1.0003	237863.41	36.950	37.597	0.376	1.4085	1.0002
1.4755	101.757	0.9222	0.9989	0.9990	0.9998	1.0000	0.9985	265081.16	36.908	37.553	0.331	1.5697	0.9990
1.6280	101.820	1.0000	1.0002	1.0002	1.0000	1.0000	1.0003	292478.57	36.952	37.600	0.378	1.7319	1.0000
1.8150	101.717	1.1344	0.9981	0.9982	0.9997	1.0000	0.9973	326074.08	36.879	37.524	0.302	1.9309	0.9982
2.2000	101.825	1.3750	1.0003	1.0003	1.0001	1.0000	1.0005	395241.31	36.956	37.603	0.381	2.3404	1.0003
Point 752, M=0.85													
0.0240	16.798	0.0133	0.5934	0.6177	0.8928	0.9939	0.2535	307.72	19.047	19.209	-11.955	0.0200	0.6096
0.0330	17.177	0.0183	0.6311	0.6549	0.8981	0.9943	0.3064	423.12	20.195	20.387	-10.777	0.0275	0.6470
0.0420	17.403	0.0233	0.6522	0.6757	0.9012	0.9946	0.3378	538.51	20.836	21.045	-10.118	0.0350	0.6679
0.0500	17.530	0.0278	0.6637	0.6870	0.9030	0.9947	0.3553	641.09	21.183	21.403	-9.760	0.0417	0.6793
0.0580	17.661	0.0322	0.6753	0.6983	0.9048	0.9948	0.3734	743.66	21.532	21.763	-9.401	0.0484	0.6907
0.0700	17.769	0.0389	0.6847	0.7074	0.9062	0.9950	0.3882	897.52	21.813	22.053	-9.111	0.0584	0.6999
0.0840	18.015	0.0467	0.7054	0.7275	0.9096	0.9952	0.4217	1077.03	22.433	22.693	-8.470	0.0701	0.7202
0.0960	18.099	0.0533	0.7123	0.7341	0.9107	0.9953	0.4331	1230.89	22.638	22.905	-8.258	0.0801	0.7269
0.1100	18.250	0.0611	0.7245	0.7459	0.9127	0.9955	0.4536	1410.39	23.000	23.280	-7.883	0.0917	0.7388
0.1257	18.336	0.0698	0.7313	0.7524	0.9139	0.9956	0.4651	1611.70	23.202	23.489	-7.674	0.1048	0.7455
0.1470	18.522	0.0817	0.7458	0.7663	0.9163	0.9958	0.4900	1884.80	23.628	23.931	-7.232	0.1226	0.7595

Table 6. Continued
(b) Continued

y, in.	pitot pressure, psia	y/δ	M/M_e	u/u_e	ρ/ρ_e	$T_r/T_{t,e}$	$(T_r-T_w)/(T_{t,e}-T_w)$	y^+	u^+	u'/u_τ	$(u'-u_e')/u_\tau$	y/δ_u	u'/u_e'
0.1760	18.742	0.0978	0.7624	0.7821	0.9192	0.9960	0.5193	2256.63	24.117	24.439	-6.725	0.1468	0.7756
0.2150	18.932	0.1194	0.7763	0.7953	0.9217	0.9963	0.5443	2756.68	24.525	24.863	-6.300	0.1793	0.7891
0.2660	19.237	0.1478	0.7980	0.8158	0.9256	0.9966	0.5841	3410.59	25.156	25.522	-5.642	0.2219	0.8100
0.3260	19.519	0.1811	0.8174	0.8340	0.9292	0.9969	0.6204	4179.89	25.716	26.106	-5.058	0.2719	0.8285
0.3960	19.818	0.2200	0.8372	0.8524	0.9330	0.9972	0.6584	5077.42	26.286	26.702	-4.462	0.3303	0.8474
0.4750	20.168	0.2639	0.8595	0.8731	0.9373	0.9976	0.7023	6090.34	26.924	27.371	-3.792	0.3962	0.8687
0.5660	20.498	0.3144	0.8798	0.8918	0.9414	0.9979	0.7431	7257.12	27.501	27.977	-3.186	0.4721	0.8879
0.6360	20.757	0.3533	0.8952	0.9060	0.9445	0.9981	0.7746	8154.64	27.937	28.436	-2.727	0.5304	0.9025
0.7165	21.122	0.3981	0.9164	0.9252	0.9489	0.9985	0.8185	9186.79	28.529	29.061	-2.102	0.5976	0.9223
0.7960	21.388	0.4422	0.9313	0.9387	0.9521	0.9988	0.8500	10206.12	28.946	29.501	-1.662	0.6639	0.9363
0.8780	21.642	0.4878	0.9452	0.9512	0.9551	0.9990	0.8797	11257.51	29.332	29.910	-1.253	0.7323	0.9493
0.9770	21.922	0.5428	0.9602	0.9646	0.9584	0.9993	0.9120	12526.86	29.745	30.349	-0.814	0.8148	0.9632
1.0770	22.179	0.5983	0.9736	0.9766	0.9613	0.9995	0.9414	13809.04	30.114	30.741	-0.422	0.8982	0.9756
1.2010	22.468	0.6672	0.9883	0.9897	0.9647	0.9998	0.9739	15398.93	30.518	31.170	0.007	1.0017	0.9892
1.3240	22.551	0.7356	0.9925	0.9934	0.9656	0.9999	0.9832	16976.01	30.632	31.291	0.128	1.1043	0.9931
1.4755	22.642	0.8197	0.9970	0.9974	0.9666	0.9999	0.9934	18918.51	30.755	31.423	0.260	1.2306	0.9973
1.6280	22.678	0.9044	0.9988	0.9990	0.9670	1.0000	0.9973	20873.83	30.804	31.475	0.312	1.3578	0.9989
1.8150	22.704	1.0000	1.0001	1.0001	0.9673	1.0000	1.0002	23271.50	30.839	31.512	0.349	1.5138	1.0000
2.0005	22.666	1.1114	0.9982	0.9984	0.9669	1.0000	0.9960	25649.93	30.788	31.457	0.294	1.6685	0.9984
2.2000	22.685	1.2222	0.9992	0.9993	0.9671	1.0000	0.9981	28207.87	30.813	31.485	0.322	1.8349	0.9992

Point 915, M=0.85

y, in.	pitot pressure, psia	y/δ	M/M_e	u/u_e	ρ/ρ_e	$T_r/T_{t,e}$	$(T_r-T_w)/(T_{t,e}-T_w)$	y^+	u^+	u'/u_τ	$(u'-u_e')/u_\tau$	y/δ_u	u'/u_e'
0.0240	24.397	0.0141	0.6548	0.6816	0.8936	0.9986	1.3927	1536.14	23.265	23.647	-11.117	0.0233	0.6732
0.0330	24.653	0.0194	0.6713	0.6977	0.8964	0.9986	1.3888	2112.20	23.815	24.217	-10.546	0.0321	0.6895
0.0420	25.033	0.0247	0.6949	0.7205	0.9006	0.9987	1.3803	2688.25	24.594	25.029	-9.734	0.0408	0.7126
0.0500	25.189	0.0294	0.7043	0.7296	0.9023	0.9987	1.3760	3200.30	24.903	25.351	-9.413	0.0486	0.7217
0.0580	25.348	0.0341	0.7137	0.7386	0.9040	0.9987	1.3712	3712.35	25.211	25.672	-9.091	0.0564	0.7309
0.0700	25.506	0.0412	0.7229	0.7474	0.9057	0.9987	1.3660	4480.42	25.511	25.985	-8.778	0.0680	0.7398
0.0840	25.822	0.0494	0.7408	0.7645	0.9091	0.9988	1.3545	5376.50	26.094	26.595	-8.169	0.0816	0.7572
0.0960	25.971	0.0565	0.7491	0.7723	0.9107	0.9988	1.3485	6144.57	26.361	26.874	-7.889	0.0933	0.7651
0.1100	26.137	0.0647	0.7581	0.7808	0.9125	0.9988	1.3416	7040.66	26.653	27.180	-7.583	0.1069	0.7738
0.1257	26.252	0.0739	0.7643	0.7867	0.9137	0.9988	1.3366	8045.55	26.852	27.389	-7.374	0.1222	0.7798
0.1470	26.556	0.0865	0.7803	0.8017	0.9169	0.9989	1.3226	9408.88	27.366	27.929	-6.835	0.1429	0.7951
0.1760	26.786	0.1035	0.7921	0.8128	0.9193	0.9989	1.3114	11265.05	27.743	28.326	-6.438	0.1710	0.8064
0.2150	27.129	0.1265	0.8092	0.8288	0.9228	0.9990	1.2938	13761.28	28.289	28.900	-5.863	0.2089	0.8228
0.2660	27.532	0.1565	0.8288	0.8469	0.9269	0.9991	1.2718	17025.59	28.906	29.551	-5.212	0.2585	0.8413
0.3260	27.946	0.1918	0.8481	0.8647	0.9311	0.9991	1.2481	20865.94	29.515	30.195	-4.569	0.3168	0.8596
0.3960	28.416	0.2329	0.8694	0.8841	0.9358	0.9992	1.2199	25346.36	30.177	30.896	-3.867	0.3848	0.8796
0.4750	28.862	0.2794	0.8888	0.9017	0.9402	0.9993	1.1921	30402.83	30.779	31.536	-3.227	0.4616	0.8978
0.5660	29.337	0.3329	0.9089	0.9198	0.9449	0.9994	1.1616	36227.37	31.395	32.191	-2.572	0.5500	0.9165
0.6360	29.790	0.3741	0.9274	0.9363	0.9492	0.9995	1.1317	40707.79	31.959	32.793	-1.970	0.6181	0.9336
0.7165	30.242	0.4215	0.9453	0.9522	0.9536	0.9996	1.1014	45860.27	32.501	33.373	-1.391	0.6963	0.9501
0.7960	30.620	0.4682	0.9599	0.9650	0.9572	0.9997	1.0756	50948.74	32.940	33.843	-0.921	0.7736	0.9635
0.8780	30.942	0.5165	0.9720	0.9757	0.9602	0.9998	1.0534	56197.23	33.304	34.233	-0.531	0.8533	0.9746

Table 6. Continued
(b) Continued

y, in.	pitot pressure, psia	y/δ	M/M_e	u/u_e	ρ/ρ_e	T_t/T_t,e	(T_t-T_w)/(T_t,e-T_w)	y^+	u^+	u'/u_τ	(u'-u_e')/u_τ	y/δ_u	u'/u_e'
0.9770	31.260	0.5747	0.9838	0.9860	0.9632	0.9999	1.0313	62533.82	33.654	34.609	-0.154	0.9495	0.9853
1.0770	31.516	0.6335	0.9931	0.9940	0.9655	1.0000	1.0135	68934.42	33.930	34.906	0.143	1.0466	0.9938
1.2010	31.639	0.7065	0.9975	0.9979	0.9667	1.0000	1.0048	76871.16	34.061	35.047	0.283	1.1672	0.9978
1.3240	31.677	0.7788	0.9989	0.9990	0.9670	1.0000	1.0022	84743.89	34.101	35.090	0.327	1.2867	0.9990
1.4755	31.683	0.8679	0.9991	0.9992	0.9671	1.0000	1.0017	94440.80	34.107	35.097	0.333	1.4339	0.9992
1.6280	31.707	0.9576	1.0000	1.0000	0.9673	1.0000	1.0001	104201.70	34.133	35.124	0.361	1.5821	1.0000
1.8150	31.709	1.0000	1.0000	1.0000	0.9673	1.0000	0.9999	116170.82	34.135	35.126	0.363	1.7638	1.0000
2.2000	31.677	1.2941	0.9989	0.9990	0.9670	1.0000	1.0022	140813.11	34.101	35.090	0.327	2.1380	0.9990

Point 945, M=0.85

y, in.	pitot pressure, psia	y/δ	M/M_e	u/u_e	ρ/ρ_e	T_t/T_t,e	(T_t-T_w)/(T_t,e-T_w)	y^+	u^+	u'/u_τ	(u'-u_e')/u_τ	y/δ_u	u'/u_e'
0.0240	35.155	0.0141	0.6659	0.6932	0.8937	0.9980	2.3823	2176.11	24.126	24.573	-10.941	0.0241	0.6850
0.0330	35.490	0.0194	0.6807	0.7076	0.8963	0.9980	2.3509	2992.15	24.626	25.094	-10.420	0.0332	0.6996
0.0420	35.965	0.0247	0.7010	0.7272	0.9000	0.9981	2.3028	3808.19	25.308	25.806	-9.708	0.0423	0.7194
0.0500	36.196	0.0294	0.7106	0.7364	0.9018	0.9981	2.2781	4533.56	25.629	26.142	-9.373	0.0503	0.7287
0.0580	36.440	0.0341	0.7206	0.7460	0.9037	0.9982	2.2511	5258.93	25.961	26.489	-9.026	0.0584	0.7384
0.0700	36.745	0.0412	0.7328	0.7576	0.9060	0.9982	2.2162	6346.99	26.366	26.912	-8.602	0.0704	0.7502
0.0840	37.106	0.0494	0.7469	0.7710	0.9088	0.9983	2.1734	7616.39	26.832	27.401	-8.114	0.0845	0.7638
0.0960	37.340	0.0565	0.7558	0.7794	0.9106	0.9983	2.1449	8704.44	27.126	27.709	-7.805	0.0966	0.7725
0.1100	37.598	0.0647	0.7655	0.7886	0.9125	0.9984	2.1128	9973.84	27.444	28.044	-7.471	0.1107	0.7818
0.1257	37.821	0.0739	0.7737	0.7963	0.9142	0.9984	2.0845	11397.38	27.714	28.327	-7.187	0.1265	0.7897
0.1470	38.215	0.0865	0.7880	0.8097	0.9171	0.9985	2.0336	13328.67	28.179	28.817	-6.698	0.1479	0.8033
0.1760	38.543	0.1035	0.7996	0.8205	0.9195	0.9985	1.9902	15958.14	28.556	29.214	-6.301	0.1771	0.8144
0.2150	39.006	0.1265	0.8156	0.8354	0.9229	0.9986	1.9278	19494.32	29.072	29.759	-5.756	0.2163	0.8296
0.2660	39.569	0.1565	0.8345	0.8527	0.9270	0.9988	1.8501	24118.55	29.678	30.399	-5.116	0.2676	0.8474
0.3260	40.171	0.1918	0.8540	0.8706	0.9314	0.9989	1.7654	29558.83	30.299	31.057	-4.457	0.3280	0.8658
0.3960	40.789	0.2329	0.8733	0.8882	0.9358	0.9990	1.6770	35905.82	30.911	31.707	-3.807	0.3984	0.8839
0.4750	41.469	0.2794	0.8939	0.9068	0.9406	0.9992	1.5783	43068.85	31.558	32.395	-3.120	0.4779	0.9031
0.5660	42.132	0.3329	0.9133	0.9241	0.9453	0.9993	1.4811	51319.93	32.162	33.039	-2.475	0.5694	0.9210
0.6360	42.834	0.3741	0.9332	0.9418	0.9501	0.9994	1.3773	57666.92	32.776	33.696	-1.819	0.6398	0.9393
0.7165	43.414	0.4215	0.9492	0.9558	0.9541	0.9996	1.2912	64965.96	33.265	34.219	-1.295	0.7208	0.9539
0.7960	43.966	0.4682	0.9640	0.9688	0.9579	0.9997	1.2090	72174.32	33.716	34.703	-0.811	0.8008	0.9674
0.8780	44.394	0.5165	0.9752	0.9786	0.9608	0.9998	1.1452	79609.36	34.056	35.068	-0.446	0.8833	0.9776
0.9770	44.884	0.5747	0.9878	0.9895	0.9641	0.9999	1.0722	88585.82	34.436	35.477	-0.037	0.9829	0.9890
1.0770	45.149	0.6335	0.9945	0.9953	0.9659	1.0000	1.0327	97652.94	34.638	35.694	0.180	1.0835	0.9950
1.2010	45.276	0.7065	0.9977	0.9980	0.9667	1.0000	1.0138	108896.18	34.733	35.797	0.283	1.2082	0.9979
1.3240	45.355	0.7788	0.9997	0.9997	0.9672	1.0000	1.0020	120048.75	34.793	35.861	0.347	1.3320	0.9997
1.4755	45.354	0.8679	0.9996	0.9997	0.9672	1.0000	1.0022	133785.44	34.792	35.860	0.346	1.4844	0.9997
1.6280	45.377	0.9576	1.0002	1.0002	0.9674	1.0000	0.9987	147612.81	34.809	35.879	0.365	1.6378	1.0002
1.8150	45.355	1.0000	0.9997	0.9997	0.9672	1.0000	1.0020	164568.33	34.793	35.861	0.347	1.8260	1.0000
2.2000	45.364	1.2941	0.9999	0.9999	0.9673	1.0000	1.0007	199476.77	34.799	35.868	0.354	2.2133	0.9999

Point 855, M=0.85

y, in.	pitot pressure, psia	y/δ	M/M_e	u/u_e	ρ/ρ_e	T_t/T_t,e	(T_t-T_w)/(T_t,e-T_w)	y^+	u^+	u'/u_τ	(u'-u_e')/u_τ	y/δ_u	u'/u_e'
0.0240	45.740	0.0141	0.6669	0.6931	0.8969	0.9926	0.5021	2872.11	24.547	24.967	-11.057	0.0249	0.6858
0.0330	46.290	0.0194	0.6855	0.7113	0.9000	0.9930	0.5268	3949.15	25.189	25.633	-10.391	0.0342	0.7041

Table 6. Continued
(b) Continued

y, in.	pitot pressure, psia	y/δ	M/M_e	u/u_e	ρ/ρ_e	$T_t/T_{t,e}$	$(T_t-T_w)/(T_{t,e}-T_w)$	y^+	u^+	u'/u_τ	$(u'-u_e')/u_\tau$	y/δ_u	u'/u_e'
0.0420	46.971	0.0247	0.7077	0.7327	0.9039	0.9934	0.5568	5026.19	25.948	26.422	-9.602	0.0436	0.7258
0.0500	47.185	0.0294	0.7145	0.7392	0.9051	0.9936	0.5661	5983.56	26.179	26.662	-9.361	0.0519	0.7324
0.0580	47.559	0.0341	0.7262	0.7504	0.9072	0.9938	0.5822	6940.93	26.575	27.075	-8.949	0.0602	0.7437
0.0700	47.919	0.0412	0.7372	0.7609	0.9092	0.9940	0.5975	8376.98	26.947	27.462	-8.562	0.0726	0.7543
0.0840	48.479	0.0494	0.7538	0.7768	0.9123	0.9944	0.6210	10052.38	27.508	28.048	-7.976	0.0871	0.7704
0.0960	48.701	0.0565	0.7603	0.7829	0.9135	0.9945	0.6302	11488.43	27.725	28.275	-7.749	0.0996	0.7767
0.1100	49.010	0.0647	0.7692	0.7913	0.9152	0.9947	0.6429	13163.83	28.022	28.585	-7.438	0.1141	0.7852
0.1257	49.431	0.0739	0.7811	0.8025	0.9175	0.9950	0.6601	15042.67	28.418	29.000	-7.024	0.1304	0.7966
0.1470	49.842	0.0865	0.7924	0.8131	0.9198	0.9952	0.6766	17591.66	28.795	29.395	-6.629	0.1525	0.8074
0.1760	50.338	0.1035	0.8058	0.8256	0.9225	0.9955	0.6963	21062.13	29.239	29.860	-6.164	0.1826	0.8202
0.2150	50.879	0.1265	0.8201	0.8389	0.9254	0.9958	0.7175	25729.31	29.708	30.353	-5.671	0.2230	0.8337
0.2660	51.672	0.1565	0.8404	0.8576	0.9297	0.9963	0.7479	31832.54	30.372	31.051	-4.973	0.2759	0.8529
0.3260	52.451	0.1918	0.8596	0.8753	0.9338	0.9967	0.7772	39012.81	30.997	31.710	-4.314	0.3382	0.8710
0.3960	53.222	0.2329	0.8781	0.8921	0.9379	0.9971	0.8056	47389.79	31.592	32.338	-3.685	0.4108	0.8883
0.4750	54.229	0.2794	0.9013	0.9131	0.9432	0.9977	0.8418	56843.81	32.336	33.126	-2.898	0.4927	0.9099
0.5660	55.002	0.3329	0.9186	0.9285	0.9472	0.9981	0.8689	67733.89	32.883	33.706	-2.317	0.5871	0.9259
0.6360	55.845	0.3741	0.9368	0.9448	0.9515	0.9985	0.8979	76110.87	33.459	34.318	-1.706	0.6598	0.9427
0.7165	56.602	0.4215	0.9528	0.9589	0.9554	0.9989	0.9234	85744.40	33.957	34.849	-1.175	0.7433	0.9572
0.7960	57.240	0.4682	0.9659	0.9704	0.9586	0.9992	0.9446	95258.26	34.365	35.284	-0.740	0.8257	0.9692
0.8780	57.875	0.5165	0.9787	0.9815	0.9619	0.9995	0.9653	105071.30	34.760	35.706	-0.318	0.9108	0.9808
0.9770	58.439	0.5747	0.9898	0.9912	0.9647	0.9998	0.9834	116918.75	35.103	36.072	0.048	1.0135	0.9908
1.0770	58.754	0.6335	0.9960	0.9965	0.9663	0.9999	0.9934	128885.87	35.291	36.273	0.249	1.1172	0.9964
1.2010	58.960	0.7065	0.9999	0.9999	0.9673	1.0000	0.9999	143725.09	35.412	36.403	0.379	1.2459	0.9999
1.3240	58.991	0.7788	1.0005	1.0005	0.9675	1.0000	1.0009	158444.65	35.430	36.423	0.399	1.3734	1.0005
1.4755	58.924	0.8679	0.9992	0.9993	0.9671	1.0000	0.9988	176574.84	35.391	36.380	0.357	1.5306	0.9993
1.6280	58.993	0.9576	1.0006	1.0005	0.9675	1.0000	1.0009	194824.69	35.432	36.424	0.400	1.6888	1.0005
1.8150	58.916	1.0000	0.9991	0.9992	0.9671	1.0000	0.9985	217203.20	35.386	36.375	0.352	1.8828	1.0000
2.2000	59.043	1.2941	1.0015	1.0013	0.9677	1.0000	1.0025	263276.61	35.461	36.455	0.432	2.2822	1.0014

Point 856, M=0.85

y, in.	pitot pressure, psia	y/δ	M/M_e	u/u_e	ρ/ρ_e	$T_t/T_{t,e}$	$(T_t-T_w)/(T_{t,e}-T_w)$	y^+	u^+	u'/u_τ	$(u'-u_e')/u_\tau$	y/δ_u	u'/u_e'
0.0240	45.746	0.0141	0.6666	0.6928	0.9273	0.9925	0.5071	2852.84	24.541	24.959	-11.070	0.0248	0.6855
0.0330	46.377	0.0194	0.6879	0.7136	0.9310	0.9929	0.5352	3922.65	25.275	25.720	-10.309	0.0341	0.7064
0.0420	46.992	0.0247	0.7079	0.7329	0.9345	0.9933	0.5620	4992.46	25.958	26.430	-9.599	0.0434	0.7259
0.0500	47.179	0.0294	0.7139	0.7386	0.9356	0.9934	0.5701	5943.41	26.160	26.640	-9.389	0.0517	0.7317
0.0580	47.556	0.0341	0.7256	0.7498	0.9378	0.9937	0.5861	6894.35	26.560	27.056	-8.973	0.0600	0.7431
0.0700	47.973	0.0412	0.7383	0.7620	0.9402	0.9939	0.6037	8320.77	26.990	27.504	-8.524	0.0724	0.7554
0.0840	48.532	0.0494	0.7549	0.7777	0.9434	0.9943	0.6269	9984.92	27.548	28.087	-7.941	0.0869	0.7715
0.0960	48.721	0.0565	0.7604	0.7829	0.9445	0.9944	0.6347	11411.34	27.733	28.280	-7.749	0.0993	0.7767
0.1100	48.911	0.0647	0.7659	0.7881	0.9456	0.9945	0.6424	13075.49	27.916	28.471	-7.557	0.1138	0.7820
0.1257	49.447	0.0739	0.7810	0.8024	0.9486	0.9949	0.6640	14941.72	28.422	29.000	-7.028	0.1300	0.7965
0.1470	49.833	0.0865	0.7917	0.8124	0.9508	0.9951	0.6794	17473.62	28.776	29.372	-6.657	0.1520	0.8067
0.1760	50.263	0.1035	0.8033	0.8233	0.9532	0.9953	0.6963	20920.79	29.161	29.776	-6.253	0.1820	0.8178
0.2150	50.883	0.1265	0.8197	0.8385	0.9566	0.9957	0.7203	25556.65	29.701	30.342	-5.687	0.2223	0.8334
0.2660	51.615	0.1565	0.8385	0.8558	0.9607	0.9961	0.7482	31618.92	30.314	30.987	-5.041	0.2751	0.8511

Table 6. Concluded

(b) Continued

y, in.	pitot pressure, psia	y/δ	M/M_e	u/u_e	ρ/ρ_e	$T_t/T_{t,e}$	$(T_t-T_w)/(T_{t,e}-T_w)$	y^+	u^+	u'/u_τ	$(u'-u_e')/u_\tau$	y/δ_u	u'/u_e'
0.3260	52.428	0.1918	0.8586	0.8743	0.9652	0.9966	0.7784	38751.01	30.969	31.677	-4.352	0.3371	0.8701
0.3960	53.222	0.2329	0.8776	0.8916	0.9695	0.9970	0.8073	47071.78	31.582	32.325	-3.704	0.4095	0.8878
0.4750	54.196	0.2794	0.9001	0.9120	0.9748	0.9976	0.8419	56462.36	32.302	33.087	-2.942	0.4912	0.9088
0.5660	54.996	0.3329	0.9180	0.9280	0.9791	0.9980	0.8697	67279.36	32.870	33.689	-2.340	0.5853	0.9253
0.6360	55.810	0.3741	0.9356	0.9437	0.9834	0.9984	0.8973	75600.13	33.426	34.280	-1.749	0.6577	0.9415
0.7165	56.566	0.4215	0.9516	0.9578	0.9874	0.9988	0.9225	85169.02	33.925	34.811	-1.218	0.7410	0.9561
0.7960	57.184	0.4682	0.9643	0.9690	0.9906	0.9991	0.9427	94619.03	34.321	35.233	-0.795	0.8232	0.9677
0.8780	57.882	0.5165	0.9784	0.9812	0.9943	0.9995	0.9652	104366.22	34.757	35.698	-0.331	0.9080	0.9805
0.9770	58.449	0.5747	0.9896	0.9910	0.9972	0.9997	0.9832	116134.17	35.101	36.066	0.037	1.0103	0.9906
1.0770	58.760	0.6335	0.9956	0.9962	0.9988	0.9999	0.9929	128020.98	35.287	36.264	0.236	1.1138	0.9961
1.2010	58.974	0.7065	0.9997	0.9998	0.9999	1.0000	0.9996	142760.63	35.413	36.400	0.371	1.2420	0.9998
1.3240	59.026	0.7788	1.0007	1.0006	1.0002	1.0000	1.0012	157381.41	35.443	36.432	0.404	1.3692	1.0007
1.4755	58.933	0.8679	0.9990	0.9991	0.9997	1.0000	0.9983	175389.93	35.389	36.374	0.345	1.5259	0.9991
1.6280	59.021	0.9576	1.0006	1.0006	1.0002	1.0000	1.0010	193517.32	35.440	36.429	0.401	1.6836	1.0006
1.8150	58.934	1.0000	0.9990	0.9991	0.9997	1.0000	0.9983	215745.66	35.389	36.374	0.346	1.8769	1.0000
2.2000	59.080	1.2941	1.0018	1.0015	1.0005	1.0000	1.0029	261509.89	35.475	36.466	0.438	2.2751	1.0016

Table 7. Preston Tube Data at Station 2

NTF Test 83, Station 2

Point	M_e	R/ft	R'/ft	T_t °F	T_w °F	c_f	R_θ'	c_f'
M=0.4, hot								
451	0.401	6.0666E+06	5.8889E+06	119.4	115.3	1.9910E-03	5.8180E+04	2.0250E-03
452	0.402	6.0612E+06	5.8842E+06	119.8	115.7	1.9910E-03	5.8140E+04	2.0250E-03
453	0.401	6.0602E+06	5.8801E+06	119.7	116.0	1.9890E-03	5.8130E+04	2.0230E-03
457	0.401	6.0585E+06	5.8717E+06	120.0	117.1	1.9650E-03	5.8110E+04	2.0010E-03
458	0.402	6.0596E+06	5.8713E+06	120.0	117.3	1.9680E-03	5.8120E+04	2.0040E-03
459	0.401	6.0539E+06	5.8664E+06	120.3	117.5	1.9680E-03	5.8070E+04	2.0040E-03
469	0.402	6.0502E+06	5.8543E+06	120.7	118.9	1.9860E-03	5.8040E+04	2.0230E-03
470	0.401	6.0494E+06	5.8526E+06	120.6	119.0	1.9840E-03	5.8040E+04	2.0210E-03
471	0.401	6.0483E+06	5.8516E+06	120.7	119.0	1.9860E-03	5.8030E+04	2.0240E-03
352	0.401	1.5015E+07	1.4505E+07	121.0	120.4	1.7540E-03	1.2910E+05	1.7890E-03
353	0.400	1.5007E+07	1.4498E+07	121.0	120.4	1.7510E-03	1.2900E+05	1.7860E-03
354	0.400	1.5008E+07	1.4497E+07	121.0	120.5	1.7490E-03	1.2900E+05	1.7840E-03
358	0.401	1.5026E+07	1.4508E+07	120.7	120.5	1.7260E-03	1.2920E+05	1.7610E-03
359	0.401	1.5020E+07	1.4505E+07	120.9	120.5	1.7270E-03	1.2910E+05	1.7610E-03
360	0.400	1.5013E+07	1.4500E+07	121.0	120.5	1.7300E-03	1.2910E+05	1.7640E-03
370	0.401	1.5055E+07	1.4519E+07	119.8	120.4	1.7430E-03	1.2940E+05	1.7790E-03
371	0.400	1.5055E+07	1.4521E+07	119.7	120.3	1.7410E-03	1.2940E+05	1.7770E-03
372	0.400	1.5055E+07	1.4520E+07	119.7	120.2	1.7460E-03	1.2940E+05	1.7830E-03
373	0.400	1.5078E+07	1.4544E+07	119.0	119.4	1.7420E-03	1.2960E+05	1.7780E-03
374	0.400	1.5088E+07	1.4553E+07	118.7	119.2	1.7420E-03	1.2970E+05	1.7780E-03
375	0.400	1.5078E+07	1.4553E+07	119.1	119.1	1.7420E-03	1.2960E+05	1.7780E-03
379	0.400	1.5082E+07	1.4556E+07	118.9	119.0	1.7270E-03	1.2960E+05	1.7620E-03
380	0.400	1.5080E+07	1.4555E+07	118.9	118.9	1.7270E-03	1.2960E+05	1.7620E-03
381	0.400	1.5077E+07	1.4553E+07	119.0	118.9	1.7250E-03	1.2960E+05	1.7610E-03
395	0.401	1.5073E+07	1.4554E+07	119.9	119.5	1.7540E-03	1.2950E+05	1.7890E-03
396	0.401	1.5068E+07	1.4551E+07	120.0	119.6	1.7530E-03	1.2950E+05	1.7880E-03
397	0.401	1.5067E+07	1.4549E+07	120.0	119.7	1.7540E-03	1.2950E+05	1.7890E-03
401	0.401	1.5063E+07	1.4543E+07	120.1	119.8	1.7350E-03	1.2950E+05	1.7700E-03
402	0.401	1.5057E+07	1.4539E+07	120.2	119.8	1.7340E-03	1.2940E+05	1.7690E-03
403	0.401	1.5056E+07	1.4537E+07	120.2	119.9	1.7330E-03	1.2940E+05	1.7680E-03
413	0.401	1.5043E+07	1.4525E+07	120.7	120.3	1.7510E-03	1.2930E+05	1.7860E-03
414	0.401	1.5043E+07	1.4524E+07	120.7	120.4	1.7510E-03	1.2930E+05	1.7870E-03
415	0.401	1.5040E+07	1.4521E+07	120.7	120.4	1.7510E-03	1.2930E+05	1.7870E-03
M=0.7, hot								
473	0.703	6.0654E+06	5.4877E+06	121.4	116.8	1.9640E-03	4.8160E+04	2.0780E-03
474	0.702	6.0386E+06	5.4699E+06	122.6	117.2	1.9680E-03	4.7970E+04	2.0810E-03
475	0.703	6.0521E+06	5.4726E+06	121.9	117.6	1.9610E-03	4.8050E+04	2.0760E-03
M=0.85, hot								
476	0.851	6.0490E+06	5.1857E+06	119.8	119.2	1.9350E-03	4.5570E+04	2.1100E-03
477	0.851	6.0191E+06	5.1831E+06	122.9	119.2	1.9400E-03	4.5360E+04	2.1100E-03
478	0.853	5.9904E+06	5.1692E+06	125.1	119.6	1.9410E-03	4.5170E+04	2.1090E-03
482	0.852	6.0146E+06	5.1751E+06	123.3	119.8	1.9180E-03	4.5330E+04	2.0870E-03
483	0.852	6.0429E+06	5.1854E+06	121.3	119.7	1.9130E-03	4.5530E+04	2.0850E-03
484	0.852	6.0411E+06	5.1866E+06	121.4	119.6	1.9170E-03	4.5510E+04	2.0880E-03
495	0.853	6.0324E+06	5.1840E+06	122.0	119.4	1.9320E-03	4.5460E+04	2.1040E-03
496	0.852	6.0372E+06	5.1859E+06	121.7	119.4	1.9290E-03	4.5490E+04	2.1010E-03
497	0.852	6.0392E+06	5.1868E+06	121.5	119.4	1.9320E-03	4.5500E+04	2.1040E-03
498	0.852	6.0370E+06	5.1866E+06	121.7	119.3	1.9310E-03	4.5490E+04	2.1030E-03
499	0.852	6.0387E+06	5.1874E+06	121.5	119.2	1.9320E-03	4.5500E+04	2.1040E-03

Table 7. Concluded

Point	M_e	R/ft	R'/ft	T, °F	T_w, °F	c_f	$R_\theta{}'$	$c_f{}'$
500	0.853	6.0435E+06	5.1891E+06	121.2	119.2	1.9310E-03	4.5530E+04	2.1040E-03
513	0.852	6.0482E+06	5.2010E+06	120.8	117.8	1.9340E-03	4.5560E+04	2.1050E-03
514	0.852	6.0485E+06	5.2008E+06	120.9	117.9	1.9310E-03	4.5570E+04	2.1020E-03
515	0.852	6.0473E+06	5.1998E+06	120.9	117.9	1.9300E-03	4.5560E+04	2.1010E-03
M=0.4, cold								
617	0.402	1.5159E+07	1.4605E+07	-251.1	-251.7	1.7800E-03	1.3020E+05	1.8160E-03
618	0.402	1.5135E+07	1.4586E+07	-250.8	-251.5	1.7780E-03	1.3000E+05	1.8130E-03
621	0.401	1.5126E+07	1.4548E+07	-250.8	-251.1	1.7620E-03	1.2990E+05	1.7980E-03
622	0.402	1.5136E+07	1.4550E+07	-250.7	-250.9	1.7600E-03	1.3000E+05	1.7970E-03
629	0.402	3.5230E+07	3.3351E+07	-250.5	-247.5	1.5640E-03	2.7330E+05	1.6130E-03
630	0.401	3.5446E+07	3.3509E+07	-251.5	-248.2	1.5630E-03	2.7480E+05	1.6130E-03
631	0.402	5.0631E+07	4.8006E+07	-251.4	-249.1	1.4620E-03	3.7610E+05	1.5080E-03
632	0.401	5.0347E+07	4.7947E+07	-250.9	-249.5	1.4740E-03	3.7410E+05	1.5160E-03
633	0.401	6.5624E+07	6.2506E+07	-251.2	-250.2	1.4220E-03	4.7240E+05	1.4650E-03
634	0.402	6.5650E+07	6.2572E+07	-251.2	-250.3	1.4180E-03	4.7260E+05	1.4600E-03
637	0.402	6.5583E+07	6.2634E+07	-251.0	-250.6	1.4090E-03	4.7210E+05	1.4490E-03
638	0.402	6.5543E+07	6.2603E+07	-251.0	-250.6	1.4090E-03	4.7190E+05	1.4490E-03
M=0.6, cold								
601	0.601	3.5252E+07	3.2015E+07	-250.9	-249.5	1.5650E-03	2.5490E+05	1.6490E-03
602	0.601	3.5233E+07	3.1995E+07	-250.8	-249.4	1.5670E-03	2.5490E+05	1.6510E-03
589	0.602	5.0142E+07	4.6565E+07	-250.3	-254.2	1.4990E-03	3.5010E+05	1.5620E-03
590	0.602	5.0208E+07	4.6591E+07	-250.4	-254.2	1.4980E-03	3.5040E+05	1.5620E-03
573	0.602	6.5535E+07	6.0300E+07	-250.8	-253.1	1.4340E-03	4.4550E+05	1.5030E-03
574	0.602	6.5528E+07	6.0235E+07	-250.8	-252.9	1.4330E-03	4.4550E+05	1.5040E-03
569	0.602	8.0121E+07	7.4142E+07	-250.1	-253.9	1.4100E-03	5.3410E+05	1.4760E-03
570	0.602	8.0213E+07	7.4150E+07	-250.2	-253.8	1.4110E-03	5.3470E+05	1.4780E-03
555	0.603	9.0406E+07	8.3760E+07	-250.2	-254.7	1.3840E-03	5.9500E+05	1.4490E-03
556	0.602	9.0296E+07	8.3622E+07	-250.4	-254.6	1.3910E-03	5.9500E+05	1.4560E-03
559	0.602	9.0283E+07	8.3602E+07	-250.3	-254.6	1.3770E-03	5.9490E+05	1.4420E-03
560	0.602	9.0308E+07	8.3633E+07	-250.3	-254.6	1.3780E-03	5.9500E+05	1.4430E-03
567	0.602	9.0162E+07	8.3582E+07	-250.1	-254.6	1.3940E-03	5.9410E+05	1.4590E-03
568	0.602	9.0168E+07	8.3543E+07	-250.1	-254.5	1.3910E-03	5.9420E+05	1.4560E-03
M=0.7, cold								
603	0.701	3.5233E+07	3.1218E+07	-251.0	-251.0	1.5570E-03	2.3800E+05	1.6610E-03
604	0.701	3.5236E+07	3.1195E+07	-250.9	-250.8	1.5580E-03	2.3790E+05	1.6630E-03
591	0.702	5.0164E+07	4.4922E+07	-250.6	-253.4	1.4920E-03	3.2770E+05	1.5850E-03
592	0.702	5.0223E+07	4.4848E+07	-250.7	-252.9	1.4880E-03	3.2800E+05	1.5830E-03
575	0.702	6.5241E+07	5.8341E+07	-250.2	-253.2	1.4380E-03	4.1580E+05	1.5310E-03
576	0.702	6.5236E+07	5.8374E+07	-250.3	-253.3	1.4430E-03	4.1590E+05	1.5360E-03
571	0.702	8.0364E+07	7.2048E+07	-250.5	-254.3	1.4010E-03	5.0260E+05	1.4920E-03
572	0.702	8.0344E+07	7.2061E+07	-250.4	-254.4	1.4010E-03	5.0240E+05	1.4920E-03
M=0.85, cold								
605	0.850	3.5125E+07	2.9655E+07	-250.8	-252.0	1.5450E-03	2.2570E+05	1.6900E-03
606	0.852	3.5179E+07	2.9644E+07	-250.9	-251.8	1.5430E-03	2.2600E+05	1.6900E-03
609	0.852	3.5107E+07	2.9566E+07	-250.6	-251.4	1.5290E-03	2.2560E+05	1.6750E-03
610	0.850	3.5113E+07	2.9551E+07	-250.7	-251.3	1.5300E-03	2.2560E+05	1.6770E-03
593	0.852	4.9993E+07	4.2554E+07	-249.8	-253.5	1.4830E-03	3.1120E+05	1.6180E-03
594	0.851	5.0107E+07	4.2604E+07	-250.2	-253.6	1.4820E-03	3.1180E+05	1.6180E-03
577	0.850	6.5086E+07	5.5394E+07	-250.2	-254.1	1.4260E-03	3.9560E+05	1.5580E-03
578	0.851	6.5082E+07	5.5443E+07	-250.1	-254.3	1.4280E-03	3.9550E+05	1.5600E-03
581	0.851	6.5139E+07	5.5614E+07	-250.3	-254.9	1.4160E-03	3.9590E+05	1.5450E-03
582	0.852	6.5202E+07	5.5646E+07	-250.3	-255.0	1.4140E-03	3.9620E+05	1.5430E-03

Table 8. Balance Data at Station 2

Point	M_e	R/ft	Roll, deg	τ, grams	c_f	By Reference Temperature $c_f{}'$	From Surveys $R_\theta{}'$
Runs 172-182							
1790	0.401	1.505E+07	0.003	55.623	1.791E-03	1.825E-03	1.2937E+05
1791	0.401	1.505E+07	0.004	55.646	1.793E-03	1.826E-03	1.2937E+05
1792	0.401	1.505E+07	0.005	55.615	1.791E-03	1.824E-03	1.2937E+05
1820	0.401	1.504E+07	-0.017	55.732	1.795E-03	1.828E-03	1.2929E+05
1821	0.401	1.504E+07	-0.023	55.850	1.800E-03	1.833E-03	1.2929E+05
1822	0.401	1.504E+07	-0.019	55.601	1.791E-03	1.824E-03	1.2929E+05
1858	0.400	1.503E+07	-0.097	55.555	1.791E-03	1.825E-03	1.2921E+05
1859	0.401	1.504E+07	-0.096	55.648	1.794E-03	1.827E-03	1.2929E+05
1860	0.401	1.504E+07	-0.103	52.540	1.693E-03	1.725E-03	1.2929E+05
Runs 183-193							
1934	0.401	1.507E+07	-0.087	57.788	1.856E-03	1.890E-03	1.2952E+05
1935	0.401	1.506E+07	-0.088	59.476	1.910E-03	1.945E-03	1.2944E+05
1936	0.401	1.506E+07	-0.085	58.003	1.863E-03	1.897E-03	1.2944E+05
Runs 194-206							
2220	0.402	1.509E+07	-0.068	58.027	1.862E-03	1.897E-03	1.2967E+05
2221	0.401	1.508E+07	-0.068	58.966	1.893E-03	1.929E-03	1.2959E+05
2222	0.401	1.509E+07	-0.068	59.106	1.897E-03	1.933E-03	1.2967E+05
2241	0.401	1.508E+07	-0.025	58.768	1.887E-03	1.922E-03	1.2959E+05
2242	0.402	1.509E+07	-0.068	57.771	1.854E-03	1.888E-03	1.2967E+05
2243	0.401	1.508E+07	-0.064	57.147	1.835E-03	1.869E-03	1.2959E+05
Runs 207-228							
2249	0.201	6.044E+06	-0.060	13.446	2.099E-03	2.109E-03	5.5916E+04
2250	0.200	6.041E+06	-0.059	13.409	2.094E-03	2.104E-03	5.5893E+04
2251	0.200	6.041E+06	-0.057	13.436	2.098E-03	2.108E-03	5.5893E+04
2270	0.201	6.045E+06	0.040	13.388	2.087E-03	2.097E-03	5.5924E+04
2271	0.201	6.045E+06	-0.051	13.415	2.091E-03	2.101E-03	5.5924E+04
2272	0.201	6.044E+06	-0.044	13.401	2.090E-03	2.100E-03	5.5916E+04
2303	0.401	6.050E+06	-0.049	25.879	2.078E-03	2.116E-03	5.8042E+04
2304	0.401	6.048E+06	-0.051	25.905	2.079E-03	2.118E-03	5.8024E+04
2305	0.402	6.053E+06	-0.050	25.862	2.075E-03	2.114E-03	5.8066E+04
2324	0.402	6.063E+06	-0.039	25.821	2.071E-03	2.110E-03	5.8150E+04
2325	0.401	6.061E+06	-0.042	25.813	2.072E-03	2.110E-03	5.8134E+04
2326	0.401	6.061E+06	-0.043	25.834	2.073E-03	2.112E-03	5.8134E+04
2358	0.602	6.048E+06	0.023	36.083	2.040E-03	2.126E-03	5.2017E+04
2359	0.602	6.031E+06	0.024	36.131	2.043E-03	2.128E-03	5.1877E+04
2360	0.601	6.042E+06	0.026	36.089	2.042E-03	2.127E-03	5.1979E+04
2379	0.602	6.041E+06	-0.058	36.109	2.041E-03	2.126E-03	5.1950E+04
2380	0.602	6.041E+06	-0.056	36.130	2.042E-03	2.128E-03	5.1954E+04
2381	0.602	6.041E+06	-0.054	36.074	2.039E-03	2.125E-03	5.1954E+04
2412	0.850	6.028E+06	-0.069	46.042	2.006E-03	2.174E-03	4.5421E+04
2413	0.850	6.017E+06	-0.069	46.037	2.007E-03	2.175E-03	4.5344E+04
2414	0.850	6.012E+06	-0.067	46.236	2.016E-03	2.185E-03	4.5310E+04
2433	0.850	6.028E+06	-0.056	45.878	1.999E-03	2.166E-03	4.5421E+04
2434	0.850	6.026E+06	-0.058	46.105	2.010E-03	2.178E-03	4.5406E+04
2435	0.850	6.024E+06	-0.059	45.949	2.004E-03	2.171E-03	4.5392E+04
2463	0.850	6.036E+06	-0.060	45.963	2.004E-03	2.171E-03	4.5475E+04
2464	0.850	6.036E+06	-0.062	46.219	2.015E-03	2.183E-03	4.5475E+04

Table 8. Continued

Point	M_e	R/ft	Roll, deg	τ, grams	c_f	By Reference Temperature c_f'	From Surveys R_θ'
2465	0.850	6.036E+06	-0.057	45.976	2.004E-03	2.172E-03	4.5475E+04
2499	0.849	6.041E+06	-0.067	45.991	2.006E-03	2.173E-03	4.5509E+04
2500	0.850	6.041E+06	-0.072	46.103	2.010E-03	2.178E-03	4.5509E+04
2501	0.850	6.040E+06	-0.071	45.983	2.005E-03	2.173E-03	4.5502E+04
2551	0.850	6.042E+06	-0.051	45.972	2.004E-03	2.171E-03	4.5516E+04
2552	0.850	6.042E+06	-0.053	46.012	2.006E-03	2.173E-03	4.5516E+04
2553	0.850	6.041E+06	-0.056	46.379	2.022E-03	2.191E-03	4.5509E+04
Runs 229-236							
2615	0.202	3.547E+07	-0.035	14.624	1.575E-03	1.583E-03	2.8538E+05
2616	0.201	3.561E+07	-0.041	14.536	1.567E-03	1.574E-03	2.8647E+05
2617	0.201	3.576E+07	-0.042	14.559	1.570E-03	1.577E-03	2.8764E+05
2633	0.202	3.503E+07	-0.027	14.648	1.575E-03	1.582E-03	2.8195E+05
2634	0.202	3.503E+07	-0.031	14.713	1.582E-03	1.590E-03	2.8195E+05
2635	0.201	3.498E+07	-0.028	14.645	1.577E-03	1.584E-03	2.8156E+05
2636	0.401	6.463E+07	-0.009	49.335	1.498E-03	1.526E-03	4.6601E+05
2637	0.401	6.466E+07	-0.009	49.494	1.501E-03	1.529E-03	4.6623E+05
2638	0.401	6.464E+07	-0.008	49.627	1.507E-03	1.535E-03	4.6607E+05
2654	0.401	6.534E+07	0.001	48.681	1.475E-03	1.502E-03	4.7057E+05
2655	0.401	6.535E+07	-0.007	48.591	1.473E-03	1.500E-03	4.7063E+05
2656	0.401	6.528E+07	-0.002	48.364	1.466E-03	1.494E-03	4.7017E+05
Runs 237-250							
2709	0.601	9.040E+07	0.010	89.449	1.393E-03	1.451E-03	5.9598E+05
2714	0.401	3.517E+07	0.008	28.813	1.626E-03	1.656E-03	2.7292E+05
2715	0.401	3.512E+07	0.007	28.773	1.625E-03	1.655E-03	2.7256E+05
2716	0.401	3.518E+07	0.006	28.772	1.623E-03	1.653E-03	2.7299E+05
2732	0.401	3.519E+07	0.020	28.740	1.621E-03	1.651E-03	2.7306E+05
2733	0.401	3.516E+07	0.010	28.744	1.621E-03	1.651E-03	2.7285E+05
2734	0.401	3.517E+07	0.012	28.776	1.622E-03	1.653E-03	2.7292E+05
2735	0.601	3.493E+07	0.027	40.065	1.597E-03	1.664E-03	2.5285E+05
2736	0.601	3.497E+07	0.017	40.031	1.595E-03	1.662E-03	2.5309E+05
2737	0.601	3.493E+07	0.024	40.049	1.596E-03	1.662E-03	2.5281E+05
2789	0.601	3.490E+07	0.045	39.962	1.591E-03	1.658E-03	2.5258E+05
2790	0.601	3.494E+07	0.042	39.978	1.592E-03	1.659E-03	2.5286E+05
2791	0.602	3.492E+07	0.044	40.013	1.592E-03	1.659E-03	2.5268E+05
2792	0.849	3.483E+07	0.050	52.161	1.633E-03	1.769E-03	2.2397E+05
2793	0.849	3.481E+07	0.049	51.010	1.598E-03	1.731E-03	2.2385E+05
2794	0.849	3.483E+07	0.046	51.536	1.613E-03	1.748E-03	2.2397E+05
2810	0.850	3.488E+07	0.055	49.996	1.563E-03	1.694E-03	2.2427E+05
2811	0.850	3.482E+07	0.051	50.522	1.579E-03	1.711E-03	2.2392E+05
2812	0.850	3.488E+07	0.055	51.068	1.597E-03	1.730E-03	2.2427E+05
2813	0.402	1.504E+07	0.053	13.633	1.786E-03	1.820E-03	1.2929E+05
2814	0.402	1.502E+07	0.057	13.619	1.787E-03	1.820E-03	1.2914E+05
2815	0.402	1.503E+07	0.057	13.618	1.787E-03	1.820E-03	1.2922E+05
2831	0.402	1.506E+07	0.062	13.598	1.782E-03	1.815E-03	1.2944E+05
2832	0.402	1.504E+07	0.060	13.587	1.783E-03	1.817E-03	1.2929E+05
2833	0.402	1.503E+07	0.061	13.602	1.783E-03	1.816E-03	1.2922E+05
Runs 251-266							
2975	0.402	1.511E+07	0.068	31.600	4.142E-03	4.219E-03	1.2982E+05
2939	0.402	1.509E+07	0.042	13.744	1.800E-03	1.834E-03	1.2967E+05
2977	0.402	1.511E+07	0.069	33.285	4.360E-03	4.441E-03	1.2982E+05
2976	0.402	1.512E+07	0.068	37.657	4.932E-03	5.025E-03	1.2990E+05
2940	0.402	1.514E+07	0.041	13.756	1.801E-03	1.835E-03	1.3005E+05
2941	0.402	1.515E+07	0.041	13.745	1.799E-03	1.833E-03	1.3012E+05

Table 8. Concluded

Point	M_e	R/ft	Roll, deg	τ, grams	c_f	By Reference Temperature c_f'	From Surveys R_θ'
2913	0.600	3.527E+07	0.125	39.924	1.595E-03	1.662E-03	2.5520E+05
2912	0.601	3.521E+07	0.137	39.942	1.595E-03	1.662E-03	2.5474E+05
2883	0.601	6.532E+07	0.419	66.761	1.437E-03	1.497E-03	4.4465E+05
2925	0.601	3.523E+07	0.059	39.895	1.592E-03	1.659E-03	2.5485E+05
2924	0.601	3.518E+07	0.065	39.869	1.591E-03	1.657E-03	2.5451E+05
2926	0.601	3.523E+07	0.061	39.853	1.590E-03	1.656E-03	2.5484E+05
2904	0.601	9.025E+07	0.269	86.264	1.342E-03	1.398E-03	5.9498E+05
2903	0.601	9.034E+07	0.330	86.604	1.347E-03	1.403E-03	5.9551E+05
2937	0.601	3.522E+07	0.043	39.873	1.590E-03	1.657E-03	2.5474E+05
2900	0.601	6.529E+07	0.252	63.268	1.360E-03	1.417E-03	4.4436E+05
2936	0.601	3.516E+07	0.048	39.904	1.591E-03	1.658E-03	2.5433E+05
2881	0.601	6.537E+07	0.421	66.743	1.435E-03	1.495E-03	4.4482E+05
2882	0.601	6.541E+07	0.420	66.378	1.427E-03	1.486E-03	4.4506E+05
2905	0.601	9.016E+07	0.258	86.578	1.346E-03	1.402E-03	5.9437E+05
2938	0.601	3.522E+07	0.039	39.878	1.590E-03	1.656E-03	2.5470E+05
2902	0.601	6.540E+07	0.253	63.494	1.364E-03	1.421E-03	4.4497E+05
2914	0.601	3.529E+07	0.128	39.939	1.591E-03	1.658E-03	2.5514E+05
2901	0.601	6.539E+07	0.251	63.302	1.360E-03	1.417E-03	4.4488E+05

Table C1. Instrumentation Locations
(a) Plug Locations

Plug Centers

Plug	x, in.	z, in.
1	13.25	0.000*
2	13.25	3.500
3	13.25	-3.500
4	30.75	0.000*
5	30.75	3.500
6	30.75	-3.500
7	48.25	0.000*
8	48.25	3.500
9	48.25	-3.500

Note:
* center of skin friction balance at
   Stations 1, 2, and 3

Table C1. Continued
(b) Pressure Orifice Locations

Orifice	x, in.	z, in.
1	4.250	0.000
2	6.250	0.000
3	8.250	0.000
4	10.250	0.000
5	16.250	0.000
6	18.250	0.000
7	20.250	0.000
8	22.250	0.000
9	24.250	0.000
10	26.250	0.000
11	27.750	0.000
12	33.750	0.000
13	35.750	0.000
14	37.750	0.000
15	39.750	0.000
16	41.750	0.000
17	43.750	0.000
18	45.250	0.000
19	51.250	0.000
20	53.250	0.000
21	55.250	0.000
22	57.250	0.000
23	4.250	4.375
24	16.250	4.375
25	22.250	4.375
26	33.750	4.375
27	39.750	4.375
28	51.250	4.375
29	4.250	-4.375
30	16.250	-4.375
31	22.250	-4.375
32	33.750	-4.375
33	39.750	-4.375
34	51.250	-4.375
35	10.250	6.000
36	10.250	4.500
37	10.250	3.000
38	10.250	1.500
39	10.250	-1.500
40	10.250	-3.000
41	10.250	-4.500
42	10.250	-6.000
43	27.750	6.000
44	27.750	4.500
45	27.750	3.000
46	27.750	1.500
47	27.750	-1.500
48	27.750	-3.000
49	27.750	-4.500
50	27.750	-6.000
51	45.250	6.000
52	45.250	4.500
53	45.250	3.000
54	45.250	1.500
55	45.250	-1.500
56	45.250	-3.000
57	45.250	-4.500
58	45.250	-6.000

Table C1. Continued
(c) Plug Orifice Locations

Station 1
Large Plug

Orifice	x, in.	z, in.
59	12.050	1.200
60	12.050	-1.200
61	12.400	0.850
62	12.400	-0.850
63	13.250	1.700
64	13.250	1.200
65	13.250	-1.200
66	13.250	-1.700
67	14.100	0.850
68	14.100	-0.850
69	14.450	1.200
70	14.450	-1.200

Small Plug

71	13.003	-0.247

Station 2

Orifice	x, in.	z, in.
59	17.500	1.200
60	17.500	-1.200
61	17.500	0.850
62	17.500	-0.850
63	17.500	1.700
64	17.500	1.200
65	17.500	-1.200
66	17.500	-1.700
67	17.500	0.850
68	17.500	-0.850
69	17.500	1.200
70	17.500	-1.200

71	17.500	-0.247

Station 3

Orifice	x, in.	z, in.
59	47.050	1.200
60	47.050	-1.200
61	47.400	0.850
62	47.400	-0.850
63	48.250	1.700
64	48.250	1.200
65	48.250	-1.200
66	48.250	-1.700
67	49.100	0.850
68	49.100	-0.850
69	49.450	1.200
70	49.450	-1.200

71	48.003	-0.247

Table C1. Concluded
(d) Thermocouple Locations

TC No.	x, in.	z, in.
1	5.250	0.000
2	17.250	0.000
3	25.250	0.000
4	34.750	0.000
5	42.750	0.000
6	52.250	0.000
7	4.250	2.625
8	12.250	2.625
9	16.250	2.625
10	29.750	2.625
11	47.250	2.625
12	12.250	4.375
13	29.750	4.375
14	47.250	4.375
15	4.250	-2.625
16	12.250	-2.625
17	16.250	-2.625
18	29.750	-2.625
19	47.250	-2.625
20	12.250	-4.375
21	29.750	-4.375
22	47.250	-4.375

23	backside, below T12
24	backside, below T13
25	backside, below T14
26	balance cannister
27	balance cannister
28	rake
29	rake
30	terminal strip - forward
31	terminal strip - mid
32	terminal strip - aft

Table C2. Rake Tube Locations

Tube No.	y, in.	Tube No.	y, in.
1	0.005	16	0.318
2	0.015	17	0.395
3	0.012	18	0.483
4	0.020	19	0.598
5	0.063	20	0.731
6	0.088	21	0.814
7	0.068	22	0.896
8	0.085	23	0.995
9	0.073	24	1.099
10	0.107	25	1.221
11	0.112	26	1.346
12	0.149	27	1.492
13	0.177	28	1.638
14	0.221	29	1.815
15	0.262	30	2.009
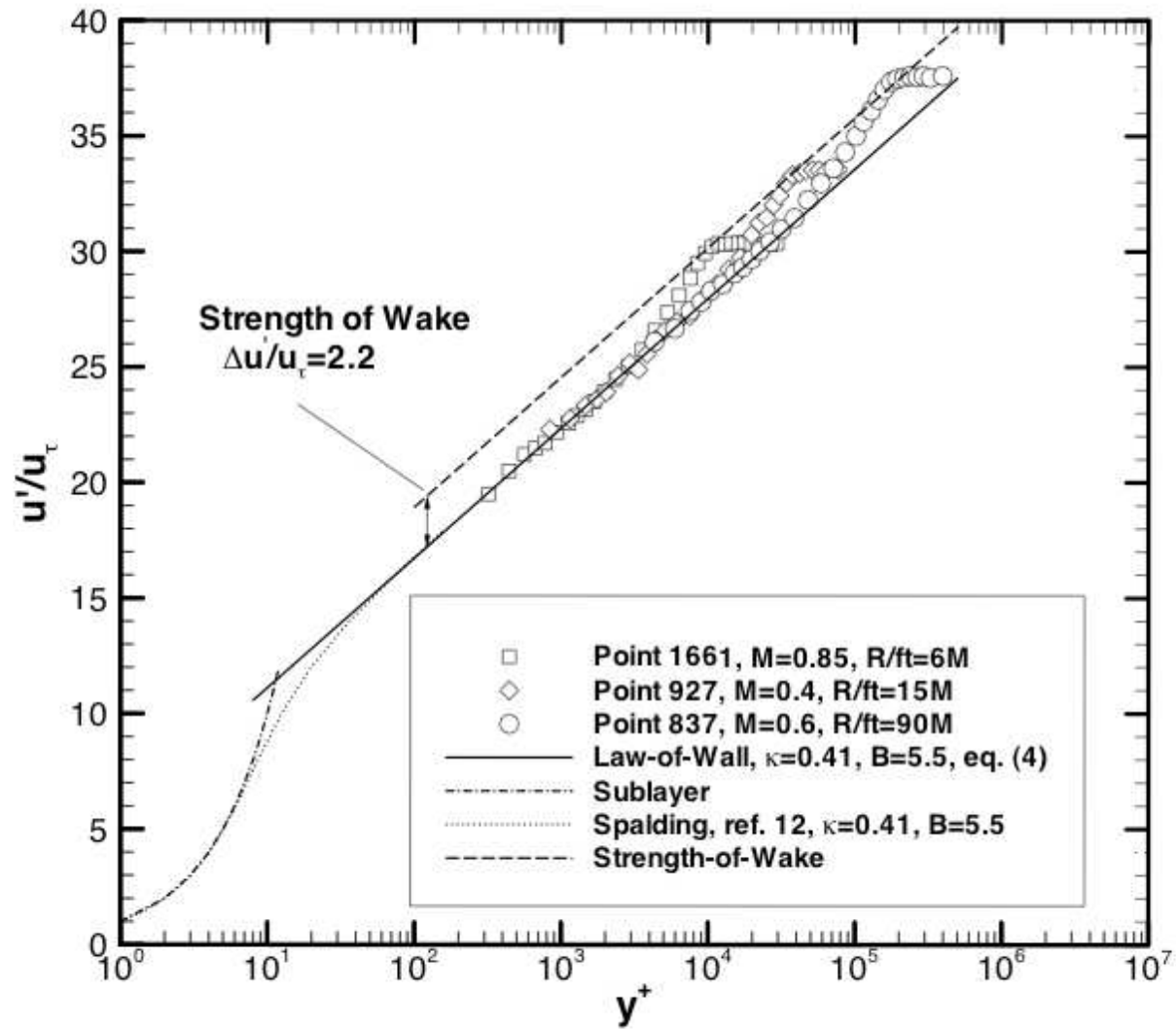
Figure 1. Transformed velocity profiles in law-of-wall coordinates—NTF data.
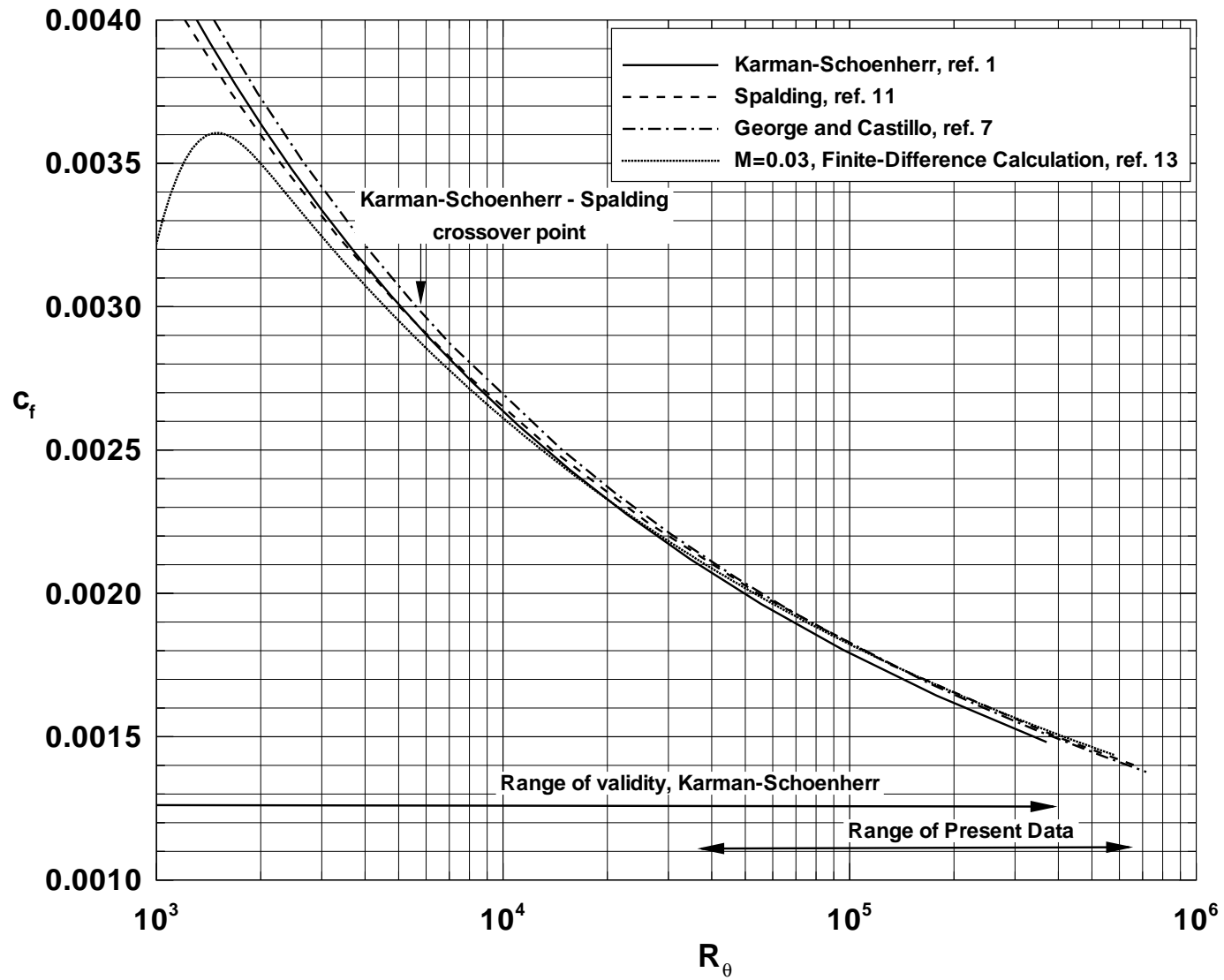
Figure 2. Incompressible flat plate skin friction theories.
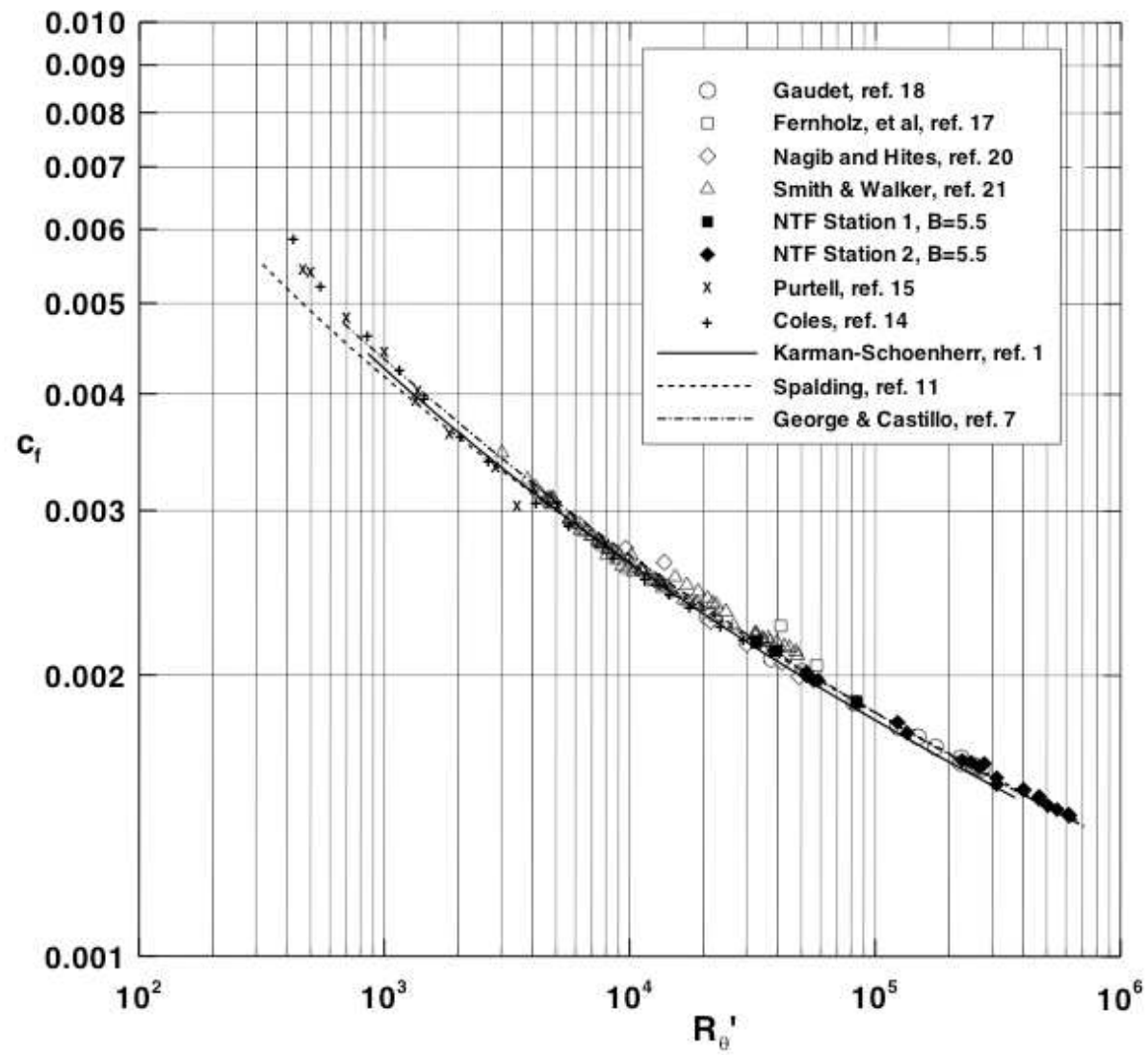
Figure 3. High Reynolds number c_f compared with theory.
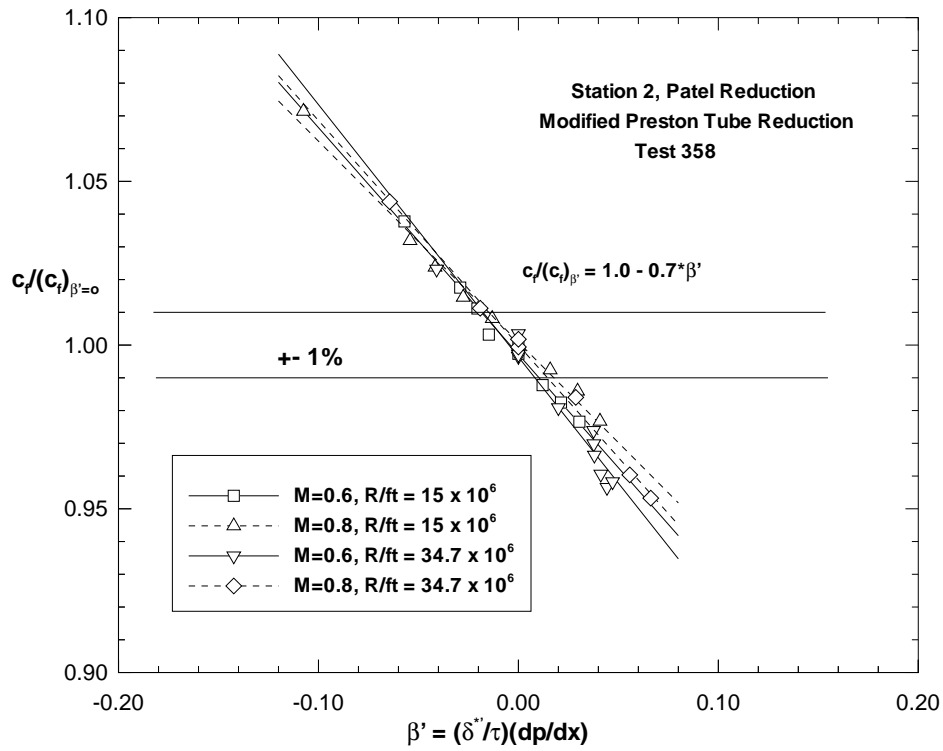
Figure 4. Effect of pressure gradient on Preston tube measured skin friction.

In the figure above:

Station 2, Patel Reduction
Modified Preston Tube Reduction
Test 358

$c_f/(c_f)_{\beta'} = 1.0 - 0.7 * \beta'$

+- 1%

$c_f/(c_f)_{\beta'=o}$

$\beta' = (\delta^{*}/\tau)(dp/dx)$

- M=0.6, R/ft = 15 x 10^6
- M=0.8, R/ft = 15 x 10^6
- M=0.6, R/ft = 34.7 x 10^6
- M=0.8, R/ft = 34.7 x 10^6
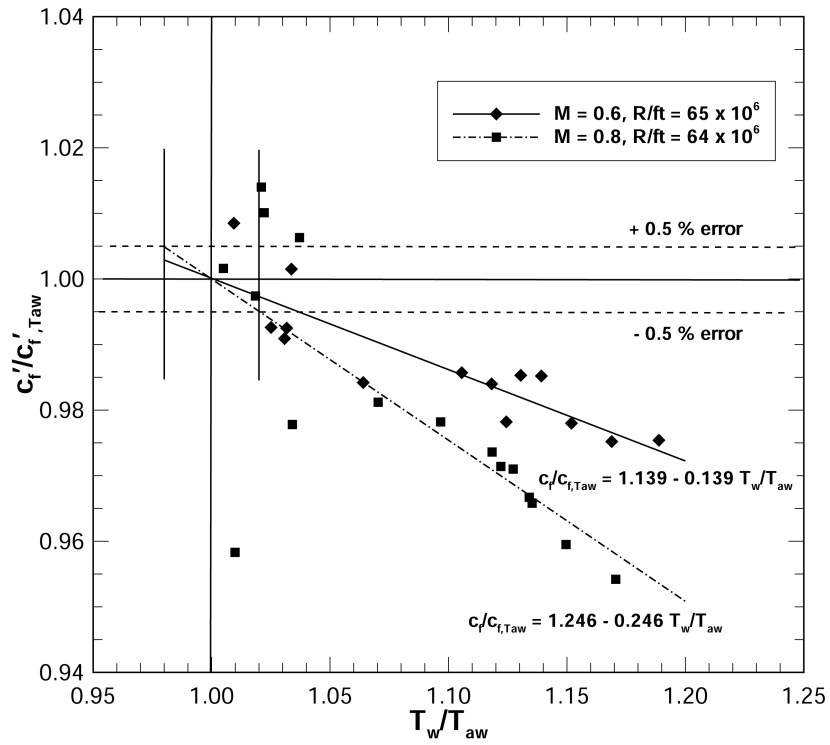
Figure 5. Effect of heat transfer on Preston tube measured skin friction.

In the figure above:

- M = 0.6, R/ft = 65 x 10^6
- M = 0.8, R/ft = 64 x 10^6

+ 0.5 % error

- 0.5 % error

$c_f'/c_{f,Taw}'$

T_w/T_{aw}

$c_f/c_{f,Taw} = 1.139 - 0.139\, T_w/T_{aw}$

$c_f/c_{f,Taw} = 1.246 - 0.246\, T_w/T_{aw}$

91
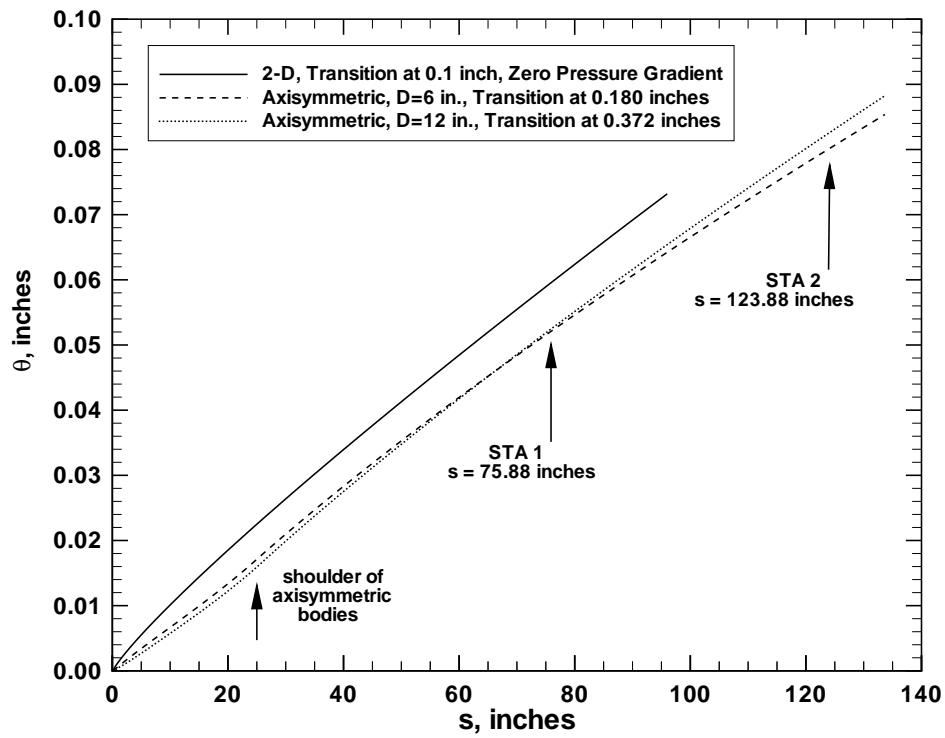
Figure 6. Effect of model geometry and pressure gradient on the downstream growth of momentum thickness at Mach 0.9.
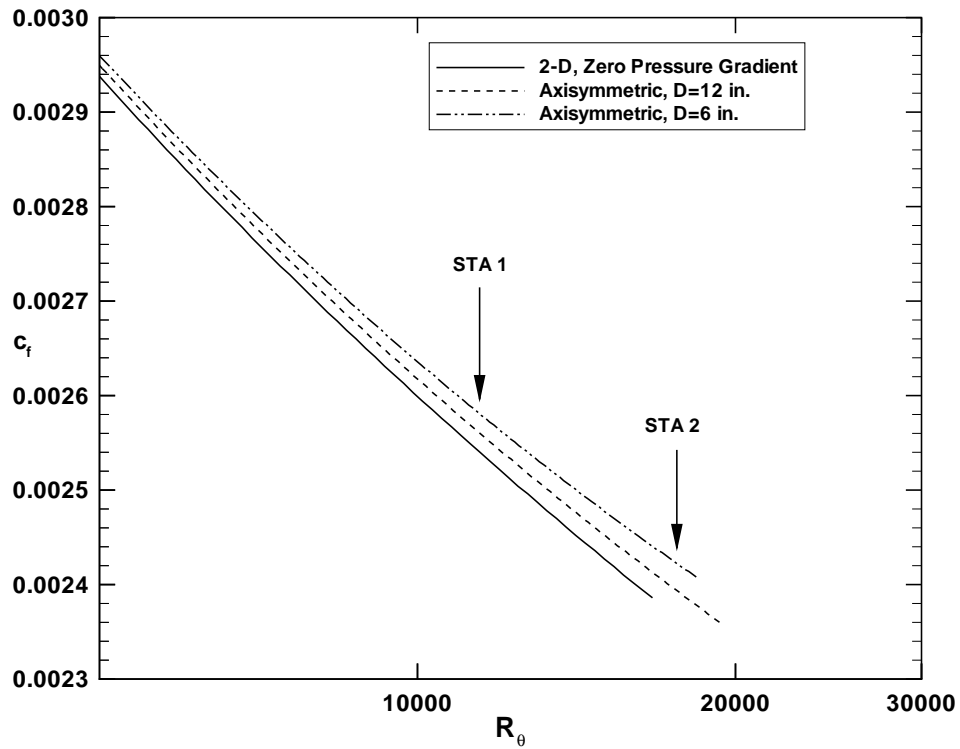
Figure 7. Comparison of flat plate and axisymmetric skin friction coefficients.
(a) Mach = 0.2, R/in = 1.48 x 10^6.
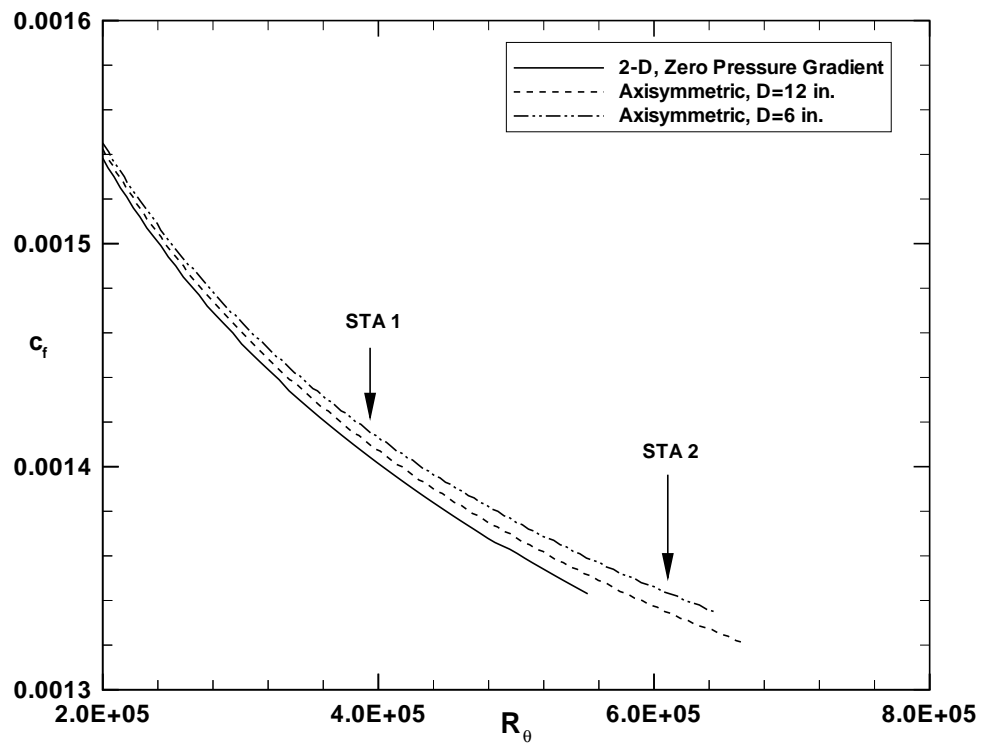
Figure 7. Concluded.
(b) Mach = 0.9, R/in = 90.5 x 10^6.
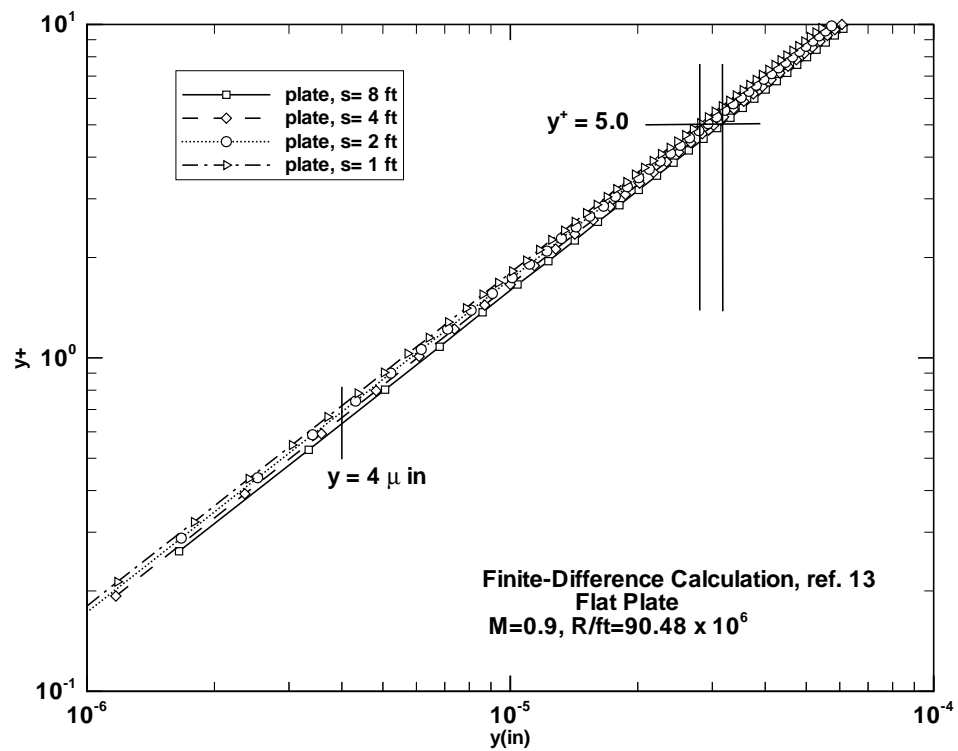
Figure 8. Calculated turbulent wall scaling.

Figure 9. Photograph of model in tunnel.
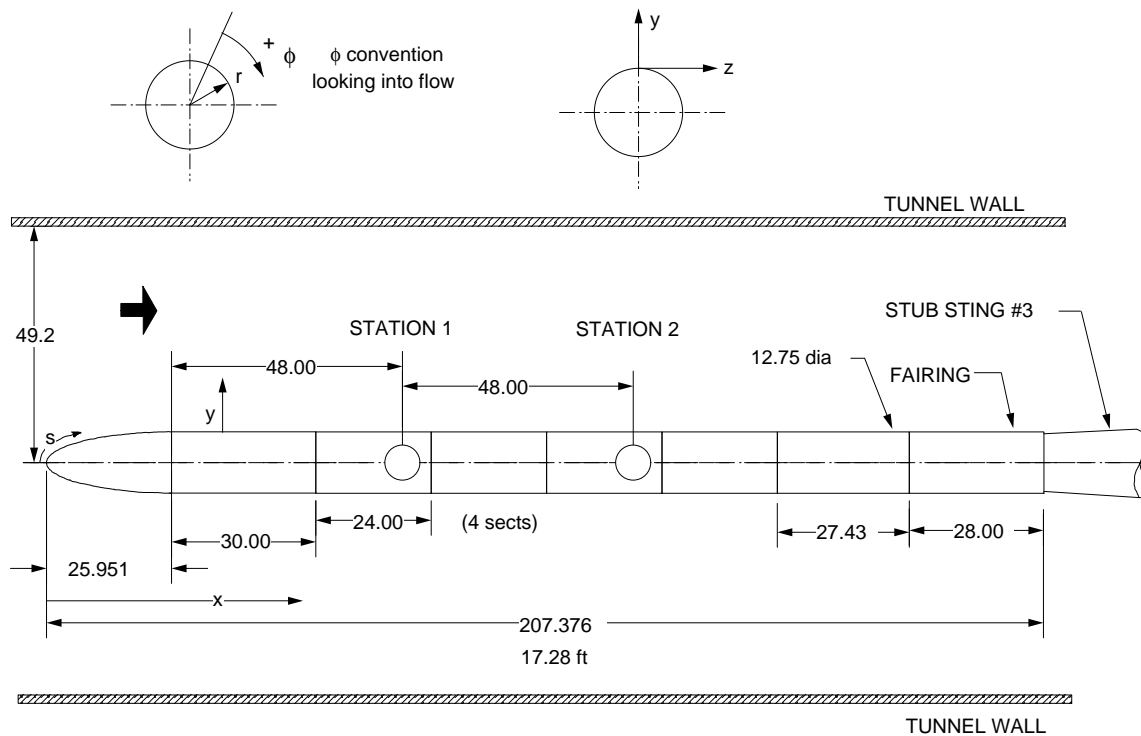
dimensions in inches unless noted

Figure 10. Model and instrumentation dimensions.
(a) Sketch of model in tunnel

94

NTF HIGH REYNOLDS NUMBER SKIN FRICTION MODEL
PLAN VIEW SURFACE LAYOUT, SECTIONS 3 & 5

Dimensions in inches.
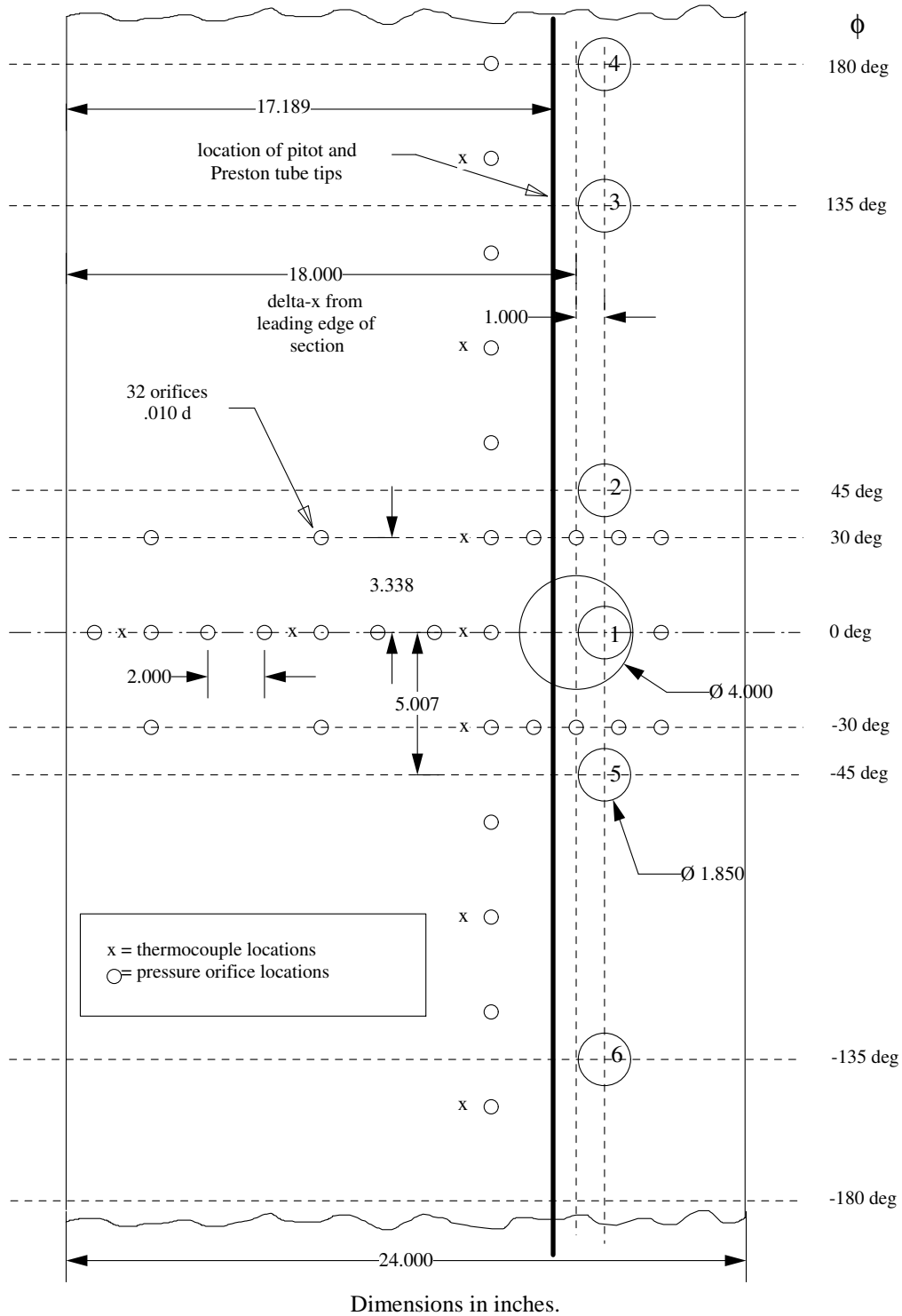
Figure 10. Continued
(b) Dimensions in vicinity of survey stations.

Ø 1.850

Ø .188   drill thru for Preston tube

1.000

5.0

.500

0.811

0.188

1.561

0.058 d
Preston Tube

0.062
extension
tube

.638

2.311

SECTION

TUBE TIP
LOCATION

TOP VIEW
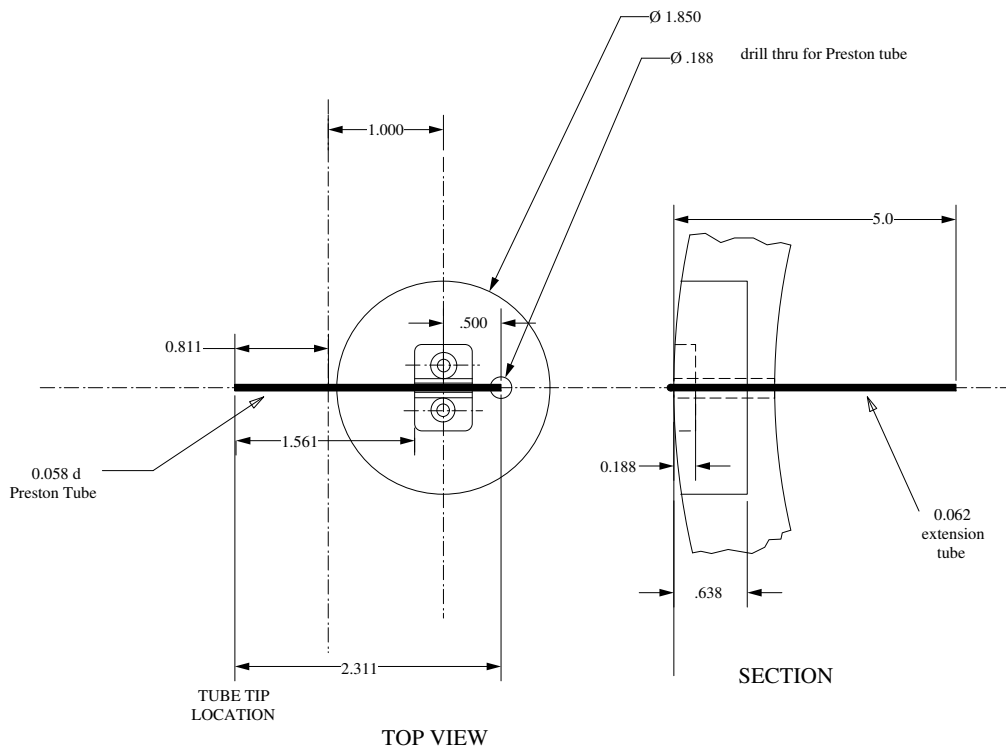
Figure 10. Continued.
(c) Sketch of Preston tube mounted on small plug.

SECTION

TOP VIEW

Ø 1.850

Ø .188   drill thru for Preston tube

Ø 4.000

1.000

5.0

.500

.811

.188

1.561

.058 d
Preston Tube

.638

.062
extension
tube

.750

.675

2.311

1.425

TUBE TIP
LOCATION
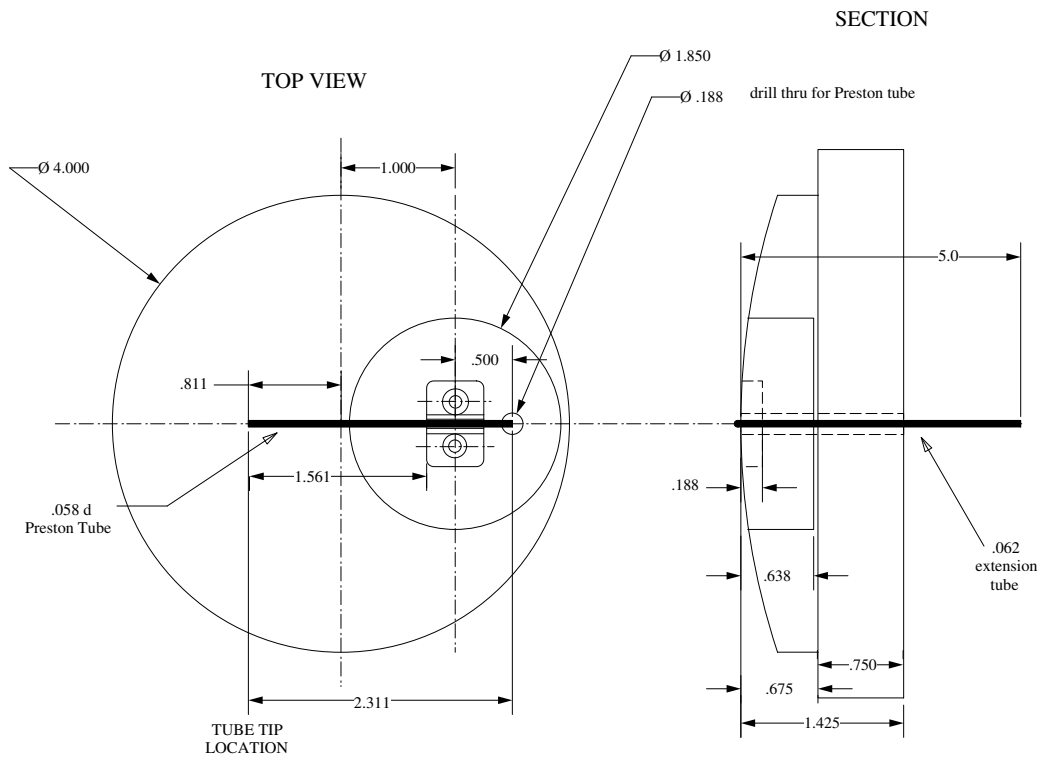
Figure 10. Continued.
(d) Sketch of Preston tube mounted on large plug.

96
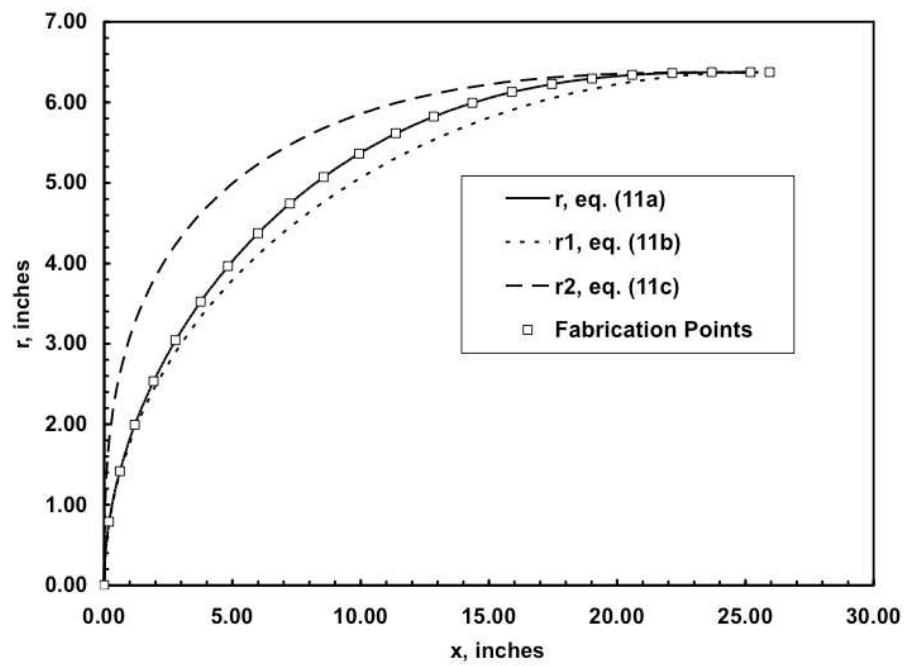
Figure 10. Continued.
(e) Nose Coordinates.
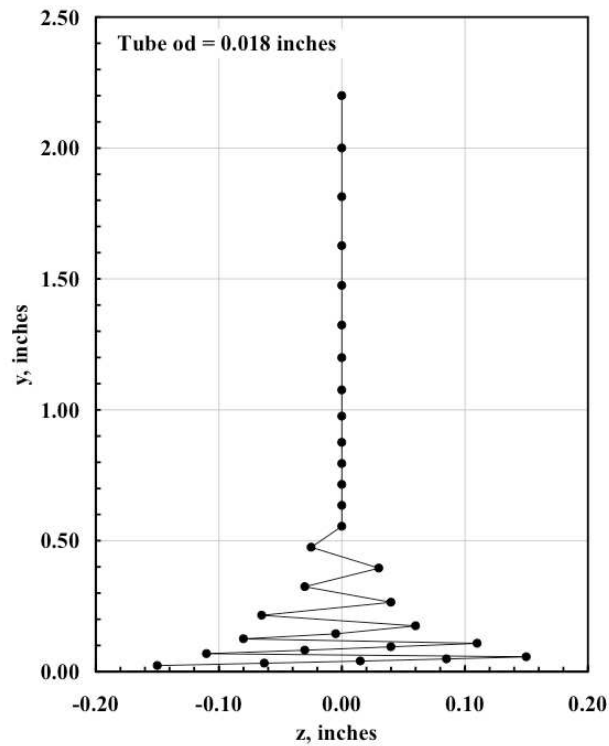
Figure 10. Concluded.
(f) Boundary layer rake tube placement.
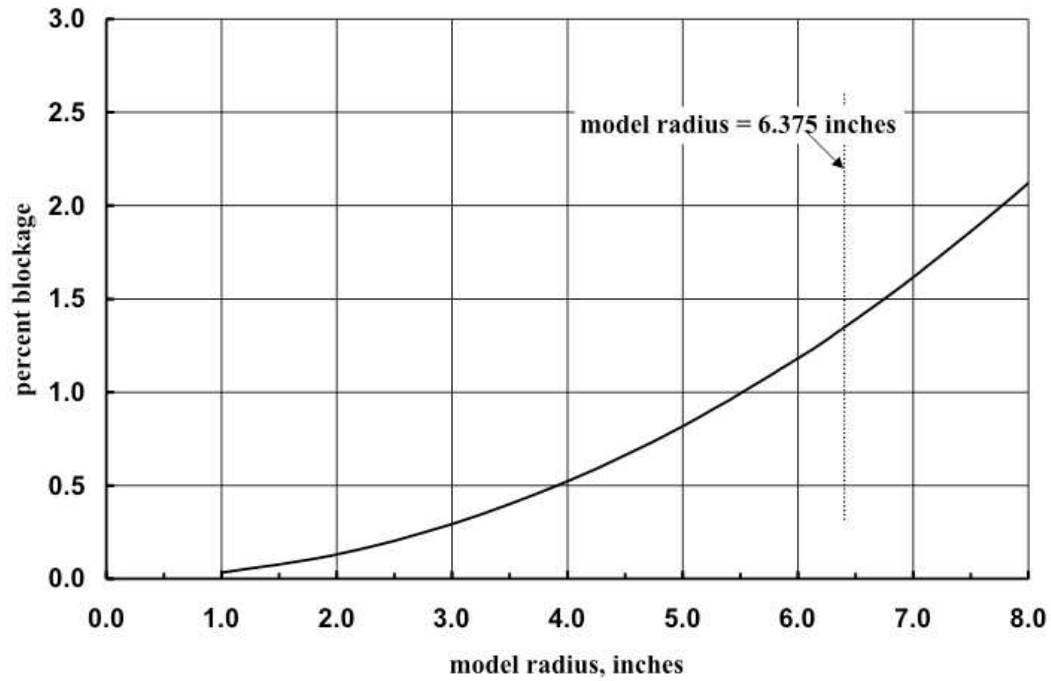
Figure 11. Area blockage of cylindrical model in NTF.

Figure 12. Instrumentation photographs.
(a) Skin friction balance.
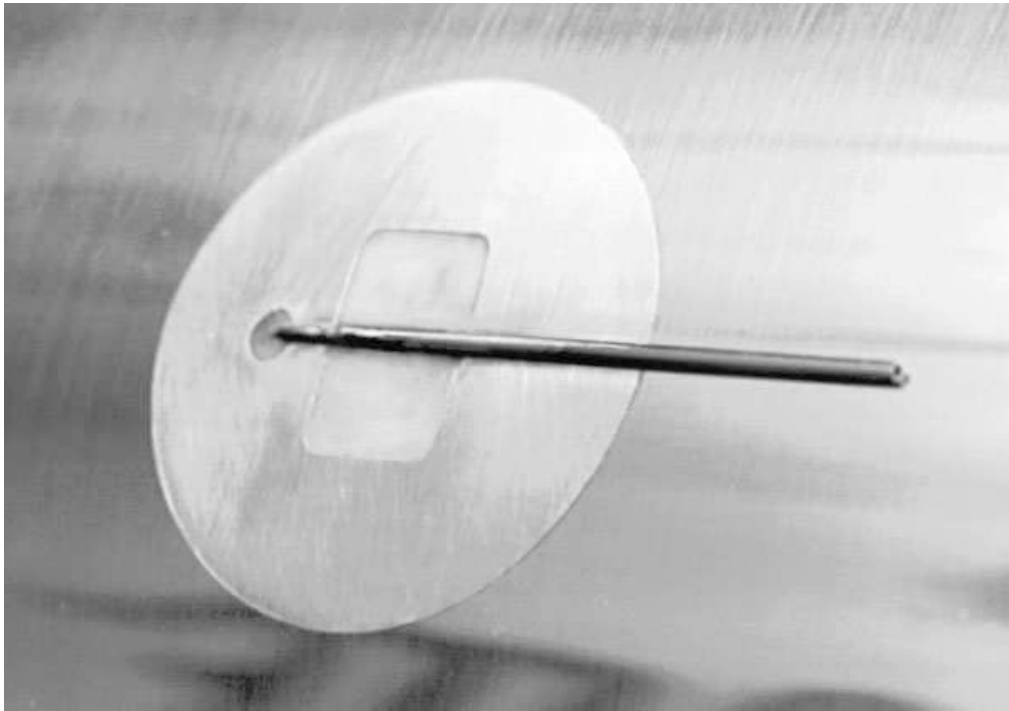
Figure 12. Continued.
(b) Preston tube.
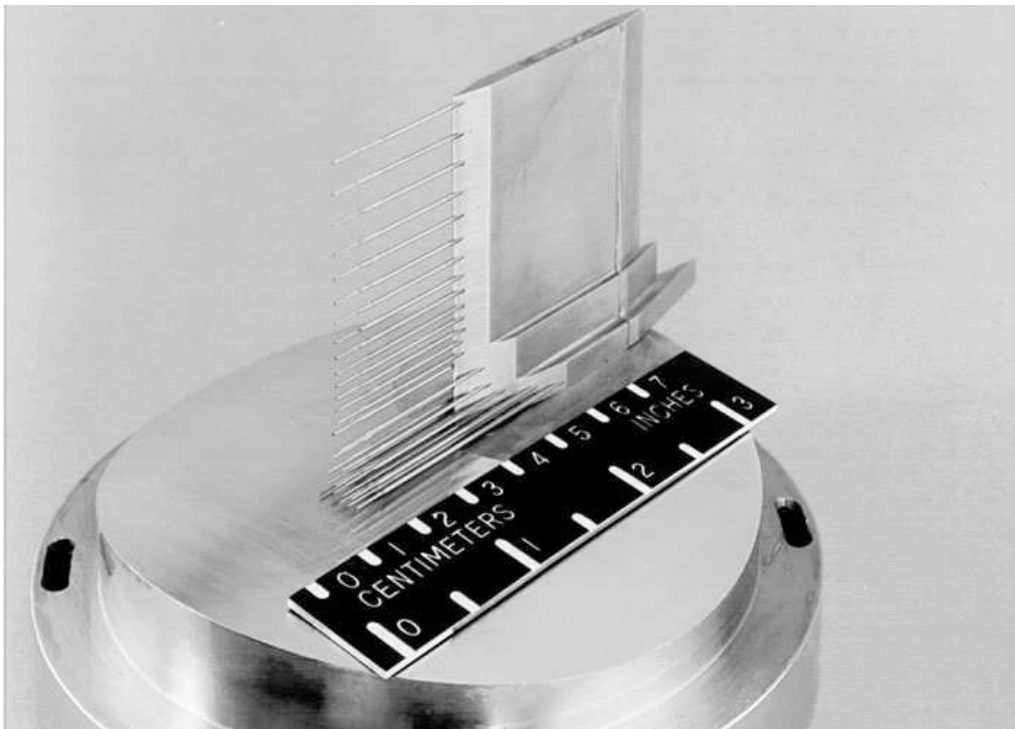
Figure 12. Concluded.
(c) Boundary layer rake mounted on model plug.
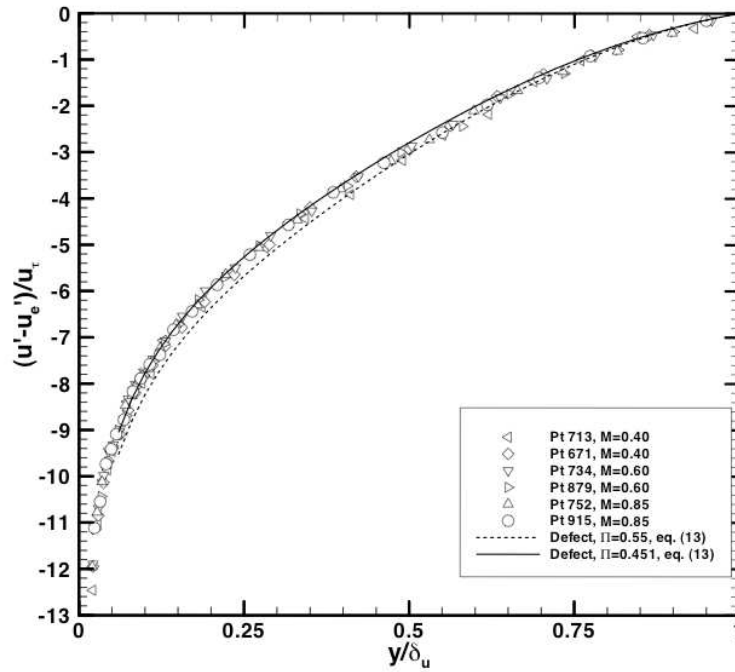
Figure 13. Laws of the wall and wake.
(a) Transformed profiles in Law-Of-Wake parameters.
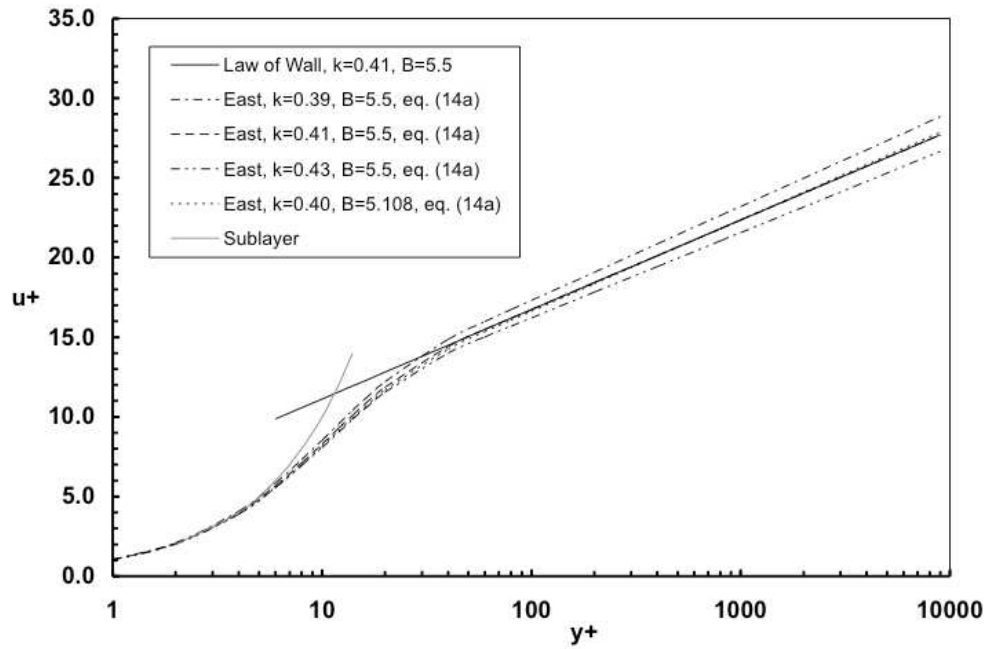
Figure 13. Concluded.
(b) East Profile compared with law-of-wall and sublayer.

100
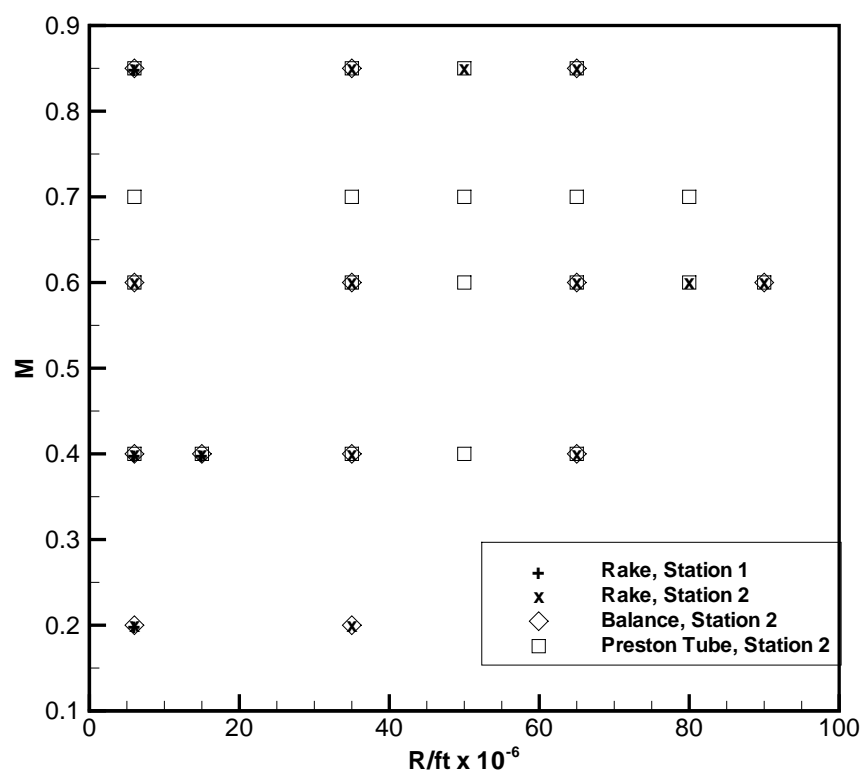
Figure 14. Mach number-Reynolds number data acquisition map.
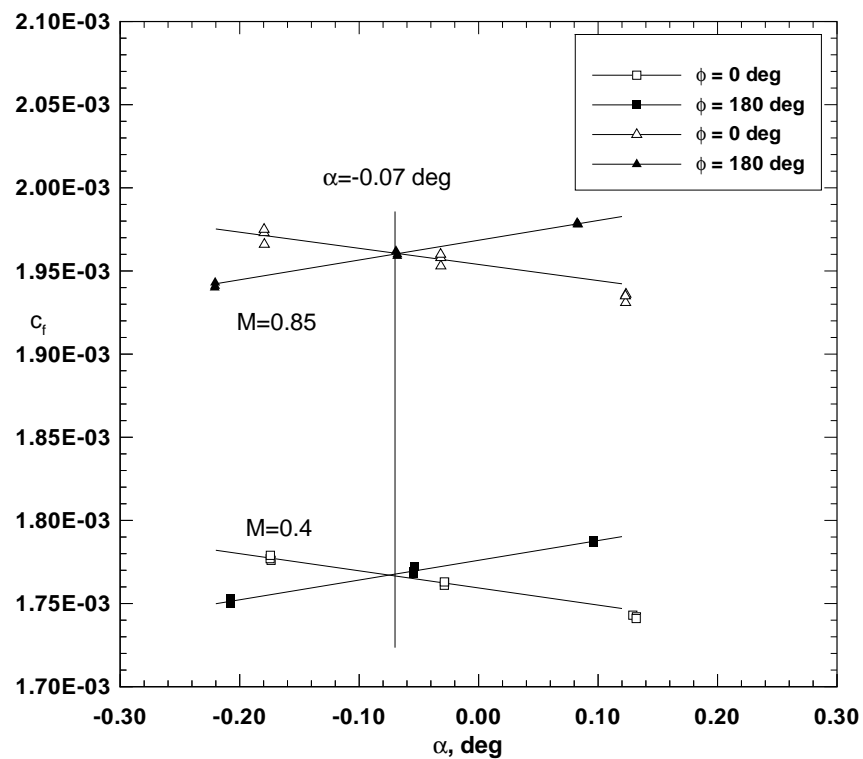
Figure 15. Model alignment in vertical plane by Preston tubes.
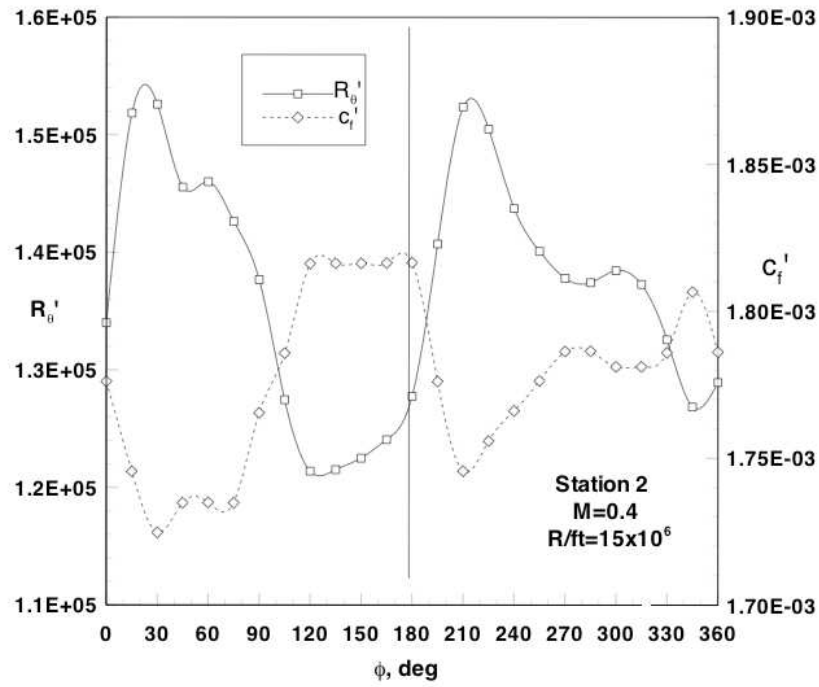
Figure 16. Variations of c_f' and R_θ' with model roll.
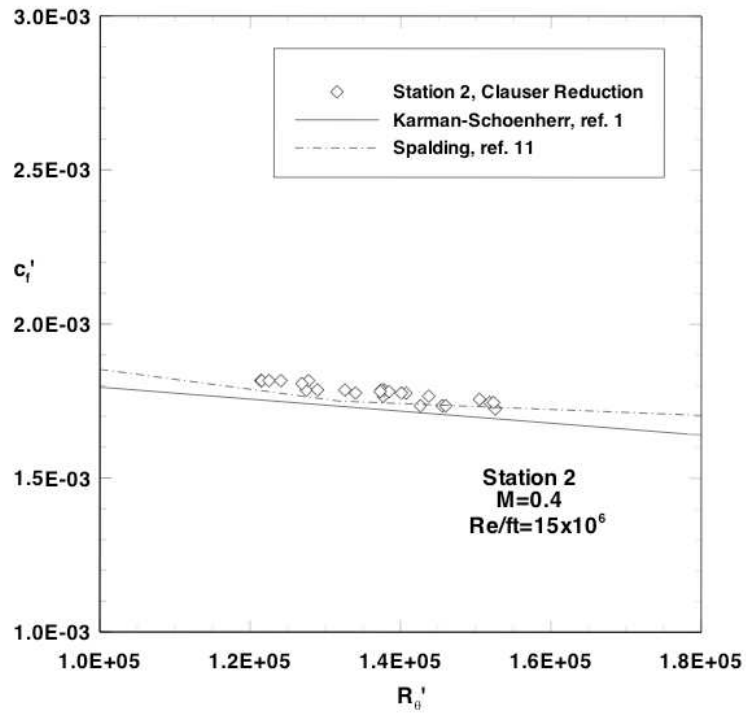
Figure 17. Circumferential c_f' as a function of R_θ'.

102
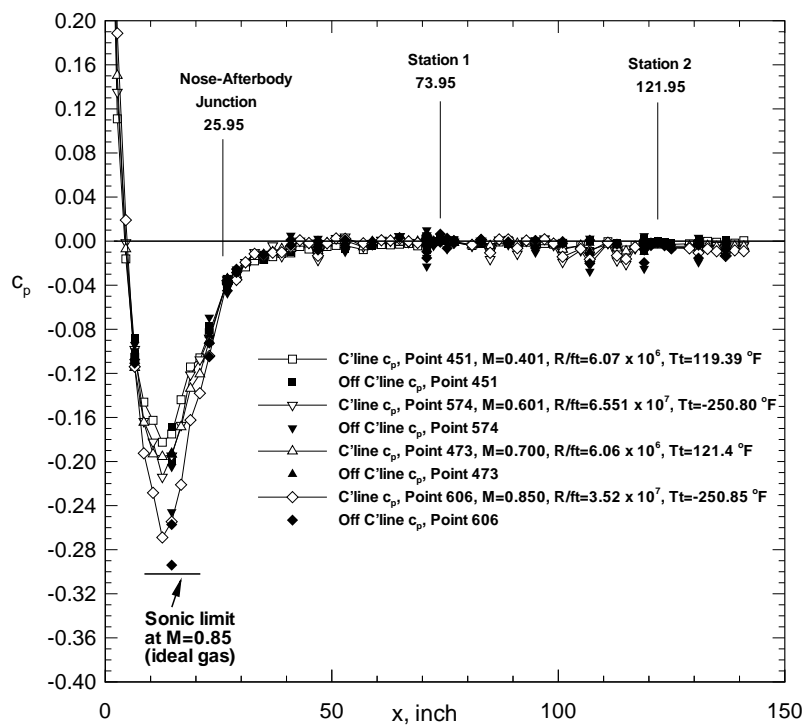
Figure 18. Representative model pressure and temperature distributions.
(a) Pressure distributions at M = 0.4, 0.6, 0.7, and 0.85.
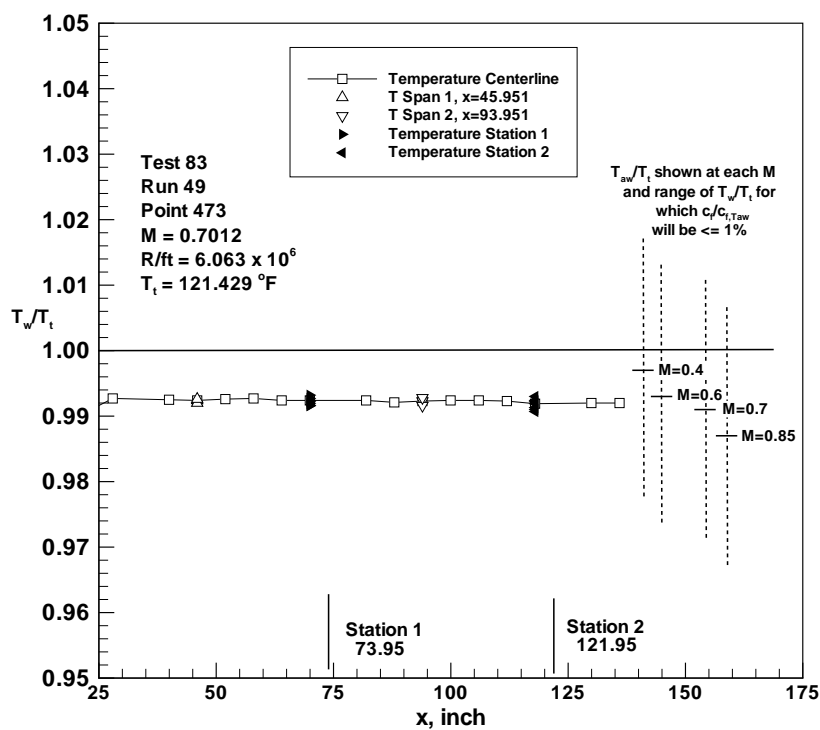
Figure 18. Continued.
(b) Temperature distribution, ambient run at M = 0.7.

103

Test 83
Run 73
Point 617
M = 0.4021
R/ft = 1.519 x 10^7
T$_t$ = -251.07 ^{o}F

T$_w$/T$_t$

Temperature Centerline
T Span 1, x=45.951
T Span 2, x=93.951
Temperature Station 1
Temperature Station 2

T$_{aw}$/T$_t$ shown at each M
and range of T$_w$/T$_t$ for
which c$_f$/c$_{f,Taw}$
will be <= 1%

M=0.4
M=0.6
M=0.7
M=0.85

Station 1
73.95

Station 2
121.95

x, inch
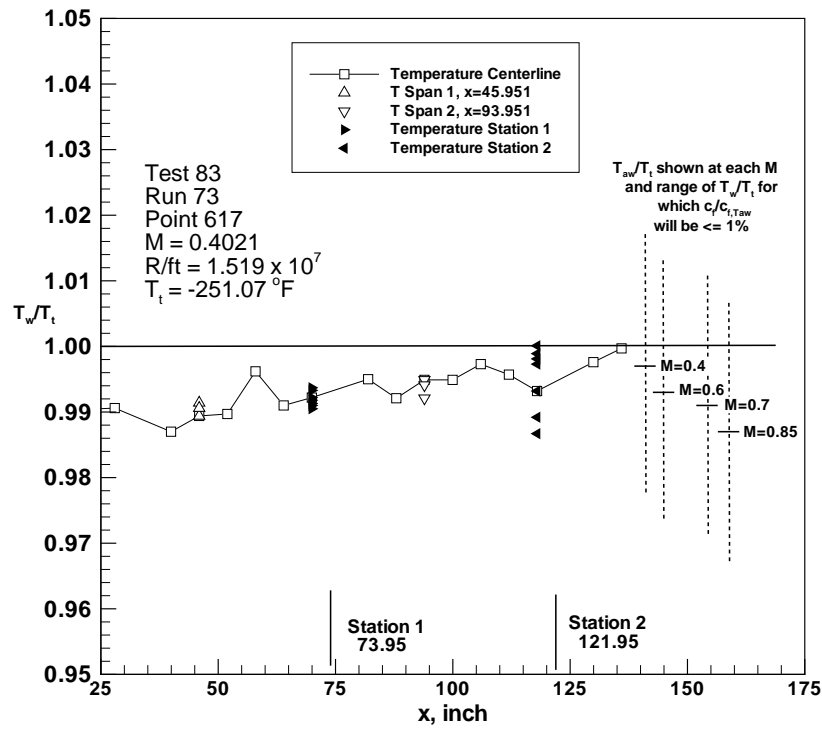
Figure 18. Continued.
(c) Temperature distribution, cold run at M = 0.4.

Test 83
Run 61
Point 569
M = 0.6009
R/ft = 8.010 x 10^7
T$_t$ = -250.05 ^{o}F

T$_w$/T$_t$

Temperature Centerline
T Span 1, x=45.951
T Span 2, x=93.951
Temperature Station 1
Temperature Station 2

T$_{aw}$/T$_t$ shown at each M
and range of T$_w$/T$_t$ for
which c$_f$/c$_{f,Taw}$
will be <= 1%

M=0.4
M=0.6
M=0.7
M=0.85

Station 1
73.95

Station 2
121.95

x, inch
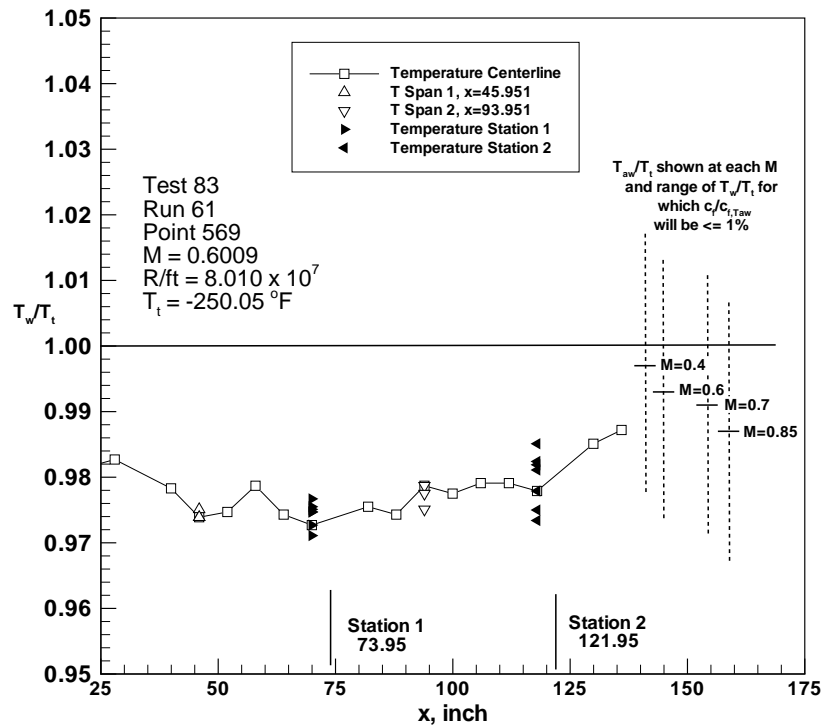
Figure 18. Continued.
(d) Temperature distribution, cold run at M = 0.6.

104
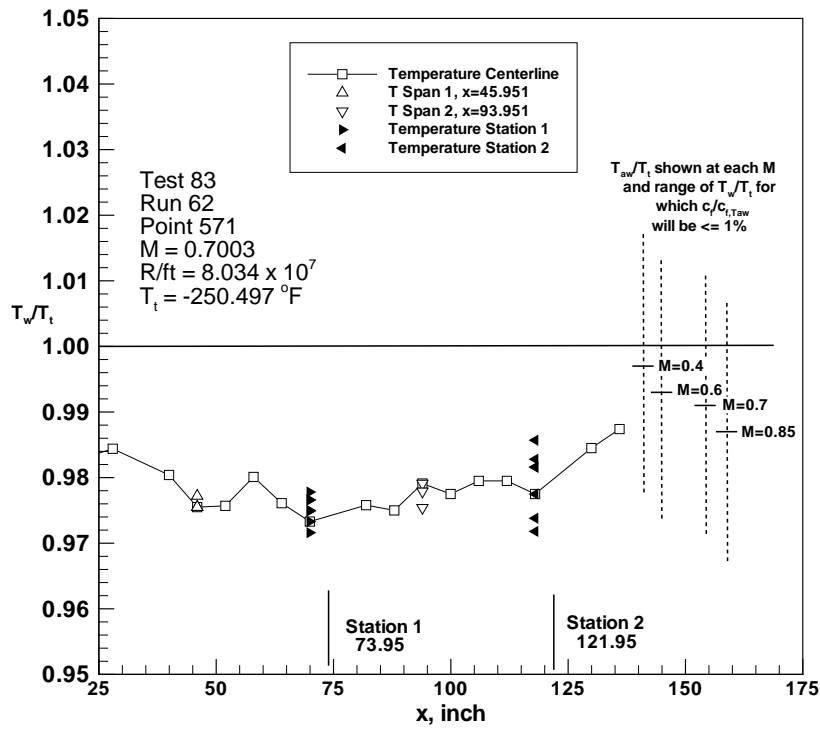
Figure 18. Continued.
(e) Temperature distribution, cold run at M = 0.7.
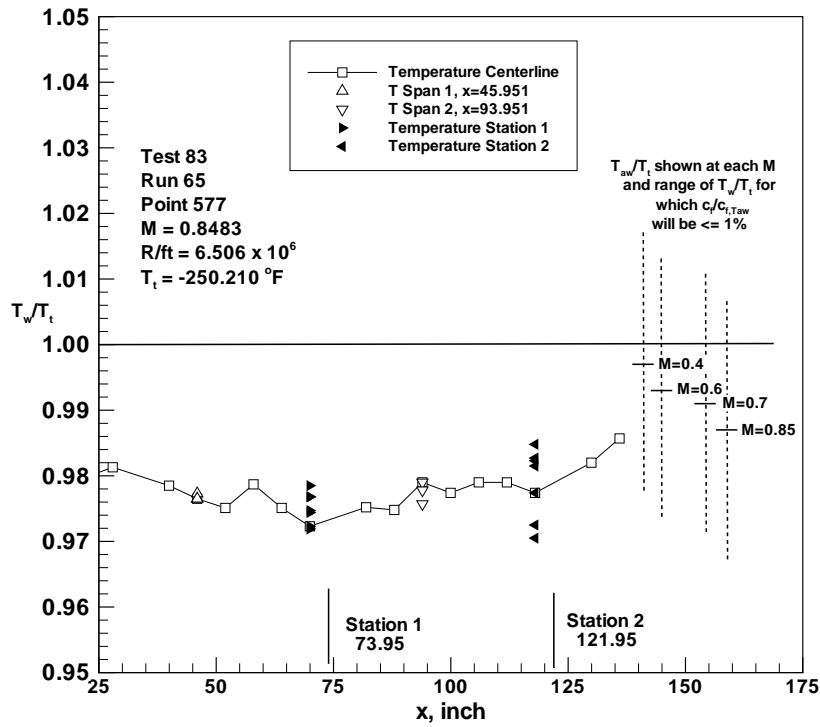
Figire 18. Concluded.
(f) Temperature distribution, cold run at M = 0.85.

105
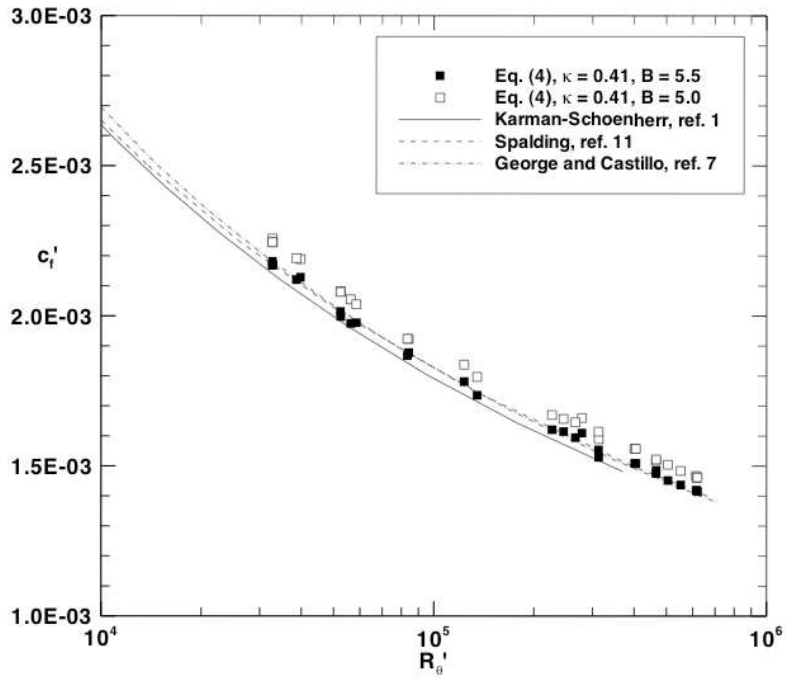
Figure 19. Data derived from velocity profiles.
(a) Effect of additive constant on Clauser-derived skin friction coefficients.
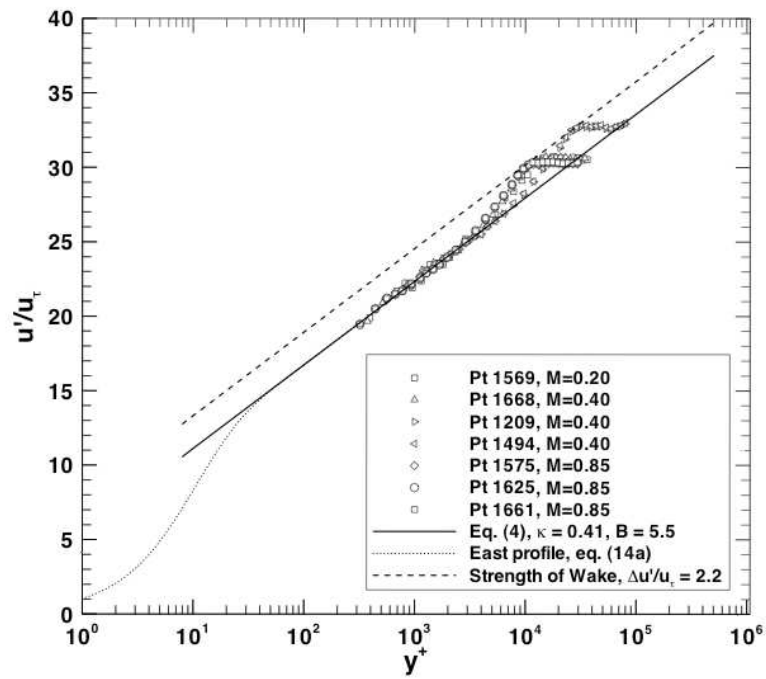
Figure 19. Continued.
(b) Transformed wall profiles at Station 1.
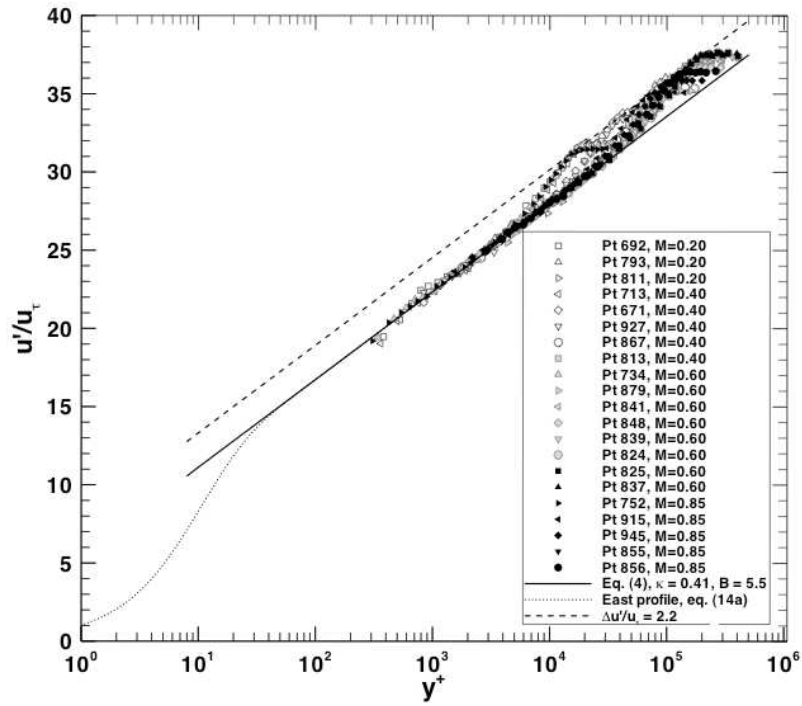
Figure 19. Continued.
(c) Transformed wall profiles at Station 2.
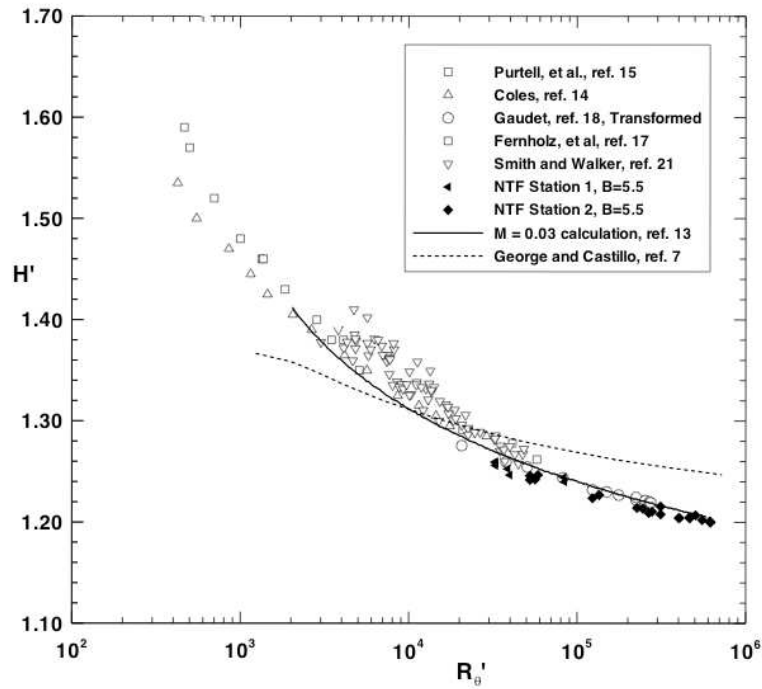
Figure 19. Continued.
(d) Transformed shape factors.
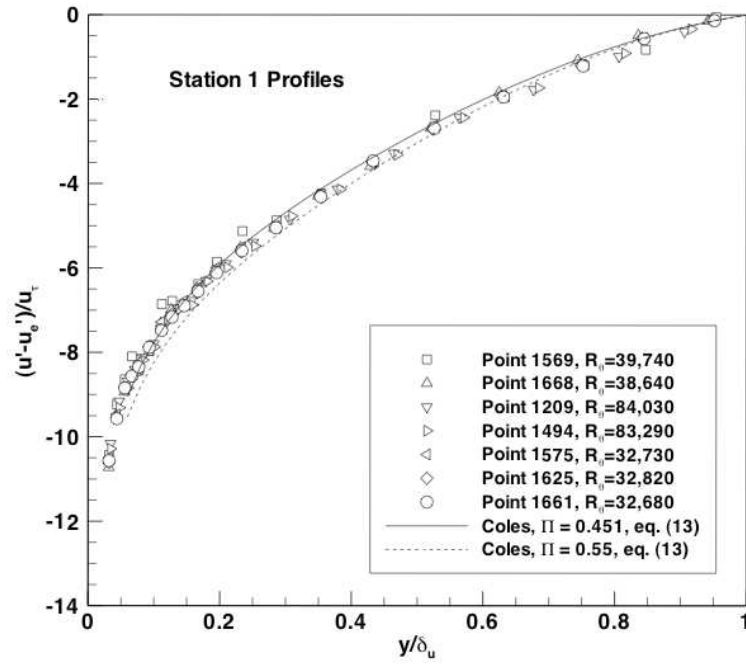
Figure 19. Continued.
(e) Transformed wake profiles at Station 1.
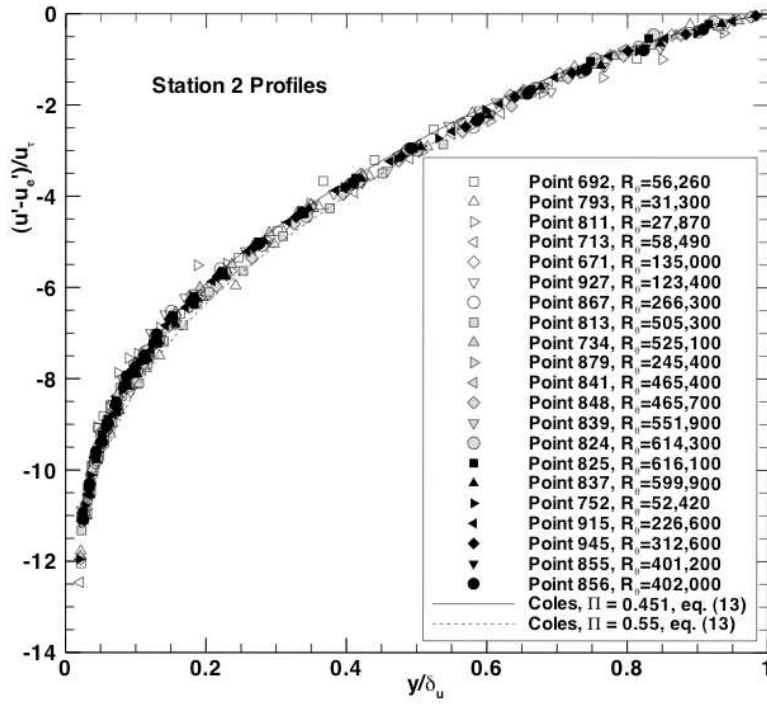
Figure 19. Continued.
(f) Transformed wake profiles at Station 2.

108
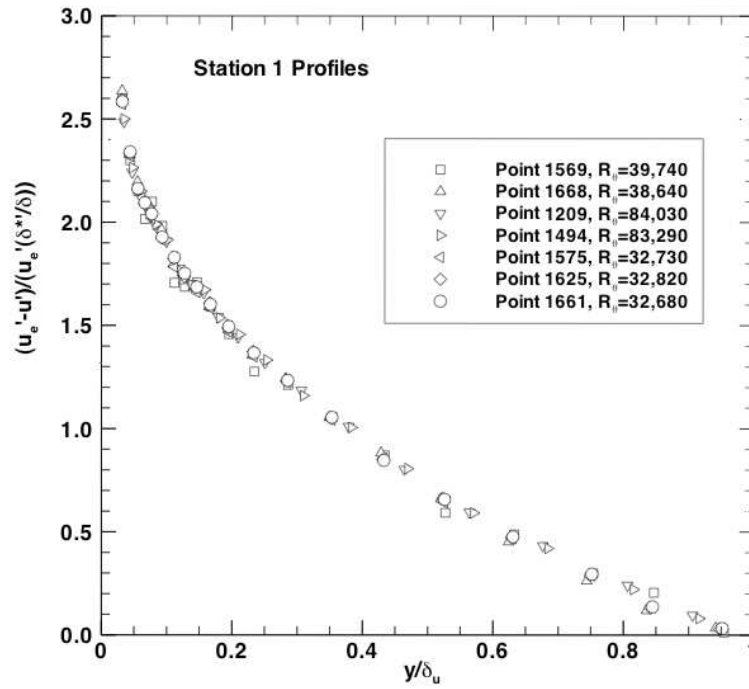
Figure 19. Continued.
(g) Transformed wake profiles at Station 1, parameters of ref. 45.
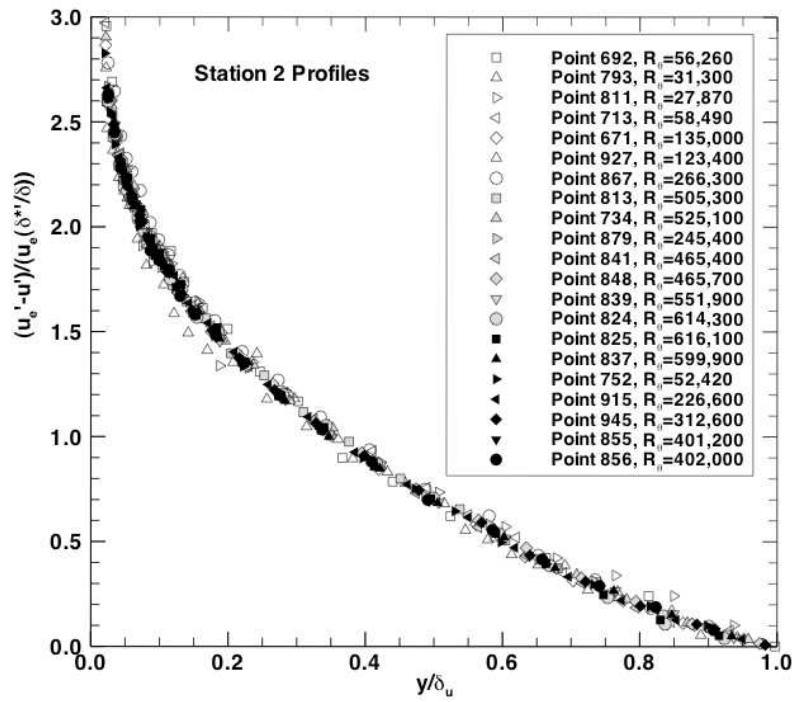
Figure 19. Concluded.
(h) Transformed wake profiles at Station 2, parameters of ref. 45.

109
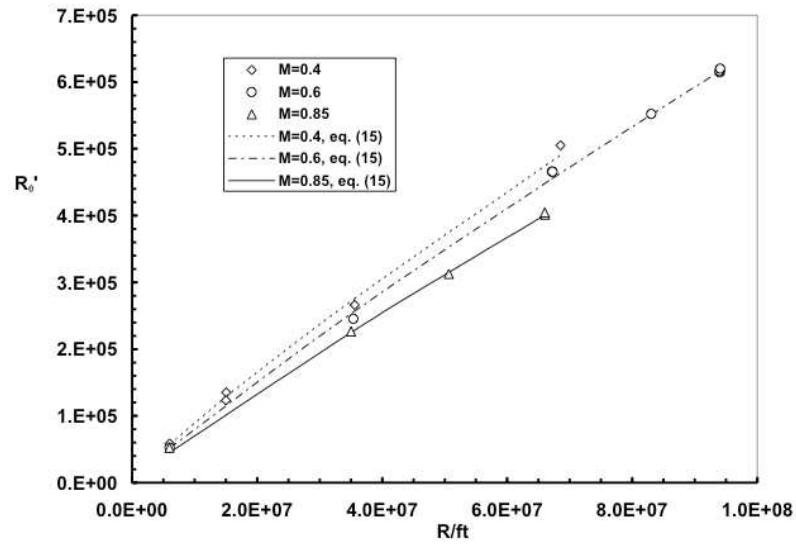
Figure 20. R_θ' from rake at Station 2.
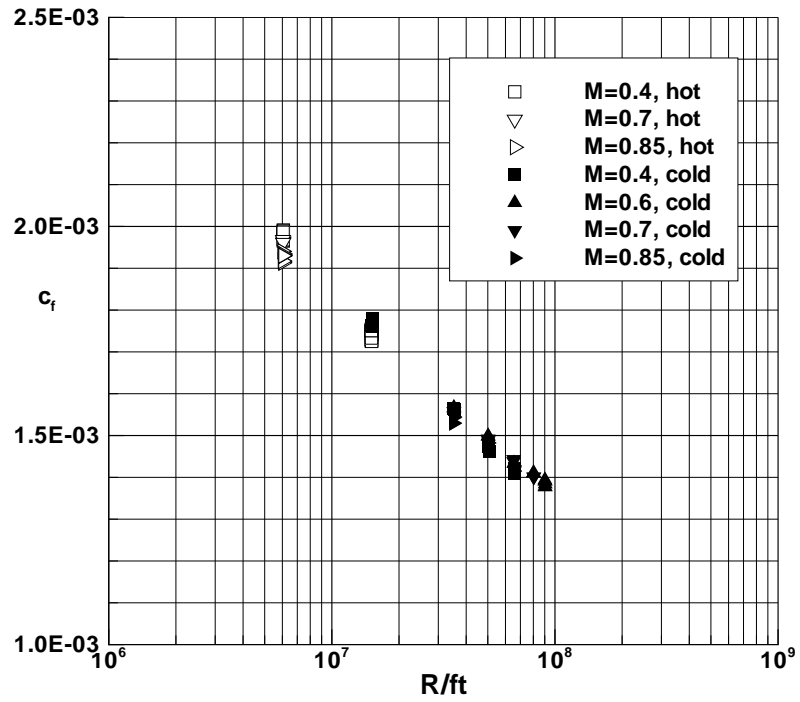
Figure 21. Preston tube data at Station 2.
(a) Compressible variables.
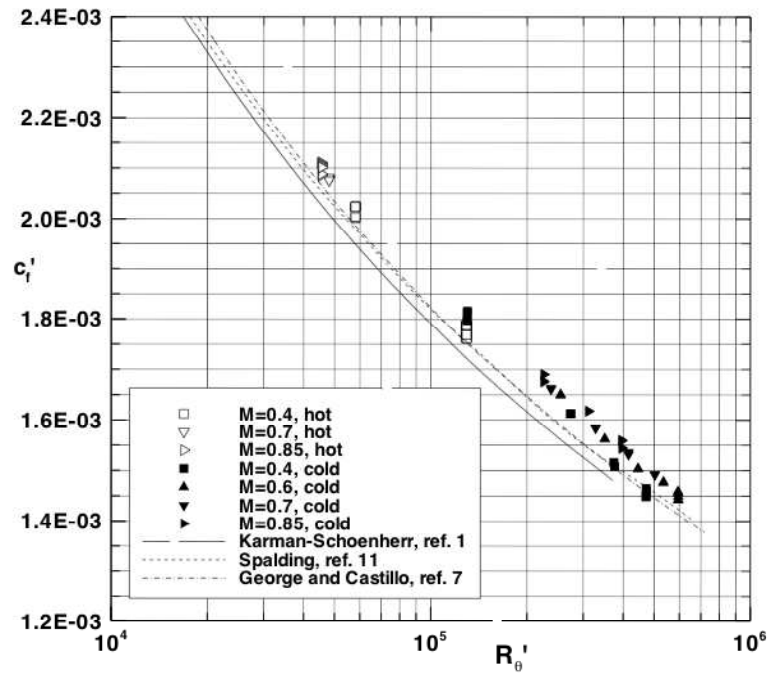
Figure 21. Concluded.
(b) Incompressible variables.
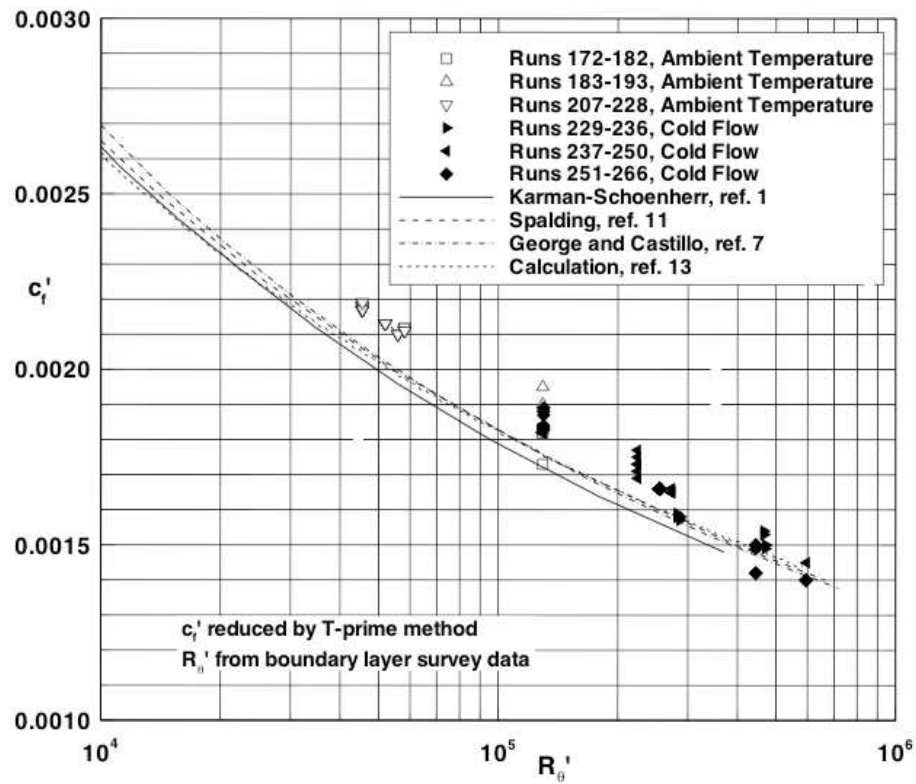
Figure 22. Balance data at Station 2—incompressible parameters.

111
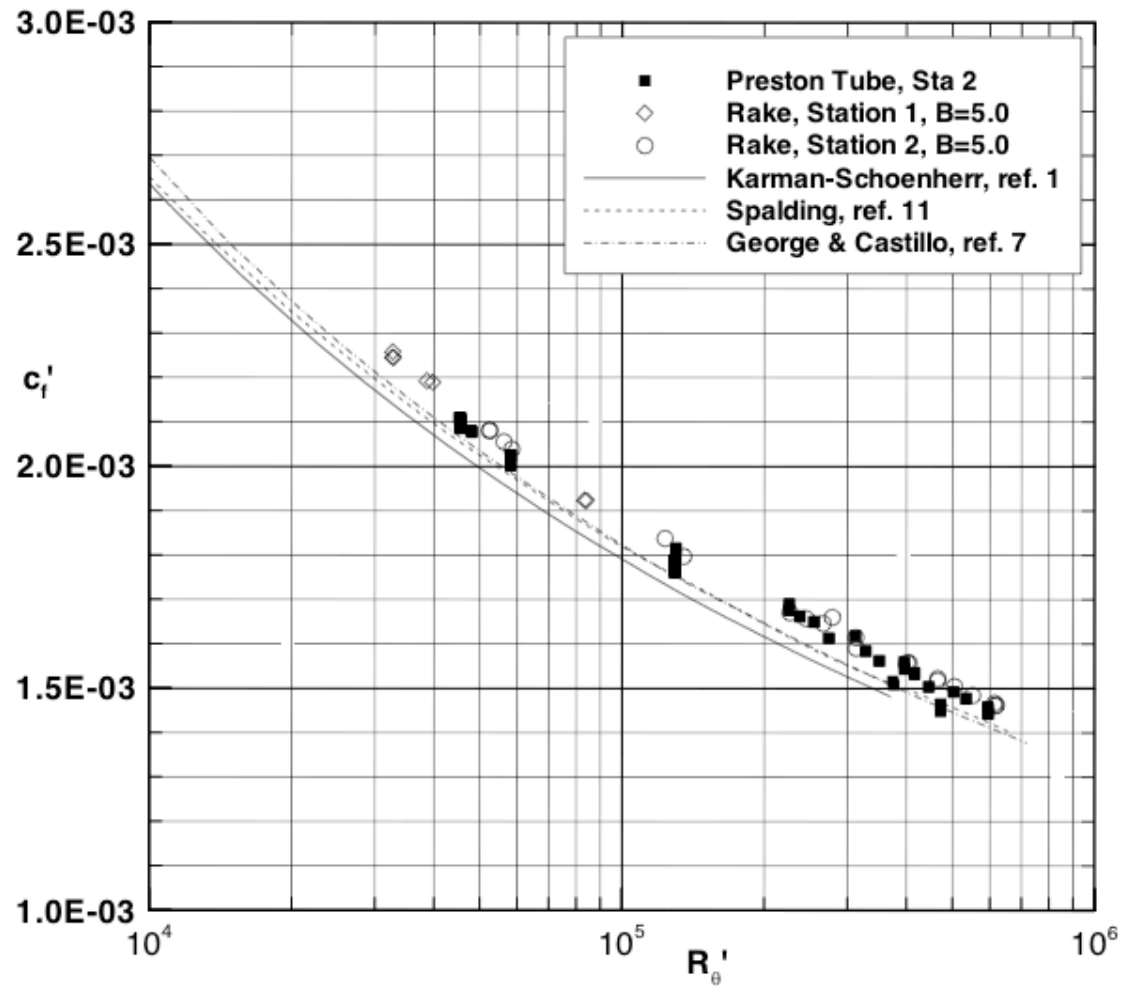
Figure 23. Comparison of Preston tube and rake data.
(a) B = 5.0 in Law of Wall reduction.
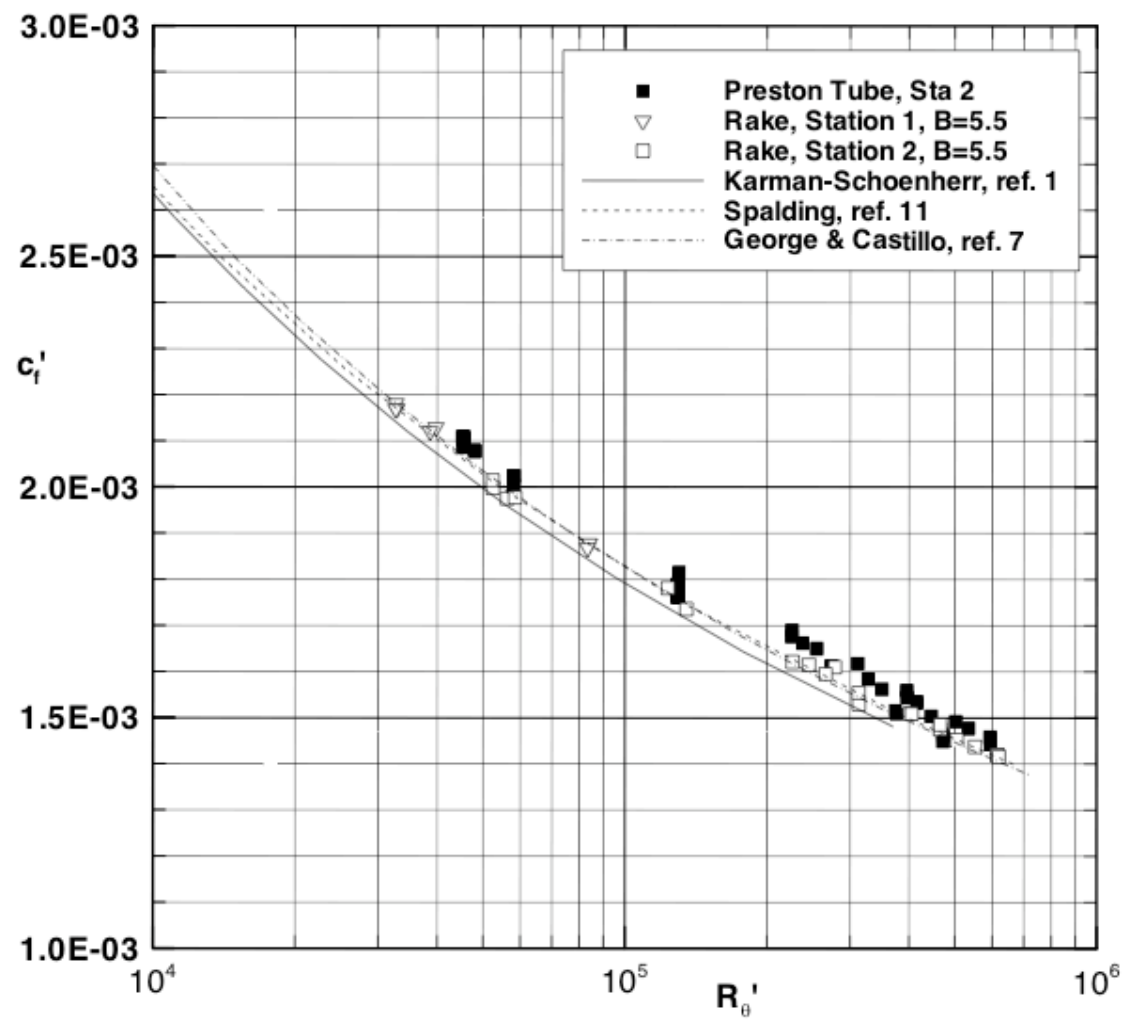
Figure 23. Continued.
(b) B = 5.5 in Law of Wall reduction.

113
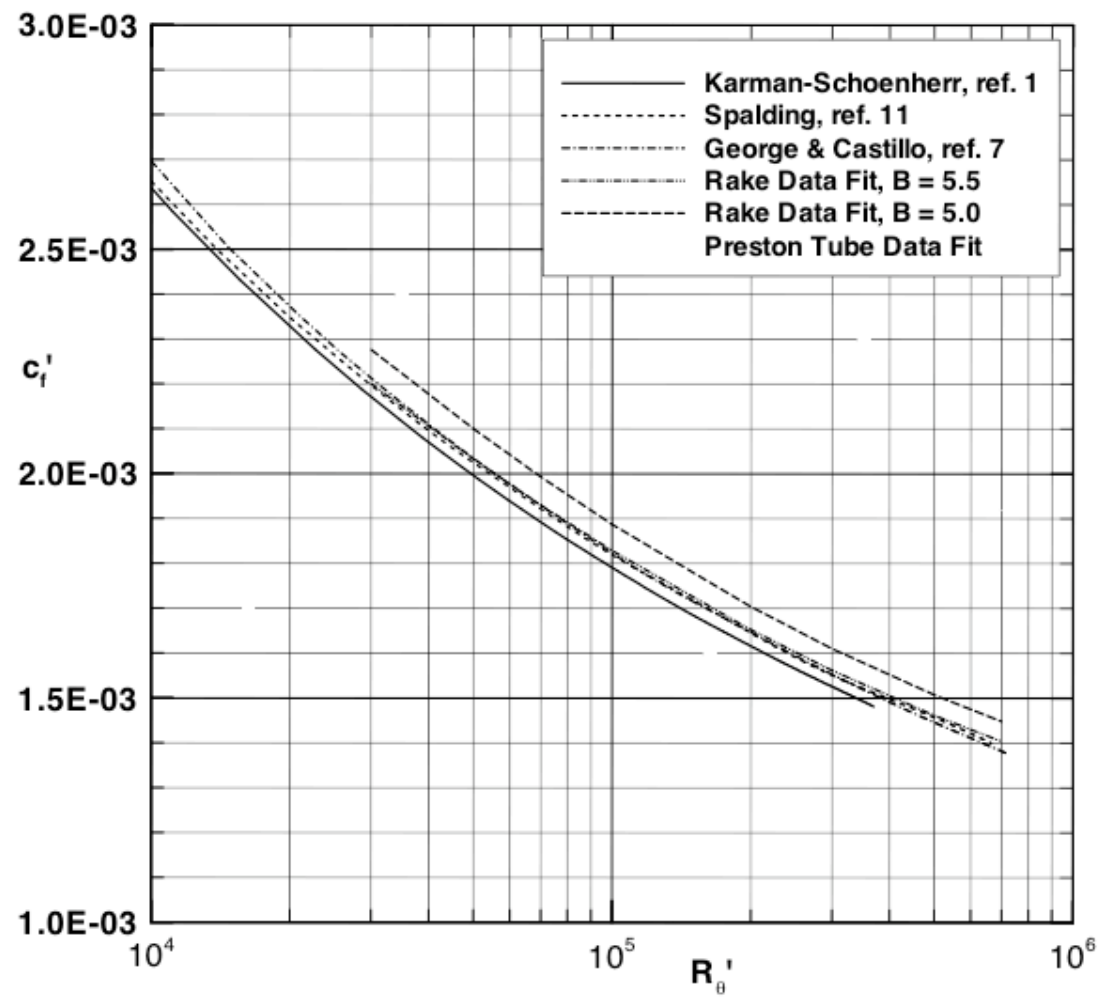
Figure 23. Concluded.
(c) Polynomial fits to Preston tube and rake data.
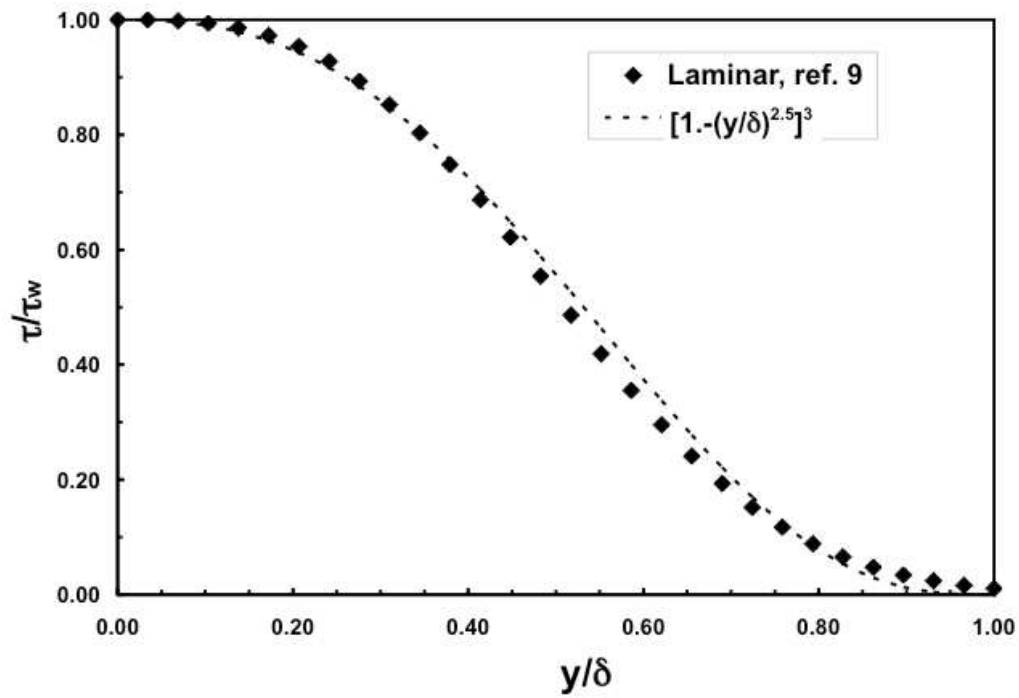
Figure A1. Incompressible boundary layer shear stress distributions.
(a) Laminar calculation by Howarth.
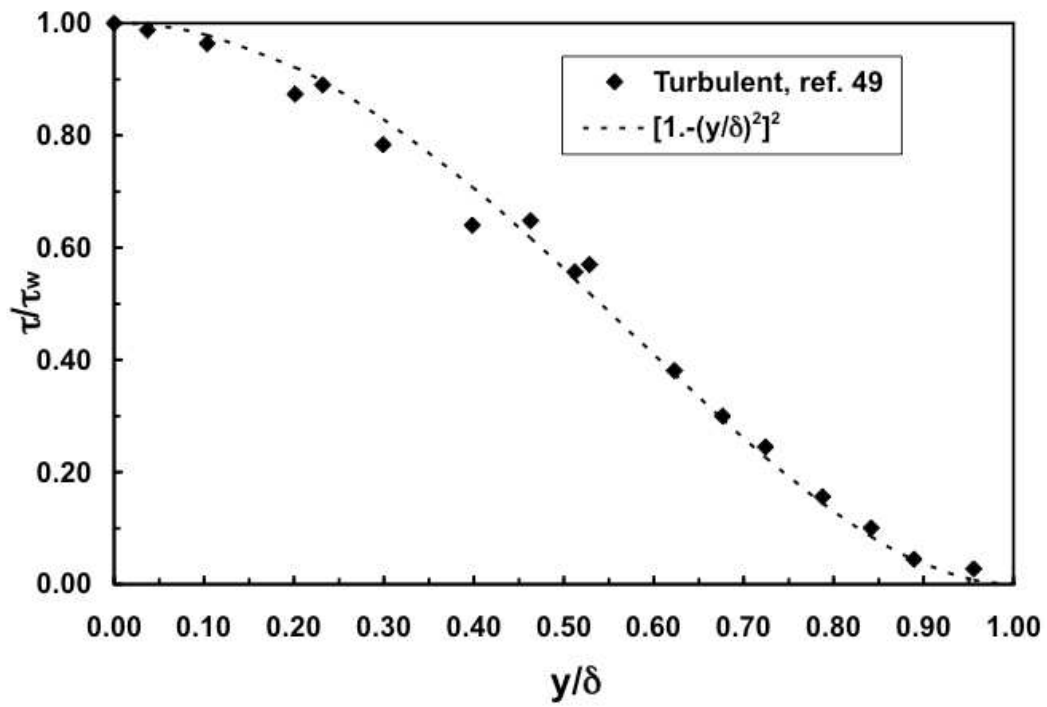
Figure A1. Concluded.
(b) Turbulent measurement from Klebanoff.
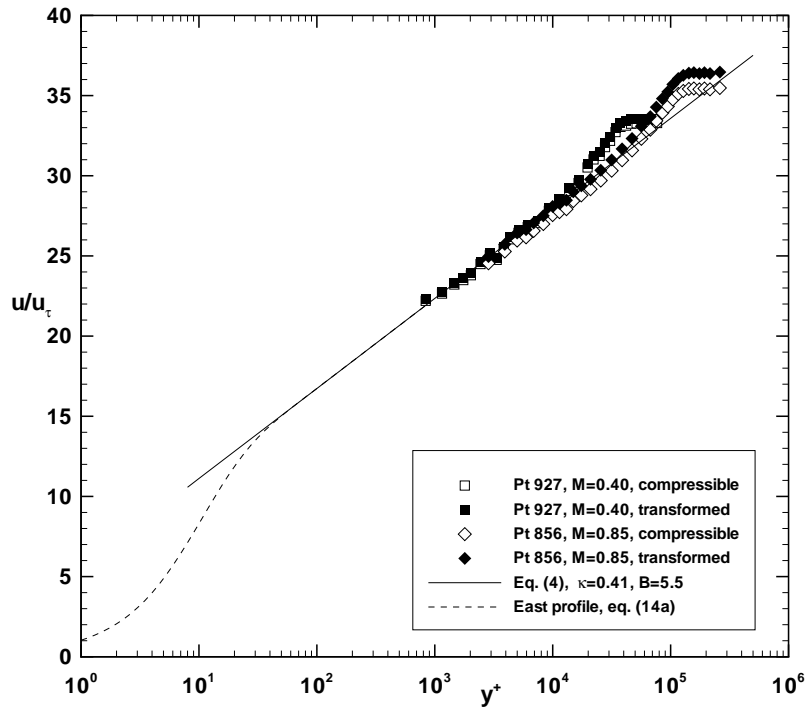
Figure A2. Van Driest transformation applied to velocity profiles.
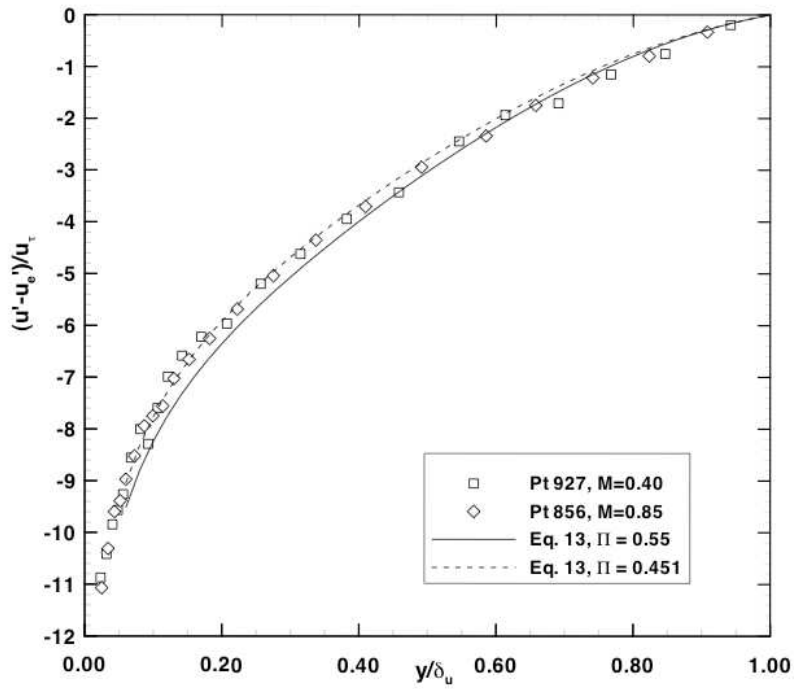
Figure A3. Transformed velocity profiles in outer coordinates.
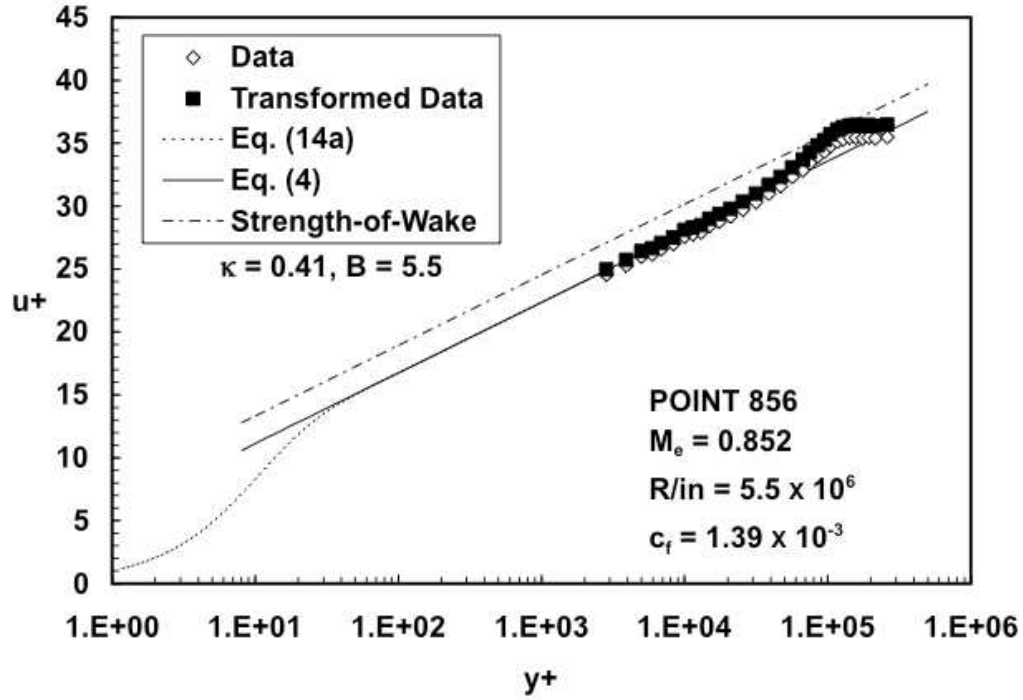
Figure B1. Profile point 856.
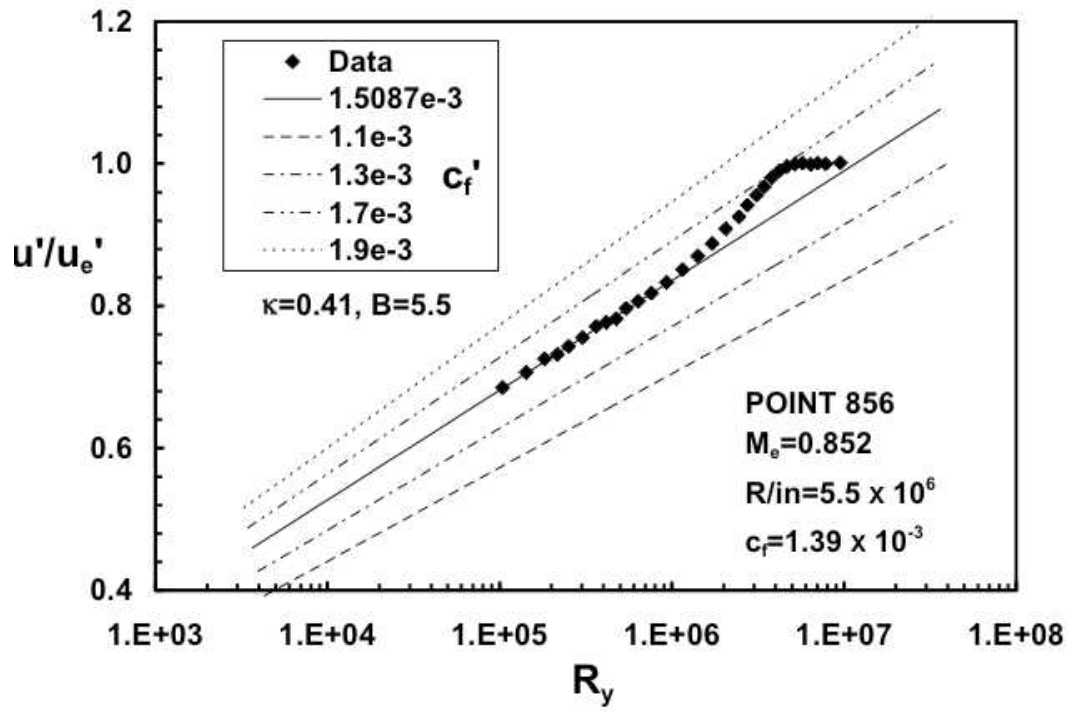
Figure B2. Clauser method applied to transformed data.

117
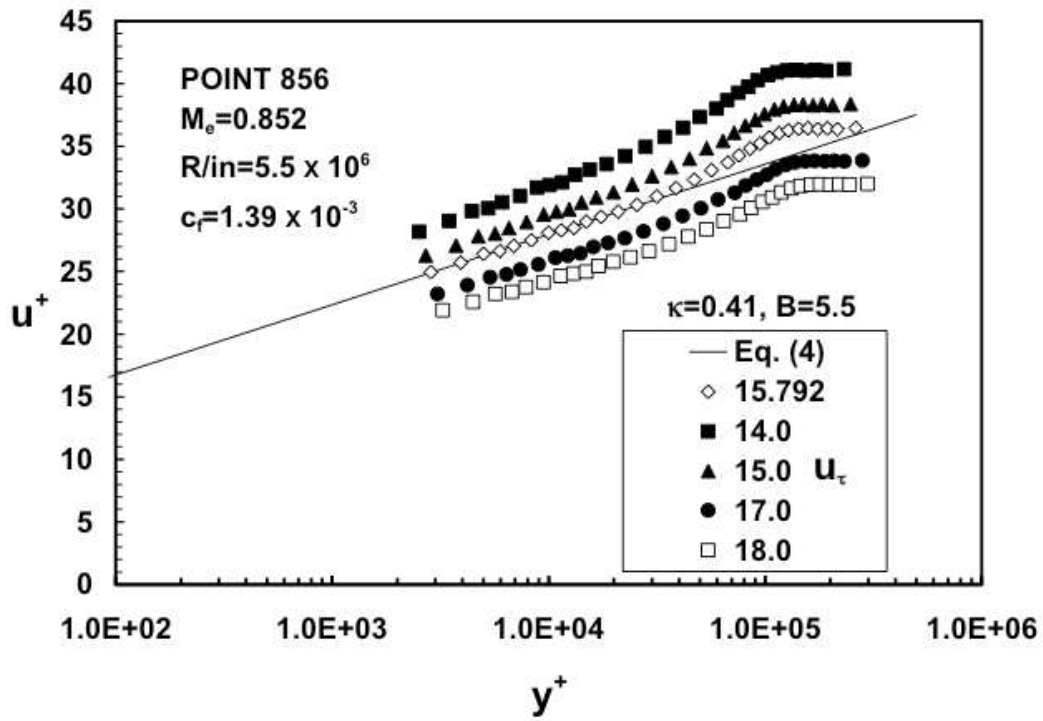
Figure B3. Modified Clauser method applied to transformed data.

Dimensions in inches.
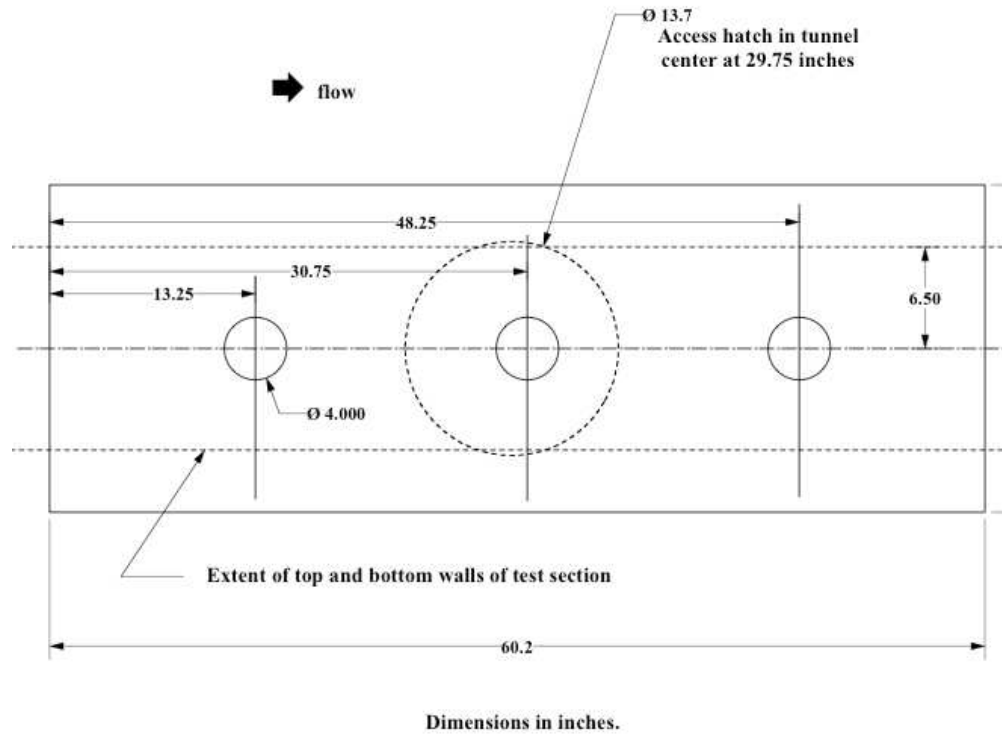
Figure C1. Tunnel wall test surface.
(a) Balance locations.

118

orifice i.d. = 0.020 inch
58 orifices total
filled orifices located at y=4.5 and -4.5

Dimensions in inches.

Figure C1. Continued.
(b) Pressure orifice locations.

22 thermocouples total
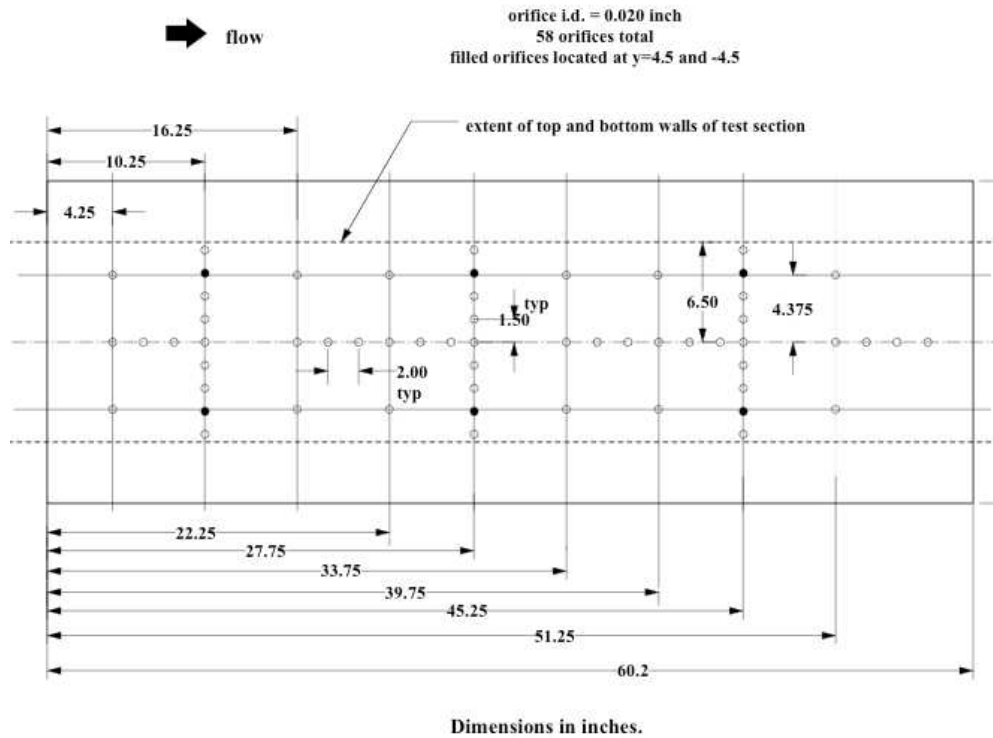
Dimensions in inches.
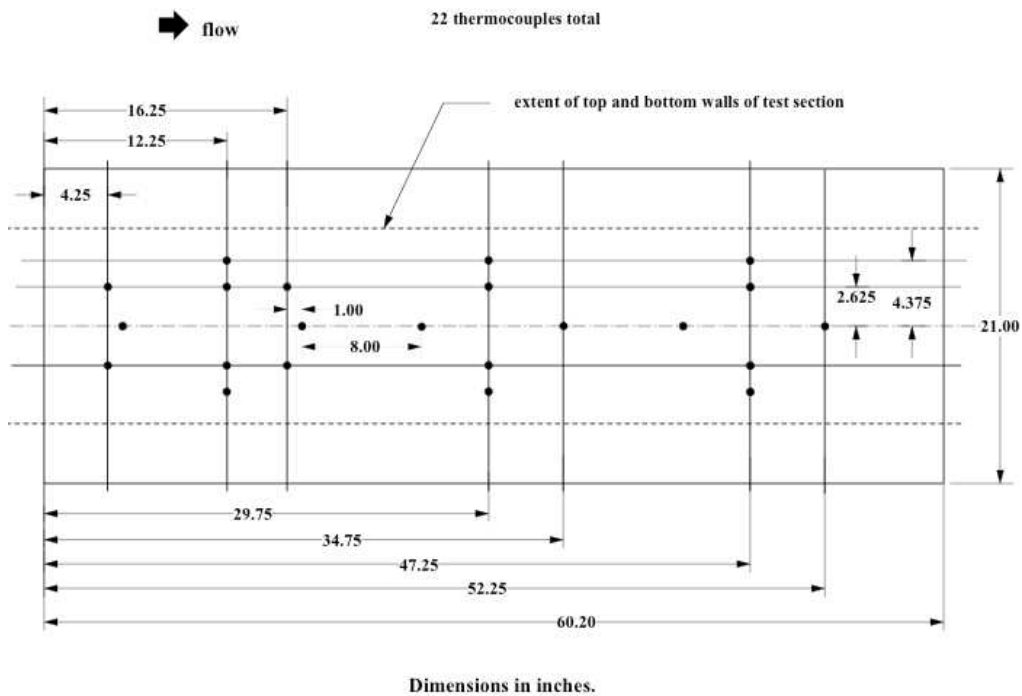
Figure C1. Concluded.
(c) Thermocouple locations.

119

center of plugs at 13.250, 30.750, and 48.250

open symbols denote
pressure orifices
solid symbols denote
thermocouples

4.375

3.500

2.625

1.500

1.500 at
2nd and 3rd
stations
2.000 at
1st station

3.000

Ø 4.000

2 thermocouples
at this location
only at 1st station

oval plugs 3 x 1

1.000

3.000

Dimensions in inches.
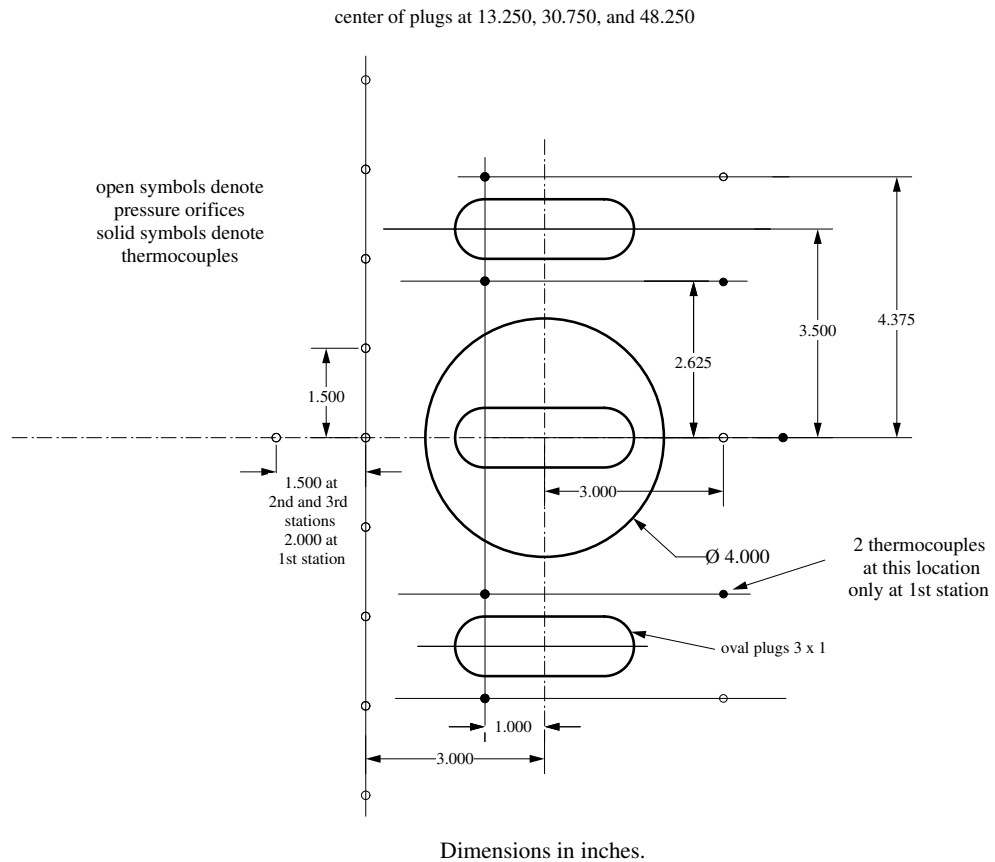
Figure C2. Test surface dimensions in vicinity of survey locations.
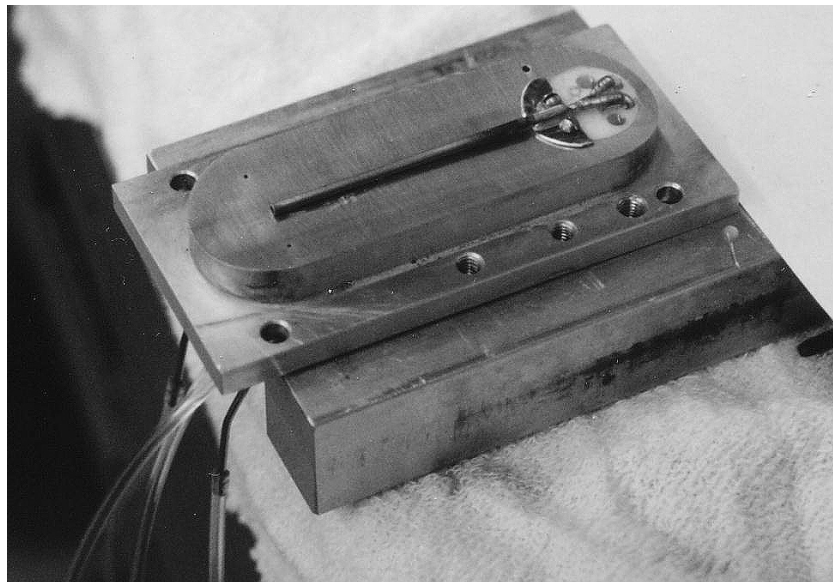
Figure D1. Photograph of Preston tube mounted on Superpipe plug.
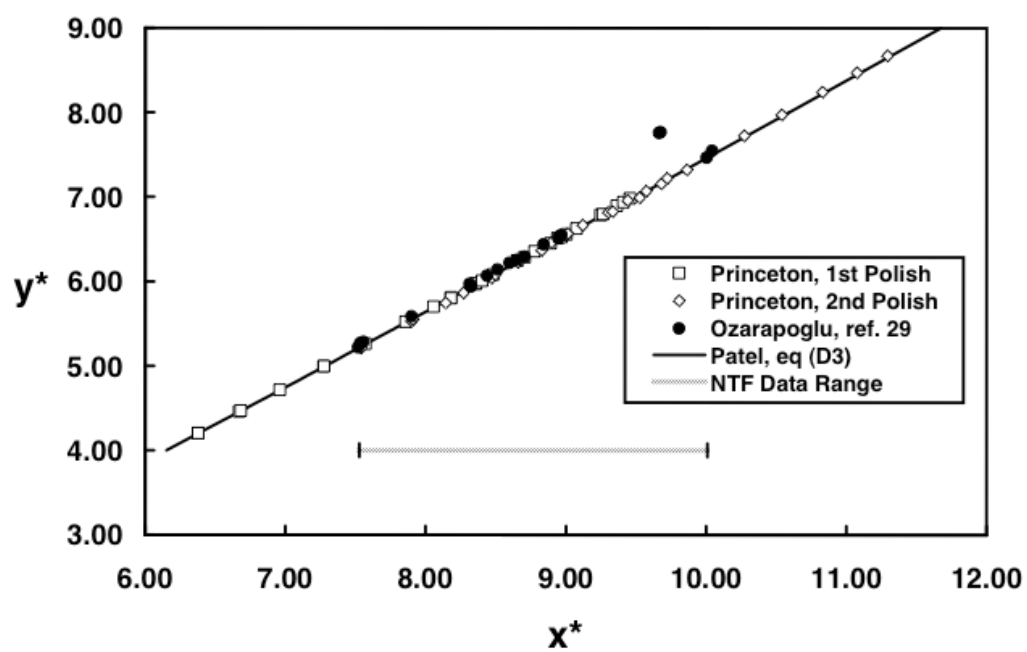
Figure D2. Preston tube calibration at high Reynolds numbers.

1. REPORT DATE *(DD-MM-YYYY)*	2. REPORT TYPE	3. DATES COVERED *(From - To)*
01- 08 - 2006	Technical Publication	

4. TITLE AND SUBTITLE	5a. CONTRACT NUMBER
Skin Friction at Very High Reynolds Numbers in the National Transoinc Facility	
	5b. GRANT NUMBER
	5c. PROGRAM ELEMENT NUMBER

6. AUTHOR(S)	5d. PROJECT NUMBER
Watson, Ralph D.; Anders, John B.; and Hall, Robert M.	
	5e. TASK NUMBER
	5f. WORK UNIT NUMBER
	732759.07.03

7. PERFORMING ORGANIZATION NAME(S) AND ADDRESS(ES)	8. PERFORMING ORGANIZATION REPORT NUMBER
NASA Langley Research Center Hampton, VA 23681-2199	L-19270

9. SPONSORING/MONITORING AGENCY NAME(S) AND ADDRESS(ES)	10. SPONSOR/MONITOR'S ACRONYM(S)
National Aeronautics and Space Administration Washington, DC 20546-0001	NASA
	11. SPONSOR/MONITOR'S REPORT NUMBER(S)
	NASA/TP-2006-214497

12. DISTRIBUTION/AVAILABILITY STATEMENT

Unclassified - Unlimited
Subject Category 34
Availability: NASA CASI (301) 621-0390

13. SUPPLEMENTARY NOTES
An electronic version can be found at http://ntrs.nasa.gov

14. ABSTRACT

Skin friction coefficients were derived from measurements using standard measurement technologies on an axisymmetric cylinder in the NASA Langley National Transonic Facility (NTF) at Mach numbers from 0.2 to 0.85. The pressure gradient was nominally zero, the wall temperature was nominally adiabatic, and the ratio of boundary layer thickness to model diameter within the measurement region was 0.10 to 0.14, varying with distance along the model. Reynolds numbers based on momentum thicknesses ranged from 37,000 to 605,000. The measurements approximately doubled the range of available data for flat plate skin friction coefficients. Three different techniques were used to measure surface shear. The maximum error of Preston tube measurements was estimated to be 2.5 percent, while that of Clauser derived measurements was estimated to be approximately 5 percent. Direct measurements by skin friction balance proved to be subject to large errors and were not considered reliable.

15. SUBJECT TERMS

Karman-Schoenherr prediction; NTF; National Transonic Facility; Preston tube measurements; Skin friction coefficients

16. SECURITY CLASSIFICATION OF:			17. LIMITATION OF ABSTRACT	18. NUMBER OF PAGES	19a. NAME OF RESPONSIBLE PERSON
a. REPORT	b. ABSTRACT	c. THIS PAGE			STI Help Desk (email: help@sti.nasa.gov)
U	U	U	UU	130	19b. TELEPHONE NUMBER *(Include area code)* (301) 621-0390